University of Alberta

STUDIES OF COPPER(II,I) COORDINATION AND ELECTRON-TRANSFER KINETICS IN ACETONITRILE

By

JAPHET KIGUNDA IRANGU

A thesis submitted to the Faculty of Graduate Studies and Research in partial fulfillment of the requirements for the degree of Doctor of Philosophy

Department of Chemistry

Edmonton, Alberta

Spring, 2004

Library and Archives Canada

Published Heritage Branch

395 Wellington Street
Ottawa ON K1A 0N4
Canada

Bibliothèque et Archives Canada

Direction du Patrimoine de l'édition

395, rue Wellington
Ottawa ON K1A 0N4
Canada

Your file Votre référence
ISBN: 0-612-96280-6
Our file Notre référence
ISBN: 0-612-96280-6

The author has granted a non-exclusive license allowing the Library and Archives Canada to reproduce, loan, distribute or sell copies of this thesis in microform, paper or electronic formats.

The author retains ownership of the copyright in this thesis. Neither the thesis nor substantial extracts from it may be printed or otherwise reproduced without the author's permission.

L'auteur a accordé une licence non exclusive permettant à la Bibliothèque et Archives Canada de reproduire, prêter, distribuer ou vendre des copies de cette thèse sous la forme de microfiche/film, de reproduction sur papier ou sur format électronique.

L'auteur conserve la propriété du droit d'auteur qui protège cette thèse. Ni la thèse ni des extraits substantiels de celle-ci ne doivent être imprimés ou aturement reproduits sans son autorisation.

In compliance with the Canadian Privacy Act some supporting forms may have been removed from this thesis.

While these forms may be included in the document page count, their removal does not represent any loss of content from the thesis.

Conformément à la loi canadienne sur la protection de la vie privée, quelques formulaires secondaires ont été enlevés de cette thèse.

Bien que ces formulaires aient inclus dans la pagination, il n'y aura aucun contenu manquant.

Canada

Abstract

The structures of diaquabis(acetonitrile)bis(trifluoromethylsulfonato)copper(II), tetrakis(acetonitrile)bis(trifluoromethylsulfonato)copper(II) and tetrakis(acetonitrile)-copper(I) triflate crystals determined here indicate four-coordinate tetrahedral Cu(I) and six-coordinate tetragonal Cu(II) geometries, and average Cu(I)-N and Cu(II)-N distances of 1.975, 1.989 and 2.002 Å, respectively.

Reactions of Cu(II) in 50, 80, 90, 95 and 97.5% vol/vol CH_3CN/H_2O gives the respective rate constants at 25 °C of 4.15, 5.97, 22.2, 198, and 1.88 x 10^3 M^{-1} s^{-1} with ferrocene, and 16.1, 25.4, 103, 862, and 7.92 x 10^3 M^{-1} s^{-1} with dimethylferrocene. The Cu(II/I) self-exchange rate constant, ~5 x 10^{-9} M^{-1} s^{-1}, from these results, is relatively constant in various % AN. In Cu(II) solutions with added NO_3^- ions, mono and bis complexes with β values of 1.09 x 10^3 M^{-1} and 1.39 x 10^4 M^{-2} in 80% AN and 4.02 x 10^3 M^{-1} and 3.96 x 10^4 M^{-2} in 95% are obtained. The NO_3^- shows no detectable effect on rate constants of the Cu(II)-ferrocenes reactions in 80% AN, but these are smaller in 95% AN. The respective k_0, k_1 and k_2 values for free Cu^{2+}, mono and bis complexes are 195, 185 and 17.5 M^{-1} s^{-1} with ferrocene, and 1040, 969 and <100 M^{-1} s^{-1} with dimethylferrocene. When the anion is Cl^-, the β values are 883 M^{-1} and 5.06 x 10^4 M^{-2} in 80% AN, and 3.52 x 10^5 M^{-1} and 4.35 x 10^9 M^{-2} in 95% AN, for the mono and bis complexes. Then the respective k_0, k_1 and k_2 are 4.43, 120 and 3.64 x 10^3 M^{-1} s^{-1} with ferrocene, and 29.2, 376 and 1.27 x 10^4 M^{-1} s^{-1} with dimethylferrocene, in 80% AN, and 189, 4.59 x 10^3 and 1.69 x 10^5 M^{-1} s^{-1} with ferrocene, in 95% AN. With dimethylferrocene rates are too fast. The β and k_n values suggest self-exchange rate constants on the order of 10^{-6} and 10^{-4} M^{-1} s^{-1} for Cu(II/I)(NO_3^-) and Cu(II/I)(Cl^-) couples in 95% AN.

The hitherto unexplained anomalous temperature dependence of $^{63}Cu(I)$-NMR linewidths in acetonitrile is shown to be due to some dissociation of $Cu(NCCH_3)_4^+$ to $Cu(NCCH_3)_3^+$. The linewidths also increase with increasing solution viscosity and ion-pairing (triflate salt).

Dedication

To Mercy, Kenan, Makena, Stella and Jediel

Acknowledgments

I am forever grateful to my supervisor, Professor R. B. Jordan for his unwavering support throughout this work. Encouraging and thoughtful discussions with Professor Jordan, during the write-up of this Thesis have helped to bring it to a logical completion. Professor Jordan was always available, in and out of the lab, and he never hesitated to help with almost anything. His help with the instruments or glass blowing and vacuum line as well as computer programming is gratefully appreciated.

I am indebted to my family, Mercy Nkirote, Kenan Muthuri and Karen Makena, who missed much time that they would have loved to spend with me, and gave me such great and steadfast support. I thank my parents, Stella and Jediel Irangu, and parents-in-law, Judith and Douglas Kaumbuthu for their love and support. Thanks to Rev. Gus and Doris Wentland, for their friendship and heartening encouragements to my family and me. Thanks also to Dr. M. Sisley, Dr. P. Kamau and Dr. G. Wangila, for their friendship.

Many thanks to my TA supervisor, Dr. N. Gee, for guidance and comments that helped in my teaching, and therefore led to a Teaching Excellence award.

I am very thankful to Professor D. B. Rorabacher for providing me with a pre-publication copy of his recent review (Rorabacher, D. B. *Chem. Rev.* 2004, *104*, 651) that was helpful in the preparation of this Thesis, and to my supervisory committee for many very thoughtful suggestions.

I appreciate the terrific work of the personnel at the NMR, MicroAnalytical and X-Ray Crystallography Labs in the Chemistry of Department, University of Alberta.

Finally, I acknowledge the financial assistance from the University of Alberta.

Table of Contents

Chapter 1. Introduction 1

Copper(II/I) Structures 9

Cu(II)-Ferrocenes Cross Reactions 15

Counterion Effects 17

Cu(I) NMR Linewidth 22

References 26

Chapter 2. Crystal Structures of Cu(II/I)-Acetonitrile Solvates 32

Introduction 32

Experimental 34

Results and Discussion 36

Conclusion 46

References 49

Chapter 3. Kinetic Study of the Cu(II)-Ferrocenes Reaction: Cu(II/I) Self-Exchange in Acetonitrile 51

Introduction 51

Experimental 55

Results 61

Discussion 75

Conclusion 84

References 85

Chapter 4. Nitrate and Chloride Effects on the Cu(II)-Ferrocenes Reactions **88**

Introduction 88

Experimental 93

Results 94

Discussion 125

Conclusion 136

References 137

Chapter 5. Study on the Cu(I)-63 NMR Linewidth in Acetonitrile **139**

Introduction 139

Experimental 144

Results 146

Discussion 148

Conclusion 179

References 180

Chapter 6. Conclusions **183**

References 193

Appendix. Figures and Table of Experimental Data **195**

List of Tables

Table		Page
1.1	Cross-Reaction Estimates of $Cu(II/I)_{(aq)}$ Self-Exchange Rate Constants at 25 °C	6
1.2	Some Examples of Anion Effects on Electron-Transfer Reactions	21
2.1	Comparison of the M(II)-Ligand (M = Cu, Cr) Distances from Crystal Structures of Six-Coordinate Complexes	41
2.2	Summary of Structural Parameters for $Cu(NCCH_3)_4^+$ Salts	44
2.3	A Comparison of Interatomic Distances (Å) and Interatomic Angles (deg) in $Cu(NCCH_3)_2(H_2O)_2(F_3CSO_3)_2$, **1a**, $Cu(NCCH_3)_4(F_3CSO_3)_2$, **1b**, $Cu(NCCH_3)_4(F_3CSO_3)$, **2**, and the CH_3CN solvate in $Cu(NCCH_3)_4PF_6$	48
3.1	Kinetic Results for Reactions of Cu(II) with Fc and Dmfc in 50% AN at 25 °C	68
3.2	Kinetic Results for Reactions of Cu(II) with Fc and Dmfc in 80% AN at 25 °C	69
3.3	Kinetic Results for Reactions of Cu(II) Triflate with Fc and Dmfc in 90% AN at 25 °C	71
3.4	Kinetic Results for Reactions of Cu(II) with Fc and Dmfc in 95% AN at 25 °C	72
3.5	Kinetic Results for Reactions of Cu(II) Triflate with Fc and Dmfc in 97.5% AN at 25 °C	74

3.6	Experimental and Calculated Parameters in the Marcus Cross-Relationship for the Reactions of Cu(II) with Fc and Dmfc at 25 °C	81
4.1	Absorbances of Cu(II) in the Presence of Nitrate Ion in 95% Acetonitrile	102
4.2	Summary of Results for Complexation of Cu(II) by Nitrate Ion in Acetonitrile	103
4.3	Absorbances of Cu(II) in the Presence of Nitrate Ion in 80% Acetonitrile	105
4.4	Absorbances of Cu(II) in the Presence of Chloride Ion in 95% Acetonitrile	107
4.5	Summary of the Results for Complexation of Cu(II) by Chloride Ion in Acetonitrile	108
4.6	Absorbances in the Presence of Chloride Ion in 80% Acetonitrile	110
4.7	Rate Constants (M^{-1} s^{-1}) for Reaction of Cu(II) with Fc and Dmfc in Presence of Nitrate Ion in 95% AN	114
4.8	Summary of Rate Constants (M^{-1} s^{-1}) for Reaction of Cu(II) with Fc and Dmfc in the Presence of Nitrate Ion	117
4.9	Rate Constants (M^{-1} s^{-1}) for Reaction of Cu(II) with Fc and Dmfc in the Presence of Nitrate Ion in 80% AN	118
4.10	Rate Constants (M^{-1} s^{-1}) for Reaction of Cu(II) with Fc in the Presence of Added Chloride Ion in 95% AN	120
4.11	Summary of Rate Constants for Cu(II) with Fc and Dmfc in the Presence of Chloride Ion	121
4.12	Rate Constants (M^{-1} s^{-1}) for Reaction of Cu(II) with Fc and Dmfc in the Presence of Added Chloride Ion in 80% AN	124

4.13 Summary of Extinction Coefficients (ε_i, M^{-1} cm^{-1}) for $Cu(II)X_n$ Complexes 126

4.14 Summary of Stepwise Formation Constants (M^{-1}) for Cu(II) complexes 128

4.15 Summary of Specific Rate constants (M^{-1} s^{-1}) for Electron-Transfer Involving $Cu(II)X_n$ complexes 132

4.16 Rate Constant Ratios for Reactions of Cu(II) with Fc and Dmfc in the Presence of Nitrate and Chloride Ions in 80 and 95% AN 134

5.1 $^{63}Cu(I)$ NMR Linewidths of $Cu(NCCH_3)_4X$ Salts in Acetonitrile 141

5.2 Water Dependence of $^{63}Cu(I)$ NMR Linewidths for $Cu(NCCH_3)_4X$ in Acetonitrile 160

5.3 Triflate Ion Dependence of $^{63}Cu(I)$ NMR Linewidths in Acetonitrile 167

List of Figures

Figure		Page
2.1	Three dimensional view showing the relative atom position and some bond distances and angles in **1a**.	38
2.2	Three dimensional view showing the relative atom position and some bond distances and angles in **1b**.	39
2.3	Three dimensional view showing the relative atom positions and the bond lengths and angles at the Cu(I) center in **2**. Angles of the Cu-N-C less than 175° are also shown. The CH_3 groups are not shown.	43
2.4	The unit cell structure showing anion contacts of ≤ 3.6 Å. The view is oriented to optimize the view of triflate-acetonitrile contacts.	45
2.5	Ligand coordination around the Cu(I) in copper(I) complexes of a dinuclear hexaaza macrocycle t-butylisonitrile and CO ligands from reference 21.	47
3.1	Plot of k_{obs} vs. [Cu(II)] for reactions of Cu(II) triflate in 95% AN at 25 °C: with Fc (□) no H^+ added, (■) 0.202 mM perchloric acid; with Dmfc (O) no H^+ added, (●) 0.202 mM perchloric acid.	64
3.2	Plot of k_{obs} vs. [Cu(II)] for reactions of Cu(II) triflate in 95% AN at 25 °C with Fc (O,□) no H^+ added, (●) 0.423 mM triflic acid, (■) 0.285 mM perchloric acid.	65
3.3	Plot of log k_{12} vs. ΔE^0 for the cross-reaction of Cu(II) triflate with Fc (o)	

and Dmfc (●) at 25 °C. The solid line represents a linear fit of all data and has a slope of 8.5 ± 0.3 and intercept value of -0.89 ± 0.11. 79

4.1 Extinction coefficients as a function of wavelength from the electronic spectra of: 2.05 mM $Cu(H_2O)_4(Trif)_2$ in neat AN (a); 0.404 mM $Cu(NO_3)_2.3H_2O$ in neat AN (b) and in 99% AN (c), 97% AN (d), 95% AN (e), 90% AN (f). 96

4.2 Variation of the apparent extinction coefficient (ε_{Cu}) with nitrate ion concentration for solutions of Cu(II) in 95% acetonitrile at 280 nm in 0.101 mM (○) and 0.24 mM (■) $HClO_4$. 101

4.3 Variation of the apparent extinction coefficient (ε_{Cu}) with chloride ion concentration for solutions of Cu(II) in 95% acetonitrile at 260 nm (○), 280 nm (●), and 300 nm (■). 106

4.4 Variation of k_{2obs} with $[NO_3^-]$ in 95 % AN: for Fc with 0.256 mM Cu(II) (□) and 0.252 mM Cu(II) (+); for Dmfc with 0.252 mM Cu(II) (○), 0.241 mM Cu(II) (■) and 0.256 mM Cu(II) (●). 115

4.5 Variation of k_{2obs} with $[Cl^-]$ in 80 % AN fitted to a mono/bis complex model (– – –) and a mono/bis/tris complex model (——). Insert shows an expansion of the low $[Cl^-]$ region. 123

4.6 Distribution of Cu(II) complexes with the nitrate (A) ($[Cu(II)]_t$ = 0.25 mM) and chloride (B) ($[Cu(II)]_t$ = 2.5 mM) in 95% AN as calculated on the basis of the formation constants from the present study. 130

4.7 Distribution of Cu(II) complexes with the nitrate (A) ($[Cu(II)]_t$ = 0.5 x

[NO_3^-]) and chloride (B) ([Cu(II)]$_t$ = 0.20 mM) in 80% AN as calculated on the basis of the formation constants from the present study. 131

5.1 Temperature dependence of the ^{63}Cu(I) linewidth for $Cu(AN)_4X$ salts in acetonitrile. (●) 0.00494 M $F_3CSO_3^-$; present study. (◇) 0.10 M ClO_4^-; reference 2. (○) 0.117 M $F_3CSO_3^-$; present study. (+) 0.10 M BF_4^-; reference. (■) 0.0621 M ClO_4^-; present study. 149

5.2 Concentration dependence of the ^{63}Cu(I) linewidth for $Cu(AN)_4X$ salts in acetonitrile. (●) X = $F_3CSO_3^-$; present study. (◇) X = ClO_4^-; reference 2. (□) X = ClO_4^-; present study: (◉) X = PF_6^-; reference 1. (+) X = BF_4^-; reference 1. 150

5.3 Concentration dependence of the ^{63}Cu(I) linewidth for $Cu(AN)_4X$ salts in acetonitrile. (●) X = $F_3CSO_3^-$; present study. (◇) X = ClO_4^-; reference 2. (□) X = ClO_4^-; present study. (+) X = BF_4^-; reference 1. Dashed lines are eye guides only. 156

5.4 Temperature dependence of ^{14}N linewidths after viscosity normalization: in pure CD_3CN (●) reference 20, (○) reference 21 and 0.045 M $Cu(F_3CSO_3)$ in CH_3CN (+). 157

5.5 Temperature dependence of ^{63}Cu(I) NMR linewidth for 0.0613 M Cu(I) perchlorate in 10% water, 90% AN. The solvent composition is 10% H_2O, 10% CD_3CN and 80% CH_3CN. 162

5.6 Temperature and concentration dependence of the ^{63}Cu(I) linewidth for $Cu(AN)_4(F_3CSO_3)$ in acetonitrile. (+) 0.00494 M. (□) 0.045 M. (○)

0.117 M. (—), curve calculated from the ion-pair model for 0.00494 M, K_i = 1.5 (25 °C), $\Delta H°$ = 6.0 kcal mol^{-1} and $\Delta S°$ = 20.93 cal mol K^{-1}. (– – –), curve calculated for 0.00988 M and the same $\Delta H°$ and $\Delta S°$. 170

5.7 Temperature and concentration dependence of the $^{63}Cu(I)$ linewidth divided by viscosity for the $Cu(AN)_4(ClO_4)$ in acetonitrile. (□) 0.00621 M. (+) 0.0621 M. 173

5.8 Temperature and concentration dependence of the $^{63}Cu(I)$ linewidth divided by viscosity for $Cu(AN)_4(BF_4)$ in acetonitrile. (●) 0.10 M; reference 1. (○) 0.09 M; reference 2. 175

5.9 Temperature and concentration dependence of the $^{63}Cu(I)$ linewidth divided by viscosity for $Cu(AN)_4(F_3CSO_3)$ in acetonitrile. (+) 0.00494 M; (□) 0.00988 M; (○) 0.117 M. The calculated curves for first two solutions are indistinguishable. 178

List of Terms and Symbols

ΔE^0	cross-reaction electrode potential difference
k_{obs}	observed pseudo-first-order rate constant
k_{calc}	calculated pseudo-first-order rate constant
K_{12}	cross-reaction equilibrium constant
k_{12}	cross-reaction rate constant
k_{11}, k_{22}	electron self-exchange rate constants
k_{2obs}	observed second-order rate constant
k_{2calc}	calculated second-order rate constant
ε_n	molar extinction coefficient of species
β_n	overall formation constant of species
K_{exp}	experimental equilibrium constant
K_i	ion-pair formation Constant
K_f	complex formation constant
k_n	rate constant for a given species
μ	ionic strength
$W_{1/2}$	full linewidth at half-maximum (FWHM)
I	absorbance, nuclear spin
I_0	initial absorbance
I_∞	final absorbance
l	optical pathlength
λ	wavelength

τ	correlation time for molecular tumbling
ν_0	nuclear precession frequency
η	asymmetry parameter, Viscosity
eq	electric field gradient (efg)
eQ	quadrupole moment
h	Planck's constant
ΔH^0	standard enthalpy change
ΔS^0	standard entropy change
K_c	coordination change equilibrium constant
K_{ci}	coordination change equilibrium constant for ion-pair
$[\,]_t$	total concentration for a given species
AN	acetonitrile
Fc	ferrocene
Dmfc	dimethylferrocene
efg	electric field gradient
triflate	trifluoromethanesulfonate
G^*	free energy of a species
f_{12}, f_{21}	correction for differences in G^* of cross-reactants
W_{12}, W_{21}	correction for coulombic interactions in cross-reactions

Chapter 1. Introduction

The general area of exploration of this work is the kinetics and mechanisms of reactions of copper ions in solution. Copper belongs to the group 11 (1B) elements, collectively called coinage metals, because of their use in such materials. Copper metal also is used extensively in wiring and piping, its compounds are useful in synthetic chemistry, and it is an important component in redox-active metalloproteins.[1]

The chemistry of copper in solution may occur in any of four oxidation states,[2] with the predominant states determined by the reduction potentials such as those shown in Scheme 1.1 for acidic aqueous solution.[3]

Scheme 1.1

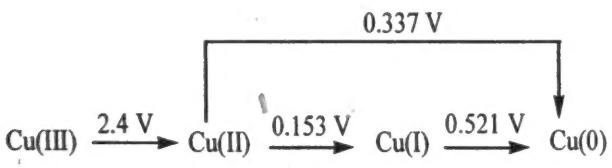

Because the reduction potential for $Cu(I/0)_{(aq)}$ is more positive than that for $Cu(II/I)_{(aq)}$, as shown in Scheme 1.1, $Cu(I)_{(aq)}$ disproportionates spontaneously to Cu(II) and Cu(0). Although metastable aqueous solutions of Cu(I) at millimolar concentrations can be prepared, this disproportionation is a major impediment to studies involving Cu(I) in water.

One of the important reactions whose study has been limited by the instability of Cu(I) with respect to disproportionation is the so-called electron self-exchange reaction. Such a reaction involves electron-transfer between two oxidation states of an element. For the two main oxidation states of copper, i.e. I and II, the electron self-exchange

reaction would involve the reversible transfer of an electron from Cu(I) to Cu(II) as shown in eq. 1.1;

$$Cu(II) + {}^{*}Cu(I) \underset{k_{11}}{\overset{k_{11}}{\rightleftharpoons}} Cu(I) + {}^{*}Cu(II) \qquad (1.1)$$

The self-exchange rate constant for this reaction will be a subject of much discussion in this work and it is designated as k_{11} throughout this thesis.

Self-exchange reactions of solvated metal ions are basic to the understanding of their electron-transfer reactions with other chemical species. As such, the rates of electron self-exchange reactions have been determined for most hydrated cations of the first-row transition metal ions[4,5] in their available oxidation states, and for many complexes of these metals. In the case of copper, there are many electron self-exchange studies, and these are thoroughly reviewed by Rorabacher.[6] These include the study of McConnell and Weaver[7] in 12 M HCl, where the self-exchange rate constant was determined to be 5 x 10^7 M^{-1} s^{-1} from ^{63}Cu NMR T_2 measurements. This value represents the rate constant for the somewhat undefined system $Cu(II)(Cl)_x/Cu(I)(Cl)_y$, and may be operating via an inner-sphere mechanism involving a chloride bridge. The studies also include recent ones on low molecular weight complexes, with many workers pointing to the relevance of such studies to biological systems.[6] Nonetheless, the self-exchange for the aqueous Cu(II/I) system remains a glaring unknown in a vast body of information.

Apart from the Cu(I) disproportionation problem, the study of the aqueous Cu(II/I) system is hindered by the limitation of suitable methods that can be used. This is more of a general problem in studies of self-exchange reactions because of the fact that

the reactants and products are identical. NMR line broadening and isotope scrambling methods can be used to resolve these values under favorable circumstances. If suitable methods for direct determination are not available, then k_{11} values are often calculated from experimental rate constants measured from reactions of M^{z+} or $M^{(z-1)+}$ species with appropriately selected reducing or oxidizing agents. Reactions of this type are termed cross-reactions. Using the Cu(II/I) couple as an example, the cross-reaction with some reagent A is

$$A_{Red} + Cu(II) \underset{k_{21}}{\overset{k_{12}}{\rightleftharpoons}} A_{Ox} + Cu(I) \qquad (1.2)$$

where A_{Red} and A_{ox} represents the reduced and oxidized states of A respectively. The cross-reaction rate constant is commonly designated k_{12} in the one direction and k_{21} in the opposite direction. This designation also will be used throughout this thesis.

The cross-reactants are carefully selected to try to insure that the electron-transfer occurs via an outer-sphere mechanism. In this mechanism, as opposed to an inner-sphere mechanism, the reaction involves no bond bridging between the reactants. Outer-sphere cross-reactions are desirable because the measured k_{12} or k_{21} values then can be used in the famous Marcus cross-relationship to calculate the self-exchange rate constant as described in several books and reviews.[5] Without going into the details here, the cross-relationship, after rearrangement, gives k_{11} by eq. 1.3,

$$k_{11} = \frac{(k_{12})^2}{k_{22}K_{12}f_{12}(W_{12})^2} \quad \text{or} \quad k_{11} = \frac{(k_{21})^2}{k_{22}K_{21}f_{21}(W_{21})^2} \qquad (1.3)$$

where k_{22} represents the rate constant for the self-exchange reaction for the selected cross reagent,

$$A_{Red} + {}^{\bullet}A_{Ox} \underset{k_{22}}{\overset{k_{22}}{\rightleftharpoons}} A_{Ox} + {}^{\bullet}A_{Red} \qquad (1.4)$$

The K_{12} or K_{21} in eq. 1.3 is the equilibrium constant for the cross-reaction and it is related to the electromotive driving force by $\Delta E^0 = RT\ln(K_{12} \text{ or } K_{21})/nF$; where R is the gas constant, T is the absolute temperature, n is the number of moles of electrons transferred and F is the Faraday constant. The nonlinear correction term f_{12} is used to try to account for the fact that the potential energy surfaces for the reactants and products are not linear in the region of their intersection. The work term correction W_{12} or W_{21} is commonly used to account for electrostatic interactions between the reactants.[5]

The f_{12} and W_{12} or W_{21} terms in the Marcus cross-relationship are dependent upon the effective contact radii of the cross-reagents as well as the distance between their centers of charge at the time of electron-transfer. These latter parameters are generally regarded as rough estimates only. Due to the uncertainty of the several parameters involved in the various terms in eq. 1.3 and the fact that k_{11} varies as the square of k_{12} or k_{21}, self-exchange rate constants obtained from the Marcus cross-relationship tend to have large errors[5] and they are generally regarded as estimates of directly measured self-exchange rate constants. For this reason, and the fact that cross-reactions may sometimes not be truly outer-sphere, direct measurement of self-exchange rates is always desirable.

A number of k_{11} estimates from eq. 1.3 for aqueous Cu(II/I) are summarized in

Table 1.1. The values of Davies[8] have been recalculated by Sisley and Jordan[9] by adjusting the E^o values to the appropriate ionic strength, and then these k_{11} values fall in the range of ~(2-9) x 10^{-7} M^{-1} s^{-1}. Overall, the k_{11} values have a wide spread but seem to fall into two categories, those in the 10^{-5} - 10^{-7} M^{-1} s^{-1} range and the others in the 10^{-2} - 10^{5} M^{-1} s^{-1} range. The latter values could be the result of inner-sphere pathways or some catalysis of the cross-reactions used to derive them. Therefore, it seems that the outer-sphere k_{11} value for aqueous Cu(II/I) is of the order of 10^{-5} - 10^{-7} M^{-1} s^{-1} and is ~10^5 times smaller than that of other aqua ions of the first-row transition metals[4,5] except for the aqueous Cr(III/II) system, which is only about 10^2 larger.

The apparently smaller self-exchange rate constant for the aqueous Cu(II/I) compared to other first-row transition metals points to a further somewhat unique aspect for this couple. As a d^9 system, the Cu(II) ion is usually in a 6-coordinate octahedral geometry with significant Jahn-Teller[10] distortion.[11] This distortion is expected to be significant for Cu(II) because it causes splitting of the occupied e_g^* orbitals which are involved in σ-bonding to the ligands. Even so, the main difference between the Cu(II/I) couple and the rest of the aqua ions of the first-row transition metals appears to be in the coordination number and geometry of the Cu(I) center. Due to its d^{10} configuration, the Cu(I) ion provides no ligand field stabilization energy in any geometry. It is most commonly found to be 4-coordinate and tetrahedral.[11] Because Jahn-Teller inversion on Cu(II) is a very rapid process ($\tau \sim 10^{-11}$ s),[12] it seems that the apparently large structural changes would come mainly from the tetragonal to tetrahedral rearrangement.

Table 1.1 Cross-Reaction Rate Constants and Estimates of $Cu(II/I)_{(aq)}$ Self-Exchange Rate Constants at 25 °C

Oxidant	Reductant	μ,M	k_{12} or k_{21}, $M^{-1} s^{-1}$	k_{11}, $M^{-1} s^{-1}$	Reference
$Cu(II)_{(aq)}$	ferrocytochrome c	-	5.7	5.2	a
$Cu(II)_{(aq)}$	V(II)	1.0	26.6	3×10^{-2}	b
$Cu(II)_{(aq)}$	Cr(II)	1.0	0.17	7×10^{-6}	b
$Cu(II)_{(aq)}$	Co(II)(sep) [c]	0.5	5	5.0×10^{-7}	d
$Cu(II)_{(aq)}$	Ascorbic acid	1.0	4.4	2.0×10^{5}	e
$Ru(III)(NH_3)_5py$ [f]	$Cu(I)_{(aq)}$	1.0	48	1.9×10^{-4}	g
$Ru(III)(NH_3)_5isn$ [i]	$Cu(I)_{(aq)}$	1.0	540	1.9×10^{-4}	g
$Ru(III)(NH_3)_4bpy$ [h]	$Cu(I)_{(aq)}$	1.0	3800	1.9×10^{-4}	g
$Ru(III)(NH_3)_4(isn)_2$ [h]	$Cu(I)_{(aq)}$	1.0	4.4×10^{4}	1.9×10^{-4}	g
$Ru(III)L_3$ [j]	$Cu(I)_{(aq)}$	0.5	2.6×10^{8}	1.0×10^{-5}	k
$Co(III)(TIM)(OH_2)_2$ [l]	$Cu(I)_{(aq)}$	1.0	4.3×10^{4}	2.0×10^{5}	m

[a] μ not specified. Yandell, J. K. *Aust. J. Chem.* **1981**, *34*, 99. [b] Parker, O. J.; Espenson, J. H. *Inorg. Chem.* **1969**, *8*, 185. Shaw, K.; Espenson, J. H. *Inorg. Chem.* **1968**, *7*, 1619. [c] sep = 1,3,6,8,10,13,16,19-octaazabicyclo[6.6.6]eicosane (sepulchrate). [d] Reference 9. [e] Xu, J. Jordan, R. B. *Inorg. Chem.* **1990**, *29*, 2933. [f] py = pyridine. [g] Reference 8. [h] isn = isonicotinamide. [i] bpy = 2,2'-bipyridine. [j] L represents bipyridine, 1,10-phenantroline, 4,4'-dimethylbipyridine or 5-chloro-1,10-phenantroline. [k] Hoselton, M. A.; Lin, C.-T.; Schwartz, H. A.; Sutin, N. *J. Am. Chem. Soc.* **1978**, *100*, 2383. [l] TIM = 2,3,9,10-tetramethyl-1,4,8,11-tetraazacyclotetradeca-1,3,8,10-tetraene. [m] Martin, M. J.; Endicott, J. F.; Ochrymowycz, L. A.; Rorabacher D. B. *Inorg. Chem.* **1987**, *26*, 3012.

The present work was designed to try to seek ways around the problems outlined above and lead to the determination of the self-exchange rate constant for the solvated Cu(II/I) couple. To overcome the problem of Cu(I) stability, acetonitrile (AN) has been chosen as the solvent. In acetonitrile, solvation effects seem to favor Cu(I) or disfavor Cu(II) but one cannot say which factor may be dominant. Because stabilities of many Cu(II) complexes increase by about 10^6 relative to their aqueous values whereas those of the corresponding Cu(I) complexes decrease by a similar magnitude,[13] Rorabacher[6] has suggested that, relative to water, solvation effects in acetonitrile both favor Cu(I) and disfavor Cu(II). In any case, the result is that Cu(II) and Cu(0) comproportionate to Cu(I) with an overall potential of 1.192 V in acetonitrile,[14] compared to –0.368 V in water. It is thus clear that Cu(I) and Cu(II) will be stable in acetonitrile so that a study of the electron exchange rate should be possible. Although there is certainly more interest in this reaction in water than in acetonitrile, such a determination would no doubt be a great step forward.

There is no clear indication as to how fast the reaction in acetonitrile might be. Manahan[15] used ^{64}Cu(I) and ^{64}Cu(II) tracers to measure the rate in acetonitrile and his value of $k_{11} \geq 0.3\ M^{-1}\ s^{-1}$ suggests that the reaction is moderately rapid. On the other hand, various estimates from the Marcus cross-relationship, such as those by Sisley and Jordan,[9] suggest that k_{11} is much smaller in water, but no cross-reactions have been studied in acetonitrile. Obviously, it would be a great advantage, in designing the self-exchange experiment, to have some idea of the time-scale of the reaction, especially if it involves expensive reagents such as isotopically-enriched copper.

Reference is made to isotopically-enriched copper because NMR line broadening

and isotope scrambling are most useful for measuring electron self-exchange rates. The proposal is that these methods can be used for the Cu(II/I) couple because of the favorable natural abundances and magnetogyric ratios of the two NMR active nuclei, that is ^{63}Cu (69.09%, 7.0974 x 10^7 rad T^{-1} s^{-1}) and ^{65}Cu (30.91%, 7.6031 x 10^7 rad T^{-1} s^{-1}).[16] If the rate is moderately fast, then the so-called slow exchange region can be exploited. Because Cu(II) is paramagnetic and Cu(I) diamagnetic, broadening of the Cu(I)-63 or 65 signal is expected to occur and increase with increasing total concentration of Cu(II). This broadening is related to the self-exchange rate constant by

$$\pi\left(W_{1/2(P,D)} - W_{1/2(D)}\right) = k_{11}[Cu(II)]_t \qquad (1.5)$$

where $W_{1/2}$ is the linewidth at half-height in Hz and the subscripts P and D refer to the paramagnetic and diamagnetic components. The self-exchange rate constant k_{11} can then be obtained as the slope in a plot of the left hand side of eq. 1.5 against the total Cu(II) concentration, $[Cu(II)]_t$. It should be noted that a reasonably measurable linewidth difference of 10 Hz and $[Cu(II)]_t \approx 0.1$ M requires $k_{11} = 3 \times 10^2$ M^{-1} s^{-1} from eq. 1.5. This estimate is much larger than current estimates for the aqueous Cu(II/I) and suggests that no line broadening might be observed in acetonitrile. One would then have to turn to what we call here the very slow exchange region, in which NMR is used as an isotope tracer monitor, exploiting the differences in the isotopic abundances of the two stable isotopes of copper. The electron exchange experiment might start by mixing isotopically enriched ^{63}Cu(I) with natural abundance Cu(II). As the electron exchange proceeds, the ^{63}Cu(I) NMR signal intensity will decrease. This method has been used for the aqueous

Ru(III/II) system, in which ^{99}Ru is NMR active.[17] Based on the current estimates for the aqueous Cu(II/I) system, this is likely to be the method required for the Cu(II/I) reaction in acetonitrile.

Because it has been shown that knowledge of structure is vital to understanding and interpreting electron-transfer reactions, studies in the present work include the synthesis and X-ray crystal structures for Cu(II,I) acetonitrile solvates. This study is presented in the next Chapter. Then the Marcus cross-relationship is used to estimate the Cu(II/I) self-exchange in acetonitrile using relevant data from the cross-reactions of Cu(II) with ferrocene or 1,1′-dimethylferrocene. This study, which appears in Chapter 3, is followed by a study to evaluate counterion effects on the Cu(II)-ferrocenes cross-reaction using nitrate and chloride ions as examples. Finally, a linewidth study of ^{63}Cu(I)-NMR in acetonitrile is presented. The latter study began as an exploration of the possibility of using this method to measure the self-exchange rate in acetonitrile. The linewidth became the subject of detailed study due to sensitivity problems associated with the broad signals, which are normally observed in ^{63}Cu(I)-NMR in acetonitrile at ambient temperatures. Some relevant chemistry and published work are reviewed briefly in the following sections.

Copper(II,I) Structures

Structures of solvated metal ions in solids have been determined using X-ray crystallography methods,[18] while the corresponding solution structures often have been studied by experimental (e.g. X-ray and neutron scattering) and computer (e.g. molecular dynamics and Monte Carlo simulation) methods, which are described in reviews by Marcus[19] and Ohtaki and Radnai.[20] Data obtained by solution structure methods are less

accurate than those from crystallographic methods. However, solutions are independent of lattice and packing forces and their study may yield information that is more relevant to solution reactivity, although sometimes different from the crystallographic results, as shown for Cu(II,I) solvates discussed below.

Copper(II). Tetragonal geometry (6-coordinate with two longer trans Cu(II)-O bonds) is predominant in crystal structures,[21] of aqua Cu(II) and this is attributable to its d^9 electronic configuration. Sometimes the Cu(II) center, as in $[Cu(OH_2)_6](BrO_3)_2$[21e] and in one of the two independent Cu(II) sites in $[Cu(OH_2)_6](SiF_6)$[21f], and those in Tutton salts of the type $M_2[Cu(OH_2)_6](SO_4)_2$ ($M = NH_4^+, Cs^+, Na^+$)[21f,22] is found to have regular octahedral geometry where the Cu(II)-O(OH_2) bonds are equivalent. Other aqua Cu(II) structures are found to have four or five H_2O ligands as in $[Cu(OH_2)_4(SO_4)].H_2O$,[23] $[Cu(OH_2)_4(SiF_6)]$,[24] and $[Cu(OH_2)_5(C_7H_2O_6)].H_2O$[25], and the octahedral geometry is completed by the anions at the more distant axial positions.

Although the majority of the crystal structures of the aqua Cu(II) ion tend to be 6-coordinate, 5-coordinate Cu(II) structures are not uncommon and examples are given by Wells[22] and Hathaway.[26] Recently, a 5-coordinate square-pyramidal aqua Cu(II) moiety was found by Bramsen, Bond and McKenzie[27] in the crystal structure of hydronium pentaaquacopper(II) triperchlorate, $(H_3O)[Cu(OH_2)_5](ClO_4)_3$. Because this structure contains two Cu-O(ClO_4) bonds of 3.305 Å, the geometry has been described by the authors as "5+2", which is extremely rare in Cu(II) salts.

Crystal structures of Cu(II) nitrile solvates are not common. The crystal structure of the benzonitrile solvate, $[Cu(NCC_6H_5)_6](SbF_6)_2$,[28] has the usual tetragonal distortion, but there are no crystal structures of Cu(II)-acetonitrile solvates.

In solution, there are several EXAFS (extended X-ray absorption fine structure) and LAXS (large angle X-ray scattering) studies of Cu(II) in acetonitrile,[29,30] and in water.[31,32,33] With the exception of the neutron diffraction and molecular dynamics study of Pasquarello et al.,[32] where aqueous $Cu(ClO_4)_2$ was claimed to contain 5-coordinate aqua Cu(II), the "4+2" tetragonal geometry found in crystal structures also is found in solution structures of the aqua ion.[30b,31,33] Interestingly, the most recent work by Persson et al.,[33] using EXAFS and LAXS found that solutions of $[Cu(OH_2)_6](BrO_3)_2$ and $[Cu(OH_2)_6](SiF_6)$ show the usual Jahn–Teller induced tetragonal distortion, with mean equatorial and axial Cu–O bond distances of 1.96(1) and 2.32(2) Å, and 1.95(1) and 2.27(3) Å, respectively, although the crystal structures of these salts show regular octahedral geometry.[21e,f] Furthermore, Persson et al.,[33] through a study of aqueous $Cu(ClO_4)_2$ solutions, found that a six-coordinate model, rather than a five coordinate model, gave better fits of their EXAFS and LAXS data, in contradiction of the earlier conclusions by Pasquarello et al.[32] Funahashi and coworkers[30b] also found tetragonal $Cu(II)(OH_2)_n(NCCH_3)_{6-n}$ (n = 0-3) structures using EXAFS, where the O atoms fill equatorial positions at the normal distance of 1.96 Å and Cu-N_{eq} and Cu-N_{ax} distances are ~2.00 and 2.46 Å, respectively. Tetragonally distorted Cu(II) structures in solution are consistent with the fast[34] water and acetonitrile exchange ($k_{ex} \approx 10^7 - 10^9$ M^{-1} s^{-1} at 25 °C) on Cu(II) compared to exchange of the same solvents on other divalent first-row transition metal ions.[35]

Tetragonal elongation also was detected by Funahashi and coworkers[30] in acetonitrile solutions of Cu(II) triflate using EXAFS. They reported Cu(II)-N_{eq} bond lengths of ~1.99 Å in two independent studies but their earlier Cu(II)-N_{ax} bond length of

2.18 Å[30a] is much shorter than the 2.49 Å[30b] they report later, and no explanation is offered for the apparent discrepancy. One possible cause is the difference in the references for the fitting parameters. In the earlier work, an EXAFS spectrum of an aqueous solution of Cu(II) ion was used as a standard sample on the basis of the structure parameters determined by the X-ray diffraction method[19,20] whereas the crystal structure of $[Cu(NCCH_3)_4(pz)](BF_4)_2$ (pz = pyrazine)[36] was used in the more recent work. The latter contains a one-dimensional linear cationic chain based on 6-coordinate Cu(II), the tetragonally distorted geometry of which comprises two bridging pz ligands (equatorial) and four terminal $NCCH_3$ ligands (two equatorial, two axial). Because crystal structures are more reliable than EXAFS structures, the more recent Cu-N_{ax} bond length by Funahashi and coworkers[30b] is probably the more accurate value, and it is interesting to note that the earlier Cu-N_{ax} value[30a] is more consistent with the Cu-$O_{ax}(H_2O)$ values of 2.29 Å.[30b,37]

Accuracy problems are not uncommon in the determination of axial bond lengths of Jahn-Teller distorted ions using solution structure methods.[19,20,38] In fact, the EXAFS and LAXS study on 1.0 M solutions of Cu(II) triflate by Persson et al.[29] reported bond distances of 1.99 Å for Cu(II)-N_{eq}, in agreement with Funahashi and coworkers,[30] but the authors[29] could not observe the axial acetonitrile ligands. Appropriate Cu(II)-acetonitrile crystal structures, that we are interested in here, can be more helpful in the analysis of data from solution structure measurements on Cu(II) acetonitrile systems.

It is to be noted that there are several crystal structures for the Cu(I)–acetonitrile system (see below) so that the lack of equivalent Cu(II) structures is somewhat surprising. There is no indication of whether the Cu(II)-acetonitrile crystals are unstable,

but the availability of solution structures is a clear indication that there is interest in this system. From the wide variation in the structures of the aqua Cu(II) salts, one cannot easily anticipate the structure for Cu(II) with acetonitrile ligands. Since solvated Cr(II), like Cu(II), is a well known Jahn-Teller distorted ion, the Cu(II) structure might be expected to be comparable to that for $Cr(NCCH_3)_4(BF_4)_2$ determined recently by Henriques et al.[39]. As in similar aqua Cu(II) and Cr(II) crystal structures,[23,24] the acetonitrile ligands occupy equatorial positions at shorter distances than the axial BF_4^- anions.

Copper(I). As noted previously, there is no crystal field stabilization for Cu(I) in any geometry because of its d^{10} electronic configuration, and ligand-dependent structures may be expected but it is most commonly found to be 4-coordinate and tetrahedral.[2,11]

Because of the disproportionation problem, the structures are unknown for the aqueous ion but acetonitrile structures have been widely studied. Many complexes, $Cu(NCCH_3)_4X$ ($X = NO_3^-$,[40] ClO_4^-,[41] PF_6^-,[42] BF_4^-,[41b,43,44] $B(C_6F_5)_4^-$,[45] or $CF_3SO_3^-$[43]), have been synthesized using the reaction of cuprous oxide with the appropriate acid,[42,41c] the comproportionation reaction,[41a,b,43,44] or by metathesis[45] of a $Cu(NCCH_3)_4Y$ salt with an LiX salt. Crystal structures of the ClO_4^-,[46] PF_6^-,[47] and BF_4^- [48] salts show disorder with three independent, tetrahedrally coordinated copper units. Each unit also shows a significant variation in chemically equivalent bond lengths and angles. This contrasts with the situation in the crystal structures of $Cu(NCC_6H_5)_4^+$ [28] and $Cu(NC_5H_5)_4^+$ [49] where the copper sites are equivalent and bond lengths and angles are very similar. Packing forces and donor abilities of the ligands may be responsible for these differences, but the structures do not seem to depend on the nature of the anion.

Solution structures for Cu(I) acetonitrile solvates have been determined using EXAFS by Persson et al.,[29] Kuchiyama, Kobayashi and Takagi,[50] and Funahashi and coworkers.[51] These studies found that the Cu(I)-N bond lengths determined for Cu(I) perchlorate solutions are very similar to the Cu(II)-N_{eq} distances (1.99 Å) in the Cu(II) structures.[29,30] Persson et al.[29] also found a correlation between the difference in Cu(II)-$solv_{eq}$ and Cu(I)-solv bond lengths and the Cu(I) disproportionation constants in water, dimethylsulfoxide, pyridine and acetonitrile. By extrapolation to water, Persson et al.[29] estimated a Cu(I)-OH_2 bond length of ~2.13 Å from their EXAFS study. On the basis of similar ionic radii of 4-coordinate Cu(II,I) ions,[2] this estimate appears large, and it will be interesting to see how Cu(II,I)-N(acetonitrile) bond lengths compare.

Bonding. As already implied in the previous sections, acetonitrile is σ-bonded to Cu(II) or Cu(I) via the lone electron pair on the nitrogen; i.e. Cu-N-C1-C2 where C1 and C2 are the *sp* and sp^3 carbons respectively. In the EXAFS studies, Persson et al.[29] further found that the Cu(II)…C1 distance was equal to the sum of Cu(II)-N plus N-C1 distance so that the acetonitrile ligands are predicted to be linearly bonded to Cu(II). On the other hand, they found a shorter Cu(I)…C1 distance compared to the Cu(I)-N plus N-C1 distance. From their distances for Cu(I)…C1, Cu-N and N-C1, they calculated a Cu(I)-N-C1 angle of ~152° ± 10°. This angle is smaller than that in the crystal structures (average ~174°), which in turn is smaller than the linear angle of 180°. However the acetonitrile ligands are found to be linear. A similar bending of the Cu(I)-solvent also has been seen in a Cu(I) dimer with *t*-butylisonitrile ligands,[52] which are isoelectronic with nitriles. It appears that significant bonding differences exist between Cu(II) and Cu(I) with acetonitrile perhaps due to substantial back-bonding from the $3d^{10}$ orbitals of the Cu(I)

ion to the π^* orbital of the nitrile group.

The back-bonding aspect is somewhat controversial because the single C≡N stretch in $Cu(NCCH_3)_4^+$, which is independent of the nature of the counterion,[42,41b,43,45] shifts to higher frequency relative to the free nitrile. The N-C distances in the crystal and solution are in the range 1.10 - 1.15 Å[29,46-48,50,51], and do not show significant lengthening relative to the free CH_3CN solvate (N-C 1.125 Å).[47] Recent studies[52,53] have shown non-classical trends in the bonding in Cu(I) carbonyl complexes where the ν(C≡O) value increases instead of decreasing with respect to ν(C≡O) of free CO. Some of the C-O bond lengths also were non-classical in that the distance decreased instead of increasing on coordination. Since CO is a better π-acceptor than CH_3CN, one might expect less back bonding in $Cu(NCCH_3)_4^+$ but CH_3CN is a stronger σ-donor and this could increase the tendency for back-bonding.

Cu(II)-Ferrocenes Cross-Reactions

Determination of the Cu(II/I) self-exchange rate constant in acetonitrile using the Marcus cross-relationship requires a judicious choice of the reaction partners that are to be used. They should provide a reasonable assurance that the reaction will be outer-sphere and have known self-exchange rate constants and reduction potentials in acetonitrile (so that the net equilibrium constant can be calculated). In addition, they must have suitable physical and chemical properties, such as solubility and stability in acetonitrile, and moderately intense absorbances in the uv-visible spectrum for convenient monitoring of the kinetics of the net reaction.

Ferrocene and its methylsubstituted derivatives are quite soluble in acetonitrile[54] and they are substitution inert[55]. Ferrocene (designated as Fc) and its dimethyl derivative

1,1′-dimethylferrocene (designated as Dmfc) are popular outer-sphere cross-reductants in acetonitrile also because there are several published studies of the electron self-exchange rate constants in this solvent. The self-exchange rate constants (25 °C) reported from several NMR studies are 5-9 x 10^6 M^{-1} s^{-1} for Fc/Fc^+ [56,57,58] and 8.3 x 10^6 M^{-1} s^{-1} for $Dmfc/Dmfc^+$.[56] These are in excellent agreement with values of 6.5 x 10^6 and 8.9 x 10^6 M^{-1} s^{-1} for Fc/Fc^+ and $Dmfc/Dmfc^+$ couples, respectively, estimated using the Marcus cross-relationship for a large number of organic oxidants.[59]

The reduction potentials for Cu(II/I) and $Dmfc^+/Dmfc$ are 0.646[14] and -0.11[60] V vs. Fc^+/Fc in acetonitrile. Thus, the reaction of Cu(II) with Fc or Dmfc should be thermodynamically spontaneous, as shown in eq. 1.6.

$$\begin{aligned} Fc + Cu(II) &\rightarrow Fc^+ + Cu(I) \qquad \Delta E^0 = 0.646\ V \\ Dmfc + Cu(II) &\rightarrow Dmfc^+ + Cu(I) \qquad \Delta E^0 = 0.756\ V \end{aligned} \tag{1.6}$$

These large and positive ΔE^0 values are the result of the solvation preferences for Cu(II) and Cu(I) that were noted previously, and this is in contrast to the situation in water where the ΔE^0 value for reaction of Fc with Cu(II) is predicted to be -0.247 V.[3] The values of ΔE^0 can also be calculated for the reaction of Fc with Cu(II) in AN/water mixtures using redox potentials of Cox and coworkers[14] in these solvents. The values are 0.006 - 0.348 V for 4 - 95% AN, and if one assumes that the reduction potential for $Dmfc/Dmfc^+$ versus Fc/Fc^+ does not deviate much from that in acetonitrile, the corresponding ΔE^0 values for the reaction of Dmfc with Cu(II) would be ~0.12 – 0.46 V. Therefore, one can introduce an additional dimension for the cross-reaction, namely, that

of changing the overall driving force by adding water to the acetonitrile. In so doing, the cross-reaction takes the form:

$$Fc \text{ (or Dmfc)} + Cu(II)(AN)_{6-n}(H_2O)_n \rightarrow Fc^+ \text{ (or Dmfc}^+) + Cu(I)(AN)_{4-m}(H_2O)_m \quad (1.7)$$

where m and n are 0, 1, 2, ... and the coordination numbers are 6 for Cu(II) and 4 for Cu(I) and different solvation patterns have been assumed.[29,61] Such a study then provides an opportunity to test how the self-exchange in the Cu(II/I)-aqueous system may be obtained by extrapolation from values in the acetonitrile systems.

The self-exchange rate constants for the ferrocenes in acetonitrile/water mixtures that would be required in the application of the Marcus cross-relationship for eq. 1.7 are not available in the literature. However, the values in various pure solvents are in the narrow range of (5 - 30) x 10^6 M^{-1} s^{-1},[56,58] and a recent study by Swaddle and coworkers[62] indicates that effects of solvent dynamics on the self-exchange rate constant for the ferrocenes are not huge. Therefore, it seems possible to at least determine the magnitudes for the Cu(II/I) self-exchange rate constants in the mixed solvents using the acetonitrile self-exchange rate constants of the ferrocenes.

Counterion Effects

During the course of the study on the Cu(II)-ferrocenes cross-reactions, it was noted that the rates were slower when the Cu(II) source was the nitrate salt, compared to the perchlorate or the triflate. This observation led to a study of some anion effects on the reaction kinetics and the Cu(II) species formed as anions are added.

Counterion effects on electron-transfer rates are not uncommon. They usually are

attributed to various degrees of ion-association, also referred to as ion-paring, or to inner-sphere complexation of the metal cation by the anion. The terminology and nature of the species that may form is shown in Scheme 1.2,

Scheme 1.2

$\{M(L)_n^{Z+}(S)_n(X^-)\}$	$\{M(L)_n^{Z+}(X^-)\}$	$\{M(L)_{n-1}(X)^{(Z-1)+}\}$
Solvent-separated ion-pair	Contact or tight ion-pair	Inner-sphere complex

where M^{Z+} is the metal ion, L are the ligands in the first coordination sphere of the metal, S is the solvent and X^- is the anion. In cases such as that studied here, L and S are the same species.

The formation of the species in Scheme 1.2 is considered a rapidly maintained equilibrium[5] that can be represented generally by eq. 1.8.

$$M^{z+} + X^{z-} \underset{\longleftarrow}{\xrightarrow{K_i}} \left\{M^{z+} \bullet X^{z-}\right\} \qquad (1.8)$$

Values of the equilibrium constant K_i can be determined by various methods including conductivity, kinetics, spectrophotometry and NMR. The assignment of the particular nature of the species formed in a given system is often difficult and somewhat subjective. The Eigen-Fuoss electrostatic model[5] often is used to estimate K_i for the contact ion-pair. If the measured K_i is much smaller than this estimate, then a solvent-separated species might be assumed. Inner-sphere complex formation is expected to produce significant changes in spectral properties, but contact ion-pairs are known to affect electronic and

NMR spectra. If the metal-ion complex, $M(L)_n^{z+}$, is kinetically inert to substitution of the L ligands, then only solvent-separated or contact ion-pairs can form. But many complexes, such as those for Cu(II), are substitution labile so that rapid complex formation must be considered.

For all these types of association, the magnitude of K_i changes as expected for a largely electrostatic interaction. Thus K_i increases with the charge on the ions and decreases as their size increases, or as the dielectric constant of the solvent increases. Thus, effects of ion association can be minimized by using a large anion, such as $B(Ph)_4^-$ and/or using a solvent with a high dielectric constant, such as water. However, these options are not always available due to solubility or solvent restrictions, as in the case of this study. Fortunately, the EXAFS studies of Funahashi et al.[29] indicate, for the triflate salt used in Chapter 3, that the solvation structure around the Cu(II) ion is maintained over a wide range of Cu(II) concentrations and that contact ion-pairing between the Cu(II) and $F_3CSO_3^-$ ions in acetonitrile is negligible up to at least 0.5 M Cu(II).

The kinetic effect of ion association or complexation depends on the relative reactivities of the free and associated species and the magnitude of K_i. If the associated species is less reactive, then the observed rate of the reaction will decrease with increasing anion concentration as X^- is added to the system. If the ion-associated species is more reactive, then as long as $K_i[X^-] \geq 1$, the rate will increase as X^- is added. If ion-pairing is not significant, anion effects may be analyzed within the Debye-Hückel theory, as a classical ionic strength effect.[5]

Effects of anions such as BF_4^-, PF_6^-, ClO_4^-, NO_3^-, Cl^- and Br^- are observed for cross-reaction electron-transfer as well as electron self-exchange reactions in acetonitrile

and solvents with lower dielectric constants.[63] The rate constant for the free-ion path and that for the ion-paired path are related to the overall observed rate constant by,

$$k_{obs} = \frac{k_0 + k_1 K_i [X]}{1 + K_i [X]} \tag{1.9}$$

where k_0 is the specific rate constant for the reaction of the solvated ion and k_1 is the equivalent for the ion-pair. The ratio of k_1 to k_0 is a measure of the magnitude of the anion effect on the reaction rate.

To see how this ratio changes from reaction to reaction, a review of some studies on counterion effects is presented in Table 1.2. The first entry in Table 1.2 involves inner-sphere complexation because of the substitution lability of Cu(II). For Cu(II)(pdto), the tetrafluoroborate ion also might coordinate to the Cu center at the vacant axial site. Except for the entries with the Cu(II)(pdto) oxidant, ion-pair association seems to give $k_1/k_0 < 1$ in the nonaqueous systems and $k_1/k_0 > 1$ in water. For five of the seven systems in acetonitrile, the k_1/k_0 are remarkably similar. In CH_2Cl_2, which has a much lower dielectric constant than acetonitrile, the ratio is about 30 or more times smaller.

For the reactions of Cu(II) with ferrocene and dimethylferrocene, it is interesting to determine the nature of the observed nitrate effect. This study is discussed in Chapter 4. The chloride ion also was studied because it is known to complex Cu(II) and it has been observed to be both a catalyst and an inhibitor (first and last entries in Table 1.2).

Table 1.2. Some Examples of Anion Effects on Electron-Transfer Reactions[a]

Reaction Couple [b]	Anion	Solvent	K_i	k_1/k_0
$Cu(II)/Co(sep)^{2+}$ [c]	Cl^-	Water	(2.3) [d]	320
$Cu(pdto)^{2+}/Fc$ [e]	BF_4^-	Acetonitrile	5	24
$Cu(pdto)^{2+}/Fc$ [e]	PF_6^-	Acetonitrile	-	No effect
Fc/Fc^+ [f]	PF_6^-	Acetonitrile	7	0.46
Fc/Fc^+ [f]	ClO_4^-	Acetonitrile	18	0.58
$Co(dmg)_3(BF)_2^+/Fc$ [g]	BF_4^-	Acetonitrile	9	0.48
$Co(dmg)_3(BF)_2^+/Fc$ [h]	PF_6^-	Acetonitrile	270	0.61
$Co(dmg)_3(BF)_2^+/Fc$ [h]	Br^-	Acetonitrile	65	0.45
$Co(dmg)_3(BF)_2^+/Fc$ [h]	BF_4^-	CH_2Cl_2	2.3×10^8	0.0022
$Co(dmg)_3(BF)_2^+/Fc$ [h, i]	Cl^-	CH_2Cl_2	6.9×10^6	0.015
$Co(dmg)_3(BF)_2^+/Fc$ [h, i]	NO_3^-	CH_2Cl_2	4.6×10^7	0.0061

[a] At 25 °C unless specified otherwise. [b] Abbreviations are as in the original literature [c] Reference 9. [d] Formation constant for $CuCl^+$ as reported by Ramette, R. W. *Inorg. Chem.* **1986**, *25*, 2481. [e] Davies, K. M.; Whyte, K. D.; Gilbert, A. H. *Inorg. Chim. Acta* **1990**, *177*, 121. [f] Reference 56. [g] Reference 55. [h] Reference 63. [i] At -20 °C.

Cu(I) NMR Linewidth

It was noted earlier that Manahan[15] reported a study on Cu(II/I) electron self-exchange in acetonitrile in 1967. No subsequent work on the system has been published and Manahan's study has been largely ignored. As stated previously, Manahan used the radioactive ^{64}Cu isotope to monitor the changes in the amounts of Cu(II) and Cu(I) upon mixing either $^{64}Cu(II)$ with normal Cu(I) or $^{64}Cu(I)$ with normal Cu(II). The problem with this method is that the reaction must be quenched and the Cu(I) and Cu(II) species have to be separated in order to measure the radioactivity in each oxidation state. In the experiment, Manahan cooled the system to -40 °C in order to precipitate $Cu(I)ClO_4$ and leave $Cu(II)ClO_4$ in the filtrate. He then measured the radioactivity in the separated Cu(I) and Cu(II) material by a scintillation counter. The problem is that one cannot tell how much of the exchange is induced by the separation process.

NMR is the better method to measure the self-exchange rate constant for the Cu(II/I) couple in acetonitrile because the need for quenching and separation is avoided. It was described in a previous section how this can be done. In the present section, a review of Cu(I) NMR linewidths is presented with the aim of determining conditions that will be most helpful to such a study. As alluded to earlier, the paramagnetic Cu(II) ion is not expected to be observed in Cu-NMR.

The abundances and magnetogyric ratios for the two stable and NMR active Cu isotopes, i.e. ^{63}Cu and ^{65}Cu were given earlier. Both have nuclear spin I = 3/2 so that the quadrupolar mechanism is expected to dominate the spin-lattice or longitudinal (T_1) and spin-spin or transverse (T_2) nuclear relaxation times. The magnitude of the nuclear quadrupolar relaxation constant depends on the value of quadrupole moments (-0.211 and

-0.195 barns for ^{63}Cu and ^{65}Cu respectively[16]) and the electric field gradient (efg) at the nucleus. The efg is expected to be near zero if the copper nucleus is in a cubic symmetry. The quadrupolar relaxation rate also depends directly on the molecular tumbling correlation time which in turn varies as solvent viscosity and inversely as temperature.

The linewidth of the NMR signal for a given nucleus is inversely proportional to T_2 so that the smaller the T_2 value, the broader the signal and, of course, the poorer the intensity. Because of its greater natural abundance, $^{63}Cu(I)$ NMR is the most commonly studied and reports on $^{65}Cu(I)$ NMR linewidths are few. Most of the reported values for $^{63}Cu(I)$ NMR linewidths in acetonitrile at ambient temperatures are in the range 500 to 600 Hz, although there are a few in the 400 to 450 Hz range and very few greater than 600 Hz.[64] The range of these values is surprising because the structural measurements suggest that the Cu nucleus in the Cu(I)-acetonitrile system is in a tetrahedral symmetry and the $^{63}Cu(I)$-NMR linewidth in aqueous tetracyanocopper(I), $Cu(CN)_4^{3-}$, at ambient temperature is 70 Hz[65] even though water is a more viscous solvent than acetonitrile. A series of $L^{R1,R2}Cu(I)CO$ complexes, where $L^{R1,R2}$ are hydrotris(pyrazolyl)borate ligands with R1 and R2 as methyl, *iso*-propyl or *tert*-butyl groups, also were found by Moro-oka and coworkers[66], to have sharp ^{63}Cu NMR signals with linewidths of about 70 Hz even though the Cu(I) is in a much lower than cubic symmetry. The issue of apparently broader than expected linewidths for the Cu(I)-acetonitrile system has been noted but never addressed adequately in the literature.

Two temperature-dependence studies by Ochsenbein and Schläpfer[67] and Kroneck et al.[68] of the $^{63}Cu(I)$ NMR linewidth for ClO_4^-, BF_4^- and PF_6^- salts in acetonitrile show a minimum linewidth at about -5 °C and then the linewidth increases as the temperature is

increased through the ambient region. If a single Cu(I) species is in these solutions, with dominant quadrupolar relaxation, then the ^{63}Cu(I) NMR linewidth should simply decrease with increasing temperature due to the increased molecular tumbling rate (i.e. shortened reorientational correlation time). Therefore, the increase in linewidth above -5 °C is anomalous. The linewidth at ~25 °C (≈ 500 Hz) is consequently much greater than would be predicted from the extrapolation of the low temperature linewidths.

The cause for the anomaly in the temperature dependence for the ^{63}Cu(I)-NMR linewidth is to be investigated in this work. Before this study, the cause of this anomaly was unknown. The only attempted rationalizations were by Ochsenbein and Schläpfer[67] and Kroneck et al.[68] These authors suggested that the effect might be due to a coordination change[67] or due to ion-pairing.[68] However, the explanations by these authors are inadequate because no effort was made to quantify contributions from the proposed species and viscosity changes with temperature were not considered.

Ochsenbein and Schläpfer[67] and Kroneck et al.[68] also studied the Cu(I) concentration dependence of the ^{63}Cu(I) NMR linewidth for the ClO_4^-, BF_4^- and PF_6^- salts. The linewidths increased with concentrations as expected from viscosity changes, but the authors did not seek to correct for these changes to determine if other factors, such as ion-pairing were contributing. In 1995, Gill et al.[69] reported the dependence of the linewidth on the concentration of $CuClO_4$ (0.008 to 0.45 M) in benzonitrile, and the behavior is similar to that in AN, even after correction for viscosity changes. Somehow, the authors concluded that "linewidths, after correction for viscosity, are also independent of concentration", even though Figure 4 in the paper shows a change in linewidth from ~4 x 10^3 to ~7 x 10^3 Hz after viscosity correction. The authors used this "evidence" and

earlier conductivity studies by Gill et al.[70] to argue against ion-pairing, but later in the paper they acknowledge the concentration dependence in benzonitrile and suggest ion-pairing as the cause. In the same paper,[69] it is suggested that the ^{63}Cu(I) linewidths are so large because of the Sternheimer antishielding factor (γ_∞), which has a value of -17 and contributes a factor of $(1-\gamma_\infty)$ to the electric field gradient. Clearly, this ignores the fact that the temperature dependence is not that expected for simple quadrupolar relaxation in one species.

In Chapter 5, the study of the ^{63}Cu(I) NMR linewidth for the Cu(I)-acetonitrile system employing solutions of Cu(I) triflate and perchlorate is presented and the issue of the anomalous temperature dependence as well as concentration dependencies of the linewidths has been addressed. As part of the same study, experiments to try to seek reasons for the wide variation in the reported linewidths at ambient conditions were designed and performed.

The conclusions from the present studies and some of the experimental data are summarized in Chapter 6, and details of results are given in the Appendix section.

References

(1) Nriagu, J. O. *Copper in the Environment*, Wiley, New York, **1990**. Howell, J. M.; Gawthorne, J. M. eds., *Copper in Animals and Man*, CRC: Boca Raton, Florida, **1987**. Linder, M. C. *Biochemistry of Copper*, Plenum, New York, **1991**.

(2) Huheey, J. E.; Keiter, E. A.; Keiter, R. L. *Inorganic Chemistry: Principles of Structure and Reactivity*, HarperCollins, New York, **1994**.

(3) *Handbook of Chemistry and Physics*, 79th edition, CRC Press, **1998–9**, p. 12-26-9.

(4) Creutz, C.; Sutin, N.; in *Inorganic Reactions and Methods*, Zuckerman, J. J. Ed. **1986**, Vol. 15, and references therein.

(5) Jordan, R. B. *Reaction Mechanisms of Inorganic and Organometallic Systems*, Oxford University Press, New York, **1998**. Cannon, R. D. *Electron Transfer Reactions*, Butterworths London, **1980**. Sutin, N. *Prog. Inorg. Chem.* **1983**, 30, 441. Wherland, S. *Coord. Chem. Rev.* **1993**, *123*, 169.

(6) Rorabacher, D. B. *Chem. Rev.* **2004**, *104*, 651.

(7) McConnell, H. M.; Weaver, H. E., Jr. *J. Chem. Phys.* **1956**, *25*, 307.

(8) Davies, K. M. *Inorg. Chem.* **1983**, *22*, 615.

(9) Sisley, M. J.; Jordan, R. B. *Inorg. Chem.* **1992**, *31*, 2880.

(10) Jahn-Teller distortion lowers the symmetry of a nonlinear molecule in an electronically degenerate state, and removes the degeneracy to lower the energy. Distortions also are common in d^1, d^2, d^4, low spin d^5, high spin d^6, and d^7 ions.

(11) Hathaway B. J.; Billing, D. E. *Coord. Chem. Rev.* **1970**, *5*, 143. Hathaway, B. J. *Coord. Chem. Rev.* **1981**, *35*, 211.

(12) Lewis, W. B.; Alei, M., Jr.; Morgan, L. O. *J. Chem. Phys.* **1966**, *44*, 2409; **1966**, 45, 4003. Noack, M.; Kokoszka, G. F.; Gordon, G. *J. Chem. Phys.* **1971**, *54*, 1342.

(13) Aronne, 1.; Dunn, B.C.; Vyvyan, J. R.; Souvignier, C. W.; Mayer, M. J.; Howard, T. A.; Salhi, C. A.; Goidie, S. N.; Ochrymowycz, L. A.; Rorabacher, D. B. *Inorg. Chem.* **1995**, *34*, 357.

(14) Cox, B. G.; Jedral, W.; Palou, J. *J. Chem. Soc., Dalton Trans.* **1988**, 733. Johnsson, M.; Persson, I. *Inorg. Chim. Acta* **1987**, *127*, 15.

(15) Manahan, S. E. *Can. J. Chem.* **1967**, *45*, 2451.

(16) *Handbook of Chemistry and Physics*, 79th edition, CRC Press, **1998–9**, p. 11-53.

(17) Bernhard, P.; Helm, L.; Ludi, A.; Merbach, A. E. *J. Am. Chem. Soc.* **1985**, *107*, 312.

(18) Ladd, M. F. C.; Palmer, R. A. *Structure Determination by X-Ray Crystallography*, Plenum Press, New York, **2003**.

(19) Marcus, Y. *Chem. Rev.* **1988**, *88*, 1475.

(20) Ohtaki, H.; Radnai, T. *Chem. Rev.* **1993**, *93*, 1157.

(21) (a) Mani, N. V.; Ramaseshan, S. *Z. Kristallogr.* **1961**, *115*, 97. (b) Ray, S.; Zalkin, A.; Templeton, D. H. *Acta Cryst.* **1973**, *B29*, 2748. (c) Silver, B. L.; Getz, D. *J. Chem. Phys.* **1974**, *61*, 638. (d) Couldwell, C.; Prout, K.; Robey, D.; Taylor, R.; Rossotti, F. J. C. *Acta Cryst.* **1978**, *B34*, 1491. (e) Blackburn, A. C.; Gallucci, J.

C.; Gerkin, R. E. *Acta Cryst.* **1991**, *C47*, 2019. (f) Cotton, F. A.; Daniels, L. M.; Murillo, C. A.; Quesada, J. F. *Inorg. Chem.* **1993**, *32*, 4861.

(22) Wells, A. F. *Structural Inorganic Chemistry*, 5th Ed.; Oxford University Press, London, **1986**.

(23) Beevers, C. H.; Lipson, H. *Proc. R. Soc. London Ser. A* **1934**, *146*, 570. Bacon, G. E.; Curry, N. A. *Proc. R. Soc. London Ser. A* **1962**, *266*, 95. Baur, W. H.; Rolin, J. L. *Acta Cryst.* **1972**, *B28*, 1448. Varghese, J. N.; Maslen, E. N. *Acta Cryst.* **1985**, *B41*, 184.

(24) Cotton, F. A.; Daniels, L. M.; Murillo, C. A. *Inorg. Chem.* **1993**, *32*, 4868.

(25) Manojlovic-Muir, L.; Muir, K. W.; Campbell, R. A.; McKendrick, J. E.; Robins, D. J. *Acta Cryst.* **1999**, *C55*, 178.

(26) Hathaway B. J. in *Comprehensive Coordination Chemistry*, Wilkinson, G. Ed. Pergamon, Oxford, **1987**, Vol. 5.

(27) Bramsen, F.; Bond A. D.; McKenzie, C. J. *Acta Cryst.* **2003**. *E59*, i105.

(28) Brownstein, S.; Han, N. F.; Gabe, E.; Le Page, Y. *Can. J. Chem.* **1989**, *67*, 2222.

(29) Persson, I.; Penner-Hahn, J. E.; Hodgson, K. O. *Inorg. Chem.* **1993**, *32*, 2497.

(30) (a) Inada, Y.; Sugimoto, Y.; Nakamo, Y.; Itoh, Y.; Funahashi, S. *Inorg. Chem.* **1998**, *37*, 5519. (b) Inamo, M.; Kamiya, N.; Inada, Y.; Nomura, M.; Funahashi, S. *Inorg. Chem.* **2001**, *40*, 5636.

(31) (a) Sham, T. K.; Hastings, J. B.; Perlman, M. L. *Chem. Phys. Lett.* **1981**, *83*, 391. (b) Magini, M. *Inorg. Chem.* **1982**, *21*, 1535.

(32) Pasquarello, A.; Petri, I.; Salmon, P. S.; Parisel, O.; Car, R.; Töth, E.; Powell, D. H.; Fischer, H. E.; Helm, L.; Merbach, A. E. *Science* **2001**, *291*, 856.

(33) Persson, I.; Persson, P.; Sandström, M.; Ullström, A.-S. *J. Chem. Soc., Dalton Trans.* **2002**, 1256, and references therein.

(34) Powell, D. H.; Fuller, P.; Pittet, P.-A. Merbach, A. E. *J. Phys. Chem.* **1995**, *99*, 16622. West, R. J.; Lincoln, S. F. *J. Chem. Soc., Dalton Trans.* **1974**, 281.

(35) Frey, U.; Merbach, A. E.; Powell, D. H. In *Dynamics* of *Solutions and Fluid Mixtures by NMR*; Delpuech, J.-J., Ed.; Wiley: Chichester, **1995**.

(36) Begley, M. J.; Hubberstey, P.; Stroud, J. *J. Chem. Soc., Dalton Trans.* **1996**, 2323.

(37) D'Angelo, P.; Bottari, E.; Festa, M. R.; Notting, H.-F.; Pavel, N. V. *J. Chem. Phys.* **1997**, *107*, 2807.

(38) Okan, S. E.; Salmon, P. S. *Mol. Phys.* **1995**, *85*, 981, and references therein.

(39) Henriques, R. T.; Herdtweck, E.; Kühn, F. E; Lopes, A. D.; Mink, J.; Romão, C. C. *J. Chem. Soc., Dalton Trans.* **1998**, 1293.

(40) Morgan, H. H. *J. Chem. Soc.* **1923**, 2901.

(41) (a) Liang, H.-C.; Karlin, K. D.; Dyson, R.; Kaderli, S.; Jung, B.; Zuberbühler, A. D. *Inorg. Chem.* **2000**, *39*, 5884. (b) Hathaway, B. J.; Holah, D. G.; Postlethwaite, J. D. *J. Chem. Soc.* **1961**, 3215. (c) Hemmerich, P.; Sigwart, C. *Experientia* **1963**, *19*, 488.

(42) Kubas, G. J. *Inorg. Synth.* **1979**, *19*, 90. *ibid.* **1990**, *28*, 68.

(43) Ogura, T. *Transition Met. Chem.* **1976**, *1*, 179.

(44) Sorrell, T. N.; Jameson, D. L. *J. Am. Chem. Soc.* **1982**, *104*, 2053.

(45) Liang, H-C.; Kim, E.; Incarvito, C. D.; Rheingold, A. L.; Karlin, K. D. *Inorg. Chem.* **2002**, *41*, 2209.

(46) Csoregh, I.; Kierkegaard, P.; Norrestam, R. *Acta Cryst.* **1975**, *B31*, 314.

(47) Black, J. R.; Levason, W.; Webster, M. *Acta Cryst.* **1995**, *C51*, 623.

(48) Jones, P. G.; Crespo, O. *Acta Cryst.* **1998**, *C54*, 18.

(49) Nilsson, K.; Oskarsson, Å.; *Acta Chem. Scand.* A **1982**, *36*, 605.

(50) Kuchiyama, Y.; Kobayashi, N.; Takagi, H. D. *Inorg. Chim. Acta* **1998**, *277*, 31.

(51) Inada, Y.; Tsutsui, Y.; Wasada, H.; Funahashi, S. *Z. Naturforsch.* **1999**, *54b*, 193.

(52) Costas, M.; Xifra, R.; Llobet, A.; Sola, M.; Robles, J.; Parella, T.; Stoeckli-Evans, H.; Neuburger, M. *Inorg. Chem.* **2003**, *42*, 4456.

(53) Strauss, S. H. *J. Chem. Soc., Dalton Trans.* **2000**, 1, and references therein.

(54) Brisset, J.-L. *J. Chem. Eng. Data* **1982**, *27*, 153.

(55) Murguia, M. A.; Wherland, S. *Inorg. Chem.* **1991**, *30,* 139, and references therein.

(56) Yang, E. S.; Chan, M.-S.; Wahl, A. C. *J. Phys. Chem.* **1980**, *84*, 3094.

(57) Kirchner, K.; Dang, S.-Q.; Stebler, M.; Dodgen, H. W.; Wherland, S.; Hunt, J. P. *Inorg. Chem.* **1989**, *28*, 3604.

(58) McManis, G. E.; Nielson, R. M.; Gochev, A.; Weaver, M. J. *J. Am. Chem. Soc.* **1989**, *111,* 5533, and references therein.

(59) Nelsen, S. F; Ismagalov, R. F.; Gentile, K. E.; Nagy, M. A.; Tran, H. Q.; Qu, Q.; Halfen, D. T.; Odegard, A. L.; Pladziewicz, J. R. *J. Am. Chem. Soc.* **1998**, *120,*

8230.

(60) Nelsen, S. F; Chen, L.-J.; Ramm, M. T.; Voy, G. T.; Powell, D. R.; Accola, M. A.; Seehafer, T. R.; Sabelko, J. J.; Pladziewicz, J. R. *J. Org. Chem.* **1996**, *61*, 1405.

(61) Kamau, P.; Jordan, R. B. *Inorg. Chem.* **2001**, *40*, 3879.

(62) Zahl, A.; van Eldik, R.; Matsumoto, M.; Swaddle, T. W. *Inorg. Chem.* **2003**, *42*, 3718.

(63) Pfeiffer, J.; Kirchner K.; Wherland, S. *Inorg. Chim. Acta* **2001**, *313*, 37.

(64) Malito J. *Annu. Rep. NMR Spectrosc.* **1999**, *29*, 265, and references therein.

(65) Endo, K.; Yamamoto, K.; Deguchi, K.; Matshusta K. *Bull. Chem. Soc. Jpn.* **1987**, *60*, 2803. Yamamoto, T.; Haraguchi, H.; Fujiwara, S. *J. Phys. Chem.* **1970**, *74*, 6349.

(66) Imai, S.; Fujisawa, K.; Kobayashi, T.; Shirasawa, N.; Fujii, H.; Yoshimura, T.; Kitajima, N.; Moro-oka, Y. *Inorg. Chem.* **1998**, *37*, 3066.

(67) Ochsenbein, U.; Schläpfer C. W. *Helv. Chim. Acta* **1980**, *63*, 1926.

(68) Kroneck, P.; Kodweiss, J.; Lutz, O.; Nolle, A.; Zepf, D. *Z. Naturforsch.* **1982**, *37a*, 186.

(69) Gill, D. S.; Rodehüser, L.; Rubini, P.; Delpuech, J. -J. *J. Chem. Soc., Faraday Trans.* **1995**, *91*, 2307.

(70) Gill, D. S.; Singh, R.; Ali, V.; Singh, J.; Rehan, S. K. *J. Chem. Soc., Faraday Trans.* **1994**, *90*, 583.

Chapter 2. Crystal Structures of Cu(II,I)-Acetonitrile Solvates

Introduction

It has been noted in Chapter 1 that the focus of the present studies is the illumination of factors and/or methods that would be helpful in the determination and understanding of the electron self-exchange of the Cu(II/I) couple. For such reactions, it is well known from the Franck Condon principle[1] that the reactants undergo structural reorganization towards the configuration of the products prior to the electron-exchange event. Therefore, structural differences between the reactants influence the rate. In order to have some measure of the structural reorganization required for the Cu(II/I) couple, it is necessary to know the structures of the reacting species.

There are many crystal structures of the Cu(II) aqua ion, as shown in Chapter 1, but equivalent structures for the Cu(I) aqua ion are not available, because of the instability of this ion with respect to disproportionation. Thus, it is not even possible to estimate the structural reorganization energy for the aqueous Cu(II/I) system. However, structures of both oxidation states in other solvents might permit such an estimate. Since both oxidation states are stable in acetonitrile, it is interesting to compare Cu(II) and Cu(I) acetonitrile solvates with the hope of gaining some insight into the type and magnitudes of structural differences between them.

The available structural studies on Cu(II) and Cu(I) acetonitrile solvates were given in Chapter 1 and a summary is presented here. The EXAFS study by Funahashi and coworkers[2] on Cu(II) triflate solutions reported six acetonitrile ligands around the Cu(II) center with bond distances of 2.00 Å (Cu(II)-N_{eq}) and 2.49 (Cu(II)-N_{ax}). These authors[2] also reported mixed-ligand $Cu(II)(OH_2)_n(NCCH_3)_{6-n}$ complexes with Cu(II)-N_{eq} and

Cu(II)-N_{ax} bond distances similar to those in pure acetonitrile. The Cu(II)-N_{eq} bond length agrees with the value of 1.99 Å that Funahashi and coworkers[3] reported earlier, but their earlier Cu(II)-N_{ax} bond distance of 2.18 Å is significantly shorter. In the more recent paper by these authors[2] reference is made to the earlier work[3] but there is no comment on the obvious discrepancy in the Cu(II)-N_{ax} bond distances. This inconsistency may be a reflection of the difficulty in the accurate determination of the axial bonds in EXAFS studies of the Jahn-Teller distorted d^9 Cu(II) ion.[4] The Cu(II)-N_{eq} bond distances by Funahashi and coworkers[2-3] agree with the value of 1.99 Å from the EXAFS study on acetonitrile solutions of Cu(II) triflate by Persson et al.[5] The latter authors did not report any Cu(II)-N_{ax} distances.

The Cu(I) acetonitrile solvate has been studied in solution by EXAFS[5,6,7] methods and in single crystals by X-ray crystallography[8,9,10]. In the EXAFS studies of $Cu(ClO_4)$ by Persson et al.[5], Kuchiyama et al.[6] and Funahashi and coworkers,[7] the Cu(I) is found to be 4-coordinate and Cu(I)-N bond distances are 1.99 Å, and are therefore very similar to those for Cu(II) acetonitrile solvates. The Cu(I)-N bond distances also are in excellent agreement with those found in the X-ray crystal structure studies of the perchlorate,[8] hexafluorophosphate[9] and tetrafluoroborate[10] salts.

Although Cu(II) and Cu(I) have been studied in acetonitrile to various extents, the present study is aimed at determining the structures of the triflate salts, which would be beneficial in clearly defining the structural difference. Triflate salts have been chosen because their solubilities in acetonitrile permit the widest concentration ranges for kinetic studies, as determined in preliminary studies in this laboratory.

It is somewhat ironic that there are several crystal structures of Cu(I)-acetonitrile

solvates, but none for Cu(II). This deficiency is removed by the results of this study. The Cu(II) crystal structure determined here will allow the first comparisons to be made to the solution structures.[2,3,5] The Cu(I) triflate structure will be compared to the EXAFS studies[5-7] and the crystal structure studies of the perchlorate,[8] hexafluorophosphate[9] and tetrafluoroborate[10] salts and to the Cu(II) structure. It is hoped that this information will be useful in the understanding of the chemistries of Cu(II) and Cu(I), especially concerning the electron-exchange reaction. The Cu(I) structure is also relevant to the Cu(I) NMR study in Chapter 5. This study also may be of interest to studies of the chemistry of coordinated nitriles.

Experimental

Materials. Acetonitrile (Caledon, Fisher or BDH) was dried over 4Å molecular sieves for several days before use, but the residual water content was not determined. Doubly distilled water was used. Trifluoromethanesulfonic (triflic) acid (Aldrich), copper foil (Matheson, Coleman and Bell), cupric oxide (Fisher) and diethyl ether (Fisher) were used as supplied.

$Cu(OH_2)_4(F_3CSO_3)_2$ and $Cu(F_3CSO_3)_2$. The tetrahydrate and anhydrous salts of the Cu(II) triflate were routinely prepared by a modification of literature methods[3, 11,12]. As a representative example, 5.0 mL (26.5 mmol) of 5.3 M triflic acid were added to 25 mL of water containing 1.035 g (13.0 mmol) of cupric oxide. The mixture was warmed to about 60 °C and stirred until a clear blue solution remained. The solution was filtered to remove traces of solid material and evaporated on a steam-bath to yield a light blue solid. The blue solid was redissolved in a minimum volume of water on the steam-bath, and recrystallized by cooling. This step was done to try to minimize traces of acid. The blue

solid product was finally dissolved in a small volume of acetonitrile (~10 mL) and precipitated with ether, filtered and washed with ether and dried in air. Anal.: Calcd for $CuC_2F_6H_8O_{10}S_2$; Cu, 14.65; C, 5.54; H, 1.86. Found Cu, 14.50, C, 5.20, H, 1.67.

The anhydrous Cu(II) triflate, $Cu(F_3CSO_3)_2$ was obtained as a fine, white hygroscopic powder by heating the tetrahydrate Cu(II) salt in air at ~100 °C. This solid was stored in a vial with a plastic cap in a desiccator. Anal.: Calcd. for $CuC_2F_6O_6S_2$; Cu, 17.5; C, 6.64: Found Cu, 17.6; C, 6.30.

Copper(II) Crystals. Blue crystals were obtained by slow evaporation of acetonitrile solutions of the tetrahydrate and the anhydrous Cu(II) triflates. The crystals from the solution of the tetrahydrate were obtained in an air atmosphere whereas those from the solution of the anhydrous salt were obtained under an argon atmosphere. Single crystals for the structure determination were selected from the solution-crystal mixture in the X-ray crystallography laboratory.

Copper(I) Crystals. A solution of Cu(I) triflate in acetonitrile was obtained by the reduction of the tetrahydrate Cu(II) salt in acetonitrile using a modification of the methods by Ogura[11] and Jenkins and Kochi.[12] A mixture containing 50 mL of acetonitrile, 1.0 g (2.3 mmol) of $Cu(OH_2)_4(F_3CSO_3)_2$ and 0.3 g (4.7 mmol) of copper foil was stirred in a capped parafilm-sealed Erlenmeyer flask until the solution turned colorless. Filtration on a 4-8 μ sintered glass frit gave a clear solution. The Cu(I) triflate salt was recovered as a white powder from this solution by adding anhydrous diethyl ether and collecting the product by filtration under argon. Argon was sucked through the product until it looked reasonably dry and then it was sealed under argon. A portion of the product was dissolved in 0.1 M $HClO_4$, air-oxidized, and analyzed for copper by the

KI/$S_2O_3^{2-}$ method.[13] Anal.: Calcd. for $CuC_9F_3H_{12}N_4O_3S$; Cu, 16.86; N, 14.87; C, 28.69; H, 3.21. Found: Cu, 17.10; N, 14.18; C, 27.64; H, 2.98.

A portion of the white Cu(I) salt was dissolved in dry acetonitrile and the solution was concentrated under an argon atmosphere and cooled further in the refrigerator. The resulting colorless crystals were collected by filtration under argon. A single crystal was then selected for the structure determination.

Elemental Analyses. Carbon, hydrogen and nitrogen contents in the solids were determined in the Microanalytical Service Laboratory in the Department of Chemistry, University of Alberta.

Structure Analyses. X-ray crystal structure analyses of the obtained crystals were done in the X-ray Crystallography Laboratory in the Department of Chemistry, University of Alberta, by M. Wang and Dr. M. J. Ferguson. Data were collected at -80 °C on a Bruker PLATFORM/SMART 1000 CCD diffractometer using graphite-monochromated Mo Kα (λ = 0.71073 Å) radiation using 0.2° ωscans of 20 or 25 s exposures.[14] Empirical or Multi-scan (SADABS) methods were used to correct the intensity data for decay and absorption. A summary of the crystal and refinement data for all these crystals is given in Appendix 2.1. Hydrogen atoms were not apparent in the electron density maps and thus were not included in the fitting models.

Results and Discussion

Copper(II) Structure. Blue crystals of acetonitrile solvates of Cu(II) triflate were obtained by cooling acetonitrile solutions of anhydrous and tetrahydrate Cu(II) triflate salts as described above. The structures were solved using direct methods (SHELXS-86)[15] or direct/fragment search methods (*DIRDIF–96*).[16] Data were refined by full matrix

least squares on F^2 (SHELXL-93).[17] Crystals obtained from the acetonitrile solution of the tetrahydrate salt have the composition $Cu(NCCH_3)_2(OH_2)_2(F_3CSO_3)_2$, whereas those from the solution of the anhydrous salt have the composition $Cu(NCCH_3)_4(F_3CSO_3)_2$. The structures of $Cu(NCCH_3)_2(OH_2)_2(O_3SCF_3)_2$ and $Cu(NCCH_3)_4(F_3CSO_3)_2$ are referred to as **1a** and **1b**, respectively, in the following discussion.

Perspective views of the local coordination environment of the copper(II) centers of **1a** and **1b** are shown in Appendix 2.2. Each copper atom is surrounded by a distorted octahedron of N and O atoms. Complete data tables for the various parameters are presented in the Appendix section. Some Cu-solvent and Cu-triflate distances are given in the spatial arrangements in Figures 2.1 and 2.2, which show Cu(II)-OH_2, Cu(II)-OS, Cu(II)-N, N-C bond lengths in Å and H_2O-Cu-OH_2, SO-Cu-OS, N-Cu-N, Cu-O-S, Cu-N-C and N-C-C bond angles in **1a** and **1b**, respectively.

It can be seen from Figures 2.1 and 2.2 that the Cu(II)-N distances are similar in **1a** and **1b**. The Cu(II)-OH_2 distance is similar to those reported by Cotton and coworkers[18] and to those observed in aqua-Cu(II) solutions with various counterions.[19] The N-Cu(II)-N and O-Cu(II)-O angles range from 89.0 to 90.9 in **1a** and 87.2 to 92.0 in **1b** indicating an octahedral geometry that is distorted from regular symmetry by elongation along the Cu(II)-triflate bonds. The tetragonal distortion causes a ~ 0.42 Å difference between the axial and equatorial groups in **1a** and 0.37 and 0.43 Å differences between the two axial triflates and the four equatorial acetonitrile ligands in **1b**. Packing effects may be responsible for the observed differences in the two Cu(II)-O(triflate) distances in **1b** (see Figure 2.2) compared to the identical ones in **1a**, where *trans* groups are related to one another by an inversion center at Cu(II) (see Figure 2.1).

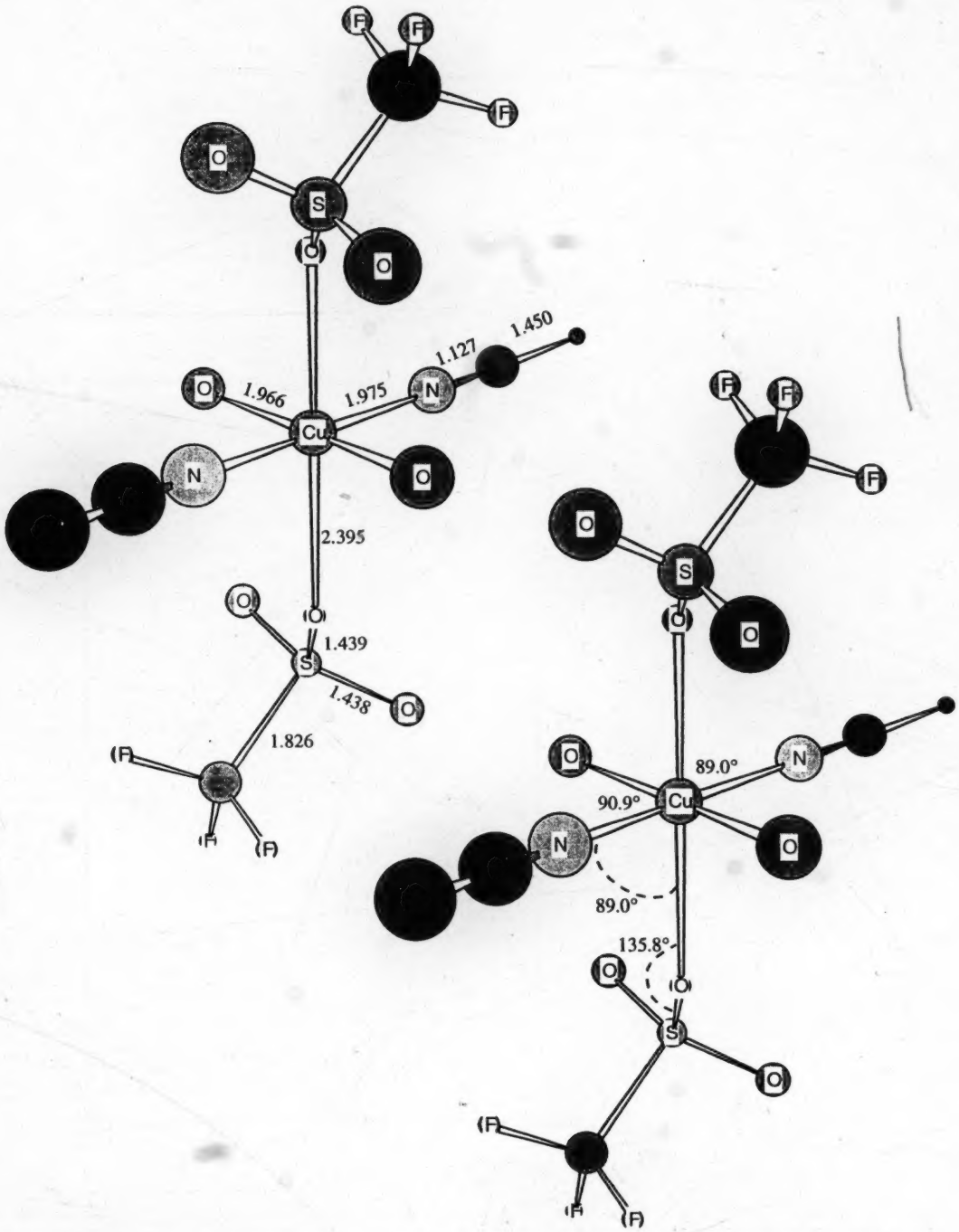

Figure 2.1. Three dimensional view showing the relative atom positions and some bond distances and angles in **1a**.

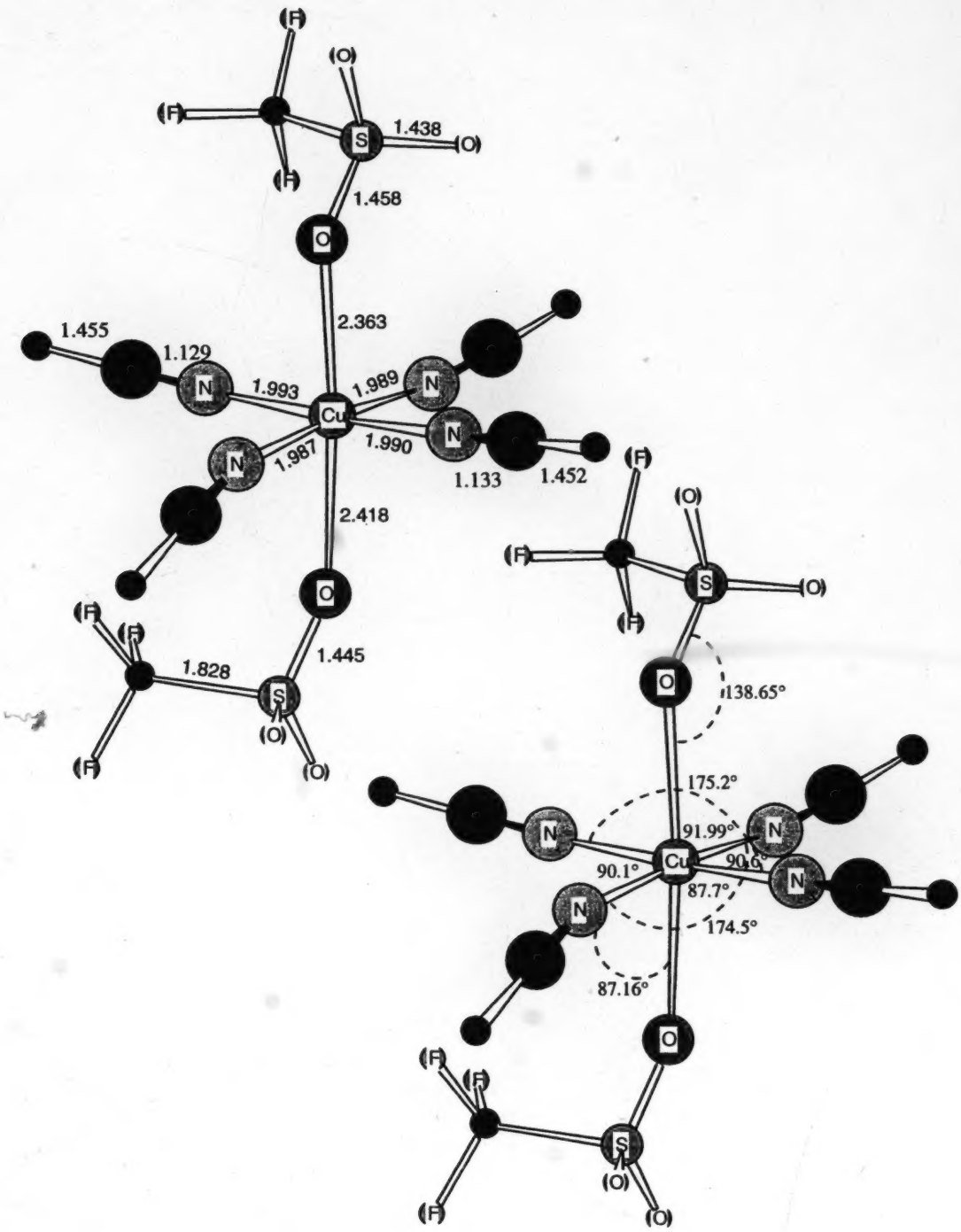

Figure 2.2. Three dimensional view showing the relative atom positions and some bond distances and angles in **1b**.

The Cu(II)-N distance is ~0.015 Å shorter in **1a** than in **1b** suggesting a weakening of the copper(II)-acetonitrile σ-bonding with increasing number of acetonitrile ligands. In **1a**, the equatorial placement of the H_2O ligands and the Cu(II)-$O(OH_2)$ distance are consistent with the EXAFS study of Funahashi and coworkers.[2] However, the Cu(II)-N distances are 0.01-0.02 Å shorter than those they report for various $Cu(OH_2)_n(NCCH_3)_{6-n}^{2+}$ species.

It is interesting to note that the Cu-N-C angles in **1a** are 175.8° whereas in **1b** they range between 161 and 177°. As a consequence, the Cu-C distances in **1b** range from 3.08 to 3.12 Å. The latter value agrees with the report of Persson et al.[5], as does the Cu(II)-N distance, for $Cu(NCCH_3)_4^{2+}$ in acetonitrile, but they did not note any irregularity in the angles. The angle variations in the crystals could be due to packing effects.

The structures of **1a** and **1b** may be compared with those for the equivalent aqua compounds and with the acetonitrile solvate of Cr(II). The data are given in Table 2.1. The Jahn-Teller distortion in the Cr(II) acetonitrile complex is of similar magnitude to that observed in Cu(II) and the elongation along the Jahn-Teller axis also is similar for both the acetonitrile and aqua Cu(II) species. The anions appear to prefer the longer axial positions, or they are forced into these positions by the more basic solvent ligands. The distances to the anions are fairly independent of nature of anion. The values are in the narrow range of 2.34 to 2.42 Å, which is similar to the axial Cu(II)-solvent bond lengths reported by Funahashi and coworkers[2] for the $Cu(OH_2)_n(NCCH_3)_{6-n}^{2+}$ complexes.

Table 2.1. Comparison of the M(II)-Ligand (M = Cu, Cr) Distances from Crystal Structures of 6-Coordinate Complexes

Compound	$M\text{-}L_{eq}$, Å	$M\text{-}L_{ax}$, Å
$Cu(OH_2)_2(NCCH_3)_2(Trif)_2$, **1a** [a,b]	1.975 (M-N)	2.395 (M-O(Trif))
	1.966 (M-O)	
$Cu(NCCH_3)_4(Trif)_2$, **1b** [a]	1.991(2)	2.3625(17) (M-O)
	1.985(2)	2.4184(18) (M-O)
$Cr(NCCH_3)_4(BF_4)_2$ [c]	2.069(2)	2.407(2) (M-F)
	2.063(2)	
$Cu(OH_2)_4SiF_6$ [d]	1.953(1)	2.3399(8) (M-F)
	1.949(1)	
$Cr(OH_2)_4SiF_6$ [d]	2.042(1)	2.3964(8) (M-F)
	2.040(1)	
$Cu(OH_2)_6(ClO_4)_2$ [e] (Site 1)	1.967 (2)	2.381(2) (M-O(OH_2))
	1.945 (2)	
$Cu(OH_2)_6(ClO_4)_2$ [e] (Site 2)	1.960 (2)	2.382(3) (M-O(OH_2))
	1.947 (3)	

[a] This study, Trif = triflate. [b] The ligands are related by a center of inversion. [c] Henriques, R. T.; Herdtweck, E.; Kühn, F. E.; Lopes, A. D.; Mink, J.; Romão, C. C. *J. Chem. Soc., Dalton Trans.* **1998**, 1293. [d] Reference 18. [e] Galluci, J. C.; Gerkin, R. E. *Acta Cryst.* **1989**, *C45*, 1279.

Copper(I) Structure. Colorless crystals were formed after cooling an acetonitrile solution of anhydrous Cu(I) triflate under argon as detailed in the experimental section. The structure was solved by direct methods (SHELXS-86).[15] Data were refined by full matrix least-squares on F^2 (SHELXL-93).[17] The X-ray analysis of the crystal revealed a monoclinic system in space group $P2_1/c$ (No. 14) and the molecular composition is $Cu(NCCH_3)_4(F_3CSO_3)$. The structure will be referred to as **2**.

Perspective views of the local coordination environment of the Cu(I) centers of **2** are shown in Appendix 2.13 along with complete data tables for the various parameters. The copper ions lie in three crystallographically independent sites and are surrounded by four N atoms. Figure 2.3 shows the coordination spheres of the three independent Cu(I) ions along with the Cu-N distances in the upper view and selected angles in the lower duplicate view. Some structural parameters for the triflate and other salts are given in Table 2.2 and closest triflate contacts are shown in Figure 2.4. The contacts of ≤ 3.6 Å, the maximum for the Van der Waal's interactions of the CH_3 or C of **2** with F or O of the triflate ions,[20] do not indicate any correlation of angular distortions and triflate contacts.

The structural information available and collected in Table 2.2 suggests that all the salts of $Cu(NCCH_3)_4^+$ show similar features. The triflate shows distortions similar to the ClO_4^-,[8] PF_6^-,[9] and BF_4^-[10] salts. The Cu-N-C angles show a similar range and average and the Cu-N distances are not significantly different. The N-Cu-N angles in the triflate salt average to the expected tetrahedral value. The C-N distances average to a value just slightly longer than the 1.125 Å for lattice $NCCH_3$ in the PF_6^- salt.[9] Overall, it would appear that the lack of strong directional bonding forces for the d^{10} Cu^+ ion allows minor disorders in the lattice and thence somewhat variable bond lengths and angles.

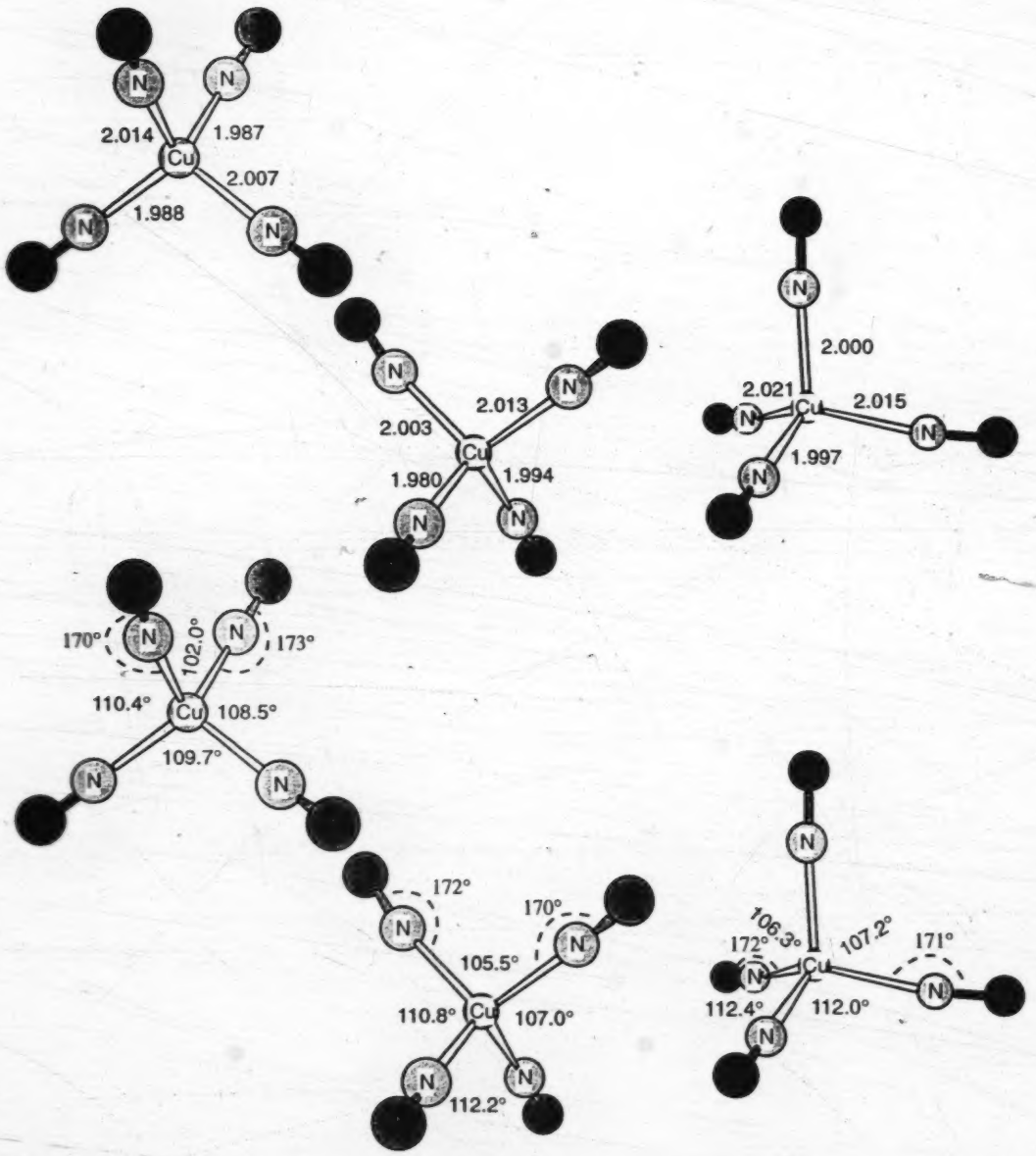

Figure 2.3. Three dimensional view showing the relative atom positions and the bond lengths and angles at the Cu(I) center in **2**. Angles of the Cu-N-C less than 175° are also shown. The CH_3 groups are not shown.

Table 2.2. Summary of Structural Parameters for $Cu(NCCH_3)_4^+$ Salts

Parameter	Salt $F_3CSO_3^-$ [a]	PF_6^- [b]	ClO_4^- [c]	BF_4^- [d]
Cu-N Range	1.980-2.022	1.968-2.030	1.95-2.02	1.964-2.028
Cu-N Ave	2.002	2.006	1.99	1.993
N-C Range	1.115-1.152		1.09-1.16	1.107-1.140
N-C Ave	1.133		1.13	1.123
N-Cu-N Range	102.0-116.3	102.7-114.0	106-113	105.4-113.4
N-Cu-N Ave	109.4	109.4		109.4
Cu-N-C Range	170.1-179.1	168.0-177.4	169-179	169.9-179.0
Cu-N-C Ave	173.8		174	174.2
N-C-C Range	178.0-179.8	176.5-179.2	176-180	175.3-179.6
N-C-C Ave	179.2		178	178.3

[a] This study. [b] Reference 9. [c] Reference 8. [d] Reference 10.

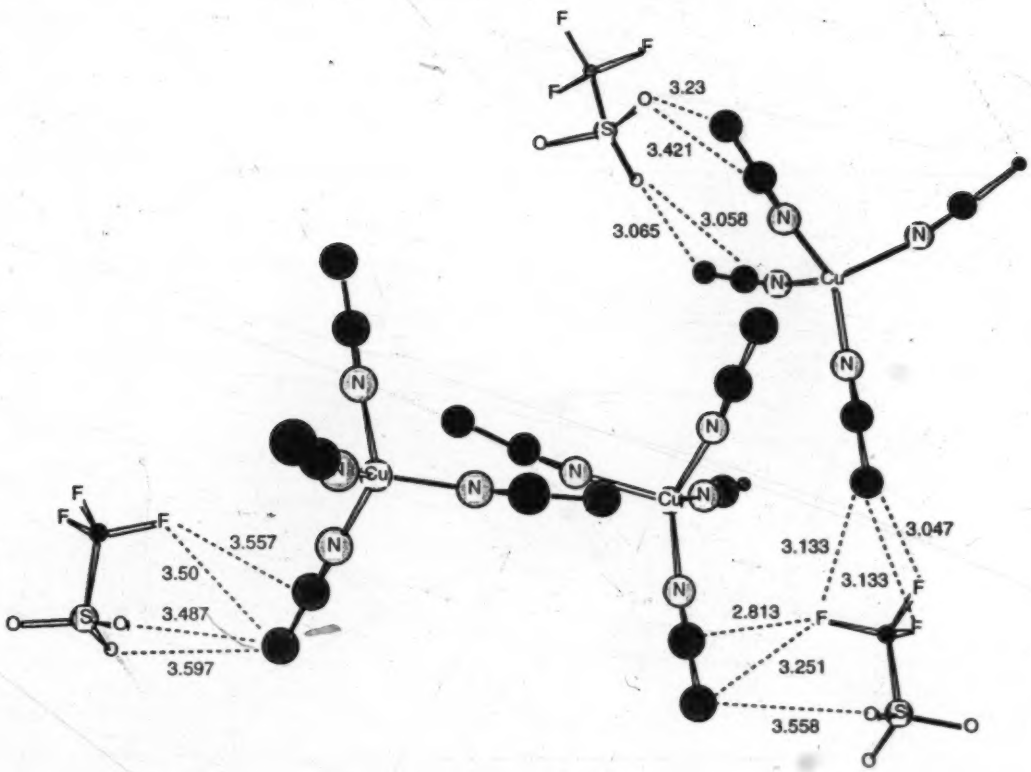

Figure 2.4. The unit cell structure of **2** showing anion contacts of ≤ 3.6 Å. The view is oriented to optimize the view of triflate-acetonitrile contacts.

It is interesting to note that Costas et al.[21] have prepared a dimeric Cu(I)-isonitrile derivative which shows variable Cu-C-N angles of 175 and 170.2° (see Figure 2.5). The specific compound is $[Cu_2(Me2m)(t\text{-}BuNC)_2]^{2+}$ (Me2m = 3,6,9,17,20,23-hexamethyl-3,6,9,17,20,23-hexaazatricyclo[23.3.1.1]triaconta-1(29),11(30),12,14,25,27-hexaene). The bending observed by Costas et al.[21] is similar to that observed in the $NCCH_3$ solvates.

Costas et. al.[21] also studied another copper(I) dimer, $[Cu_2(Me2p)(CO)_2]^{2+}$ (Me2p = 3,6,9,16,19,22-hexamethyl-3,6,9,16,19,22-hexaazatricyclo-[22.2.2.2]triaconta-1(26),11(12)13,24,27,29-hexaene), whose Cu-C-O angles are essentially identical, as can be seen in the lower views in Figure 2.5. These angles do not show as much bending as the nitrile and isonitrile compounds.

Conclusion

Some structural parameters from the present study for acetonitrile solvates of Cu(II) and Cu(I) are collected in Table 2.3, where it can be seen that the Cu-N bond lengths in the Cu(II) and Cu(I) species are almost identical. This is generally consistent with the X-ray scattering results described in the Introduction. Then it would seem that simple bond expansion and compression should not be a major contributor to the reorganization energy for electron-transfer between Cu(I) and Cu(II).

The similar Cu-N distances in the two oxidation states suggests that the same is quite probable for the aqua-species. This in turn implies that the bond length difference of ~0.14 Å suggested by Persson et al.[5] is probably a substantial overestimate. It is interesting to note that commonly tabulated ionic radii[20] for 4-coordinate Cu(II) and Cu(I) are 0.71 and 0.74 Å, respectively, and are reasonably consistent with the acetonitrile solvate structures determined here.

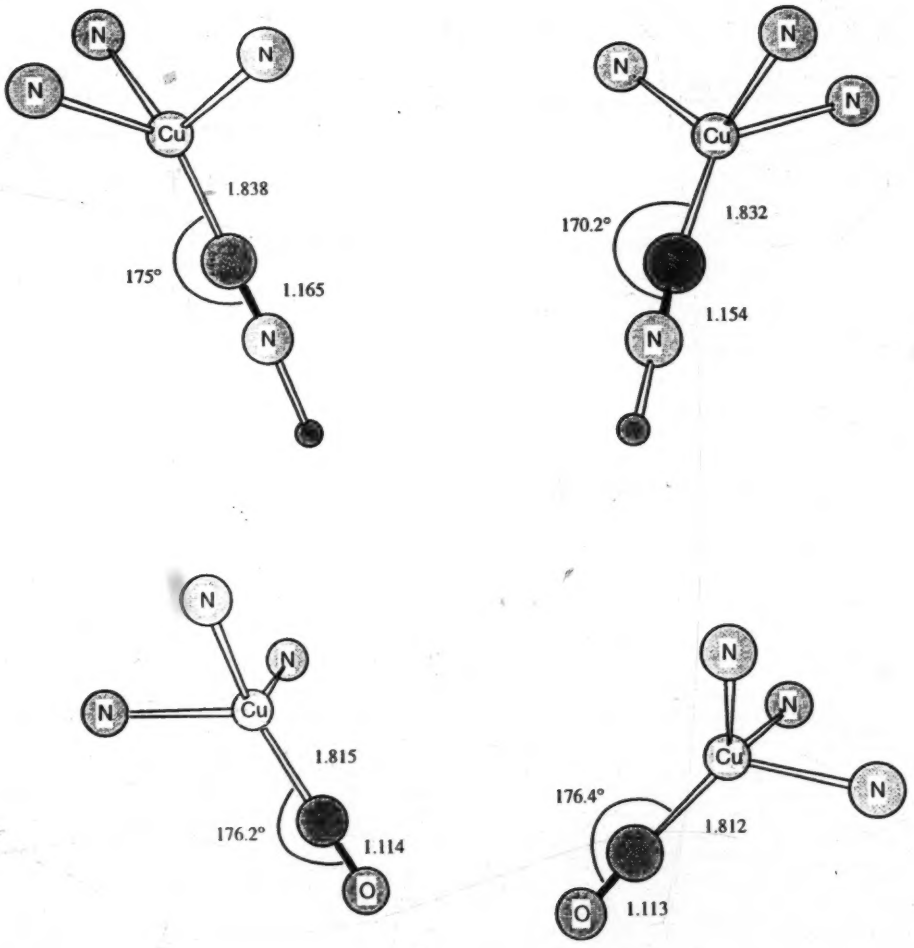

Figure 2.5. Ligand coordination around the Cu(I) in copper(I) complexes of a dinuclear hexaaza macrocycle *t*-butylisonitrile and CO ligands from reference 21.

Table 2.3. A Comparison of Interatomic Distances (Å) and Interatomic Angles (deg) in $Cu(OH_2)_2(NCCH_3)_2(F_3CSO_3)_2$, **1a**, $Cu(NCCH_3)_4(F_3CSO_3)_2$, **1b**, $Cu(NCCH_3)_4(F_3CSO_3)$, **2**, and the CH_3CN solvate in $Cu(NCCH_3)_4PF_6$

Parameter	**1a** [a]	**1b** [a]	**2** [b]	CH_3CN [d]
Cu-OH_2	1.966			
Cu-OS	2.395	2.390		
Cu-N	1.975	1.989	2.002	
N-C	1.127	1.130	1.133	1.125
C-C	1.450	1.455	1.446	1.491
N-Cu-N	180.0, 90.03	174.85, 90.06	109.4 [c]	
Cu-N-C	175.8	170.0	173.8	
N-C-C	179.2	179.1	179.2	177.90

[a] Average values. [b] These are averages over the three crystallographically independent units. [c] The average N-Cu-N angle within each unit also is ~109.4, but variations in the averages of the other parameters within a Cu unit is somewhat larger (see Figure 2.3 and/or details in the Appendix Section). [d] Reference 9.

References

(1) Marcus, R. A. *Annu. Rev. Phys. Chem.* **1964**, *15*, 155; *J. Chem. Phys.* **1965**, *43*, 679. Sutin, N. *Acc. Chem. Res.* **1982**, *15*, 275.

(2) Inamo, M.; Kamiya, N.; Inada, Y.; Nomura, M.; Funahashi, S. *Inorg. Chem.* **2001**, *40*, 5636.

(3) Inada, Y.; Sugimoto, Y.; Nakamo, Y.; Itoh, Y.; Funahashi, S. *Inorg. Chem.* **1998**, *37*, 5519.

(4) Okan, S. E.; Salmon, P. S. *Mol. Phys.* **1995**, *85*, 981, and references therein.

(5) Persson, I.; Penner-Hahn, J. E.; Hodgson, K. O. *Inorg. Chem.* **1993**, *32*, 2497.

(6) Kuchiyama, Y.; Kobayashi, N.; Takagi, H. D. *Inorg. Chim. Acta* **1998**, *277*, 31.

(7) Inada, Y.; Tsutsui, Y.; Wasada, H.; Funahashi, S. *Z. Naturforsch.* **1999**, *54b*, 193.

(8) Csoregh, I.; Kierkegaard, P.; Norrestam, R. *Acta Cryst.* **1975**, *B31*, 314.

(9) Black, J. R.; Levason, W.; Webster, M. *Acta Cryst.* **1995**, *C51*, 623.

(10) Jones, P. G.; Crespo, O. *Acta Cryst.* **1998**, *C54*, 18.

(11) Ogura, T. *Transition Met. Chem.* **1976**, *1*, 179.

(12) Jenkins, C. L.; Kochi, J. K. *J. Am. Chem. Soc.* **1972**, *94*, 843.

(13) Kolthoff, I. M.; Sandell, E. B.; Meehan E. J.; Bruckenstein, S. *Quantitative Chemical Analysis*, Collier-MacMillan Canada Ltd., Toronto, **1969**.

(14) Programs for diffractometer operation, data collection, data reduction and absorption correction were those supplied by Bruker.

(15) Sheldrick, G. M. *Acta Cryst.* **1990**, *A46*, 467.

(16) Beurskens, P. T.; Beurskens, G.; Bosman, W. P.; de Gelder, R.; Garcia Granda, S.; Gould, R. O.; Israel, R.; Smits, J. M. M. **1996**. The *DIRDIF-96* program system, Crystallography Laboratory, University of Nijmegen, The Netherlands.

(17) Sheldrick, G. M. SHELXS-93. *Program for crystal structure determination*, University of Göttingen, Germany **1993**.

(18) Cotton, F. A.; Daniels, L. M.; Murillo, C. A.; Quesada, J. F. *Inorg. Chem.* **1993**, *32,* 4868. Cotton, F. A.; Daniels, L. M.; Murillo, C. A.; Quesada, J. F. *Inorg. Chem.* **1993**, *32,* 4861.

(19) Ohtaki, H.; Radnai, T. *Chem. Rev.* **1993**, *93*, 1157, and references therein.

(20) Huheey, J. E.; Keiter, E. A.; Keiter, R. L. *Inorganic Chemistry: Principles of Structure and Reactivity*, HarperCollins, New York, **1994**.

(21) Costas, M.; Xifra, R.; Llobet, A.; Sola, M.; Robles, J.; Parella, T.; Stoeckli-Evans, H.; Neuburger, M. *Inorg. Chem.* **2003**, *42*, 4456.

Chapter 3. Kinetic Study of the Cu(II)-Ferrocenes Reaction: Cu(II/I) Self-Exchange in Acetonitrile

Introduction

Since the introduction of Marcus theory in the 1960's, it has been recognized that a knowledge of the rates of electron self-exchange reactions is fundamental to understanding and predicting the rates of outer-sphere electron-transfer reactions. Consequently, the self-exchange rates have been measured for many transition metal ions and their complexes in water. A glaring exception is the Cu(II/I) system. As noted in Chapter 1, it is unlikely that this system will ever be studied in water because of the instability of aqueous Cu(I) with respect to disproportionation.

The situation is different in acetonitrile (AN), where Cu(I) is quite stable,[1] as discussed in Chapter 1.Therefore it seems at least possible to measure the Cu(II/I) self-exchange rate in AN. However, before attempting such measurements, it obviously would be helpful to have some idea of the magnitude of the rate. Then an experimental method appropriate to the expected time scale could be chosen.

The present Chapter describes experiments to estimate the Cu(II/I) electron exchange rate in AN from the Marcus cross-relationship. The system chosen is the reaction of Cu(II) with ferrocene (Fc) and 1,1′-dimethylferrocene (Dmfc) in AN/water mixtures. The necessary background information is available from studies of reduction potentials in AN/water mixtures by Cox and coworkers[2] and the electron self-exchange studies in AN of Fc/Fc^{+} [3,4,5] and $Dmfc/Dmfc^{+}$ [3] couples.

It should be noted that there have been several applications of the Marcus cross-relationship to estimate the Cu(II/I) electron self-exchange rate in water. Sutin and

coworkers[6] studied the reaction of Cu(I) with various Ru(III) polypyridyl complexes and estimated a rate constant of ~1 x 10^{-5} M^{-1} s^{-1}. Shortly thereafter, Davies[7] measured the rates for Cu(I) reacting with several Ru(III) ammine complexes and obtained an estimate of ~2 x 10^{-4} M^{-1} s^{-1}. Most recently, Sisley and Jordan[8] used the reaction of Cu(II) with Co(II)(sep) and found a self-exchange rate constant of ~5 x 10^{-7} M^{-1} s^{-1}. These authors also re-evaluated the earlier work of Davies[7], by adjusting E^{o} values to the appropriate ionic strength, and obtained values in the range of ~(2-9) x 10^{-7} M^{-1} s^{-1}. In contrast, the rate constant of 4.3 x 10^{4} M^{-1} s^{-1} measured by Rorabacher and coworkers[9] for the oxidation of Cu(I) by $Co(TIM)(OH_2)_2^{3+}$ (TIM = 2,3,9,10-tetramethyl-1,4,8,11-tetraazacyclotetradeca-1,3,8,10-tetraene) yields a self-exchange rate constant of ~2 x 10^{5} M^{-1} s^{-1} for aqueous Cu(II/I). This large value is consistent with the authors' suggestion that the reaction might be going by an inner-sphere pathway, although the oxidant is generally assumed to go outer-sphere. For the oxidation of hydrated ions of V(II) and Cr(II) by aqueous Cu(II), Espenson and coworkers[10] obtained rate constants of 26.6 and 0.17 M^{-1} s^{-1} respectively. The Marcus cross-relationship gives self-exchange rate constants of ~3 x 10^{-2} and ~7 x 10^{-6} M^{-1} s^{-1}, respectively. The latter value is reasonably consistent with the range calculated by Sisley and Jordan[8], whereas the V(II)/Cu(II) system would appear to be using an inner-sphere mechanism.

The general conclusion from these studies is that the self-exchange rate constant for aqueous Cu(II/I) is in the range of 10^{-6} to 10^{-7} M^{-1} s^{-1}. This places it about 10^{2} smaller than that of the aqueous Cr(III/II) system, which in turn is 10^{3} times smaller than the other known aqua ions of the first-row transition metal ions. The slow electron self-exchange for the Cu and Cr systems may be due to the uniquely large Jahn-Teller

distortion for d^4 Cr(II) and d^9 Cu(II) (see Chapter 2) which causes rather energetic inner-sphere ligand rearrangements prior to electron-transfer. As indicated by studies in Chapter 2 and other literature[11], the Cu system has a further problem in that Cu(I) is probably tetrahedral whereas Cu(II) has a 6-coordinate tetragonal structure. The general type of rearrangement in the self-exchange of the Cu(II/I) system, in which the ligand is L, is shown in Scheme 3.1.

Scheme 3.1

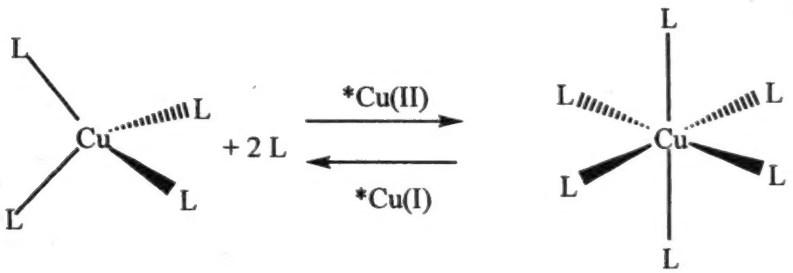

Cu(I), tetrahedral geometry

Cu(II), distorted octahedral geometry

An overview of the available information suggests that it is difficult to anticipate the magnitude of the Cu(II/I) self-exchange rate constant in AN. There are no cross-reaction studies to which Marcus theory can be applied. The lack or uncertainty in the structural information prevents any interpretation of inner-sphere rearrangement energies between water and AN.

Since the plan is to redress this situation by studies of the cross-reaction between Cu(II) and ferrocenes in AN, some background chemistry will be reviewed. Kratochvil and coworkers[12] have shown that the Cu(II)-Fc reaction proceeds to completion with 1:1 stoichiometry as shown in eq. 3.1.

$$Fc + Cu^{2+} \rightarrow Fc^{+} + Cu^{+} \qquad (3.1)$$

where Fc is the ferrocene, Cu^{2+} is the Cu(II) solvate, Fc^{+} is the ferrocenium ion and Cu^{+} is the Cu(I) solvate. As noted previously, the rate constant for the reaction in eq. 3.1 and that of the reaction of the Cu(II) solvate with Dmfc will be determined in various AN/water mixtures.

The Cu(II) speciation in the chosen solvent has been studied by Funahashi and coworkers[13] for AN with compositions $0 \leq [H_2O] \leq 0.84$ M (98.5% AN). They reported formation of $[Cu(OH_2)_n(NCCH_3)_{6-n}]^{2+}$ (n = 0 - 3) with $[Cu(OH_2)_2(NCCH_3)_4]^{2+}$ as the dominant species for $[H_2O]$ as low as 0.5 M (~99% AN). The Cu(I)-AN system has been studied by Kamau and Jordan[14] from the water-rich end. Their results suggest that the dominant species is $Cu(OH_2)(NCCH_3)_3^{+}$ for >50% AN, but the point at which this converts to $Cu(NCCH_3)_4^{+}$ is uncertain. The electrochemical studies of Cox and coworkers[2] show that the Cu(II/I) reduction potential increases smoothly with increasing % AN (50% - 100%), and do not suggest any abrupt change in species.

The reduction potentials for the Fc^{+}/Fc system in AN/water mixtures also were determined by Cox and coworkers.[2] The equivalent values for the Dmfc have not been determined under these conditions, but those for Fc show rather minor variations with solvent composition. As noted earlier, the kinetics for self-exchange of the Fc[3-5] and Dmfc[3] have been measured in AN. Fc has been studied in a number of solvents,[3-5] the variations are generally small, and it will be assumed that the self-exchange rate is independent of the AN/water composition.

Although it has been necessary to make several assumptions, it must be

remembered that the goal is to obtain a magnitude of the Cu(II/I) self-exchange rate within the inevitable limitations of simple Marcus theory.

Experimental

Materials. Acetonitrile (Caledon, Fisher or BDH), perchloric acid (Fisher), triflic acid (Aldrich), lithium perchlorate (Fisher), copper(II) nitrate trihydrate (Allied Chemicals) and 1,1'-dimethylferrocene (Alfa Inorganics) were used as supplied. Ferrocene (Strem Chemicals) was purified by sublimation. Tetraaquacopper(II) triflate ($Cu(OH_2)_4(F_3CSO_3)_2$) was prepared as described in Chapter 2.

AN/water. The AN/water solvent was made by transferring an appropriate volume of doubly distilled water, and sometimes standardized aqueous perchloric or triflic acid, to a 500 mL or 1.00 L volumetric flask and diluting to volume with AN (99.7 or 99.5%). Therefore the % AN refers to volume percentage. The acid, used to suppress hydrolysis[12] of Cu(II) in the solvent mixtures, was prepared by diluting the concentrated acid with doubly distilled water and analyzed by titration with 0.100 M NaOH. The mixed solvents were stored in volumetric flasks and used within 2 days. The densities and molarities as a function of volume % AN are given in Appendix 5.1.

Sample solutions. Cu(II) solutions (< 0.05 M) in AN/water (with and without added acid) were prepared by dissolving ~1.0 g, (~2.3 mmol) of $Cu(OH_2)_4(F_3CSO_3)_2$ or ~0.6 g, (~2.5 mmol) of $Cu(NO_3)_2 \cdot 3H_2O$ in a 50.0 mL volumetric flask and diluting to the mark. Then the solutions were standardized with $KI/S_2O_3^{2-}$. Solutions for the iodometric standardization titrations were prepared by standard methods.[15] Once the formula weight of the Cu(II) triflate salt was established, further solutions were prepared by weight.

Aliquots from these solutions were diluted to (0.4 - 4.0) x 10^{-2} M Cu(II) in 25.0 mL volumetric flasks and used as the stock solutions for the kinetic runs.

A 1.66 x 10^{-2} M aqueous solution of Cu(II) perchlorate, containing 0.199 M $HClO_4$, was used in a few runs for comparison to triflate and nitrate. Known volumes of this solution were mixed with AN to obtain the required % AN. Then the solutions were diluted with the appropriate solvent to make (8.31 - 41.6) x 10^{-5} M Cu(II) perchlorate.

Solutions of Fc and Dmfc were prepared by dissolving carefully weighed amounts of Fc (~10 mg, ~0.054 mmol) or Dmfc (~11 mg, ~0.051 mmol) in neat AN or AN/water solvent in 25.0 mL volumetric flasks. Then 10.0 mL aliquots of these solutions were diluted in 50.0 mL volumetric flasks with the appropriate solvent to give (4.0 - 6.0) x 10^{-4} M stock solutions for the kinetic runs.

Electronic spectra. For the purposes of determining molar extinction coefficients, solutions of Cu(II) and the ferrocenes were made as described above. Solutions of Cu(I) were made by dissolving weighed amounts (0.10 g, 0.265 mmol) of Cu(I) triflate (Chapter 2) in 25.0 mL of AN. The Fc^+ or $Dmfc^+$ solutions were obtained by mixing equal volumes of ~0.3 x 10^{-4} M Fc (or Dmfc) and ~0.5 x 10^{-4} M Cu(II) triflate for uv region, and ~4 x 10^{-4} M Fc (or Dmfc) and ~5 x 10^{-4} M Cu(II) triflate, for the visible region.

The uv-visible spectra for Cu(I), Cu(II), Fc, Fc^+, Dmfc and $Dmfc^+$ were recorded from 230 to 850 nm on a Cary 219 spectrophotometer using 1, 2 or 5 cm cylindrical optical cells as needed. The absorbance and wavelength were read off the chart paper and the molar extinction coefficients (ε) were calculated based on the mass of the Cu(I), Cu(II) or Fc species and the 1:1 stoichiometry.[12]

Kinetic measurements. Runs under pseudo-first-order, and a few under second-order conditions were done in 50, 80, 90, 95 or 97.5% AN on a Tritech Dynamic Instruments stopped-flow spectrophotometer. In this system, the storage and drive syringes, the observation cell and all connecting tubing are in a circulating, thermostated water bath. The temperature was monitored by a Fluke 2180A digital thermometer.

Freshly prepared Cu(II) triflate and Fc or Dmfc solutions in the appropriate solvent mixture were transferred to separate storage syringes on the stopped-flow system and thermostated at 25 ± 0.5 °C. These solutions were transferred via three-way taps to the drive syringes and mixed in equal volumes so that the species concentrations in the reaction cell were at one-half their stock values. Most runs were under pseudo-first-order conditions with [Cu(II)] > 10 [Fc] or [Dmfc].

The rate of formation of the Fc^+ or $Dmfc^+$ product was monitored by measuring the change in absorbance with time at 616 or 280 nm. The latter was used for the Cu(II) perchlorate solutions only.

The collection of kinetic traces started with a calibration experiment using the solvent in the stopped-flow cell to set the 100% and 0% transmittance voltages which gave Beer's law numbers of zero and 255 for conversion of volts to absorbance. The reactants in the drive syringes were mixed by a pneumatic drive and 256 voltages at equal time intervals were stored on a transient recorder. The data were transferred to a 486 PC using the manufacturer's kinetic version 1.2 IBM program and stored as a data file. A locally developed program read this file, converted the data to absorbance/time and fitted it by iterative least-squares to obtain the rate constants. At least 120 points were used in the analysis. The fits were excellent as judged from visual comparison of the observed

data and the calculated curves, and the standard error of the fits. The observed rate constants were taken as averages from the results of 8 - 12 kinetic traces. The basic equations[16] upon which these calculations are based are outlined in the following paragraphs.

In the developments that follows, the subscripts of zero and infinity will be used to indicate the initial and final conditions, respectively. To simplify the development, the reaction previously given as eq. 3.1, will be rewritten in terms of A, B, C, D,

$$A + B \rightarrow C + D \qquad (3.2)$$

where A is Fc or Dmfc, B is Cu(II), C is Fc^+ or $Dmfc^+$ and D is Cu(I). It is important to note that the absorbances of A and D at 616 nm are essentially zero. This is the case also at 280 nm because of the very low reagent concentrations used for the measurements at this wavelength.

For the pseudo-first-order conditions with $[B]_0 \geq 10 \times [A]_0$, the observed pseudo-first-order rate constant, k_{obs} and the concentration of A at any time during the reaction are related by eq. 3.3.

$$[A] = [A]_0 \exp(-k_{obs}t) \qquad (3.3)$$

According to mass action law, $[A] = [A]_0 - [C]$ and $[A]_0 = [C]_\infty$. Then eq. 3.3 can be rearranged to eq. 3.4.

$$[C] = [C]_\infty - [C]_\infty \exp(-k_{obs}t) \quad (3.4)$$

Applying Beer's law, the absorbances in a 1 cm cell initially, at any time, and at the end of reaction are given by $I_o = \varepsilon_B[B]_0$, $I = \varepsilon_B[B]_0 + \varepsilon_C[C]$ and $I_\infty = \varepsilon_B[B]_0 + \varepsilon_C[C]_\infty$ respectively. Then the concentrations [C] and $[C]_\infty$ are given by $[C] = (I - I_0)/\varepsilon_C$ and $[C]_\infty = (I_\infty - I_0)/\varepsilon_C$ respectively. Substitution for [C] and $[C]_\infty$ in eq. 3.4 and rearrangement gives eq. 3.5, which relates k_{obs} to the absorbance vs. time data.

$$I = I_\infty - (I_\infty - I_0)\exp(-k_{obs}t) \quad (3.5)$$

This equation also is applicable under conditions where $[A]_0 \geq 10 \times [B]_0$. The analysis to determine k_{obs} from eq. 3.5 was done using the least-squares program.

A Cary 219 spectrophotometer and the stopped-flow systems also were used to measure the rate for the reaction of Cu(II) triflate or nitrate with Fc and Dmfc under second-order conditions. For the Cary 219 runs, equal volumes of known concentrations of Cu(II) and the ferrocenes were manually transferred by syringes to a 2 cm optical cell. The absorbance change was then recorded immediately at 616 nm. The absorbance/time data were read off the chart paper and stored as data files on the 486 PC.

The expression for calculating the second-order rate constant, k_2, from the data is obtained by starting with the integrated rate law.

$$k_2 t = \frac{1}{[B]_0 - [A]_0} \ln\left(\frac{[A]_0}{[B]_0}\frac{[B]}{[A]}\right) \quad (3.6)$$

In order to express [B] and [C] in terms of the initial concentrations, one can use the stoichiometry relationship that $[C] = [A]_o - [A] = [B]_o - [B]$. Substitution for [A] from this relationship into eq. 3.6 and rearrangement yields eq. 3.7.

$$[B] = \frac{([B]_o - [A]_o)\frac{[B]_o}{[A]_o}\exp([B]_o - [A]_o)k_2 t}{\frac{[B]_o}{[A]_o}\exp([B]_o - [A]_o)k_2 t - 1} \tag{3.7}$$

This expression for [B] can now be substituted into the stoichiometry relationship for [C] and then rearrangement leads to eq. 3.8.

$$[C] = \frac{[B]_o\left[\exp([B]_o - [A]_o)k_2 t - 1\right]}{\frac{[B]_o}{[A]_o}\exp([B]_o - [A]_o)k_2 t - 1} \tag{3.8}$$

Thus, with B and C as the only absorbing species and the reaction occurring in a cell of pathlength *l*, the absorbance at any time of the reaction is given by

$$I = (\varepsilon_B[B] + \varepsilon_C[C])l \tag{3.9}$$

If $[B]_0 > [A]_0$, then ε_B and ε_C can be expressed in terms of the initial and final absorbances as shown by eq. 3.10 and 3.11:

$$\varepsilon_B = \frac{I_0}{[B]_0\, l} \tag{3.10}$$

$$\varepsilon_C = \frac{[B]_0 I_\infty - I_0([B]_0 - [A]_0)\, l}{[A]_0[B]_0\, l} \tag{3.11}$$

Then substitutions for the ε_B and ε_C in eq. 3.9 gives

$$I = \frac{I_0([B]_0 - [A]_0)\exp([B]_0 - [A]_0)k_2 t + \{[B]_0 I_\infty - I_0([B]_0 - [A]_0)l\}[\exp([B]_0 - [A]_0)k_2 t - 1]}{[B]_0 \exp([B]_0 - [A]_0)k_2 t - [A]_0} \tag{3.12}$$

The absorbance/time data were fitted to this equation by least-squares to extract k_2 values. A variable dead-time t_d and a blank absorbance I_b were allowed for in the least-squares program. The dead-time is added as a correction to time t to account for the time between when the reaction starts and when recording on the spectrophotometer starts. Five parameters, I_0, I_∞, k_2, t_d and I_b, are involved in the analysis, but I_0 and I_∞ were treated as invariants, by using the known values of ε_B and ε_C and the initial concentrations.

Results

Electronic spectra. The absorbances for the reactants Fc or Dmfc and Cu(II) and of the products Fc^+ or $Dmfc^+$ and Cu(I) were measured in the uv-visible region. At 280 nm the ε values (with triflate counterion) for Cu(II), Cu(I), Fc, Fc^+, Dmfc and $Dmfc^+$ in AN were found to be 32.7, 3.1, 756, 6.18×10^3, 1.65×10^3, and $1.25_5 \times 10^4$ M^{-1} cm^{-1}, respectively. This wavelength was used for monitoring the reaction of $(8.31 - 41.6) \times 10^{-5}$ M Cu(II) perchlorate with 8.17×10^{-6} M Fc and 8.02×10^{-6} M Dmfc in 95% AN.

In the visible region, the ε_{max} for Fc and Dmfc in AN are 95 and 102 M^{-1} cm^{-1} at

440 and 432 nm, respectively and neither species absorbs significantly above 600 nm. For Fc^+ and $Dmfc^+$, the ε_{max} are 482 and 357 M^{-1} cm^{-1} at 616 and 644 nm, respectively. These are in reasonable agreement with literature values of 513 at 617 nm[4] and 446 at 620 nm[17] for Fc^+, and 332 at 650 nm[18] for $Dmfc^+$. At 616 nm, the ε value for the $Dmfc^+$ ion in AN is 320 M^{-1} cm^{-1}. All these ε values show minor changes (± 10 M^{-1} cm^{-1}) with the % AN in 80, 90 and 95% AN.

The ε values for the Cu(II) ion in AN at 616 nm were found to be 3.65 and 14.1 M^{-1} cm^{-1} for the triflate and nitrate salts, respectively. The former agrees with the value of ~4 M^{-1} cm^{-1} determined by Funahashi and coworkers[13] These values decrease with decreasing % AN. In 95% AN, 80% AN and water, the ε values for the triflate salt are 2.21, 1.64 and 1.47 M^{-1} cm^{-1}, respectively. This trend also was observed by Funahashi and coworkers.[13] for 100 to 98.3% AN. The equivalent values for the nitrate salt are 4.92, 2.25, and 1.56 M^{-1} cm^{-1}, respectively. At 644 nm, the ε values for Cu(II) in AN are 6.81 and 24.4 M^{-1} cm^{-1} for the triflate and nitrate salts, respectively. For the reduced Cu(I) state, ε values in the visible region are negligible.

Kinetics and rate law. The kinetics generally involved observations of the formation of Fc^+ or $Dmfc^+$ at 616 nm. For the Dmfc there was no considerable advantage in carrying out the measurements at 644 nm because the higher ε values for Cu(II) offset to some extent the higher ε for $Dmfc^+$.

For the conditions of [Cu(II)] >> [Fc] or [Dmfc], the absorbance vs. time data gave excellent fits to eq. 3.5. The k_{obs} values increase linearly with [Cu(II)], indicating a first-order dependence on [Cu(II)]. A few runs under second-order conditions are fitted well by eq. 3.12 as shown in Appendix 3.1 and 3.2 for the reaction of 0.385 mM Cu(II)

and 0.208 mM Dmfc in 80% AN. This gives a second-order rate constant (k_2) of 28.5 ± 0.5 M^{-1} s^{-1}. As will be shown later in this Chapter (see Table 3.2), this k_2 value agrees well with the slopes of the plots of k_{obs} vs. [Cu(II)] in 80% AN. This indicates that the rate is first-order in the concentration of Cu(II) and the Fc species.

There are two minor complications with the rate law, which are illustrated in Figures 3.1 and 3.2. Figure 3.1 shows representative data for the reaction of Fc and Dmfc in 80% AN, and the effect of adding 0.202 mM $HClO_4$ in each. Without added acid, the plots tend to have a small positive intercept. Addition of acid lowers the k_{obs} and effectively eliminates the intercept, but does not affect the slope significantly.

Analogous observations can be made for the reaction of Fc in 95 % AN, shown in Figure 3.2. These data also show that runs on entirely different solutions are reasonably reproducible, and that the same effect of acid is observed with triflic or perchloric acids. The results in triflic acid are systematically slightly smaller than in perchloric acid, but the differences are within the normal day-to-day precision of the k_{obs} values. Because the triflic and perchloric acid concentrations are different, the similarity of the results suggests that the ion-pairing differences between triflate and perchlorate, observed in the Cu(I)-NMR study in Chapter 5, are not significant under the more dilute and partially aqueous conditions of the stopped-flow studies.

The most important result from the above observations is that the slopes of the k_{obs} vs. [Cu(II)] plots are essentially unaffected by the addition of acids. Therefore, the rate constant obtained from the slopes of such plots (equal to k_2 for the cross-reaction) is essentially independent of whether H^+ has been added or not.

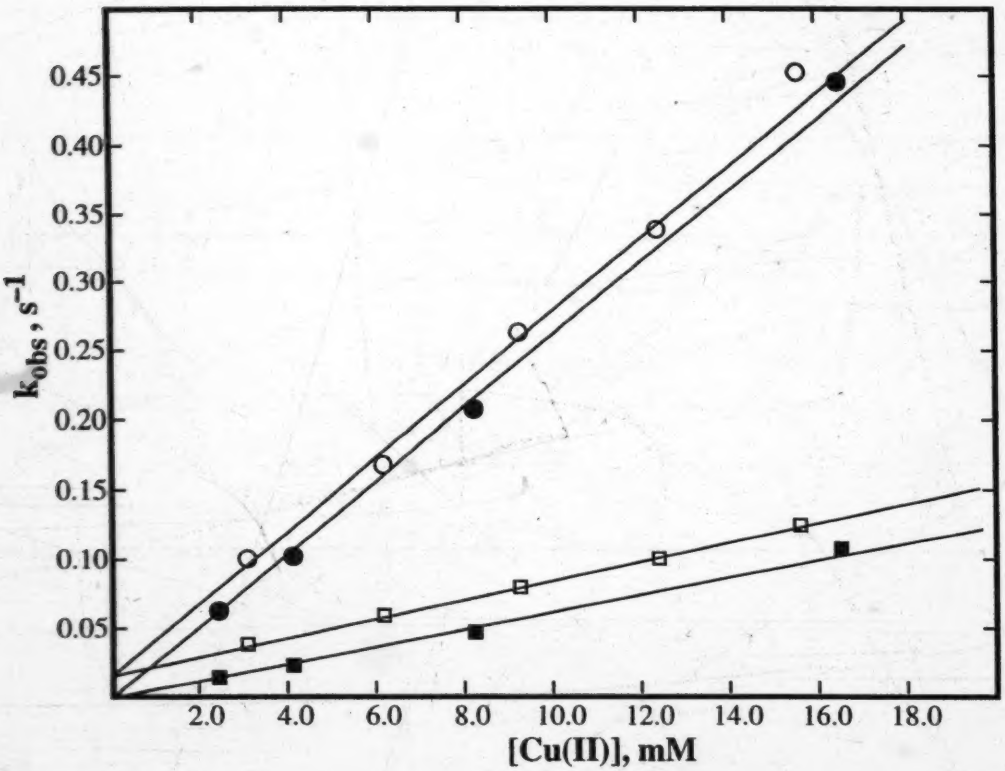

Figure 3.1. Plot of k_{obs} vs. [Cu(II)] for reactions of Cu(II) triflate in 80% AN at 25 °C and variable μ: with Fc (□) no H^+ added, (■) 0.202 mM $HClO_4$; with Dmfc (○) no H^+ added, (●) 0.202 mM $HClO_4$.

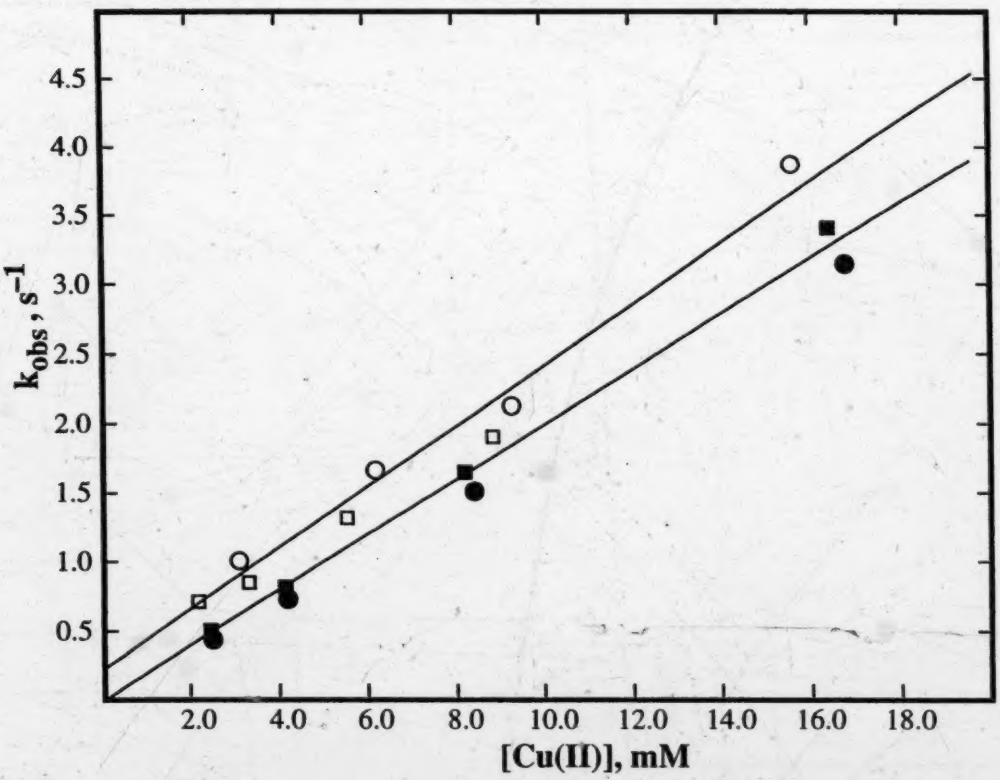

Figure 3.2. Plot of k_{obs} vs. [Cu(II)] for reactions of Cu(II) triflate in 95% AN at 25 °C and variable μ: with Fc (○, □) no H^+ added, (●) 0.423 mM triflic acid, (■) 0.285 mM perchloric acid.

The source of the H^+ effect on the intercept remains uncertain. It cannot be rapid proton equilibria involving either protonation of Fc or hydrolysis of $Cu(OH_2)^{2+}$ to $Cu(OH)^+$. Either of these would affect the concentration of Fc and Cu(II) and should then affect the slope of the k_{obs} vs. [Cu(II)] plots. Nonetheless, it has been shown that the spectrum of Fc is unaffected by the addition of H^+ (0.285 mM H^+ to 0.485 mM Fc in 95% AN and 0.202 mM H^+ to 1.63 mM Fc in 80% AN). It cannot be a systematic proportional error in [Cu(II)] but would have to be an additive error of ~2.0 mM. However, there is no reason that such an error would disappear on addition of H^+, because the stock solutions are prepared by the same general procedure whether or not acid is added.

One general possibility is the presence of some ubiquitous oxidant that gives a kinetic pathway first-order in [Fc] but independent of [Cu(II)]. The latter rules out some impurity being added together with the Cu(II). Since the absorbance vs. time profiles always appear to be first-order, the concentration of this oxidant must be $\geq 5 \times$ [Fc] ≈ 1 mM. This seems to rule out something being added with Fc, and it has been found that resublimed Fc does not change the observations.

An oxidant that might fit the requirements is dioxygen (O_2). Based on its solubility in water it would be present at 0.2-0.3 mM, and since it is a 4-electron oxidant if reduced to H_2O, its effective concentration is suitable. However, the oxidation of Fc by O_2 in aqueous AN is quite slow, as evidenced by the stability of the stock solutions. Therefore some catalyst for the reaction must be added along with the Cu(II). At this point it can only be suggested that the catalyst might be some form of hydrolyzed Fe(III), which might be converted to less active form by H^+. The Fe(III) species would be reduced to Fe(II) by Fc and the latter would be oxidized to Fe(III) by O_2 in a catalytic

cycle. The H^+ also might inhibit the latter reaction.

Cross-reaction rates constants. The pseudo-first-order rate constants, k_{obs}, for the measurements in 50, 80, 90, 95 and 97.5% AN were obtained by fitting the absorbance vs. time data to eq. 3.5. The k_{obs} are given in Table 3.1 (50% AN), Table 3.2 (80% AN), Table 3.3 (90% AN), Table 3.4 (95% AN) and Table 3.5 (97.5% AN). The k_{obs} values are averages of 8 - 12 kinetic runs, the error limits are one standard deviation of the average. These give an indication of the reproducibility of the rate constants for a particular set of conditions.

The k_{obs} also varied linearly with [Cu(II)] in all solvents studied and the plots of the k_{obs} vs. [Cu(II)] were used to obtain the second-order rate constants, k_2. These values are given in Tables 3.1 to 3.5 along with their standard deviations. The intercepts of these plots, together with their standard deviations, also are given in the Tables as footnotes.

Some k_2 values in Tables 3.1 to 3.5 were obtained using eq. 3.12 for second-order conditions. Tables 3.1 and 3.2 for the reactions in 50% and 80% AN also include values of k_{obs} and k_2 measured using a nitrate source for Cu(II). These values appear to agree with those obtained using the triflate salt. However, nitrate ion seemed to inhibit the reaction at higher % AN (see Chapter 4). The k_{obs} and k_2 values for the reaction with Cu(II) perchlorate are given in Table 3.4. The k_2 values are more than ~10% larger than the other values in the Table but this could be due to larger errors in the very low concentrations used.

Table 3.1. Kinetic Results for Reactions of Cu(II)[a] with Fc and Dmfc in 50% AN at 25 °C [b]

[Cu(II)],	Fe		Dmfc	
mM	$10^2 k_{obs}$, s^{-1}	k_2, $M^{-1} s^{-1}$	$10^2 k_{obs}$, s^{-1}	k_2, $M^{-1} s^{-1}$
2.19 [c]	1.34 ± 0.06	4.34 ± 0.07 [d]	5.26 ± 0.22	17.1 ± 0.6 [d]
3.66 [c]	1.94 ± 0.04		7.34 ± 0.22	
7.31 [c]	3.53 ± 0.10		14.0 ± 0.3	
14.6 [c]	6.79 ± 0.17		26.7 ± 0.7	
2.61 [e,f]	1.35 ± 0.07	3.95 ± 0.18 [g]	5.32 ± 0.24 [e]	15.0 ± 0.4 [g]
4.36 [e,f]	1.93 ± 0.03		7.73 ± 0.17	
8.71 [e,f]	3.64 ± 0.11		14.2 ± 0.3	
17.4 [e,f]	7.41 ± 0.29		28.0 ± 0.8	

[a] Triflate salt unless otherwise specified (variable μ). [b] No acid added. [c] Reductants: 0.198 mM Fc; 0.221 mM Dmfc. [d] k_{obs} vs. [Cu(II)] intercept: (3.76 ± 0.27) x 10^{-3} s^{-1} Fc; (13.8 ± 2.6) x 10^{-3} $HClO_4$Dmfc. [e] Nitrate salt. [f] Reductants: 0.219 mM Fc; 0.244 mM Dmfc. [g] k_{obs} vs. [Cu(II)] intercept: (2.82 ± 0.85) x 10^{-3} s^{-1} Fc; (13.2 ± 1.8) x 10^{-3} s^{-1} Dmfc.

Table 3.2. Kinetic Results for Reactions of Cu(II)[a] with Fc and Dmfc in 80% AN at 25 °C [b]

[Cu(II)],	Fc		Dmfc	
mM	$10^2 k_{obs}$, s^{-1}	k_2, $M^{-1} s^{-1}$	$10^2 k_{obs}$, s^{-1}	k_2, $M^{-1} s^{-1}$
2.48 [c]	1.30 ± 0.06	6.14 ± 0.4 [d]	6.09 ± 0.15	26.3 ± 0.9 [d]
4.13 [c]	2.23 ± 0.10		10.1 ± 0.2	
8.26 [c]	4.56 ± 0.09		20.6 ± 0.3	
16.5 [c]	10.6 ± 0.39		44.4 ± 0.7	
3.09 [e,f]	3.68 ± 0.19	6.84 ± 0.09 [g]	9.91 ± 0.46	26.4 ± 1.3 [g]
6.18 [e,f]	5.78 ± 0.17		16.6 ± 0.9	
9.27 [e,f]	7.79 ± 0.20		26.2 ± 1.8	
12.4 [e,f]	10.0 ± 0.2		33.7 ± 2.3	
15.6 [e,f]	12.4 ± 0.5		45.1 ± 2.3	
0.385 [e,h]				28.5 ± 0.5 [k]
0.505 [i,f]		6.22 ± 0.15 [k]		25.6 ± 0.5 [k]
2.52 [i,f]	1.32 ± 0.03	5.63 ± 0.26 [l]	5.09 ± 0.10	21.2 ± 0.4 [l]
5.05 [i,f]	2.62 ± 0.07		10.3 ± 0.3	
10.1 [i,f]	5.40 ± 0.11		20.9 ± 0.7	
15.0 [i,f]	8.81 ± 0.26		32.2 ± 0.4	

Table 3.2. (Continued)

[Cu(II)],	Fc		Dmfc	
mM	$10^2 k_{obs}$, s^{-1}	k_2, $M^{-1} s^{-1}$	$10^2 k_{obs}$, s^{-1}	k_2, $M^{-1} s^{-1}$
2.85 [e,i,m]			8.83 ± 0.31	24.2 ± 1.4 [n]
4.27 [e,i,m]			11.9 ± 0.2	
7.11 [e,i,m]			20.1 ± 0.7	
9.96 [e,i,m]			25.3 ± 1.3	
2.89 [e,i,o]	2.14 ± 0.09	5.00 ± 0.15 [n]		
5.77 [e,i,o]	3.46 ± 0.12			
10.1 [e,i,o]	5.71 ± 0.17			
14.4 [e,i,o]	8.04 ± 0.41			

[a] Triflate salt unless otherwise specified (variable μ). [b] In 0.202 mM $HClO_4$ unless otherwise specified. [c] Reductants: 0.232 mM Fc; 0.251 mM Dmfc. [d] k_{obs} vs. [Cu(II)] intercept: (-2.51 ± 1.44) x 10^{-3} s^{-1} Fc; (-5.23 ± 3.62) x 10^{-3} s^{-1} Dmfc. [e] No acid added. [f] Reductants: 0.266 mM Fc; 0.247 mM Dmfc. [g] k_{obs} vs. [Cu(II)] intercept: (15.5 ± 0.6) x 10^{-3} s^{-1} Fc; (14.4 ± 8.1) x 10^{-3} s^{-1} Dmfc. [h] Reductant: 0.208 mM Dmfc. [i] Nitrate salt. [j] In 0.254 mM $HClO_4$. [k] Calculated using eq. 3.12. [l] k_{obs} vs. [Cu(II)] intercept: (-1.22 ± 1.13) x 10^{-3} s^{-1} Fc; (-2.97 ± 1.53) x 10^{-3} s^{-1} Dmfc. [m] Reductant: 0.242 mM Dmfc. [n] k_{obs} vs. [Cu(II)] intercept: (6.74 ± 0.85) x 10^{-3} s^{-1} Fc; (1.87 ± 0.67) x 10^{-2} s^{-1} Dmfc. [o] Reductant: 0.254 mM Fc.

Table 3.3. Kinetic Results for Reactions of Cu(II) Triflate with Fc and Dmfc in 90% AN at 25 °C

[Cu(II)],	$[HClO_4]$,	Fc		Dmfc	
mM	mM	$10^2 k_{obs}$, s^{-1}	k_2, $M^{-1} s^{-1}$	$10^2 k_{obs}$, s^{-1}	k_2, $M^{-1} s^{-1}$
2.51 [a]	0.242	6.78 ± 0.11	23.8 ± 1.0 [b]	27.4 ± 0.5	110 ± 3 [b]
4.18 [a]	0.404	10.4 ± 0.2		44.9 ± 0.9	
8.35 [a]	0.808	19.9 ± 0.4		89.5 ± 2.2	
16.7 [a]	1.62	42.0 ± 1.5		189 ± 8	
2.34 [c]	0.0242	18.0 ± 0.2	21.4 ± 2.4 [d]	40.9 ± 0.7	98.4 ± 3.0 [d]
3.90 [c]	0.0404	21.0 ± 0.5		55.3 ± 1.8	
7.81 [c]	0.0808	27.2 ± 0.4		91.9 ± 1.8	
15.6 [c]	0.162	48.6 ± 1.0		175 ± 7	
2.33 [c]	0.0485	13.2 ± 0.2	21.3 ± 1.8 [e]	33.5 ± 0.5	101 ± 2 [e]
3.89 [c]	0.0808	15.8 ± 0.2		47.8 ± 0.9	
7.78 [c]	0.162	23.0 ± 0.3		87.3 ± 1.6	
15.7 [c]	0.323	43.5 ± 1.6		171 ± 6	

[a] Reductants: 0.223 mM Fc; 0.233 mM Dmfc (variable μ). [b] k_{obs} vs. [Cu(II)] intercept: (6.83 ± 4.09) x 10^{-3} s^{-1} Fc; (-6.53 ± 12.1) x 10^{-3} s^{-1} Dmfc. [c] Reductants: 0.219 mM Fc; 0.219 mM Dmfc. [d] k_{obs} vs. [Cu(II)] intercept: (12.5 ± 1.4) x 10^{-2} s^{-1} Fc; (17.4 ± 1.4) x 10^{-2} s^{-1} Dmfc. [e] k_{obs} vs. [Cu(II)] intercept: (7.79 ± 0.96) x 10^{-2} s^{-1} Fc; (9.43 ± 1.03) x 10^{-2} s^{-1} Dmfc.

Table 3.4. Kinetic Results for Reactions of Cu(II)[a] with Fc and Dmfc in 95% AN at 25 °C

[Cu(II)], mM	[H^+], mM	Fc		Dmfc	
		k_{obs}, s^{-1}	$10^{-2}k_2$, M^{-1} s^{-1}	k_{obs}, s^{-1}	$10^{-2}k_2$, M^{-1} s^{-1}
2.52 [b]	0.423 [c]	0.431 ± 0.004	1.85 ± 0.04 [d]	2.09 ± 0.06	8.72 ± 0.09 [d]
4.20 [b]	0.423 [c]	0.722 ± 0.018		3.56 ± 0.06	
8.39 [b]	0.423 [c]	1.49 ± 0.044		7.30 ± 0.15	
16.8 [b]	0.423 [c]	3.13 ± 0.14		14.4 ± 0.4	
2.68 [e]	0.0254 [c]	0.728 ± 0.067	1.78 ± 0.13 [f]	2.69 ± 0.04	7.94 ± 0.21 [f]
4.47 [e]	0.0423 [c]	0.975 ± 0.019		4.06 ± 0.09	
8.94 [e]	0.0846 [c]	1.73 ± 0.06		7.90 ± 0.18	
17.9 [e]	0.169 [c]	3.62 ± 0.11		14.5 ± 0.6	
2.52 [g]	0.0635 [c]	0.561 ± 0.010	1.85 ± 0.03 [h]	2.38 ± 0.61	7.95 ± 0.24 [h]
4.21 [g]	0.106 [c]	0.854 ± 0.023		3.89 ± 0.10	
8.41 [g]	0.212 [c]	1.64 ± 0.02		7.18 ± 0.17	
16.8 [g]	0.423 [c]	3.22 ± 0.10		13.5 ± 0.7	
2.46 [i]	0.285	0.491 ± 0.014	2.03 ± 0.05 [j]	2.27 ± 0.06	8.29 ± 0.33 [j]
4.11 [i]	0.285	0.800 ± 0.019		3.78 ± 0.09	
8.21 [i]	0.285	1.63 ± 0.05		7.32 ± 0.15	
16.4 [i]	0.285	3.38 ± 0.06		13.4 ± 0.5	

Table 3.4. (Continued)

[Cu(II)],	$[H^+]$ [a]	Fc		Dmfc	
mM	mM	k_{obs}, s^{-1}	$10^{-2}k_2$, M^{-1} s^{-1}	k_{obs}, s^{-1}	$10^{-2}k_2$, M^{-1} s^{-1}
2.64 [k]	0.186	0.494 ± 0.007	1.95 ± 0.09 [l]	2.41 ± 0.12	8.42 ± 0.19 [l]
5.27 [k]	0.371	0.944 ± 0.015		4.74 ± 0.09	
10.5 [k]	0.742	2.00 ± 0.04		9.21 ± 0.21	
19.8 [k]	1.39	3.99 ± 0.09		16.5 ± 1.3	
0.0831 [m,n]	1.00	0.0430 ± 0.0063	2.43 ± 0.24 [o]	0.0993 ± 0.0088	10.4 ± 0.52 [o]
0.166 [m,n]	2.00	0.0709 ± 0.0104		0.180 ± 0.016	
0.249 [m,n]	3.00	0.0836 ± 0.0232		0.259 ± 0.033	
0.416 [m,n]	5.00	0.122 ± 0.005		0.465 ± 0.024	

[a] Triflate salt, $HClO_4$ acid unless otherwise specified (variable μ). [b] Reductants: 0.240 mM Fc; 0.255 mM Dmfc. [c] Triflic acid. [d] k_{obs} vs. [Cu(II)] intercept: (-3.98 ± 1.65) x 10^{-2} s^{-1} Fc; (-10.2 ± 3.6) x 10^{-2} s^{-1} Dmfc. [e] Reductants: 0.257 mM Fc; 0.274 mM Dmfc. [f] k_{obs} vs. [Cu(II)] intercept: (22.2 ± 6.7) x 10^{-2} s^{-1} Fc; (56.1 ± 10.2) x 10^{-2} s^{-1} Dmfc.

[g] Reductants: 0.244 mM Fc; 0.255 mM Dmfc. [h] k_{obs} vs. [Cu(II)] intercept: (9.03 ± 1.19) x 10^{-2} s^{-1} Fc; (42.1 ± 10.5) x 10^{-2} s^{-1} Dmfc. [i] Reductants: 0.242 mM Fc; 0.254 mM Dmfc. [j] k_{obs} vs. [Cu(II)] intercept: (-1.44 ± 1.95) x 10^{-2} s^{-1} Fc; (27.5 ± 13.7) x 10^{-2} s^{-1} Dmfc. [k] Reductants: 0.239 mM Fc; 0.254 mM Dmfc. [l] k_{obs} vs. [Cu(II)] intercept: (-3.27 ± 3.86) x 10^{-2} s^{-1} Fc; (21.1 ± 9.0) x 10^{-2} s^{-1} Dmfc. [m] Perchlorate salt. [n] Reductants: 0.00817 mM Fc; 0.00802 mM Dmfc. [o] k_{obs} vs. [Cu(II)] intercept: (2.44 ± 0.43) x 10^{-2} s^{-1} Fc; (1.17 ± 0.77) x 10^{-2} s^{-1} Dmfc.

Table 3.5. Kinetic Results for Reactions of Cu(II) Triflate with Fc and Dmfc in 97.5% AN at 25 °C [a]

[Cu(II)],	Fc		Dmfc	
mM	k_{obs}, s^{-1}	$10^{-3}k_2$, M^{-1} s^{-1}	k_{obs}, s^{-1}	$10^{-3}k_2$, M^{-1} s^{-1}
2.04 [b,c]	7.50 ± 0.13	1.97 ± .05 [d]	24.6 ± 0.7	7.78 ± 0.38 [d]
4.08 [b,c]	11.8 ± 0.3		41.7 ± 2.2	
6.11 [b,c]	15.7 ± 0.4		58.3 ± 3.3	
8.15 [b,c]	19.3 ± 0.3		69.9 ± 3.9	
1.98 [e]	4.77 ± 0.08	1.79 ± 0.07 [f]	18.9 ± 0.8	8.07 ± 0.26 [f]
2.97 [e]	6.84 ± 0.12		26.9 ± 1.0	
4.94 [e]	10.3 ± 0.3		41.5 ± 1.2	
7.91 [e]	15.2 ± 0.7		68.2 ± 2.9	

[a] In 0.202 mM $HClO_4$ unless otherwise specified (variable μ). [b] Reductants: 0.204 mM Fc; 0.201 mM Dmfc. [c] No acid added. [d] k_{obs} vs. [Cu(II)] intercept: 3.54 ± 0.22 s^{-1} Fc; 9.05 ± 1.46 s^{-1} Dmfc. [e] Reductants: 0.200 mM Fc; 0.205 mM Dmfc. [f] k_{obs} vs. [Cu(II)] intercept: 1.31 ± 0.23 s^{-1} Fc; 2.83 ± 0.83 s^{-1} Dmfc.

Discussion

Cu(II/I) self-exchange in AN/water. It has been shown that the cross-reactions are first-order in each of the reactants with no consequential additional term and the k_2 values in Tables 3.1 to 3.5 will be used in the further analysis to estimate the Cu(II/I) self-exchange rate by the Marcus cross-relationship. The cross-relationship, including the so-called work term corrections[19] is given by eq. 3.13;

$$k_{12} = (k_{11}k_{22}K_{12}f_{12})^{1/2} W_{12} \tag{3.13}$$

where $k_{12} = k_2$ for the present systems and k_{11} and k_{22} are the self-exchange rate constants of the Cu(II/I) and Fc/Fc^+ or $Dmfc/Dmfc^+$ couples, respectively. K_{12} is the equilibrium constant, and it can be obtained from the potential difference for the reaction as described in Chapter 1. The nonlinear correction term f_{12}, and electrostatic work term involved in bringing reactants into outer-sphere contact, W_{12}, are given by eq. 3.14 and 3.15.

$$\ln f_{12} = \frac{\left[\ln K_{12} + \left(\frac{-w_{21}}{RT}\right)\right]^2}{4\left[\ln \frac{k_{11}k_{22}}{Z^2} + \frac{w_{11}}{RT}\right]} \tag{3.14}$$

$$\ln W_{12} = \frac{-(w_{21} - w_{11})}{2RT} \tag{3.15}$$

where Z is a collision number (taken to be 10^{11} M^{-1} s^{-1}), R is the gas constant in kcal mol^{-1} K^{-1}, T is the temperature in Kelvin and w_{ij} (kcal mol^{-1}) are the individual work terms which are calculated from eq. 3.16.

$$w_{ij} = \frac{z_i z_j e^2}{\varepsilon_s r\,(1 + r\sqrt{8\pi N e^2 \mu/(10^3 \varepsilon_s k_b T)})} = \left[\frac{331.7\, z_i z_j}{\varepsilon_s r\,(1 + r\sqrt{8.497\mu/\varepsilon_s})}\right]_{T = 298\,K} \qquad (3.16)$$

where z_i and z_j are the charges on the reactants, N is Avogadro's number, *e* is the electron charge, r is the center to center distance (Å) in the outer-sphere transition state, ε_s is bulk solvent dielectric constant, μ is the ionic strength (M) and k_b is the Boltzmann constant. For the present systems, the charge product $z_i z_j = 0$ for w_{12} and w_{22}, so that these terms are zero. For w_{21} and w_{11}, the charge products are 1 and 2 respectively.

It has been noted that reduction potentials for the Cu(II/I) and Fc/Fc^+ couples in AN and AN/water mixtures at 25 °C and ionic strength of 0.1 M ($NaClO_4$) are published.[2] From formal potentials for various ferrocenes reported recently by Nelsen et al.[20], the value for $Dmfc/Dmfc^+$ in AN at 25 °C and ionic strength of 0.1 M (n-Bu_4NClO_4) is deduced to be -0.11 V vs. Fc/Fc^+. Reduction potentials measured by Noviandri et al.[21] in various solvents show that the differences between the potential for methylsubstituted ferrocene and that for ferrocene are approximately constant (~0.05 V per CH_3 group) in many of the solvents. Thus, the -0.11 V value for $Dmfc/Dmfc^+$ vs. Fc/Fc^+ at 25 °C in AN[20] also has been assumed in the AN/water mixtures. Therefore, ΔE^0 values for the cross-reaction in the various AN/water mixtures are 0.164, 0.197, 0.242, 0.348, 0.460 V for Fc and 0.274, 0.307, 0.352, 0.458, 0.570 V for Dmfc in 50, 80, 90, 95,

97.5% AN respectively.

The self-exchange rate constants (k_{22}'s) for the Fc/Fc^+ and $Dmfc/Dmfc^+$ couples have been determined in various solvents by several workers.[3-5] In AN, the range in k_{22} values is ~9 x 10^6 M^{-1} s^{-1} at 25 °C and (5-30) x 10^6 M^{-1} s^{-1} in all the solvents. Therefore the factor of 1-3 variation of k_{22} with solvent is small and is consistent with the recent suggestion by Swaddle and coworkers[22] that differences in k_{22} for ferrocene and decamethylferrocene in acetone, methylene chloride and acetonitrile can be explained on the basis of the reactant size differences, without reference to solvent dynamics. It therefore seems that constant k_{22} values for Fc and Dmfc can reasonably be assumed in the AN/water solvents.

The only study on the $Dmfc/Dmfc^+$ couple, by Yang, Chan and Wahl[3], reported a k_{22} value at 25 °C of 8.3 x 10^6 M^{-1} s^{-1} (μ = 0.016 M). However, the k_{22} value of 5.3 x 10^6 M^{-1} s^{-1} (μ = 0.035 M) for the Fc^+/Fc couple determined by these authors is somewhat smaller than that reported later by Kirchner et al.[4] (k_{22} = 9.3 x 10^6 M^{-1} s^{-1}, μ = 0) and McManis et al.[5] (k_{22} = 9.1 x 10^6 M^{-1} s^{-1}, μ = 0.65 M). Nonetheless, the finding by Yang, Chan and Wahl[3] that the k_{22} value for Dmfc is slightly larger than that for Fc is consistent with the findings that k_{22} values for decamethylferrocene are ~4-7 times larger than for Fc.[3,23] It seems that the k_{22} value for Dmfc should be 1-1.5 times larger than that for Fc. For the present work, it will be assumed that this difference is not significant so that the same k_{22} for Dmfc and Fc can be used.

The self-exchange values by Kirchner et al.[4] and McManis et al.[5] given earlier suggest that k_{22} is essentially independent of ionic strength, as might be expected for the self-exchange reaction where one of the reactants is always neutral. The Kirchner et al.[4]

value of 9.3×10^6 $M^{-1}s^{-1}$ at zero ionic strength will be used in this study.

The foregoing information will now be used to test conformity of the Cu(II)-ferrocenes reaction to the predictions of the Marcus theory. The cross-relationship (eq. 3.13) is given in logarithmic form by eq. 3.17.

$$\log k_{12} = 0.5(\log (k_{11}k_{22}) + \log K_{12} + \log f_{12}) + \log W_{12} \qquad (3.17)$$

Substitution for $0.5\log K_{12} = 0.5(nF\Delta E^0/2.303RT) = 8.5\Delta E^0$ into eq. 3.17 gives eq. 3.18.

$$\log k_{12} = 0.5\log (k_{11}k_{22}) + 8.5\Delta E^0 + 0.5\log f_{12} + \log W_{12} \qquad (3.18)$$

In order to test if the Marcus cross-relationship works at all, it is common practice to assume that the sum of the $\log f_{12}$ and $\log W_{12}$ contributions is small, or relatively constant compared to other terms in eq. 3.18. Then it is predicted that a plot of $\log k_{12}$ vs. ΔE^0 should be linear with a slope of 8.5 and an intercept at $\Delta E^0 = 0$ of $\sim 0.5\log (k_{11}k_{22})$. This plot is shown in Figure 3.3. The slope of 8.5 ± 0.3 is in excellent agreement with the prediction. The intercept of -0.89 and k_{22} of 9.3×10^6 M^{-1} s^{-1} gives $k_{11} \approx 1.7 \times 10^{-9}$ M^{-1} s^{-1}.

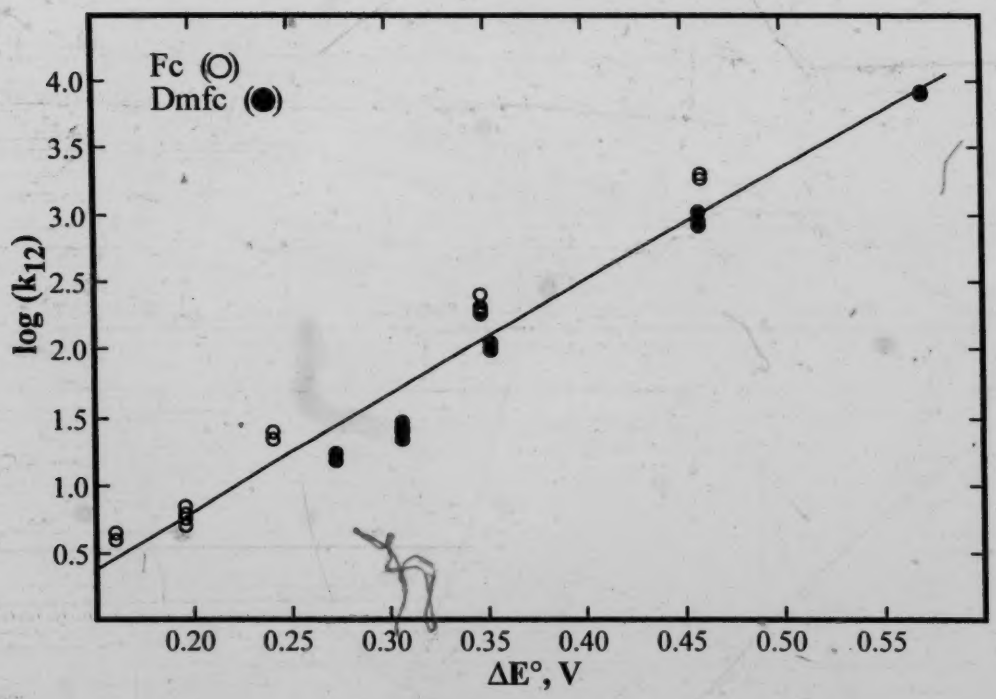

Figure 3.3. Plot of log k_{12} vs. ΔE^0 for the cross-reaction of Cu(II) with Fc (○) and Dmfc (●) at 25 °C and variable μ. The solid line represents a linear fit of all data and has a slope of 8.5 ± 0.3 and intercept value of -0.89 ± 0.11.

Since the slope in Figure 3.3 conforms so well to the prediction of Marcus theory, it seems worthwhile to examine the effect of the work term factors w_{21} and w_{11}. In order to calculate these, it is necessary to estimate the radii of the species involved. The radii for $Cu(NCCH_3)_4^{2+}$ and $Cu(NCCH_3)_4^{+}$ are estimated from the structures in Chapter 2 to be 6.0 and 6.02 Å, respectively. The radii for Fc and Dmfc have been estimated by Murguia and Wherland[24] as 3.8 and 4.3 Å, respectively. The corresponding values for Fc^+ and $Dmfc^+$ are assumed to be 0.05 Å smaller than their reduced forms.[16] These values, along with the dielectric constants for AN/water mixtures reported by Venables and Schmuttenmaer[25] can be used to estimate w_{21} and w_{11} from eq. 3.16. Then W_{12} and f_{12} can be calculated from eq. 3.15 and 3.14, respectively. The estimate of f_{12} also has used the k_{11} determined from the simplified treatment, and a typical ionic strength of 0.03 M has been used for the work terms.

The results of the above calculations are summarized in Table 3.6. In addition, values of k_{11} have been calculated from eq. 3.19, which is a rearranged form of eq. 3.18.

$$\log k_{11} = 2\log k_{12} - \log k_{22} - \log K_{12} - \log f_{12} - 2\log W_{12} \qquad (3.19)$$

The uncorrected k_{11}, omitting f_{12} and W_{12} terms, also are given in Table 3.6.

The log W_{12} is a relatively constant and a small correction. The main effect of the corrections lies in f_{12} which becomes increasingly significant as the % AN increases. This is primarily due to the corresponding increase in K_{12}. The individual work terms w_{21} and w_{11} make small contributions to the magnitude of f_{12}. As a result, uncertainties of ± 0.5 Å in the sum of the reactants' radii have an insignificant effect on f_{12}.

Table 3.6. Experimental and Calculated Parameters in the Marcus Cross-Relationship for the Reactions of Cu(II) with Fc and Dmfc at 25 °C

% AN	log k_{12} [a]	log K_{12} [b]	log W_{12} [c]	log f_{12} [d]	log k_{11} [e]	log k_{11} [f]
			Fc			
50	0.618	2.773	0.064	-0.068	-8.51	-8.57
80	0.776	3.332	0.077	-0.10	-8.75	-8.81
90	1.346	4.093	0.083	-0.15	-8.37	-8.38
95	2.297	5.885	0.087	-0.33	-8.26	-8.11
97.5	3.274	7.779	0.090	-0.59	-8.20	-7.79
			Dmfc			
50	1.207	4.634	0.073	-0.21	-9.19	-9.13
80	1.405	5.192	0.088	-0.26	-9.35	-9.27
90	2.013	5.953	0.096	-0.34	-8.90	-8.75
95	2.936	7.745	0.099	-0.59	-8.84	-8.45
97.5	3.899	9.640	0.10	-0.93	-8.81	-8.09

[a] Averages of the k_2 values from Tables 3.1 to 3.5 (variable μ). [b] Calculated using ΔE^0 for the reactions. [c] Calculated using the dielectric constants from reference 25, radii of the reacting species in the text and $\mu = 0.03$ M. [d] Calculated using $k_{22} = 9.3 \times 10^6$ M^{-1} s^{-1} and $k_{11} = 1.7 \times 10^{-9}$ M^{-1} s^{-1}. [e] Calculated without the f_{12} and W_{12} corrections. [f] Calculated with the f_{12} and W_{12} corrections.

If the results are fitted perfectly by the theory, then the calculated k_{11} values in Table 3.6 should be the same for the Fc and Dmfc systems. In fact, the latter values are 2-4 times smaller. However, this is a small factor within the commonly accepted factor of 10 for agreement between Marcus theory and experiment. To illustrate the danger in over interpreting such differences, it should be noted that the two systems do agree if ΔE^0 for Dmfc is 0.08 V instead of 0.11 V larger than that for Fc.

The uncorrected k_{11} values are essentially independent of the solvent composition. However, the f_{12} correction suggests a trend towards increasing k_{11} with increasing % AN. The "trend" is a small effect within the uncertainties of the theory, but could be ascribed to a change in Cu(II) species at the higher % AN. However, it might also be due to uncertainties in ΔE^0 because the electrochemical measurements were at 0.10 ionic strength whereas the kinetics were in the 0.01 to 0.05 M range. Sample calculations reveal that a 0.04 V increase in ΔE^0 in 97.5% AN essentially removes the appearance of a trend in both systems.

The overall conclusion of this analysis is that the kinetic results are quite consistent with the Marcus theory and yield a self-exchange rate constant for Cu(II/I) in aqueous AN of ~5 x 10^{-9} M^{-1} s^{-1}. This suggests a half-time of ~1.6 x 10^3 days or 4.4 years for 1 M concentrations of Cu(II) and Cu(I) and 10^2 times longer for 0.1 M concentrations. It seems unlikely then that anyone will have the patience to study the reaction by any direct method.

The k_{11} values in Table 3.6 may be compared to the magnitude of 10^{-7} M^{-1} s^{-1} for $Cu(II/I)_{(aq)}$ obtained previously by Sisley and Jordan[8] and other researchers.[7] By the standards of the Marcus theory, the k_{11} values from the present study are not greatly

different from those for the aqueous couple.

The k_{11} values for Cu(II/I) solvates in AN and water are very small compared to those of Cu(II/I)L_n complexes, with derivatives of bipyridyl and 1,10-phenanthroline as ligands.[26] Thus, structural changes in the solvated systems seem to be greater than for these complexes, but it should be noted that, even in structurally similar complexes, such as Cu(II/I)$(bib)_2$ (bib = 2,2'-bis(2-imidazolyl)biphenyl)[27] the k_{11} value is smaller than for systems that appear to require greater structural changes.[26] Rorabacher[26] has developed a "square-scheme" that emphasizes structural conformation, before electron-transfer, for Cu(II/I)L_n systems. Differences in k_{11} values from Cu(II) reduction and Cu(I) oxidation cross-reactions are taken as evidence of contribution from conformation changes. As shown in the Introduction, k_{11} values from Cu(II) reduction and Cu(I) oxidation cross-reactions are similar for the aqueous Cu(II/I) system. The same might be expected for k_{11} values in AN and also for Cu(II)$(OH_2)_n(NCCH_3)_{6-n}$/Cu(I)$(NCCH_3)_{4-m}(OH_2)_m$[13,14] systems that may exist in solution, as the % AN is increased. The fairly constant k_{11} values for the latter, as indicated by these studies, suggest that the structural barrier is similar in all.

Cu(II/I) self-exchange in 100% AN. Since the Cu(II)–ferrocenes cross-reactions appeared too fast to measure in 100% AN, it is of interest to determine if this is predicted by the k_{11} value of ~5 x 10^{-9} M^{-1} s^{-1}. The ΔE^0 values at 25 °C and ionic strength of 0.10 M for the reduction of Cu(II) by Fc and Dmfc in 100% AN are 0.646 V and 0.756 V, respectively.[2,20] These give log K_{12} values of 10.9 and 12.8 for Cu(II) reaction with Fc and Dmfc, respectively. Then the K_{12} values, and the k_{22} = 9.3 x 10^6 M^{-1} s^{-1} and appropriate values of f_{12} and W_{12} can be used to estimate k_{12} in 100% AN. The k_{12} values

obtained using eq. 3.17 are 2 x 10^4 and 1 x 10^5 M^{-1} s^{-1} for Fc and Dmfc, respectively. These values suggest half-lives of ~12 and ~2 ms for ~3 x 10^{-3} M concentrations of Cu(II). These time-scales are consistent with the indications that rates in 100% AN are too fast, in agreement with the observations.

Conclusion

An estimation of the electron self-exchange rate constant for Cu(II/I)-AN system has been made from an application of the Marcus cross-relationship, using rate constants for the reactions of Cu(II) with Fc and Dmfc in AN/water mixtures. The cross-reaction rate constants for the various % AN conform so well to the predictions of the cross relationship and yields a Cu(II/I) self-exchange rate constant of ~5 x 10^{-9} M^{-1} s^{-1}. There is no indication of any significant trend or variation of the rate constant with increasing % AN. Therefore, the same value of ~5 x 10^{-9} M^{-1} s^{-1} is predicted for the rate constant in pure AN, and the $k_{11} \geq 0.3$ M^{-1} s^{-1} from the study of Manahan[28] is likely to be much too large. As pointed out in Chapter 1, Manahan's value may be affected by separation-induced exchange.

The results of the aqueous AN systems and those of the aqueous systems that were described in the introductory section leads to the conclusion that the rate is so slow that it may never be determined in these solvents by direct methods. As discussed in Chapter 1, and indicated by the structure study in Chapter 2, the Cu(II) ion may be 5- or 6-coordinate and tetragonal while Cu(I) is 4-coordinate and tetrahedral. A significant portion of Cu(I) in AN at 25 °C may be 3-coordinate as suggested by the Cu(I)-63 NMR studies in Chapter 5. Thus, the structural reorganization barrier is substantial for these systems.

References

(1) Ahrland, S.; Nilsson, K.; Tagesson, B. *Acta Chem. Scand* **1983**, *37A*, 193.

(2) Cox, B. G.; Jedral, W.; Palou, J. *J. Chem. Soc., Dalton Trans.* **1988**, 733.

(3) Yang, E. S.; Chan, M.-S.; Wahl, A. C. *J. Phys. Chem.* **1980**, *84*, 3094.

(4) Kirchner, K.; Dang, S.-Q.; Stebler, M.; Dodgen, H. W.; Wherland, S.; Hunt, J. P. *Inorg. Chem.* **1989**, *28*, 3604.

(5) McManis, G. E.; Nielson, R. M.; Gochev, A.; Weaver, M. J. *J. Am. Chem. Soc.* **1989**, *111*, 5533, and references there in.

(6) Hoselton, M. A.; Lin, C.-T.; Schwartz, H. A.; Sutin, N. *J. Am. Chem. Soc.* **1978**, *100*, 2383.

(7) Davies, K. M. *Inorg. Chem.* **1983**, *22*, 615.

(8) Sisley, M. J.; Jordan, R. B. *Inorg. Chem.* **1992**, *31*, 2880.

(9) Martin, M. J.; Endicott, J. F.; Ochrymowycz, L. A.; Rorabacher D. B. *Inorg. Chem.* **1987**, *26*, 3012.

(10) Parker, O. J.; Espenson, J. H. *Inorg. Chem.* **1969**, *8*, 185. Shaw, K.; Espenson, J. H. *Inorg. Chem.* **1968**, *7*, 1619.

(11) Hathaway B. J.; Billing, D. E. *Coord. Chem. Rev.* **1970**, *5*, 143. Hathaway B. J. *Coord. Chem. Rev.* **1981**, *35*, 211. Persson, I.; Persson, P.; Sandström, M.; Ullström, A.-S. *J. Chem. Soc., Dalton Trans.* **2002**, 1256, and references therein.

(12) Quirk, P. F.; Kratochvil, B. *Anal. Chem.* **1970**, *42*, 492. Kratochvil, B.; Al-Daher, I. M. *Talanta* **1980**, *27*, 989.

(13) Inamo, M.; Kamiya, N.; Inada, Y.; Nomura, M.; Funahashi, S. *Inorg. Chem.* **2001**, *40*, 5636.

(14) Kamau, P.; Jordan, R. B. *Inorg. Chem.* **2001**, *40*, 3879.

(15) Kolthoff, I. M.; Sandell, E. B.; Meehan E. J.; Bruckenstein, S. *Quantitative Chemical Analysis*, Collier-MacMillan Canada Ltd., Toronto, **1969**.

(16) Jordan, R. B. *Reaction Mechanisms of Inorganic and Organometallic Systems*, Oxford University Press, New York, **1998**.

(17) Yang, E. S.; Chan, M.-S.; Wahl, A. C. *J. Phys. Chem.* **1975**, *79*, 2049.

(18) Pladziewicz, J. R.; Brenner, M. S.; Rodeberg, D. A.; Likar, M. D. *Inorg. Chem.* **1985**, *24*, 1450.

(19) Sutin, N. *Acc. Chem. Res.* **1982**, *15*, 275.

(20) Nelsen, S. F; Chen, L-J; Ramm, M. T.; Voy, G. T.; Powell, D. R.; Accola, M. A.; Seehafer, T. R.; Sabelko, J. J.;. Pladziewicz, J. R. *J. Org. Chem.* **1996**, *61*, 1405.

(21) Noviandri, I.; Brown, K. N.; Fleming, D. S.; Gulyas, P. T.; Lay, P. A.; Masters, A. F.; Phillips, L. *J. Phys. Chem. B.* **1999**, *103*, 6713.

(22) Zahl, A.; van Eldik, R.; Matsumoto, M.; Swaddle, T. W. *Inorg. Chem.* **2003**, *42*, 3718.

(23) Nielson, R. M.; McManis, G. E.; Safford, L. K.; Weaver, M. J. *J. Phys. Chem.* **1989**, *93*, 2152.

(24) Murguia, M. A.; Wherland, S. *Inorg. Chem.* **1991**, *30*, 139.

(25) Venables, D. S.; Schmuttenmaer, C. A. *J. Chem. Phys.* **1998**, *108*, 4935.

(26) Rorabacher, D. B. *Chem. Rev.* **2004**, *104*, 651, and references therein.

(27) Xie, B.; Wilson, L. J.; Stanbury, D. M. *Inorg. Chem.* **1999**, *38*, 12.

(28) Manahan, S. E. *Can. J. Chem.* **1967**, *45*, 2451.

Chapter 4. Nitrate and Chloride Effects on the Cu(II)-Ferrocenes Reactions

Introduction

As noted in Chapter 3, rates of the Cu(II)-ferrocenes cross-reaction appeared to be slower in 95% AN when the Cu(II) source was the nitrate salt, than when the source was triflate or perchlorate. However, there was no detectable effect for ≤ 80% AN. As pointed out in Chapter 1, anion effects on electron-transfer reactions are not uncommon, and a nitrate inhibition of the reaction of $Co(dmg)_3(BF)_2^+$ (dmg = dimethylglyoximate) with ferrocene in methylene chloride,[1] was noted therein. The study in this Chapter was undertaken to investigate the effects of adding nitrate to the reagent solutions. Since the chloride ion is known to show both catalytic[2,3,4,5] and inhibitive[1] effects on rates of electron-transfer, it was included in this study for comparison with the nitrate ion.

There are several recognized explanations for kinetic effects of non-reacting counterions. If the ionic strength is not controlled, as in this study, then the effect could be due to the change in activity coefficient(s) with ionic strength. This effect can be accommodated by classical Debye-Hückel theory,[6,7] as given by eq. 4.1,

$$\log k_\mu = \log k_{\mu=0} + \frac{2Az_1z_2\sqrt{\mu}}{1+\alpha B\sqrt{\mu}} \qquad (4.1)$$

where z_i is the charge of the ions, A and B are calculable Debye-Hückel parameters, α is the average effective diameter of the ions, and μ is the ionic strength. The effect of the latter should be minimal here because one of the reactants has zero charge.

The lower dielectric constant of AN compared to water raises the possibility of

anion-cation pairing as being significant. Ion-pairs are commonly designated as $\{MS_n^{z+} \bullet X^{z-}\}$, where S is solvent or some other ligand and X is the anion. As an example of ion-pair effects, Wherland and coworkers[1] found ion-paired pathways accounted for the effects of BF_4^- and PF_6^- ions on the reaction of $[Co(dmg)_3(BF)_2]BF_4$ with ferrocene in AN. Details of ion-pair effects on electron-transfer reactions are given in recent articles by Wherland[8] and Marcus.[9]

A third explanation involves coordination of the anion X to the metal to form an inner-sphere complex, $\{MS_{n-1}X\}$. The effect is stoichiometrically equivalent to ion-pairing when S is the solvent, and is always a possibility when one of the reaction partners is substitutionally labile, as is Cu(II)[10] in the present case. Effects of inner-sphere complex formation have been observed in aqueous solution in the electron-transfer reactions of Cu(II) with $Co(sep)^{2+}$ (sep = sepulchrate),[2] ascorbic acid,[3,4] and ferrocytochrome *c*.[5] Neutral imidazole ligands also were found to affect the rate of electron-transfer in the Cu(II)/$Co(sep)^{2+}$ system, and were attributed to inner-sphere coordination of imidazole to the aqua Cu(II) ion.[2]

It can be difficult to distinguish between ion-pairing and inner-sphere complex formation effects. Because both phenomena involve Cu(II), they will have parallel effects on the oxidation of ferrocene (Fc) and 1,1′-dimethylferrocene (Dmfc). Both effects should increase with increasing % AN, because the lower dielectric constant favors ion-pairing, and the weaker coordination power of AN compared to H_2O favors anion coordination. In certain circumstances, the two possibilities may be distinguished on the basis of the magnitude of the formation constant. If the monitoring method does not distinguish ion-pairing and coordination, then the experimental equilibrium constant

(K_{exp}) is related to the ion-pair equilibrium constant (K_i) and the complex formation constant (K_f) by $K_{exp} = K_i + K_f$. The K_i value can be estimated with a hard sphere electrostatic model and is $< 10^2$ for +2/-1 ions in AN/H_2O mixtures. If K_{exp} is much larger than this estimate, then inner-sphere coordination (K_f) is commonly assumed to be predominant.

The consequences of inner-sphere complex formation can be demonstrated by use of the reactions in Scheme 4.1. This scheme shows the relation between inner-sphere complex equilibria and the electron-transfer reactions of solvated Cu(II) or Cu(I) and of the inner-sphere complex species $Cu(II)X_n$ or $Cu(I)X_n$ (where X is the anion) with the outer-sphere[11,12] reductants $Fe(C_5H_4R)_2$ (R = H, CH_3). The solvent ligands are omitted for simplicity.

Scheme 4.1

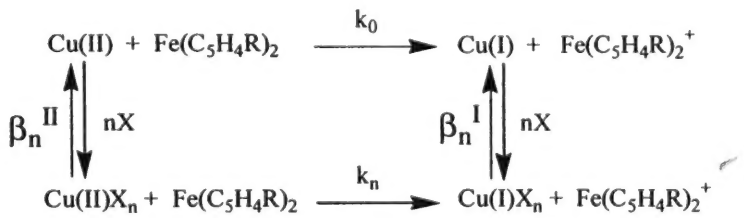

Scheme 4.1, in conjunction with the Marcus cross-relationship,[13] suggests that the potential differences between the solvated Cu(II) ion (ΔE_o^0) and the $Cu(II)X_n$ complexes (ΔE_n^0) and their respective rate constants k_0 and k_n are related to the overall inner-sphere formation constants $\beta_n^I = [Cu(I)X_n]/([Cu(I)][X]^n)$ and $\beta_n^{II} = [Cu(II)X_n]/([Cu(II)][X]^n)$, by eq 4.2 and 4.3,

$$\Delta E_n^0 = \Delta E_o^0 + \frac{RT}{nF} \ln\left(\frac{\beta_n^{I}}{\beta_n^{II}}\right) \qquad (4.2)$$

$$\frac{k_n}{k_0} \approx \left(\frac{k_{11}^n}{k_{11}^0}\right)^{1/2} \left(\frac{\beta_n^{I}}{\beta_n^{II}}\right)^{1/2} \qquad (4.3)$$

where R is the gas constant, T is the temperature in Kelvin, n is the number of electrons transferred, F is Faraday's constant and k^0_{11} and k^n_{11} are the electron self-exchange rate constants for the solvated Cu(II/I) ions and the inner-sphere complex Cu(II/I)X_n couples, respectively.

It follows from eq. 4.2 that, if the driving force is the major factor determining the rate of electron transfer, then complexation increases the rate if $\beta_n^I/\beta_n^{II} > 1$, and decreases it if $\beta_n^I/\beta_n^{II} < 1$. Alternatively, if both β_n^I/β_n^{II} and k^n_{11}/k^0_{11} make a significant contribution, then eq. 4.3 implies that the observed effect on rate will depend on which factor is dominant. It also follows that one can estimate k^n_{11}/k^0_{11} if β_n^I/β_n^{II} is known.

There do not seem to be any studies on nitrate or chloride complexation and/or counterion effects on electron-transfer rates in AN/water mixtures, but some studies involving Cu(II) and Cu(I) in the pure solvents may be relevant to the present study. In the chloride catalysis of the reaction of aqueous Cu(II) with ferrocytochrome *c* in the presence of dioxygen, Yandell[5] rationalized the effects in terms of Cu(II)Cl_n complex formation, with specific rate constants for Cu^{2+}, $CuCl^+$, and $CuCl_2$ of 5.7, 2.3 x 10^2, and 5.6 x 10^3 M^{-1} s^{-1} respectively. He ascribed the increased reactivity, using Marcus theory,[13] to the increased driving force for the reaction due to stronger chloride complexation of Cu(I) than Cu(II). However, using the Ahrland et al.[14] value of 513 M^{-1} for the formation constant of CuCl and the Ramette[15] value of 2.36 M^{-1} for $CuCl^+$, the change in

thermodynamic driving force alone predicts that $k_1/k_0 \approx 15$, compared to Yandell's value of 40. However, it should be noted that, due to the square root dependence of eq. 4.3 based on the Marcus cross-relationship, less than a factor of 10 change in k^n_{11}/k^0_{11} is needed to account for the apparent discrepancy in k_1/k_0 from the study by Yandell.[5] Sisley and Jordan[2] noted that the ratio of 40 found for k_1/k_0 by Yandell is consistent with Marcus theory predictions, but the calculated self-exchange rate constant for $Cu(II/I)_{(aq)}$ of 5.2 M^{-1} s^{-1} is much higher than the estimate by Davies[16] of ~2 x 10^{-4} M^{-1} s^{-1} and their estimate of 5 x 10^{-7} M^{-1} s^{-1} from the aqueous $Cu(II)/Co(sep)^{2+}$ system. It would appear that the reaction studied by Yandell[5] may be using an inner-sphere pathway. For the $Cu(II)/Co(sep)^{2+}/Cl^-$ system, Sisley and Jordan[2] found rate constants (0.02 M $HClO_4$, 0.48 M $LiClO_4$, 25 °C) of 5.0 ± 0.25, 1.6 x 10^3, 1.5 x 10^4 and 4.5 x 10^5 M^{-1} s^{-1} for n = 0, 1, 2, and 3, respectively. Since $Co(sep)^{2+}$ is an outer-sphere reagent[17], these authors analyzed the results in terms of the Marcus cross-relationship, and the k_1/k_0 value of 320 was accounted for in terms of a larger driving force for the cross-reaction and a larger k^1_{11} of ~2 x 10^{-4} compared to the k^0_{11} of 5 x 10^{-7} M^{-1} s^{-1}.

Because of the weaker coordination[18] of AN to Cu(II) compared to Cu(I) (opposite to H_2O), chloride ion complexation favors Cu(II) over Cu(I) in AN[19,20,21], and this situation may also pertain in 80 and 95% AN. The magnitudes of the overall formation constants β_1^I, β_2^I and β_1^{II}, β_2^{II} for the formation of $Cu(I)Cl$[19,20] and $Cu(II)Cl$[20,21] in AN are found to be 10^4, 10^{10} and 10^9, 10^{17} in 0.1 M tetraethylammonium perchlorate at 25 °C. Senne and Kratochvil[19b] studied the nitrate and chloride ions and found nitrate association with Cu(I) to be negligibly small in AN. Because of the higher charge density of Cu(II) compared to Cu(I), association of the nitrate with Cu(II) may be expected to be

greater, but nitrate ion is generally regarded as weakly coordinating. According to eq. 4.3, stronger coordination of nitrate or chloride to Cu(II) than to Cu(I) will cause a decrease in the driving force of the cross reaction. This would slow down the rate if the self-exchange rate constants remain largely unaffected by the presence of the anions.

In this Chapter, measurements are reported of the overall formation constants (β) and molar extinction coefficients (ε) for $Cu(II)X_n$ ($X = NO_3^-$, Cl^-) complexes in 80 and 95% AN/water. In addition, kinetics have been measured for the electron-transfer reactions of Cu(II) with Fc and Dmfc as a function of the concentration of X. The results are analyzed using the Marcus cross-relationship to evaluate what factors are important in determining the effect of these anions on the rates of the Cu(II)-ferrocenes reactions.

Experimental

Materials: Acetonitrile (Caledon, Fisher or BDH), perchloric acid (Fisher), tetraethylammonium chloride (Et_4NCl) (Sigma), copper(II) nitrate trihydrate (Allied Chemicals), sodium nitrate (ACP), and 1,1′-dimethylferrocene (Alfa Inorganics) were used as received. Ferrocene (Strem Chemicals) was purified by sublimation. Tetraaquacopper(II) triflate was prepared as described in Chapter 2.

AN/water mixtures and solutions. AN/water mixtures for preparing Cu(II) solutions were prepared as described in Chapter 3. For the absorbance measurements, stock solutions of Cu(II) (nitrate or triflate) and of the ferrocenes were prepared as described in Chapter 3. The concentration of Cu (II) in the stock solutions was determined by using the KI/Na_2SO_3 method.[22] Stock solutions for Cu(II) triflate or nitrate ($4.0 - 5.0 \times 10^{-4}$ M) and Fc and Dmfc ($4.0 - 6.0 \times 10^{-3}$ M), for the kinetic measurements, were prepared similarly.

Spectra and kinetics measurements. Absorbance measurements were done on a Cary 219 spectrophotometer. Absorbances were recorded in the wavelength range 250 - 400 nm. Preliminary measurements were performed using a wide distribution of concentrations to determine the relative concentration of Cu(II) and anion that maximized the formation of the mono species for Cu(II) with nitrate or chloride anion in 80 and 95% AN. For these measurements, the total [Cu(II)] concentration in the various runs was (1.0 - 4.0) x 10^{-4} M. The total anion concentration range were: nitrate; 8.0 x 10^{-5} M - 2.1 x 10^{-2} M in 95% AN and 5.6 x 10^{-4} M - 7.8 x 10^{-2} M in 80% AN, chloride; 6.6 x 10^{-6} M - 3.3 x 10^{-4} M in 95% AN and 4.7 x 10^{-6} - 1.2 x 10^{-1} M in 80% AN. The absorbance measurements were done at 22 ± 1 °C

The kinetics were determined with a pseudo-first-order excess of Fc or Dmfc except for a few runs with added Cl^- in 95% AN that were done with a pseudo-first-order excess of Cu(II) triflate. The measurements were done on a Tritech Dynamic Instruments stopped-flow spectrophotometer as described previously, and the reactions were monitored at 616 nm. The data were analyzed as described in Chapter 3 to obtain the pseudo-first order rate constants.

Results

This study was setup to examine the effects of nitrate and chloride ions on the rate of the cross-reactions of Cu(II) triflate with Fc or Dmfc in AN/water mixtures. Before delving into the study of the kinetic effects, the effects of these anions on the individual reactants were studied because this would aid the interpretation of any kinetic effects. This was done by measuring spectra in the absence and presence of the anions. The lack of any apparent change in the spectra of either Fc or Dmfc in the wavelength range

studied was considered an indication of no interactions between the ferrocenes and the nitrate or chloride ions.

For the Cu(II) solutions, changes in spectra were observed on addition of nitrate or chloride ion. Absorbances were determined at suitable wavelengths and divided by the total Cu(II) concentration and the cell pathlength to obtain the apparent molar extinction coefficient (ε). Representative results are shown in Figure 4.1. The absorbances in neat AN were obtained from the uv spectra for a 2.05 mM solution of $Cu(OH_2)_4(Trif)_2$ in a 2 cm cell and 0.404 mM solution of $Cu(NO_3)_2.3H_2O$ in a 1 cm cell. The latter salt and cell also were used for AN/water solutions. As can be seen from the plot, the ε values for the triflate in AN are negligible compared to those for the nitrate. When the AN is diluted with water, the effects of the nitrate on the Cu(II) absorbance decrease with % AN as shown in Figure 4.1.

Absorbance measurements on a 0.1 M solution of sodium nitrate in 95% AN gave an ε value at 280 nm of 2 M^{-1} cm^{-1}, compared to the equivalent value of ~500 M^{-1} cm^{-1} for $Cu(NO_3)_2.3H_2O$, from Figure 4.1. When the % AN and Cu(II) (~0.1 mM) were kept constant at 95% and the nitrate was systematically added as $NaNO_3$ the absorbance at 280 nm (for a 5 cm pathlength) increased by a factor of 5 for a 10^2 increase in total nitrate concentration. Under the same conditions of % AN and $[Cu(II)]_t$, a similar increase in absorbance is obtained with a 10^2 times smaller Et_4NCl concentration than the nitrate. These observations qualitatively indicate complex formation and suggest more favorable coordination of chloride than of nitrate.

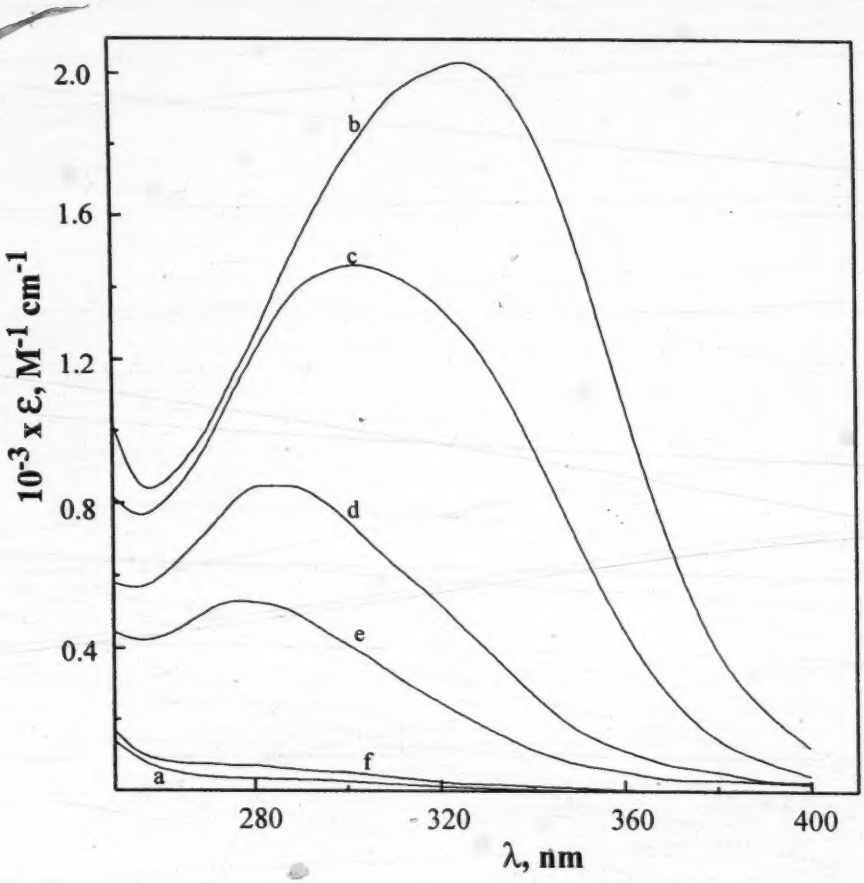

Figure 4.1. Extinction coefficients as a function of wavelength from the electronic spectra of: 2.05 mM $Cu(H_2O)_4(Trif)_2$ in neat AN (a); 0.404 mM $Cu(NO_3)_2.3H_2O$ in neat AN (b) and in 99% AN (c), 97% AN (d), 95% AN (e), 90% AN (f) at ambient temp. and variable μ.

To determine the magnitudes of the complex formation constants, the absorbances of Cu(II) solutions were recorded as a function of nitrate and chloride concentrations in 95% AN. Similar measurements were done in 80% AN for comparison. The spectra were recorded on a Cary 219 spectrophotometer in the 250 - 400 nm range, as noted in the experimental section. The absorbance values at selected wavelengths were then read off the chart paper, stored as data files on a computer, and analyzed to obtain β and ε values of the complexes as described below.

Analysis of absorbance data. For simplicity of the presentation in this section, the oxidation states and charges are omitted. The total Cu(II) and anion concentrations, $[Cu]_t$ and $[X]_t$ respectively, are given by eq. 4.4 and 4.5.

$$[Cu]_t = [Cu] + [CuX] + [CuX_2] + \cdots + [CuX_n] \quad (4.4)$$

$$[X]_t = [X] + [CuX] + 2[CuX_2] + \cdots + n[CuX_n] \quad (4.5)$$

Substitution of the expression for β_n given previously into eq. 4.4 and collecting terms gives

$$[Cu]_t = [Cu](1 + \beta_1[X] + \beta_2[X]^2 + \cdots + \beta_n[X]^n) \quad (4.6)$$

Then the concentrations of the copper species can be expressed in terms of $[Cu]_t$, β's and [X] as

$$
\begin{aligned}
[Cu] &= [Cu]_t/(1+\beta_1[X]+\beta_2[X]^2+\cdots+\beta_n[X]^n)\\
[CuX] &= \beta_1[X][Cu]_t/(1+\beta_1[X]+\beta_2[X]^2+\cdots+\beta_n[X]^n)\\
[CuX_2] &= \beta_2[X]^2[Cu]_t/(1+\beta_1[X]+\beta_2[X]^2+\cdots+\beta_n[X]^n)\\
&\vdots\\
[CuX_n] &= \beta_n[X]^n[Cu]_t/(1+\beta_1[X]+\beta_2[X]^2+\cdots+\beta_n[X]^n)
\end{aligned}
\qquad (4.7)
$$

Substitution of these expressions into eq. 4.5 and collecting terms gives

$$
[X]_t = [X] + \frac{(\beta_1[X] + 2\beta_2[X]^2+\cdots+n\beta_n[X]^n)[Cu]_t}{1+\beta_1[X]+\beta_2[X]^2+\cdots+\beta_n[X]^n} \qquad (4.8)
$$

It is apparent that cross-multiplication by the denominator of the second term on the right-hand side will produce a polynomial in [X] which can be solved in principle to give [X] in terms of $[X]_t$, $[Cu]_t$ and the β′s.

If the conditions are such that the tris and higher complex species are negligible, a cubic equation of the general form given by eq. 4.9 is obtained,

$$
[X]^3 + b[X]^2 + c[X] + d = 0 \qquad (4.9)
$$

where

$$
\begin{aligned}
b &= (\beta_1 + \beta_2(2[Cu]_t - [X]_t))/\beta_2\\
c &= (1 + \beta_1([Cu]_t - [X]_t))/\beta_2\\
d &= -[X]_t/\beta_2
\end{aligned}
\qquad (4.10)
$$

In general, such polynomials may be solved by successive iteration methods on a computer. However, these methods require an initial estimate of a root of the polynomial,

and will initially find the root closest to the initial guess. In order to avoid the complication of making a correct initial guess or designing a program that would determine if a particular root was the appropriate one, a closed solution for the cubic equation has been used. Initial trial and error determined which of these formula gave the appropriate root. The formula used is given by eq. 4.11 and 4.12.

$$
\begin{aligned}
q &= (c/3) - (b^2/9) \\
r &= (bc - 3d/6) - (b^3/27) \\
p &= r/\sqrt{-q^3} \\
\phi &= 2\,\mathrm{atan}(1) - \mathrm{atan}\left(p/\sqrt{1-p^2} \right)
\end{aligned}
\tag{4.11}
$$

Then

$$[X] = 2(\sqrt{-q})\cos(\phi/3) - (b/3) \tag{4.12}$$

In the iterative least-squares process, the value of [X] from eq. 4.12 and the initial guesses of the β's were used to calculate [Cu], [CuX] and [CuX_2]. These were combined with the initial guesses of ε_{CuX} and ε_{CuX_2} to calculate the absorbance, I, from the Beer's law expression;

$$I = \varepsilon_X[X] + \varepsilon_{Cu}[Cu] + \varepsilon_{CuX}[CuX] + \varepsilon_{CuX_2}[CuX_2] \tag{4.13}$$

It should be noted that ε_X and ε_{Cu} can be determined independently. The least-squares algorithm then iterated β and ε values with a standard unweighted regression, because small I values are most affected by uncertainties in baseline correction.

Nitrate complexation in 95% AN. The absorbances in 95% AN changed most at ~280 nm. Absorbance data collected at this wavelength were well fitted by the mono/bis model, as shown in Figure 4.2. The ε_{cu} values in Figure 4.2 were calculated from eq. 4.14,

$$\varepsilon_{Cu} = \frac{I_{obs} - l\,\varepsilon_X[X]}{l\,[Cu]_t} \qquad (4.14)$$

where l is the path length (5 cm for nitrate) and ε_X are the molar extinction coefficients for nitrate ion determined at the specified acid concentrations.

Table 4.1 gives values of I_{obs} and I_{calc} at 280 nm, with nitrate ion in 95% AN. The agreement between I_{obs} and I_{calc} is excellent, and shows that the mono/bis model works well. This model gives the best fit values and the one standard deviations for β_1, β_2, ε_1 and ε_2 shown in Table 4.2. The standard deviations of the mono/bis model, that are given in the Table, indicate that the β and ε values are reasonably well defined.

The ε values for the free nitrate ion ($\varepsilon_{Nitrate}$) shown in Table 4.2 were obtained using the $NaNO_3$ salt. The $NaNO_3$ concentrations were 0.0126 M in 0.202 mM $HClO_4$ or 0.0306 M in 0.101 mM $HClO_4$ in 95% AN, and 0.195 M $NaNO_3$ in 0.202 mM $HClO_4$ in 80% AN. The $\varepsilon_{Nitrate}$ values are obtained by dividing the absorbances at the appropriate wavelengths by the molarity of $NaNO_3$. As can be seen in Table 4.2, the $\varepsilon_{Nitrate}$ values show a small acid-dependence.

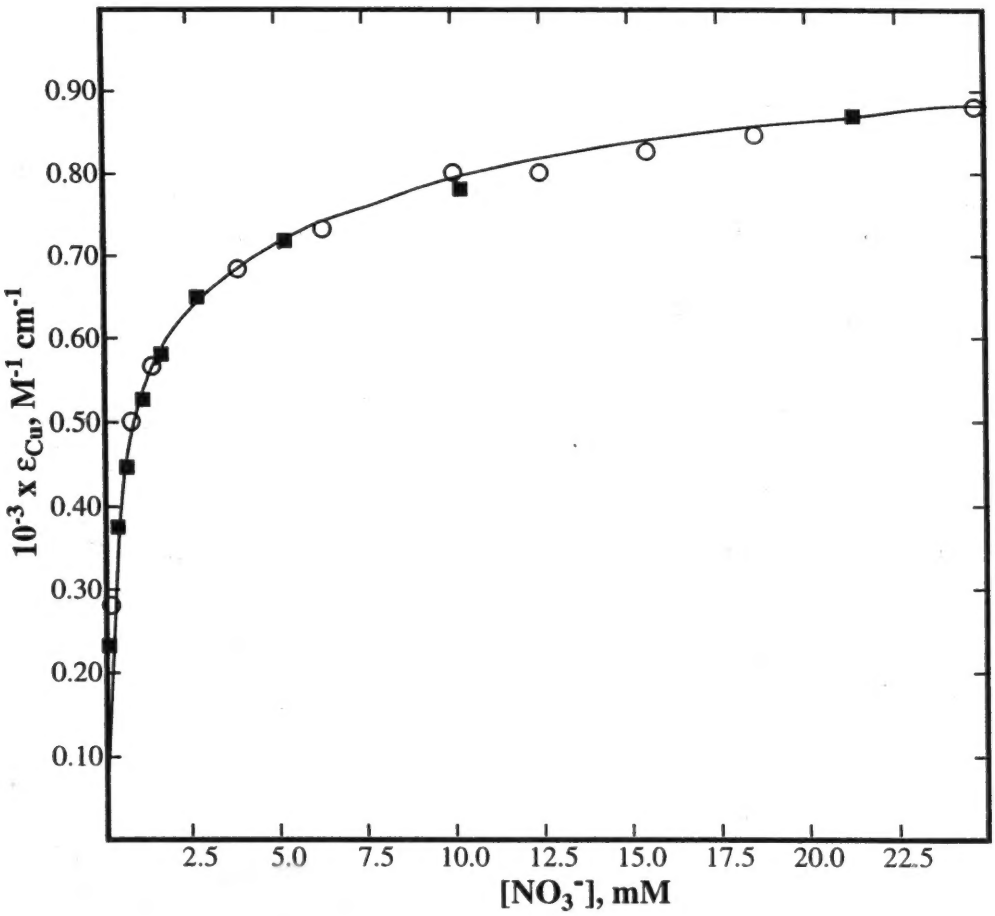

Figure 4.2. Variation of the apparent extinction coefficient (ε_{Cu}) with nitrate ion concentration for solutions of Cu(II) in 95% acetonitrile at 280 nm in 0.101 mM (O) and 0.24 mM (■) $HClO_4$ (ambient temp., variable μ).

Table 4.1. Absorbances of Cu(II) in the Presence of Nitrate Ion in 95% Acetonitrile [a,b]

$[NO_3]_t$,[c] mM	I_{obs} [d]	I_{calc}	$[NO_3]_t$,[c] mM	I_{obs} [d]	I_{calc}
0.2204	0.156	0.143	0.2026 [e]	0.119	0.126
0.8324	0.283	0.275	0.4538 [e]	0.194	0.200
1.444	0.327	0.325	0.7050 [e]	0.233	0.240
3.892	0.418	0.416	1.207 [e]	0.280	0.286
6.340	0.471	0.473	1.710 [e]	0.312	0.315
10.01	0.549	0.541	2.715 [e]	0.359	0.354
12.46	0.576	0.581	5.227 [e]	0.422	0.420
15.52	0.623	0.627	10.25 [e]	0.511	0.516
18.58	0.668	0.670	21.34 [e]	0.682	0.679
24.70	0.753	0.750			

[a] In 0.101 mM $HClO_4$ (ambient temp. and variable μ). [b] $[Cu(II)]_t$ = 0.1102 mM unless otherwise specified. [c] Added as $NaNO_3$. [d] At 280 nm in a 5 cm cell unless otherwise indicated. Absorbances in cells of pathlength l have been multiplied by $5/l$. [e] $[Cu(II)]_t$ = 0.1013 mM.

Table 4.2. Summary of Results for Complexation of Cu(II) by Nitrate Ion[a] in Acetonitrile

	95% Acetonitrile [b]	
β_1, M^{-1}	$4.02 \pm 0.53 \times 10^3$	
β_2, M^{-2}	$3.96 \pm 1.8 \times 10^5$	
ε_1, $M^{-1}\ cm^{-1}$	609 ± 32	
ε_2, $M^{-1}\ cm^{-1}$	990 ± 36	
$\varepsilon_{Nitrate}$, $M^{-1}\ cm^{-1}$	2.18 [c] (2.28) [d]	
	80% Acetonitrile [d,e]	
β_1, M^{-1}	$1.09 \pm 0.62 \times 10^3$	
β_2, M^{-2}	$1.39 \pm 1.1 \times 10^4$	
ε_1, $M^{-1}\ cm^{-1}$	24.2 ± 6.3 [f]	30.8 ± 7.5 [g]
ε_2, $M^{-1}\ cm^{-1}$	158 ± 14 [f]	193 ± 17 [g]
$\varepsilon_{Nitrate}$, $M^{-1}\ cm^{-1}$	1.49 [f]	2.76 [g]

[a] As $NaNO_3$. [b] At 280 nm in solutions containing 0.101 or 0.202 mM $HClO_4$ unless otherwise indicated. [c] In 0.101 mM $HClO_4$. [d] In 0.202 mM $HClO_4$. [e] At 270 and 280 nm. [f] At 270 nm. [g] At 280 nm.

Nitrate complexation in 80% AN. The values of β and ε for 80% AN are shown in Table 4.2. As in 95% AN, these values were obtained using the mono/bis model. The least-squares program was modified slightly to simultaneously fit the absorbance data at the two wavelengths of 270 and 280 nm. Use of the two wavelengths was found to give a smaller standard error of the fit and results in excellent agreement between I_{obs} and I_{calc}, as shown in Table 4.3. As indicated by the standard deviations in Table 4.2, the mono/bis model gives β values that are not so well defined by the absorbance data, but the ε values are well defined.

Chloride complexation in 95% AN. For the Cu(II)/Cl^- system in 95% AN, the application of the mono/bis model to absorbances at 260, 280, and 300 nm gave a good fit as shown in Figure 4.3. The Figure shows the variation of ε_{Cu} (calculated using eq. 4.14, $\varepsilon_{Cl} = 0$) with chloride ion concentration. Use of data at the three wavelengths gives a significantly lower standard deviation of the least-squares fit. The good quality of the fit also can be seen from the agreement between I_{obs} and I_{calc} values in Table 4.4. The β and ε values of the fits are summarized in Table 4.5. The standard deviations given in Table 4.5 show that the β and the ε values are well defined.

The excellent fit of the data for the Cu(II)/Cl^- system in 95% AN, using the mono/bis complex model suggests that formation of a tris complex in this medium is negligible, as might be expected for the low chloride ion concentrations used. As will be seen later in the Chapter, the kinetics were too fast to determine at higher concentrations where the tris or higher complexes might be present. Therefore, the emphasis here was on the complex formation of the mono and bis complexes.

Table 4.3. Absorbances of Cu(II) in the Presence of Nitrate Ion in 80% Acetonitrile[a,b]

	I_{obs} [d]		I_{calc}	
$[NO_3]_t$,[c] mM	270 nm	280 nm	270 nm	280 nm
0.5584	0.018	0.018	0.018	0.017
4.450	0.080	0.099	0.078	0.096
8.342	0.127	0.166	0.120	0.161
16.13	0.199	0.283	0.197	0.283
23.91	0.267	0.395	0.270	0.403
31.69	0.333	0.510	0.340	0.520
39.48	0.413 [f]	0.640 [f]	0.409	0.637
78.40	0.745 [f]	1.195 [f]	0.737	1.204
117.3	1.060 [g]	1.780 [g]	1.049	1.759
156.2	1.340 [g]	2.300 [g]	1.354	2.308
0.6227 [e]	0.026	0.025	0.026	0.023
0.934 [e]	0.035	0.036	0.036	0.034
1.562 [e]	0.049	0.052	0.052	0.052
2.335 [e]	0.064	0.070	0.068	0.071
3.114 [e]	0.080	0.088	0.081	0.087

[a] In 0.202 mM $HClO_4$ (ambient temp. and variable μ). [b] $[Cu(II)]_t$ = 0.2792 mM unless otherwise specified. [c] Added as $NaNO_3$. [d] In a 5 cm cell unless indicated otherwise. Absorbances in cells of path length l have been multiplied by $5/l$. [e] $[Cu(II)]_t$ = 0.4231 mM. [f] In a 2 cm cell. [g] In a 1 cm cell.

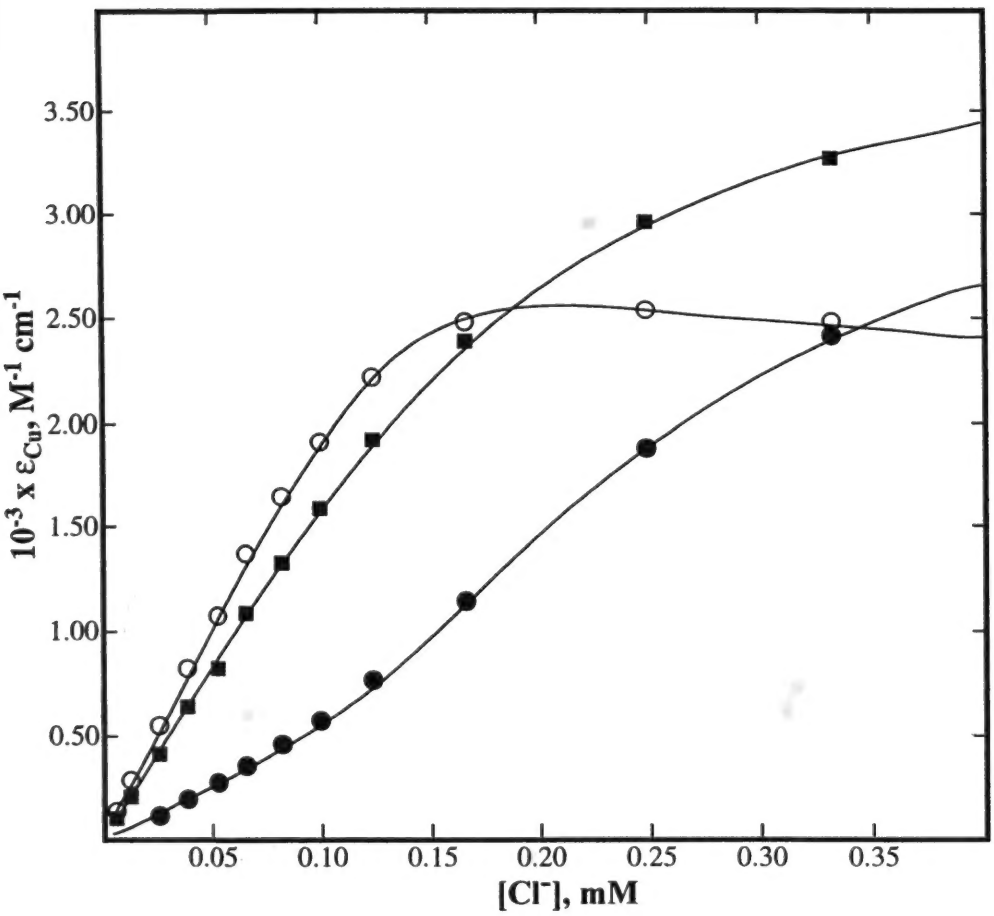

Figure 4.3. Variation of the apparent extinction coefficient (ε_{Cu}) with chloride ion concentration for solutions of Cu(II) in 95% acetonitrile at 260 nm (○), 280 nm (●), and 300 nm (■) (ambent temp., variable μ).

Table 4.4. Absorbances of Cu(II) in the Presence of Chloride Ion in 95% Acetonitrile [a]

	I_{obs} [c]			I_{calc}		
$[Cl^-]_t$,[b] mM	260 nm	280 nm	300 nm	260 nm	280 nm	300 nm
0.00663	0.037	0.025		0.038	0.030	
0.01326	0.075	0.053		0.075	0.059	
0.02652	0.148	0.110	0.030	0.150	0.118	0.036
0.03978	0.221	0.171	0.050	0.222	0.176	0.054
0.05304	0.290	0.222	0.073	0.293	0.234	0.074
0.06630	0.368	0.293	0.095	0.361	0.290	0.094
0.08288	0.444	0.357	0.121	0.440	0.359	0.121
0.09946	0.514	0.429	0.152	0.512	0.425	0.151
0.12430	0.597	0.518	0.205	0.598	0.516	0.202
0.16580	0.668	0.643	0.308	0.674	0.638	0.306
0.24860	0.683	0.800	0.504	0.686	0.797	0.510
0.33150	0.668	0.883	0.652	0.665	0.887	0.649

[a] $[Cu(II)]_t$ = 0.1352 mM in 0.202 mM $HClO_4$ (ambient temp., variable μ). [b] Added as Et_4NCl. [c] In 2 cm cell.

Table 4.5. Summary of the Results for Complexation of Cu(II) by Chloride Ion in Acetonitrile

	95% Acetonitrile [a]		
β_1, M^{-1}	$3.52 \pm 0.77 \times 10^5$		
β_2, M^{-2}	$4.35 \pm 2.0 \times 10^9$		
$10^{-3} \times \varepsilon_1$, $M^{-1}\,cm^{-1}$	2.92 ± 0.04 [b]	2.28 ± 0.025 [c]	0.671 ± 0.02 [d]
$10^{-3} \times \varepsilon_2$, $M^{-1}\,cm^{-1}$	2.18 ± 0.07 [b]	4.02 ± 0.18 [c]	3.62 ± 0.29 [d]

	80% Acetonitrile [a]			
β_1, M^{-1}	$6.65 \pm 0.33 \times 10^2$ [e]		$8.83 \pm 1.2 \times 10^2$ [f]	
β_2, M^{-2}	$9.72 \pm 1.3 \times 10^3$ [e]		$5.06 \pm 3.3 \times 10^4$ [f]	
β_3, M^{-3}			$1.27 \pm 2.7 \times 10^5$ [f]	
$10^{-3} \times \varepsilon_1$, $M^{-1}\,cm^{-1}$	1.68 ± 0.03 [g]	0.716 ± 0.03 [h]	1.43 ± 0.12 [g]	0.562 ± 0.61 [h]
$10^{-3} \times \varepsilon_2$, $M^{-1}\,cm^{-1}$	2.50 ± 0.36 [g]	2.88 ± 0.87 [h]	2.12 ± 0.16 [g]	1.58 ± 0.38 [h]
$10^{-3} \times \varepsilon_3$, $M^{-1}\,cm^{-1}$			2.79 ± 0.52 [g]	4.65 ± 2.9 [h]

[a] In 0.202 mM $HClO_4$. [b] At 260 nm. [c] At 280 nm. [d] At 300 nm. [e] Model assumes only mono and bis complex formation. [f] Model assumes mono, bis and tris complex formation. [g] At 254 nm. [h] At 280 nm.

Chloride complexation in 80% AN. For this solvent, larger absorbance changes occurred at 254 nm. The absorbance data at this wavelength, together with that at 280 nm were fit to the mono/bis model. The β and ε values from the least-squares fit using this model are given in Table 4.5 and the I_{obs} and I_{calc} values are collected in Table 4.6. As can be seen from the Tables, the mono/bis model does give satisfactory results. However, the mono/bis model did not work for the kinetics (as shown later in this Chapter) and so the complexation model was expanded to include the tris complex, which seemed to be required by the kinetics.

Following the procedure given earlier, addition of a tris complex results in a fourth order polynomial in $[Cl^-]$, as shown in eq. 4.15 and 4.16,

$$[Cl]^4 + b[Cl]^3 + c[Cl]^2 + d[Cl] + e = 0 \tag{4.15}$$

where

$$\begin{aligned} b &= (\beta_2 + \beta_3(3[Cu]_t - [Cl]_t))/\beta_3 \\ c &= (\beta_1 + \beta_2(2[Cu]_t - [Cl]_t))/\beta_3 \\ d &= (1 + \beta_1([Cu]_t - [Cl]_t))/\beta_3 \\ e &= -[Cl]_t/\beta_3 \end{aligned} \tag{4.16}$$

Equation 4.15 was solved by Newton's iterative method, using initial guesses for $[Cl^-]$ from the exact cubic solution for concentrations < 2 mM and $[Cl^-] = [Cl^-]_t$ for higher concentrations. The results of this fit also are given in Table 4.6. It can be seen that the absorbance data is consistent with tris complex formation, but the β_3 (Table 4.5) is not satisfactorily defined.

Table 4.6. Absorbances of Cu(II) in the Presence of Chloride Ion in 80% Acetonitrile [a]

	I_{obs} [c]		I_{calc} [d]		I_{calc} [e]	
$[Cl^-]_t$, [b] mM	254 nm	280 nm	254 nm	280 nm	254 nm	280 nm
0.187	0.114	0.052	0.123	0.053	0.128	0.051
0.373	0.253	0.099	0.229	0.099	0.237	0.096
0.934	0.475	0.196	0.471	0.207	0.481	0.200
1.867	0.722	0.315	0.721	0.326	0.722	0.316
4.668	1.037	0.508	1.046	0.512	1.034	0.508
9.336	1.231	0.690	1.239	0.675	1.231	0.687
23.34	1.445	0.977	1.440	0.962	1.450	0.977
46.68	1.586	1.235	1.580	1.249	1.587	1.238
70.02	1.667	1.416	1.660	1.433	1.659	1.414
116.7	1.742	1.672	1.751	1.658	1.745	1.672

[a] $[Cu(II)]_t$ = 0.4006 mM in 0.202 mM $HClO_4$ (ambient temp., variable μ). [b] Added as Et_4NCl. [c] In 2 cm cell. [d] Obtained using the mono/bis model. [e] Obtained using the mono/bis/tris model.

Kinetics. In the preceding sections, nitrate and chloride ions have been shown to complex with Cu(II) ion in 95 and 80% AN, and the absorbance data were used to obtain the β values for the complexes. These β values will be used to try to elucidate the kinetic effects of introducing these anions into the reactions of Fc or Dmfc with Cu(II) (eq. 4.17).

$$\begin{aligned} Fc + Cu^{2+} &\rightarrow Fc^{+} + Cu^{+} \\ Dmfc + Cu^{2+} &\rightarrow Dmfc^{+} + Cu^{+} \end{aligned} \qquad (4.17)$$

In Chapter 3, the rate of the reaction (triflate salt) was shown to be first-order in each reactant, but most reactions were done with a large excess of Cu(II) over the ferrocenes. A few runs were done with a large excess of the ferrocenes, and it was found that the two conditions gave similar second-order rate constants.

Most of the kinetic measurements in the present Chapter were done with a large excess of the ferrocenes. In order to ascertain that no complications (e.g. autoxidation of Fc catalyzed by Cu(II), eq. 4.18) occurred, an additional experiment was done:

$$\begin{aligned} Fc + Cu(II) &\rightarrow Fc^{+} + Cu(I) \\ 2\,Cu(I) + O_2 + 2H^{+} &\rightarrow 2\,Cu(II) + H_2O_2 \end{aligned} \qquad (4.18)$$

A 20 mL mixture of 3.03×10^{-3} M Fc and 1.01×10^{-3} M Cu(II) triflate in 95% AN was shaken in air and then transferred to a 5 cm pathlength cell. Then the spectrum of this solution was measured from 500 - 700 nm. The spectrum was recorded at time intervals of 2, 4, 9, 14, and 24 min.

For an O_2 concentration in the solution of ~0.2 - 0.3 mM, it is conceivable that the

Cu(I) initially formed in eq. 4.17 might be oxidized to Cu(II) by the dioxygen in a catalytic cycle. If this process occurs, the observed absorbance would be greater than expected from the initial Cu(II) concentration (i.e. ~0.25 at 616 nm). The absorbance at 616 nm, after 2 min was 0.248 and the spectrum stayed constant for ~30 min. The conclusion from this observation is that neither Fc nor Cu(I) is oxidized by O_2 in the presence of Cu(II), and the same was assumed for reactions with Dmfc.

Analysis. For the conditions with [Cu] >> [Fc], it was found in Chapter 3 that k_{obs} vs. $[Cu(II)]_t$ plots had constant slopes but acid-dependent intercepts (k_i). The rate law, which satisfies this situation, was proposed to be

$$\frac{d[Fc^+]}{dt} = k_i[Fc] + k_{12}[Cu][Fc] \qquad (4.19)$$

Upon rearrangements and integration, eq. 4.19 gives $k_{obs} = k_i + k_{12}[Cu]_t$, where k_{obs} is the observed pseudo-first-order rate constant and k_{12} is the second-order rate constant for the copper-dependent pathway. For conditions of $[Fc]_t >> [Cu]_t$, the rate law gives $k_{obs} = k_{2obs}[Fc]_t$, where k_{2obs} is the observed second-order rate-constant.

If Cu is present as $Cu(II)X_n$ (n = 0, 1, 2, ...), the rate law is given by eq. 4.20.

$$\frac{d[Fc^+]}{dt} = k_i[Fc] + (k_0[Cu] + k_1[CuX] + k_2[CuX_2] + \cdots + k_n[CuX_n])[Fc] \qquad (4.20)$$

where k_0, k_1, k_2, ... k_n are the species-specific rate constants. Substitution from eq. 4.7 then gives eq. 4.21.

$$\frac{d[Fc^+]}{dt} = k_i[Fc] + \left(\frac{k_0 + k_1[X] + k_2[X]^2 + \cdots + k_n[X]^n}{1 + \beta_1[X] + \beta_2[X]^2 + \cdots + \beta_n[X]^n}\right)[Cu]_t[Fc] \qquad (4.21)$$

For conditions of constant [X] and $[Fc]_t >> [Cu]_t$, the observed pseudo-first-order rate constants can then be divided by $[Fc]_t$ to give k_{2obs} values as shown in eq. 4.22.

$$k_{2obs} = \frac{k_{obs}}{[Fc]_t} = \frac{k_0 + k_1[X] + k_2[X]^2 + \cdots + k_n[X]^n}{1 + \beta_1[X] + \beta_2[X]^2 + \cdots + \beta_n[X]^n} \qquad (4.22)$$

For the reactions done with Dmfc, Fc should be replaced by Dmfc in the above expressions.

The kinetic data were fitted by iterative least-squares to eq. 4.22, using the β values from the absorbance measurements. The values of [X] were obtained as described by eq. 4.4 to 4.12 for nitrate ion in 80 and 95% AN and chloride ion in 95% AN and eq. 4.15 and 4.16 for chloride ion in 80% AN. A weighted regression was used for these fits because the error in k_{obs} is essentially independent of its magnitude. The results are given in the following sections. It should be noted that the k_0 in eq. 4.22 is essentially the same as the k_{12} determined in Chapter 3 for the reaction of Cu(II) triflate with the ferrocenes.

Nitrate effect in 95% AN. The k_{2obs} data for the reactions (eq. 4.17) of Fc and Dmfc are given in Table 4.7. A fit of the k_{obs} data using the β_1 and β_2 values from Table 4.2 gave excellent agreement between observed and calculated values for Fc and Dmfc as shown in Figure 4.4. The plot in Figure 4.4 shows an initial rapid decrease in the k_{2obs} values and then the slope decreases at total nitrate concentrations above 2 mM. This is

Table 4.7. Rate Constants (M^{-1} s^{-1}) for Reactions of Cu(II) with Fc and Dmfc in Presence of Nitrate Ion in 95% AN[a]

		Fc		Dmfc	
$[NO_3^-]_t$,[b] mM	$[HClO_4]$, mM	k_{2obs}[c]	k_{2calc}	k_{2obs}[c]	k_{2calc}
0	0.278	197 ± 3	200	1040 ± 17	1040
0.0800	0.278	197 ± 3	199	1035 ± 22	1029
0.160	0.278	195 ± 5	198	1030 ± 13	1018
0.400	0.278	191 ± 3	195	996 ± 18	990
0.482[e]	0.242			950 ± 33	980
0.512[d]	0.0171	211 ± 5	184	1041 ± 19	978
0.801	0.278	184 ± 3	179	881 ± 15	949
0.913[d]	0.0171	199 ± 4	178	978 ± 17	939
1.31[d]	0.0171	191 ± 4	171	924 ± 20	904
1.74[e]	0.242			815 ± 27	869
2.00	0.278	163 ± 4	172	794 ± 15	850
2.51[d]	0.0171	167 ± 3	166	827 ± 6	815
4.00	0.278	141 ± 1	150	675 ± 13	726
4.52[d]	0.0171	142 ± 2	145	730 ± 16	699
5.51[e]	0.242			667 ± 22	653
6.01	0.278	131 ± 2	133	638 ± 14	633
8.52[d]	0.0171	124 ± 3	117	630 ± 12	546

[a] With 0.252 mM $Cu(Trif)_2$ and 2.64 mM Fc or 2.74 mM Dmfc unless otherwise specified (25 °C, variable μ). [b] Added as $NaNO_3$. [c] With 0.241 mM $Cu(NO_3)_2$ and 2.78 mM Dmfc. [d] With 0.256 mM $Cu(NO_3)_2$. [e] Errors are standard deviations of 8 - 10 replicate runs.

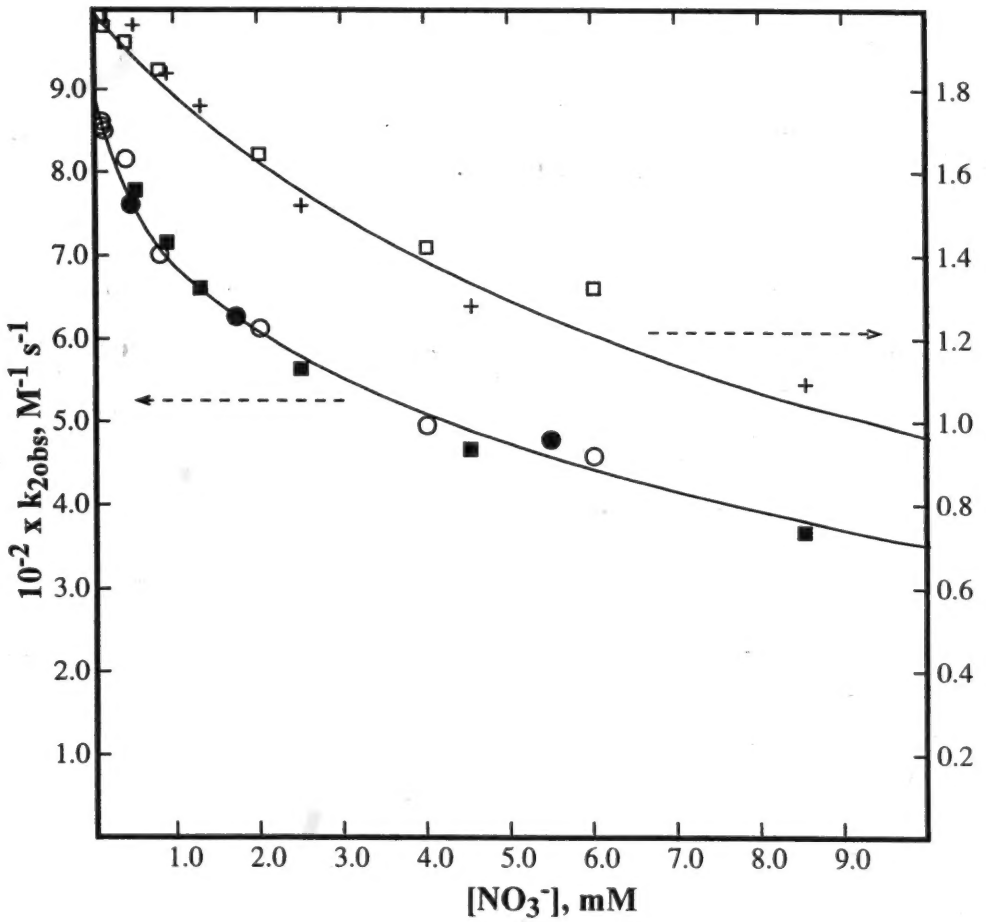

Figure 4.4. Variation of k_{2obs} with $[NO_3^-]$ in 95 % AN (25 °C, variable μ): for Fc with 0.256 mM Cu(II) (□) and 0.252 mM Cu(II) (+); for Dmfc with 0.252 mM Cu(II) (○), 0.241 mM Cu(II) (■) and 0.256 mM Cu(II) (●).

consistent with the β values, which, for the concentrations used, show the mono complex as the predominant species, and the bis complex is minor. The excellent quality of the fits demonstrated by the plot and the agreement between the k_{2obs} and k_{2calc} values in Table 4.7 further shows that the kinetic results are consistent with the assumed β values.

Table 4.8 gives a summary of specific rate constants (k_n) for reactions of $Cu(II)X_n$ ($X = NO_3^-$, n= 0, 1, or 2) with Fc or Dmfc in 95% AN. The k_0 and k_1 values in Table 4.8 are well defined, but k_2 is undefined because $Cu(NO_3)_2$ is always a minor species (≤ 7%).

The k_{12} values from Chapter 3 also are given in Table 4.8. The k_0 value for reactions with Fc is in good agreement with the k_{12} value, but the k_0 value for Dmfc is ~20% larger than the k_{12} value. This discrepancy should not be due to contamination of the Dmfc because the same source of Dmfc was used in both studies. The differences may be due to random errors and uncertainties in the formation constants.

Nitrate effect in 80% AN. The β values in 80% AN predict that solutions of $Cu(NO_3)_2$ (2 - 20 mM) contain ≥ 75% mono complex and ≤25% free Cu(II) Since the kinetics in Chapter 3 gave similar results for nitrate and triflate in 80% AN, it is interesting to see if this is consistent with the results for nitrate complexation in 80% AN.

The kinetic data obtained in Chapter 3 using variable concentrations of Cu(II) nitrate in 80% AN have been analyzed using the β values in 80% AN. The k_{2obs} values are calculated for each $[NO_3^-]$ by dividing the k_{obs} by $[Cu(II)]_t$. Because intercepts in 80% AN were negligible, an intercept of zero was assumed for these data. The results, given in Table 4.9, show good agreement between k_0 and k_{12} for Dmfc and a 20% difference for Fc.

Table 4.8. Summary of Rate Constants (M^{-1} s^{-1}) for Reactions of Cu(II) with Fc and Dmfc in the Presence of Nitrate Ion.

Parameter	80% AN		95% AN	
	Fc	Dmfc	Fc	Dmfc
k_{12} [a]	5.97	25.4	198	862
k_o	7.47 ± 0.92	25.4 ± 5.5	195±4	1040±40 [c]
k_1	4.57 ± 0.55	27.8 ± 2.3	185 ± 2	969 ± 20 [c]
k_2	11.9 ± 3.8	27.3 ± 3.5	17.5 ± 16 [b]	< 100 [d]

[a] Values taken from Chapter 3. [b] Value not well defined as indicated by the standard deviation. [c] Determined with k_2 fixed at 0; if k_2 = 100 then k_1 = 635±14. [d] Estimated upper limit that causes a 25% increase in the standard error of the least-squares fit.

Table 4.9. Rate Constants (M^{-1} s^{-1}) for Reactions of Cu(II) with Fc and Dmfc in the Presence of Nitrate Ion in 80% AN

Fc			Dmfc		
$[NO_3^-]_t$,[a] mM	k_{2obs} [d]	k_{2calc}	$[NO_3^-]_t$,[a] mM	k_{2obs} [d]	k_{2calc}
1.01 [b]	6.22 ± 0.15	6.17	1.01 [e]	25.6 ± 0.5	26.5
5.05 [b]	5.24 ± 0.10	5.43	5.70 [f]	31.0 ± 1.1	27.3
10.1 [b]	5.20 ± 0.14	5.37	8.54 [f]	27.8 ± 0.5	27.4
20.2 [b]	5.35 ± 0.11	5.54	14.2 [f]	28.3 ± 0.9	27.5
30.0 [b]	5.87 ± 0.17	5.75	19.9 [f]	25.4 ± 1.3	27.5
11.5 [c]	5.99 ± 0.21	5.38	83.4 [f,g]	24.9 ± 1.8	27.6
20.2 [c]	5.66 ± 0.16	5.54	90.0 [f,g]	26.3 ± 2.8	27.5
28.8 [c]	5.59 ± 0.29	5.72	92.5 [f,g]	26.8 ± 1.6	27.5
			95.0 [f,g]	29.8 ± 0.9	27.5
			97.5 [f,g]	32.8 ± 1.4	27.5

[a] Equals two times the total $Cu(NO_3)_2$ concentrations unless otherwise specified (25 °C, variable μ). [b] With 0.266 mM Fc and 0.254 mM $HClO_4$. [c] With 0.254 mM Fc. [d] Averages of 8-10 replicate runs. [e] With 0.247 mM Dmfc and 0.254 mM $HClO_4$. [f] With 0.242 mM Dmfc. [g] Equals two times the total $Cu(NO_3)_2$ concentrations plus the concentration of added $NaNO_3$.

The rate constants for free Cu(II) (k_0) in Table 4.9 can be compared with the k_{12} values shown in Table 4.8, for the reaction of Cu(II) triflate with Fc and Dmfc, respectively. For Dmfc, the k_0 value agrees with the k_{12} value and is the same as k_1 and k_2 values. For Fc, there appears to be a difference between the k_{12} and k_n values but the large error in k_2 shows that the difference is not significant. Similar values of k_1 and k_2 are obtained if k_0 is fixed at the k_{12} value. The k_2 also can be fixed at a moderate value without adverse effect on the fit. For example, if k_2 is taken as 5 M^{-1} s^{-1}, k_0 and k_1 are calculated to be 6.39 ± 0.81 and 5.49 ± 0.22 M^{-1} s^{-1}, respectively. It is therefore apparent that the k's for the different species are about the same in 80% AN, as expected from the lack of any real trend in the k_{2obs} values.

Chloride effect in 95% AN. For the 95% AN, the effect of the chloride ion on the Cu(II)-Fc reaction was studied with a large excess of Cu(II). The observed second-order rate constants (k_{2obs}) for the reaction were calculated from the k_{obs} values and the total Cu(II) concentration. Because the reagents were in 0.202 mM $HClO_4$ an intercept of zero was used as suggested by results under similar conditions in Chapter 3. The β_1 and β_2 values from Table 4.2 have been used. The k_{2obs} values and the corresponding k_{2calc} values are collected in Table 4.10. The k_{2obs} values increased nonlinearly by ~10^2 for a 10-fold increase in total chloride concentration. The agreement between k_{2obs} and k_{2calc} is excellent and the kinetics are therefore consistent with the assumed β_1 and β_2 values. The values of k_0, k_1, and k_2, which are summarized in Table 4.11, are well defined. The mono and bis complexes are found to be ~25 and ~900 times more reactive than the free Cu^{2+} ion. The k_0 value also agrees with the k_{12} value from Chapter 3 shown in Table 4.11.

Table 4.10. Rate Constants (M^{-1} s^{-1}) for Reactions of Cu(II) with Fc in the Presence of Chloride Ion in 95% AN [a]

$[Cl^-]_t$ [b], mM	k_{2obs} [e]	k_{2calc}
0 [c]	189 ± 6	186
0.207	585 ± 9	594
0.414	11.0 ± 0.2 x 10^2	11.0 x 10^2
0.622	17.9 ± 0.4 x 10^2	17.2 x 10^2
0.829 [d]	25.6 ± 0.5 x 10^2	25.6 x 10^2
0.829	25.1 ± 0.4 x 10^2	25.0 x 10^2
1.24	45.1 ± 1.8 x 10^2	46.7 x 10^2
2.07	14.6 ± 0.7 x 10^3	14.8 x 10^3
2.49	26.1 ± 1.1 x 10^3	25.4 x 10^3

[a] With 2.50 mM $Cu(Trif)_2$, 0.239 mM Fc and 0.202 mM $HClO_4$ and intercept = 0 unless otherwise specified (25 °C, variable μ). [b] Added as Et_4NCl. [c] With 0.225 mM $Cu(Trif)_2$ and 2.47 mM Fc. [d] With 2.46 mM $Cu(Trif)_2$ and 0.239 mM Fc. [e] Errors are standard deviations of 8 to 10 replicate runs.

Table 4.11. Summary of Rate Constants (M^{-1} s^{-1}) for Reactions of Cu(II) with Fc and Dmfc in the Presence of Chloride Ion. [a]

Parameter	80% AN		95% AN
	Fc	Dmfc	Fc
k_{12} [b]	5.97	25.4	198
k_o	4.43 ± 0.38	29.2 ± 0.53	189 ± 5
k_1	120 ± 13	376 ± 12	$4.59 \pm 0.1 \times 10^3$
k_2	$3.64 \pm 0.37 \times 10^3$	$1.27 \pm 0.03 \times 10^4$	$1.69 \pm 0.04 \times 10^5$
k_3	$1.97 \pm 0.11 \times 10^5$	$5.07 \pm 0.14 \times 10^5$	

[a] In solutions containing 0.202 mM $HClO_4$ at 25 °C. [b] Values taken from Chapter 3.

Chloride effect in 80% AN. The variation of the observed rate constant (k_{2obs}) with the chloride concentration in 80% AN is shown in Figure 4.5. The measurements were done with a large excess of Fc or Dmfc and the k_{2obs} values were calculated as described previously. As the Figure shows, the β values from the mono/bis complex model do not fit the dependence of the rate constants on chloride ion concentration. The essential problem is that the model predicts that the system would be approaching saturation in the bis complex at ~25 mM Cl^- and therefore cannot accommodate the increasing reactivity beyond this point. For this reason, the tris complex and β_3 were added to the model to fit the absorbance data as described earlier in this Chapter. Although β_3 is not statistically defined, the mono/bis/tris model gives a better fit of the kinetic data (see Figure 4.5) because higher Cl^- concentrations were used for the kinetics.

To calculate the fit using the mono/bis/tris model, β values and free chloride ion concentrations were calculated using eq. 4.15 and 4.16 and then the results were used in eq. 4.22 with additional terms for the tris complex. The k_{2calc} values from the fits are given in Table 4.12. It can be seen that the k_{2obs} and k_{2calc} values are in excellent agreement and hence consistent with the mono/bis/tris model.

The values of k_0, k_1, k_2, and k_3 are shown in Table 4.11. These values are all well defined. The k_0 value for Fc is about 30% larger than the k_{12} value (see Table 4.11) from Chapter 3 while that for Dmfc is about 15% larger. As noted previously, these discrepancies seem to be the result of random errors and uncertainties in the β values. The results in Table 4.11 show that the reactivity of the $Cu(II)Cl_n$ complexes increase with increasing n in both 80% and 95% AN.

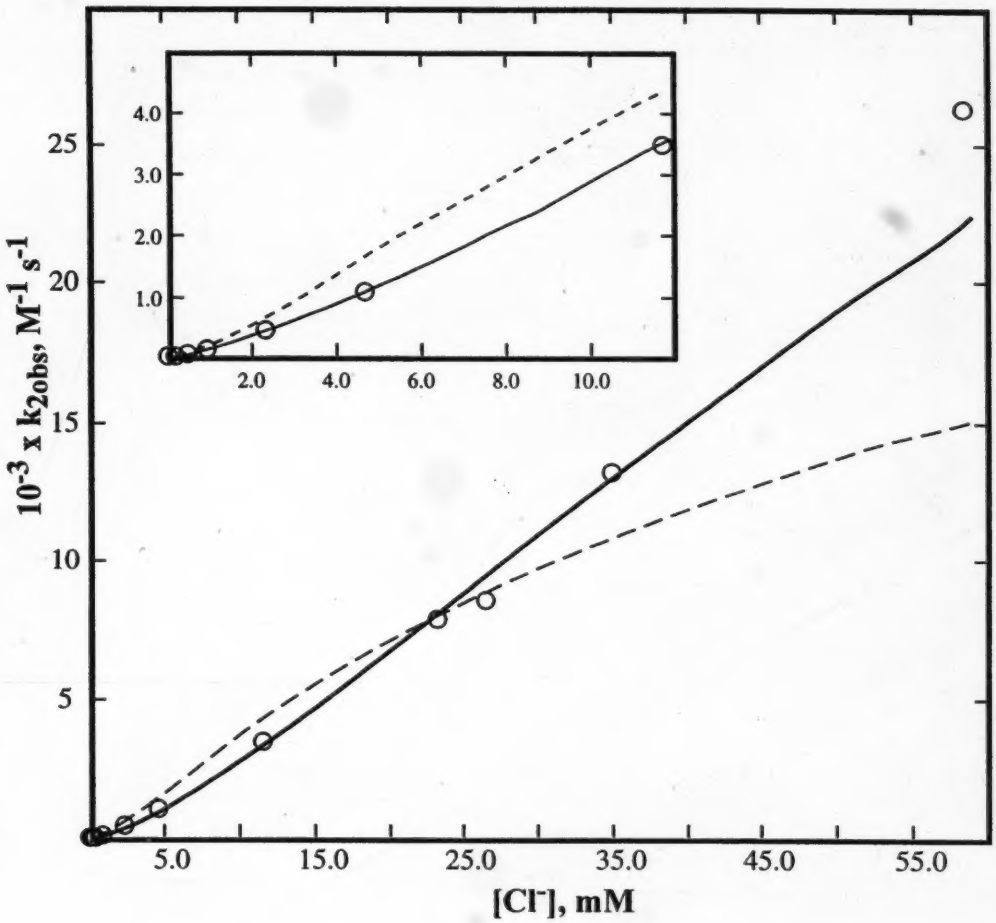

Figure 4.5. Variation of k_{2obs} with [Cl^-] in 80% AN fitted to a mono/bis complex model (– – –) and a mono/bis/tris complex model (—). Insert shows an expansion of the low [Cl^-] region (25 °C, variable μ).

Table 4.12. Rate Constants (M^{-1} s^{-1}) for Reactions of Cu(II) with Fc and Dmfc in the Presence of Chloride Ion in 80% AN [a]

	Fc		Dmfc	
$[Cl^-]$ [b], mM	k_{2obs} [c]	k_{2calc}	k_{2obs} [c]	k_{2calc}
0.00467	4.85 ± 0.13	4.83	30.3 ± 0.7	30.4
0.187	22.8 ± 0.3	23.2	88.7 ± 1.6	87.1
0.467	58.6 ± 0.7	59.1	199 ± 4	203.2
0.934	139 ± 1	135	450 ± 9	439.5
2.33	446 ± 7	433	$14.3 \pm 0.2 \times 10^2$	14.1×10^2
4.67	$10.6 \pm 0.1 \times 10^2$	10.7×10^2	$33.7 \pm 0.9 \times 10^2$	33.6×10^2
11.7	$34.5 \pm 0.9 \times 10^2$	34.8×10^2	$10.1 \pm 0.4 \times 10^3$	10.3×10^3
23.3	$78.1 \pm 1.8 \times 10^2$	81.4×10^2	$23.0 \pm 1.4 \times 10^3$	23.0×10^3
26.5 [d]	$85.3 \pm 5.1 \times 10^2$	94.4×10^2		
35.0	$13.1 \pm 0.5 \times 10^3$	13.0×10^3		
58.4	$26.3 \pm 1.2 \times 10^3$	22.2×10^3		

[a] With 0.200 mM $Cu(Trif)_2$, 2.03 mM Fc or 2.05 mM Dmfc, 0.202 mM $HClO_4$ and intercept = 0 (25 °C, variable μ). [b] Added as Et_4NCl. [c] Errors are standard deviations of 8 to 10 replicate runs. [d] With chloride initially present in the Fc solution.

Discussion

Complex formation. In this and several other studies,[20,21,23] the complex formation constants of Cu(II) have been determined by spectrophotometry. Such studies yield values for the formation constants and the extinction coefficients of the complexes used in the model to fit the absorbance vs. ligand concentration data. In general, these studies have concentrated on spectral changes in the ultraviolet region where the absorbance is typically assigned to ligand to metal charge-transfer bands.

With the anticipation that some trends might be observed in the extinction coefficients between water, water/AN mixtures and neat AN, values for nitrate and chloride complexes are collected in Table 4.13. For $Cu(II)(X)_n$ complexes, there is a general observation that, with increasing n, the maximum extinction coefficient increases and the absorbance maximum shifts slightly to longer wavelength. In addition, the extinction coefficients in water are smaller than those when AN is present.

Unfortunately it is difficult to identify trends with solvent composition because of the disagreements between the results from different studies in both water and 100% AN. In water, the work of Khan and Schwing-Weill[23] gives details of the extinction coefficients, but the β values differ from those of the more recent study of Ramette.[15] For consistency, the absorbances of Khan and Schwing-Weill[23] have been recalculated from their data and then refitted, using the β values of Ramette,[15] to obtain new extinction coefficients. Both sets of values are given in Table 4.13. The reevaluated results suggest that ε_2 is a maximum at ~260 nm and the value does not follow the typical trend of $\varepsilon_1 < \varepsilon_2 < \varepsilon_3$. The variation with wavelength of the ε_3 values also is different for the two sets. The two studies in 100% AN show some substantial differences in their extinction

Table 4.13. Summary of Extinction Coefficients (ε_i, M^{-1} cm^{-1}) for $Cu(II)X_n$ Complexes

λ, nm	Medium	X	$10^{-3}\varepsilon_1$	$10^{-3}\varepsilon_2$	$10^{-3}\varepsilon_3$
270 [a]	80% AN	NO_3^-	0.024	0.16	
280 [a]	80% AN	NO_3^-	0.031	0.19	
280 [a]	95% AN	NO_3^-	0.61	0.99	
254 [b]	Water	Cl^-	0.97[c] 1.7[d]	2.5[c] 2.9[d]	3.3[c] 1.9[d]
260	Water	Cl^-	0.845[c] 1.44[d]	2.35[c] 3.21[d]	2.85[c] 2.02[d]
280	Water	Cl^-	0.213[c] 0.362[d]	0.906[c] 1.88[d]	2.71[c] 2.01[d]
300	Water	Cl^-	0.013[c] 0.023[d]	0.440[c] 1.20[d]	1.13[c] 3.86[d]
254 [a]	80% AN	Cl^-	1.4	2.1	2.8
280 [a]	80% AN	Cl^-	0.562	1.58	4.65
260 [a]	95% AN	Cl^-	2.9	2.2	
280 [a]	95% AN	Cl^-	2.3	4.0	
300 [a]	95% AN	Cl^-	0.67	3.6	
254	100% AN	Cl^-	1.0[e] 0.015[f]	2.4[e] 1.2[f]	2.3[e] 3.2[f]
260	100% AN	Cl^-	1.1[e] 0.40[f]	2.2[e] 1.0[f]	2.2[e] 0.64[f]
280	100% AN	Cl^-	1.8[e] 2.8[f]	0.83[e] 1.9[f]	1.1[e] 1.0[f]
300	100% AN	Cl^-	2.5[e] 4.5[f]	2.3[e] 3.0[f]	2.5[e] 3.4[f]

[a] This work (ambient temp., variable μ). [b] Interpolated from published data. [c] Reference 23 (25 °C, μ = 5 M $NaClO_4$). [d] Recalculated with β's from reference 15. [e] Reference 21 (25 °C, μ = 0.1 M Et_4NClO_4). [f] Reference 20b (unspecified temp., μ = 0.1 M Et_4NClO_4).

coefficients, and are not particularly consistent with any smooth trend with increasing AN from the values determined in 80 and 95% AN in this study, but this is due at least in part to the apparent shift of the maxima to longer wavelength in 100% AN.

The discussion of complex formation constants below is done in terms of the stepwise or successive formation constants (K_n) rather than overall (β_n) values. The stepwise values are defined as $K_n = [MX_n]/[MX_{n-1}]\,[X]$, and they are related by $K_1 = \beta_1$, $K_2 = \beta_2/\beta_1$, $K_3 = \beta_3/\beta_2$. This change is made because there are generally recognized trends in successive K_n values in that they usually vary as $K_1 > K_2 > K_3$. This trend is ascribed to probability, steric and charge effects and it is found often that K_n/K_{n-1} is in the range of 5 – 50 when these factors have their normal influence. When the order is abnormal, or if there is an unusually large change in the successive values, the explanation is usually found in a change in metal ion coordination number or geometry, and/or a change in the number of unpaired electrons.

The K_n values for Cu(II), given in Table 4.14, generally follow the expected trend of $K_1 > K_2 > K_3$. A notable exception is the K_3 value with Cl^- of Ohtaki and coworkers[21] which is 10^3 times less than K_2, and is a similar magnitude smaller than that given by Manahan and Iwamoto.[20b]

Although no K value for Cu(II) with nitrate ion in AN is available, those in water, 80 and 95% AN, show a trend that suggests a K_1 for the formation of $Cu(NO_3)^+$ that would be several orders of magnitude larger in AN than in water.[24] This same trend is noted for chloride ion complexation with increasing AN, and may be ascribed to the rather weak coordination of Cu(II) by AN as well as the decreasing dielectric constant of the medium. The K_1 values for the nitrate in 80 and 95% AN seem quite large since the

Table 4.14. Summary of Stepwise Formation Constants (M^{-1}) for Cu(II) complexes

Medium	M/X	K_1	K_2	K_3	Reference
(0% AN) Water	$Cu^{(II)}/NO_3^-$	3.2	0.13		a
80% AN	$Cu^{(II)}/NO_3^-$	1.1×10^3	12.8		b
95% AN	$Cu^{(II)}/NO_3^-$	4.0×10^3	99		b
(0% AN) Water	$Cu^{(II)}/Cl^-$	2.36	0.63	0.46	c
80% AN	$Cu^{(II)}/Cl^-$	8.8×10^2	57	2.5	b
95% AN	$Cu^{(II)}/Cl^-$	3.5×10^5	1.2×10^4		b
100% AN	$Cu^{(II)}/Cl^-$	4.9×10^9	8.9×10^7	8.7×10^4	d
100% AN	$Cu^{(II)}/Cl^-$	5.0×10^9	7.9×10^7	1.3×10^7	e
100% AN	$Cu^{(I)}/NO_3^-$	0 ± 5			f
(0% AN) Water	$Cu^{(I)}/Cl^-$	1.3×10^3	2.1×10^2	0.2	a
100% AN	$Cu^{(I)}/Cl^-$	6.3×10^4	6.3×10^5		g
100% AN	$Cu^{(I)}/Cl^-$	7.9×10^4	7.9×10^5		e
100% AN	$Cu^{(I)}/Cl^-$	2.0×10^4	7.9×10^5		f

[a] Reference 24, $\mu = 0$. [b] This work (ambient temp., variable μ). [c] Reference 15 ($\mu = 5$ M $NaClO_4$). [d] Reference 21, (25 °C, $\mu = 0.1$ M Et_4NClO_4). [e] Reference 20b (unspecified temp., $\mu = 0.1$ M Et_4NClO_4). [f] Reference 19 (25 °C, $\mu = 0.1$ M Et_4NClO_4). [g] Reference 20a (25 °C, $\mu = 0.1$ M Et_4NClO_4).

nitrate ion usually is considered to be weakly coordinating. The value of K_1 may have a contribution from ion-pairing (K_i), but Eigen-Fuoss calculations suggest $K_i < 10^2$ so that its contribution to K_1 is small.

The complexation of Cu(I) in AN has been studied by several groups[19,20,24] and the results are included in Table 4.14. Nitrate ion was studied by Senne and Kratochvil[19] by potentiometry and was found to be unassociated with the Cu(I) in AN. The results for chloride ion in AN[19,20] are in reasonable agreement but are unusual in that $K_2 > K_1$. This might represent a change in geometry from tetrahedral $Cu(NCCH_3)_3(Cl)$ to trigonal $Cu(NCCH_3)(Cl)_2$ or linear $Cu(Cl)_2$. It should be noted that the K_n values in water[24] show a rather normal trend. Compared to Cu(II), the Cu(I) formation constants show a much smaller increase between water and AN. This may be attributed to the much stronger solvation or coordination of Cu(I) by AN compared to water. The strong stabilization of Cu(I) by AN has been noted elsewhere in this work.

The complexation results of the present study are summarized in Figures 4.6 and 4.7 in the form of species distribution plots. These have been calculated for conditions typical of the kinetic studies described in the following sections.

Kinetics. The species distribution diagrams given in Figures 4.6 and 4.7 indicate that for the Cu(II) concentrations used, mono, bis and tris (chloride system, 80% AN) complexes are present in addition to the free ion. The specific rate constants (k_n) for these complexes and those from the previous study in water[2] are summarized in Table 4.15.

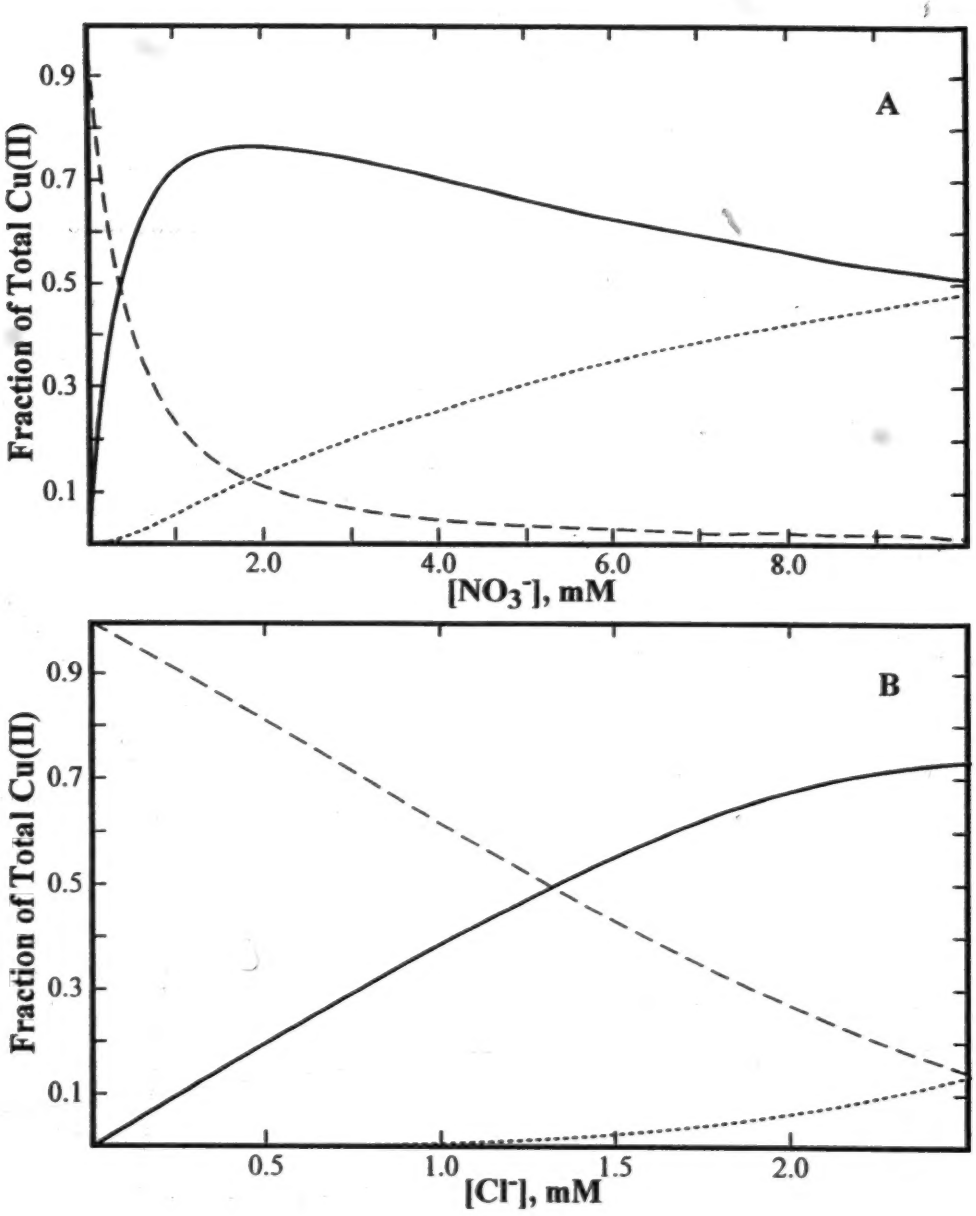

Figure 4.6. Distribution of Cu(II) complexes with the nitrate (A) ($[Cu(II)]_t$ = 0.25 mM) and chloride (B) ($[Cu(II)]_t$ = 2.5 mM) in 95% AN as calculated on the basis of the formation constants from the present study. Species are Cu^{2+} (– – –), CuX^+ (——) and CuX_2 (-------).

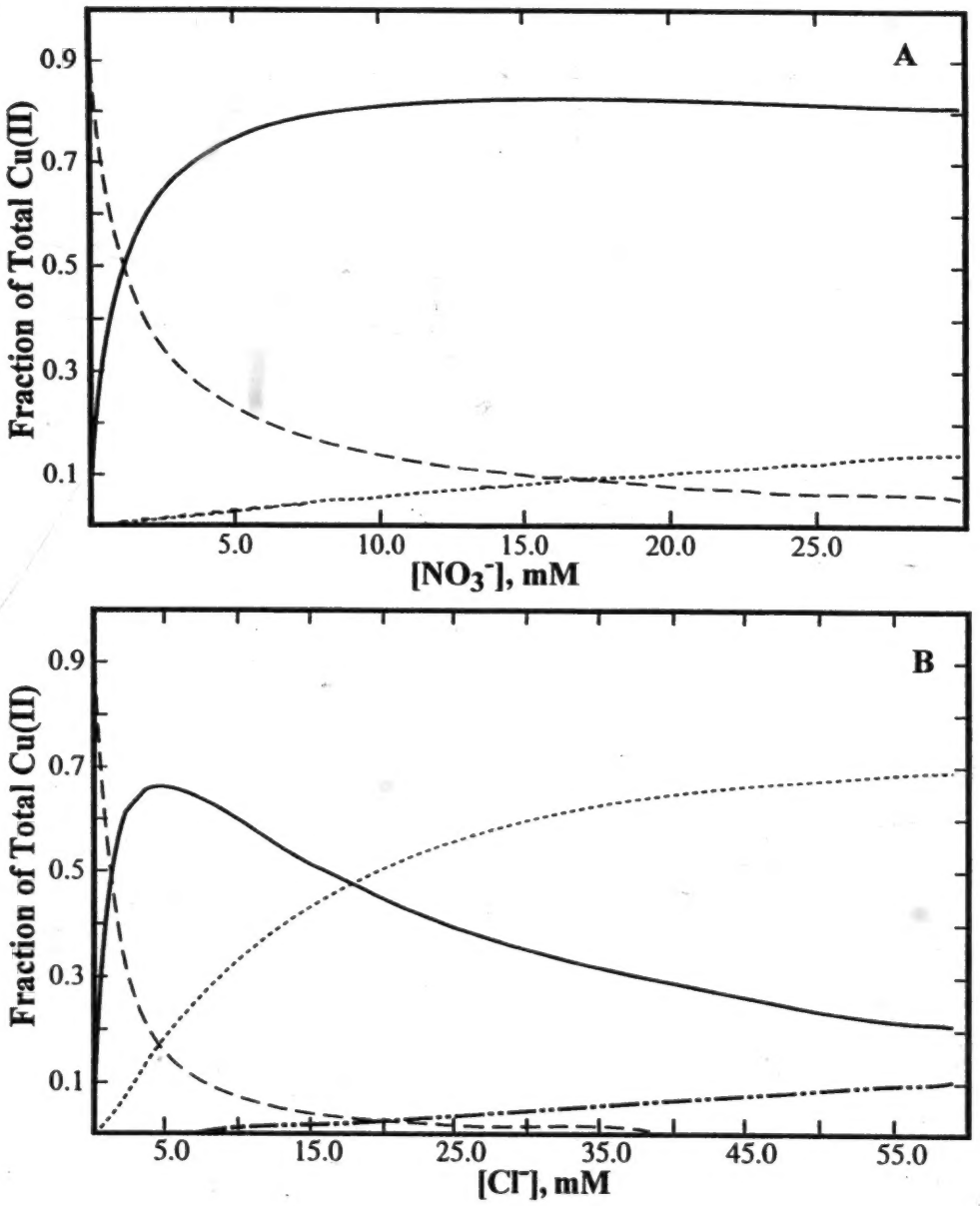

Figure 4.7. Distribution of Cu(II) complexes with the nitrate (**A**) ($[Cu(II)]_t$ = 0.5 x $[NO_3^-]$) and chloride (**B**) ($[Cu(II)]_t$ = 0.20 mM) in 80% AN as calculated on the basis of the formation constants from the present study. Species are Cu^{2+} (– – –), CuX^+ (——), CuX_2 (-------) and CuX_3^- (—·—·—).

Table 4.15. Summary of Specific Rate constants (M^{-1} s^{-1}) for Electron-Transfer Involving $Cu(II)X_n$ Complexes

Medium	X^-	Reductant	k_0	k_1	k_2	k_3
80% AN [a]	NO_3	Fc	6.40 [d]	5.49 [d]	5.00	
80% AN [a]	NO_3	Dmfc	25.4	27.8	27.3	
95% AN [a]	NO_3	Fc	195	185	7.5	
95% AN [a]	NO_3	Dmfc	1040	969	<100	
Water [b]	Cl	Co(Sep) [c]	5.0	1.6×10^3	1.5×10^4	4.5×10^5
80% AN [a]	Cl	Fc	4.43	1.20×10^2	3.64×10^3	1.97×10^5
80% AN [a]	Cl	Dmfc	29.2	3.76×10^2	1.27×10^4	5.07×10^5
95% AN [a]	Cl	Fc	189	4.59×10^3	1.69×10^5	

[a] This work (25 °C, variable μ). [b] Reference 2 (25 °C, μ = 0.5 M $HClO_4/LiClO_4$).
[c] Co(Sep) = cobalt(II) sepulchrate. [d] Calculated with a fixed k_2 of 5.00 M^{-1} s^{-1}, as explained on in the text.

The variation of the electron-transfer rate constants with the nitrate and chloride ion concentrations appears anomalous in that the k_n shows minor variations with nitrate, but increases substantially with increasing n with chloride. Based on the introductory discussion, if one assumes that the electron-transfer is always outer-sphere, and that the self-exchange rate constants for the ferrocenes are independent of anion, then eq. 4.3 predicts that k_n/k_0 should be the same for Fc and Dmfc with a particular anion in the same medium. These ratios are given in Table 4.16, and indicate that this prediction is reasonably true.

It would be of interest to learn if the changes in k_n are primarily due to variations in the thermodynamic factor β_n^I/β_n^{II} or the kinetic factor k^n_{11}. In order to do this the following version of eq. 4.3 has been used.

$$\left(\frac{k^n_{11}}{k^0_{11}}\right) \approx \left(\frac{k_n}{k_0}\right)^2\left(\frac{\beta^I_n}{\beta^{II}_n}\right)^{-1} \qquad (4.23)$$

In the present study, values of k_n, k_0 and β_n^{II} have been determined, and if β_n^I values can be obtained from previous work, then k^n_{11}/k^0_{11} can be estimated. If this kinetic factor is not influential, then the ratio should be ~1. If it is much greater, then the implication is that the complex formation facilitates the electron exchange between the Cu(II/I) species and thereby enhances the rate of the cross-reaction.

For the Cu(I)-nitrate system, a previous study in 100% AN could only place an upper limit of $\beta_n^I \leq 5\ M^{-1}$ (see Table 4.14). No doubt the value is smaller in aqueous AN, but one can still estimate an upper limit for $(\beta_1^I/\beta_1^{II}) \leq 1.25 \times 10^{-3}$ in 95% AN. This

Table 4.16. Rate Constant Ratios for Reactions of Cu(II) with Fc and Dmfc in the Presence of Nitrate and Chloride ions in 80 and 95% AN

Ratio	Anion	n	80% AN		95% AN	
			Fc	Dmfc	Fc	Dmfc
k_n/k_0	NO_3^-	1	0.86	1.1	0.95	0.93
k_n/k_0	NO_3^-	2	0.78	1.1	3.8×10^{-2}	3.8×10^{-2}
k_n/k_0	Cl^-	1	27	13	24	
k_n/k_0	Cl^-	2	8.2×10^2	4.3×10^2	8.9×10^2	
k_n/k_0	Cl^-	3	4.4×10^4	1.7×10^4		
k^n_{11}/k^0_{11} [a]	NO_3^-	1			$\geq 7.2 \times 10^2$	$\geq 7.0 \times 10^2$
k^n_{11}/k^0_{11} [a]	Cl^-	1	65	15	2.1×10^4	
k^n_{11}/k^0_{11} [a]	Cl^-	2	34	9.6	3.5×10^6	

[a] Calculated from β_n values as described in text.

combined with $k_1/k_0 = 0.95$ for Fc in 95% AN gives $(k^1_{11}/k^0_{11}) \geq 7.2 \times 10^2$. The analogous value for Dmfc is $\geq 7.0 \times 10^2$. These results suggest that complexation of Cu(II) by nitrate ion does enhance the Cu(II/I) self-exchange rate. Some increase in the rate might be expected because of the reduced electrostatic repulsion between the reactants, but estimates indicate that this is a factor of 2-3 for a 10 Å interaction distance in 95% AN. Since an estimate of β_1^I in 80% AN would be even more doubtful and there is no information on β_2^I for nitrate, the nitrate system will not be analyzed further.

With chloride ion, the β_1^I in water is just 50 times smaller than that in 100% AN (see Table 4.14), and it seems reasonable that β_1^I is $\sim 10^4$ M^{-1} in 95% and 80% AN. If one further assumes that K_2^I/K_1^I is similar in 100%, 95% and 80% AN, then K_2^I is $\sim 10^5$ and β_2^I is $\sim 10^9$ M^{-2}. Then one can calculate (k^n_{11}/k^0_{11}) for n = 1 and 2 as before and the values are collected in Table 4.16.

The general observation from these calculations is that the values from Fc and Dmfc are in reasonable agreement, and are larger than 1. This shows that the thermodynamic factor (β_n^I/β_n^{II}) is always causing the rate constant to decrease more than observed. Comparisons of nitrate to chloride are limited to Fc in 95% AN where the effect of nitrate is ~30 times less. The consequence is that k_n changes rather little with nitrate, whereas it increases with chloride. Because the estimates of β_n^I are most reliable in 95% AN, these also give the best estimates of (k^n_{11}/k^0_{11}). The values give $k^1_{11}/k^0_{11} = 2.1 \times 10^4$ and $k^2_{11}/k^1_{11} = 3.5 \times 10^6$, indicating that the effect of chloride on the self-exchange rate constant attenuates with increasing complexation. If one takes the value of $k^0_{11} = 10^{-9}$ determined in Chapter 3, then $k^1_{11} = 2.1 \times 10^{-5}$ and $k^2_{11} = 3.5 \times 10^{-3}$ M^{-1} s^{-1}. There is an analogous change in 80% AN, but it is 10^3-10^4 times smaller.

The chloride effect found in the present study is qualitatively analogous to that observed in the Cu(II)/Co(II)(sep) system (see Table 4.15) in that the rate increases with increasing chloride concentration. For aqueous Cu(I) and Cu(II) the β_3 values are small and poorly defined, however it is possible to do the above analysis for n = 1 and 2. The situation is analogous to that in 80% AN, except that the β_n^I/β_n^{II} ratio is about 10 times larger in water. The k^n_{11}/k^0_{11} ratios are 1.9×10^2 and 54 for n =1 and 2, respectively. The only anomaly is that k^2_{11} appears to be ~4 times smaller than k^1_{11}, but this may not be significant within the uncertainties in the β_n values and the usual assumptions of Marcus theory.

Conclusion

The present study has established that both nitrate and chloride ions complex appreciably with the Cu(II) in 80 and 95% AN with overall formation constants $>10^3$. For both ions, complexation seems to favor Cu(II) over Cu(I) in AN but the nitrate appears to inhibit the electron-transfer rate for Cu(II)-ferrocenes while the chloride ion has the opposite effect. It is concluded, for the chloride ion, that the effects on the electron-transfer rate constants result from an increase in the self-exchange rate constant for the $Cu(II/I)Cl_n$ species. For the nitrate ion, the inhibition of the rate above 95% AN is due to the much stronger complexation of Cu(II) which is only partially compensated by increases in the self-exchange rate constants.

References

(1) Pfeiffer, J.; Kirchner K.; Wherland, S. *Inorg. Chim. Acta* **2001**, *313*, 37, and references therein.

(2) Sisley, M. J.; Jordan, R. B. *Inorg. Chem.* **1992**, *31*, 2880.

(3) Dekker, A. 0.; Dickinson, R. G. *J. Am. Chem. Soc.* **1940**, *62,* 2165. Mapson, L. W. *Biochem. J.* **1941**, 35, 1332. Ogata, Y.; Kosugi, Y.; Morimoto, T. *Tetrahedron* **1968**, *24,* 4057.

(4) Xu, J.; Jordan, R. B. *Inorg. Chem.* **1990**, *29,* 2933. Sisley, M. J.; Jordan, R. B. *J. Chem. Soc., Dalton Trans.* **1997**, 3883.

(5) Yandell, J. K. *Aust. J. Chem.* **1981**, *34*, 99.

(6) Zahl, A.; van Eldik, R.; Swaddle, T. W. *Inorg. Chem.* **2002**, *41*, 757.

(7) Jordan, R. B. *Reaction Mechanisms of Inorganic and Organometallic Systems*, Oxford University Press, New York, **1998**.

(8) Wherland, S. *Coord. Chem. Rev.* **1993**, *123*, 149.

(9) Marcus, R. A. *J. Phys. Chem. B.* **1998**, *102*, 10071, and references therein.

(10) Powell, D. H.; Furrer, P.; Pittet, P.-A.; Merbach, A. E. *J. Phys. Chem.* **1995**, *99*, 16622.

(11) Murguia, M. A.; Wherland, S. *Inorg. Chem.* **1991**, *30*, 139.

(12) Nelsen, S. F.; Pladziewicz, J. R. *Acc. Chem. Res.* **2002**, *35*, 247.

(13) Sutin, N. *Prog. Inorg. Chem.* **1983**, *30*, 441. Marcus, R. A. *Annu. Rev. Phys. Chem.* **1964**, *15,* 155.

(14) Ahrland, S.; Rawthorne, J. *Acta Chem. Scand.* **1970**, *24,* 157.

(15) Ramette, R. W. *Inorg. Chem.* **1986**, *25*, 2481.

(16) Davies, K. M. *Inorg. Chem.* **1983**, *22*, 615.

(17) Creaser, I. I.; Harrowfield, J. M.; Herlt, A. J.; Sargeson, A. M.; Snow, M. R.; Springborg, J. *J. Am. Chem. Soc.* **1982**, *104*, 6016. Creaser, I. I.; Sargeson, A. M.; Zanella, A. W. *Inorg. Chem.* **1983**, *22*, 4022. Bernhard, P.; Sargeson, A. M. *Inorg. Chem.* **1987**, *26*, 4122.

(18) Kolthoff, I. M.; Coetzee, J. *J. Am. Chem. Soc.* **1957**, *79*, 1852.

(19) Senne, J. K.; Kratochvil, B. *Anal. Chem.* **1971**, *43*, 79.

(20) (a) Heerman, L. F.; Rechnitz, G. A. *Anal. Chem.* **1972**, *44*, 1655. (b) Manahan, S. E.; Iwamoto, R. T. *Inorg. Chem.* **1965**, *4*, 1409.

(21) Ishiguro, S.-I.; Jeliazkova, B. G.; Ohtaki, H. *Bull. Chem. Soc. Jpn.* **1985**, *58*, 1749.

(22) Kolthoff, I. M.; Sandell, E. B.; Meehan E. J.; Bruckenstein, S. *Quantitative Chemical Analysis*, Collier-MacMillan Canada Ltd., Toronto, **1969**.

(23) Khan, M. A.; Schwing-Weill, M. J. *Inorg. Chem.* **1976**, *15*, 2202.

(24) Smith, R. M.; Martell A. E.; Motekaitis, R. *NIST Critically Selected Stability Constants of Metal Complexes Database*, Version 2; NIST: Washington, DC, **1995**.

Chapter 5. Studies on ^{63}Cu(I) NMR Linewidth in Acetonitrile

Introduction

This study began as an exploration of the possibility of using ^{63}Cu(I) NMR to measure the Cu(II/I) electron-exchange rate in acetonitrile. As noted in Chapter 2, preliminary studies found that the triflate salts of Cu(I) and Cu(II) have advantageous solubilities in acetonitrile that would permit the widest concentration range for both in the electron-exchange studies. As a consequence, the studies in this thesis have focused on the triflate salts and a major concern here is the NMR behavior of $Cu(AN)_4(F_3CSO_3)$ which had not been studied previously. The NMR behavior of the perchlorate salt also has been studied for comparison purposes. In addition, the effects of chloride ion and water on the ^{63}Cu(I) NMR linewidths have been examined.

As noted in Chapter 1, ^{63}Cu(I) NMR linewidths in AN are unexpectedly broad so that the sensitivity is seriously affected. Two studies in the 1980's by Ochsenbein and Schläpfer[1] and Kroneck et al.[2] indicated that the temperature dependence of the linewidth is anomalous in that it shows a minimum at about -5 °C and then broadens through the ambient temperature region. As a result, the linewidth at ~25 °C is much greater than would be predicted from extrapolation of low temperature linewidths. For nuclei such as ^{63}Cu with spin I >1/2, the decrease in linewidth with increasing temperature is expected for quadrupolar relaxation, as described below, but the cause of the increasing linewidths above -5 °C remains unexplained. As noted in Chapter 1, earlier studies suggested that this effect might be due to a coordination change[1] or to ion-pairing.[2] One goal of this study was to seek a quantitative explanation of this anomaly, with the hope that it might then be possible to find conditions to minimize it and thereby improve the sensitivity, and

also to add to the understanding of the coordination chemistry of the Cu(I)-acetonitrile system and provide speciation information that might be critical for electron exchange studies.

In 1982, Marker and Gunter[3] also studied ^{63}Cu(I) NMR and ^{31}P NMR linewidths of Cu(I) complexes with trimethyl and triethyl phosphite in CD_2Cl_2 and $CDCl_3$ and found a temperature dependence of the ^{63}Cu(I) NMR linewidths (100-700 Hz) analogous to that observed in the acetonitrile system, with a minimum in the 0-20 °C range, and a similar dependence for the lines ($J_{Cu\text{-}P}$ ~ 1200 Hz) in the ^{31}P spectra. The latter spectra also show a singlet resonance which the authors assign to $[CuP_x(AN)_{4-x}]^+$ (x = 1-3) derived from the $Cu(AN)_4^+$ starting material. The assignment is based on phosphite concentration effects and ^{13}C chemical shifts of AN. The ^{31}P linewidths of the singlet increased with increasing temperature, while simple observation of the singlet suggested slow exchange of these species with the CuP_4^+ species. The authors interpreted the higher temperature behavior as due to ligand exchange with activation energies in the range of ~ 4 kcal mol^{-1}.

Because $Cu(AN)_4^+$ is often used as a shift standard in ^{63}Cu NMR, there have been a few other reports of the linewidths, and they all are summarized in Table 5.1. Aside from a few strange results, such as the most recent on BF_4^-, and the earliest on PF_6^-, the reported values commonly fall in the 480 to 550 Hz range. However, there are several, including those from this study, in the 400 to 440 Hz range.

Table 5.1. ^{63}Cu(I) NMR Linewidths of $Cu(AN)_4X$ Salts in Acetonitrile

X^-	$W_{1/2}$, Hz	Date	Conditions[a]	Reference
BF_4	540	1978	0.1 M, Bruker SXP, 10 mm	c
BF_4	490	1980	0.1 M, Varian XL-100, 10 mm	d
BF_4	540	1982	0.087 M, Bruker SXP, 10 mm	e
BF_4	600	1987	1.0 M, Varian FX-270, 30 °C	f
BF_4	8570	1988	Unspecified conc., Bruker WH-200	g
PF_6	800	1980	0.1 M, Varian XL-100, 10 mm	d
PF_6	400	1983	Unspecified conc., Nicolet NT-360	h
ClO_4	522 (494)[b]	1980	0.1 M, Varian XL-100, 10 mm	d
ClO_4	550	1982	0.061 M, Bruker SXP, 10 mm	e
ClO_4	580	1982	0.10 M, Bruker SXP, 10 mm	e
ClO_4	500	1984	0.05 M, JOEL FX-200, 10 mm	i
ClO_4	505 (481)[b]	1990	0.02-0.06 M, Bruker AM-400	j
ClO_4	480	1995	0.05-0.065 M, Bruker AM-400	k
ClO_4	480	1998	0.064 M, Bruker-500, 10 mm	l
ClO_4	480	1999	0.064 M, Bruker-500, 10 mm	m
ClO_4	440	1999	0.1 M, Bruker MSL-300	n
ClO_4	520	2001	0.064 M, Bruker-300, 10 mm	o
ClO_4	443	2002	0.062 M, Varian S-400	p
ClO_4	423	2002	0.0062 M, Varian S-400	p

Table 5.1. (Continued)

X^-	$W_{1/2}$, Hz	Date	Conditions[a]	Reference
F_3CSO_3	417	2002	0.00494 M, Varian S-400	p
F_3CSO_3	463	2002	0.062 M, Varian S-400	p
F_3CSO_3	460	2002	0.061 M, Varian S-400	p
F_3CSO_3	488 (492)[b]	2002	0.117 M, Varian S-400	p

[a] Temperatures are 25 °C unless stated otherwise, although sometimes not given. Sample tube diameter is 5 mm unless otherwise indicated. [b] A measured T_1 converted to the equivalent in Hz. [c] Reference 6. [d] Reference 1. [e] Reference 2. [f] Endo, K.; Yamamoto, K.; Deguchi, K.; Matsushita, K. *Bull. Chem. Soc. Jpn.* **1987**, *60*, 2803. [g] Connor, J. A.; Kennedy, R. J. *Polyhedron* **1988**, *7*, 161. [h] Reference 13. [i] Kitagawa, S.; Munakata, M. *Inorg. Chem.* **1984**, *23*, 4388. [j] Reference 8. [k] Reference 9. [l] Reference 11. [m] Gill, D. S.; Singh, L. J.; Singh, R.; Zamir, T.; Quickenden, L. *Indian J. Chem.* **1999**, *38A*, 913. [n] Szlyk, E.; Szymanska, I. *Polyhedron* **1999**, *18*, 2941. [o] Reference 12. [p] Present study.

Taken overall, the range of ~150 Hz in the values in Table 5.1 seems unexpected for materials that are relatively easy to prepare and handle, and are considered as standards. It should be noted that the spectra typically might have significant random noise, making assignment of the linewidth somewhat difficult. In this work, the uncertainties are ±10 Hz, for a signal/noise ratio of ~10, but trends within a given type of experiment on a particular instrument are clearly perceptible. The situation may be worse for some earlier, low-field measurements, although 10 mm outside diameter (o.d.) tubes often were used to improve sensitivity. The S/N ratio is much better for ≥ 400 MHz ^{1}H instruments, even with 5 mm o.d. tubes. Nevertheless, the range of linewidths seems difficult to explain on the basis of instrumentation alone. Indeed, the trend in the linewidths does not seem to be a function of advancements or differences in instrumentation. One minor objective of this work was to test the effect of various conditions and possible common contaminants that might affect the linewidths. Consequently, the effects of sample size and spinning, and of likely contaminants such as water and chloride ions have been examined in this study.

Experimental

Materials. Acetonitrile (Caledon, Fisher or BDH) was dried in 4Å molecular sieves for several days before use. Doubly distilled water was used. Anhydrous diethyl ether (Fisher), perchloric acid (Fisher), trifluoromethanesulfonic (triflic) acid (Aldrich), copper foil (Matheson, Coleman and Bell), cuprous oxide (Matheson, Coleman and Bell), cupric oxide (Fisher) were used as supplied. Tetra(n-butyl)ammonium triflate (Aldrich), tetra(n-butyl)ammonium perchlorate (Aldrich), tetramethylammonium hexafluorophosphate (Aldrich), tetramethylammonium tetrafluoroborate (Aldrich) and

tetraethylammonium chloride (Sigma) were dried in air at ~90 °C. Lithium triflate was prepared by adding ~5 M triflic acid to an aqueous slurry of the required amount of lithium carbonate (Fisher) and concentrating the resulting clear colorless solution to dryness and then washing the solid with diethyl ether and drying in vacuo. $(NH_3)_5Co(OH_2)Br_3$ was synthesized by adding 1.0 g (3.76 mmol) of $[(NH_3)_5CoCO_3]NO_3$ to 20 mL of water containing 20 mL of 48% HBr (Anachemia) in an ice bath. The mixture was stirred for ten minutes and then the solid product was allowed to settle before collecting by filtration. The product was washed with ethanol and ether and air dried.

$Cu(CH_3CN)_4(ClO_4)$. In a modification of the method used by Hemmerich and Sigwart[4], 1.8 mL of 70% (~11.6 M) perchloric acid was added to 100 mL of acetonitrile containing 1.43 g (10 mmol) of cuprous oxide and stirred at ~40 °C for 1 hour. The resulting mixture was filtered and, on adding diethyl ether to the colorless filtrate, a crystalline white product was obtained which was recovered by filtration through a porous frit. This product is stable in air for several months with no color change if the sample is kept in a tightly-capped container when not in use.

$Cu(CH_3CN)_4(F_3CSO_3)$. The tetrakis(acetonitrile)copper(I) triflate was prepared from the reaction of $Cu(H_2O)_4(F_3CSO_3)_2$ and Cu metal and recovered as a white solid from the acetonitrile solution using anhydrous diethyl ether, as described in Chapter 2. This product also was recovered by removing the solvent by vacuum distillation. An ice/water slush was used to trap the solvent and pumping was stopped just when the solid appeared to be reasonably dry. A liquid nitrogen trap or prolonged pumping seemed to give a more air and moisture sensitive product. The product was then transferred to a

glove bag and stored under prepurified nitrogen. This product seemed more air-sensitive than that obtained in Chapter 2.

NMR samples. On the bench top, stock solutions were made by quickly weighing and transfering the Cu(I) triflate/perchlorate salt to a measured volume of 90%CH_3CN/10%CD_3CN mixture in a vial which was then capped and covered with parafilm. Aliquots of freshly prepared stock were diluted to obtain the required concentration. Samples of 0.6 mL (5 mm o.d. tubes) or 4 mL (10 mm o.d. tubes) were then drawn using a gastight syringe fitted with a Teflon needle and immediately transferred on to an nmr tube which had been dearated by flushing with argon for 5 minutes. The argon was bubbled through the solution for a further 1 minute before placing a septum cap and sealing with parafilm. Cu(I) triflate or perchlorate samples containing added salts (tetraethylammonium chloride, lithium triflate, tetramethylammonium hexafluorophosphate/tetrafluoroborate, tetra(n-butyl)ammonium triflate/perchlorate) were similarly prepared. Samples also were prepared on a vacuum line by distilling CH_3CN/CD_3CN onto a weighed amount of $Cu(CH_3CN)_4(O_3SCF_3)$ in a weighed NMR tube. Then the tube was sealed and reweighed to determine the final concentration. Samples containing small amounts of water were prepared on the vacuum line by collecting the water released from weighed amounts of $(NH_3)_5Co(OH_2)Br_3$, (heated at ~100 °C)[5] onto the Cu(I)-acetonitrile sample in a dry-ice slush. The tube was then sealed under vacuum and the composition determined from the mass. A sample contanining 5.61 M water also was prepared on the bench top by dissolving 4.01×10^{-2} g (0.123 mmol) of the Cu(I) perchlorate salt in 2 mL of 80%CH_3CN/10%CD_3CN/10%H_2O v/v/v mixture.

NMR measurements. NMR measurements were done in the NMR Laboratory in the Department of Chemistry, University of Alberta. The ^{63}Cu NMR spectra were recorded using broadband probe heads on Varian S 400 and Bruker AM 200 spectrometers. The latter also was used for the ^{14}N spectra. Samples were in 5 mm o.d. tubes, except for one ^{63}Cu measurement at 25 °C in a 10 mm o.d. on the Bruker system. Typical NMR parameters for a given experiment were: 45° pulse, delay ~$5T_1$, spectroscopic window of 50 kHz, exponential filter of 10 Hz. For the ^{63}Cu spectra, about 10000 scans (Bruker) or 1000 scans (Varian) were collected, whereas ~400 scans were used for ^{14}N. The variable temperature ^{63}Cu and a few ^{65}Cu (at 25 °C) NMR spectra were recorded on the Varian S 400. The probe temperature was calibrated using methanol for temperatures below ambient and ethylene glycol for temperatures above ambient. The linewidths were determined by fitting to a Lorentzian lineshape using the spectrometer's software, as well as locally developed programs. Both methods were in good agreement (i.e. within ±20 Hz). In all linewidth measurements it was observed, in agreement with Marker and Gunter,[3] that when an exponential filter was applied to the FID the resultant line broadening needed to be subtracted to obtain the correct linewidth.

The T_1 was determined by a (π-τ-$\pi/2$-acquire-delay)n (n = 1500 transients at each of 11τ values) sequence on a 0.117 M $Cu(CH_3CN)_4(F_3CSO_3)$ and analyzed using the Varian software.

Results

For ^{63}Cu with nuclear spin I = 3/2 and magnetogyric ratio $\gamma = 7.097 \times 10^7$ rad s^{-1} $Tesla^{-1}$, nuclear relaxation is expected to be dominated by the quadrupolar relaxation mechanism and to be in the extreme narrowing limit. The latter requires that the nuclear

precession rate ($\pi\nu_o$) times the correlation time for molecular tumbling (τ_Q) should satisfy the condition $(\pi\nu_o\tau_Q)^2 << 1$. For ^{63}Cu(I) on a 400 MHz ^{1}H spectrometer, $\pi\nu_o = 3.3 \times 10^8$ s^{-1} and $\tau_Q \leq 5 \times 10^{-11}$ s for species such as $Cu(AN)_4^+$ in a normal fluid, so that the extreme narrowing condition should be applicable. Then the quadrupolar relaxation rate is given by

$$\frac{1}{T_2} = \pi W_{1/2} = \frac{3\pi^2(2I+3)}{10\{I^2(2I-1)\}}\left(1+\frac{\eta^2}{3}\right)\left(\frac{e^2qQ}{h}\right)^2\tau_Q \qquad (5.1)$$

where η is the asymmetry parameter, eq is the electric field gradient and eQ is the quadrupole moment. Because all of these factors are unknown, the last two terms in brackets in eq. 5.1 are commonly grouped together as an effective quadrupole coupling constant (QCC), and the expression becomes

$$\frac{1}{T_2} = \pi W_{1/2} = \frac{3\pi^2(2I+3)}{10\{I^2(2I-1)\}}(QCC)^2\tau_Q = 3.9478(QCC)^2\tau_Q \,. \qquad (5.2)$$

Quadrupolar relaxation is consistent with the ^{63}Cu(I) and ^{65}Cu(I) linewidths determined by Lutz and coworkers.[6] The ratio of the linewidths (540/470 = 1.149) is in reasonable agreement with the square of the nuclear quadrupolar coupling constants (1.1686).[7] Similar measurements in this study on 0.062 M Cu(I) perchlorate and triflate gave values of 443/380 = 1.166, and 465/399 = 1.165, respectively. As expected for a system in the extreme narrowing condition, T_1 and T_2 values for ^{63}Cu(I) in AN also were found by

Ochsenbein and Schläpfer,[1] Gill et al.[8] and in this study to be essentially equal.

Some ^{63}Cu(I) NMR linewidths at 25 °C from this study were given previously in Table 5.1. Linewidths also were measured as a function of salt concentration and temperature. Figures 5.1 and 5.2 show some representative results of temperature and concentration effects from the systematic studies of ^{63}Cu(I) NMR linewidths of Cu(I) salts in acetonitrile from this study and by Ochsenbein and Schläpfer[1] and Kroneck et al.[2] The linewidth increases with increasing concentration of the Cu(I) salt and, as noted previously, its temperature dependence typically shows a minimum at about -5 °C. The results of this study with the triflate and perchlorate salts are at least qualitatively similar to those obtained previously. The present results show that the triflate salt gives slightly broader lines than the perchlorate. It can be seen from the Figures that there are considerable differences in the linewidths of the perchlorate salt from this study and an earlier study.[2] Nonetheless, the trends from all these studies are quite similar.

Discussion

The temperature dependence of the ^{63}Cu(I) NMR linewidth above ~-5 °C ($10^3/T$ = 3.7) is anomalous because quadrupolar relaxation should show a simple decrease in linewidth with increasing temperature due to the shortening of the correlation time (τ_Q) for this relaxation process. Kroneck et al.[2] suggested that ion-pairing effects cause the observed broadening above ~-5 °C, and this is supported qualitatively by the concentration effects shown in Figure 5.2, but no attempt was made to provide a quantitative analysis of the results. Ochsenbein and Schläpfer[1] favored formation of complex(es) of different coordination number at higher temperatures to explain the increasing linewidths, and gave no explanation of the concentration effects.

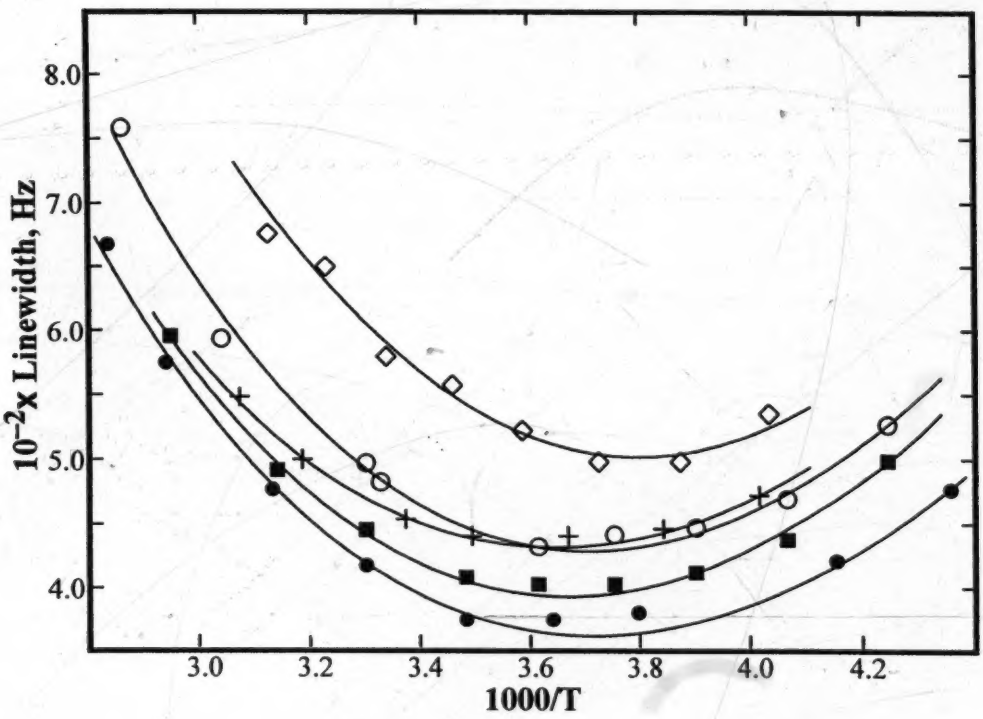

Figure 5.1. Temperature dependence of the $^{63}Cu(I)$ linewidth for $Cu(AN)_4X$ salts in acetonitrile. (●) 0.00494 M $F_3CSO_3^-$; present study. (◇) 0.10 M ClO_4^-; reference 2. (○) 0.117 M $F_3CSO_3^-$; present study. (+) 0.10 M BF_4^-; reference 1. (■) 0.062[illegible] ClO_4^-; present study.

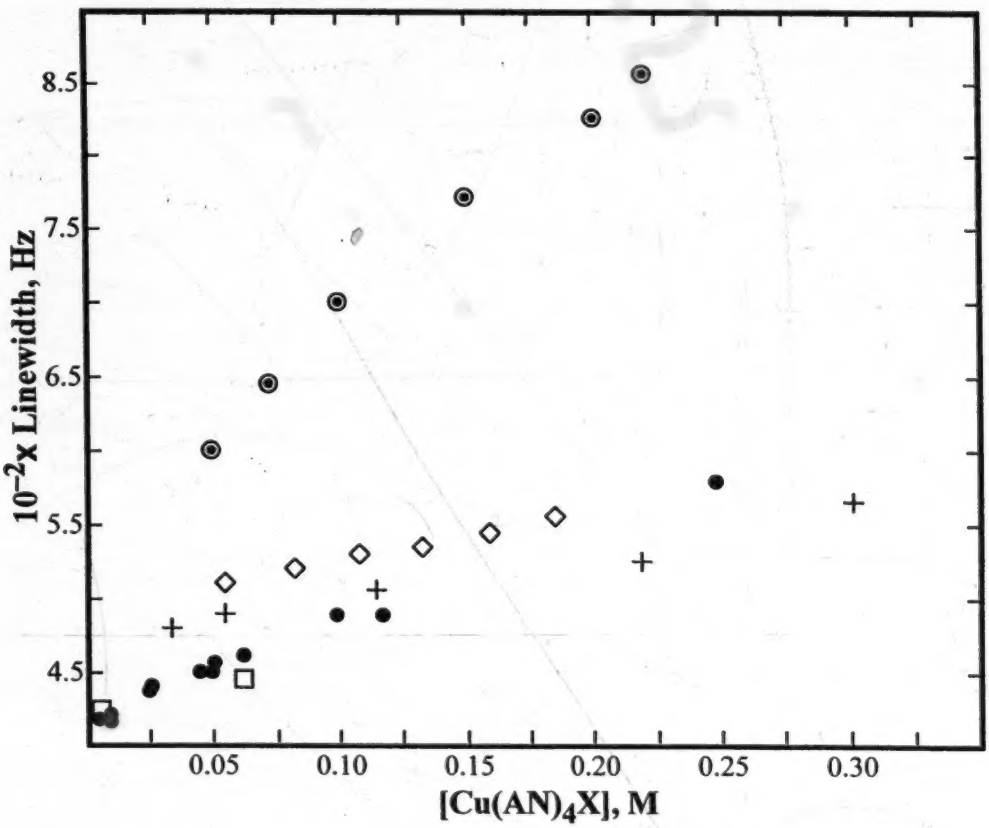

Figure 5.2. Concentration dependence of the ^{63}Cu(I) linewidth for $Cu(AN)_4X$ salts in acetonitrile. (●) X = $F_3CSO_3^-$; present study. (◇) X = ClO_4^-; reference 2. (□) X = ClO_4^-; present study: (◉) X = PF_6^-; reference 1. (+) X = BF_4^-; reference 1.

Gill and coworkers have published a series of studies which mainly deal with the changes in the $^{63}Cu(I)$ linewidth at 25 °C as cosolvents are added to AN. The lines inevitably broaden with the addition of another solvent and this is attributed primarily to the formation of mixed complexes. The observations have been used to estimate quadrupolar coupling constants (QCC) for these species, but the temperature dependence was not studied, although it is probably anomalous for quadrupolar relaxation, as in the pure AN systems. In 1995, Gill et al.[9] reported the dependence of the linewidth on the concentration of $CuClO_4$ (0.008 to 0.45 M) in benzonitrile, and the behavior is similar to that in AN, even after correction for viscosity changes. However, the authors used earlier conductivity results by Gill et al.[10] to argue against ion-pairing but thereafter, they acknowledge the concentration dependence in benzonitrile and suggest ion-pairing as the cause. These authors also suggested that the $^{63}Cu(I)$ linewidths are so large because of the Sternheimer antishielding factor (γ_∞), which has a value of -17 and contributes a factor of ($1-\gamma_\infty$) to the electric field gradient. As noted previously, this ignores the fact that the temperature dependence is not that expected for simple quadrupolar relaxation in one species. In a more recent paper by Gill, Byrne and Quickenden,[11] the Sternheimer factor is not mentioned and the Stokes-Einstein equation is used to calculate a correlation time of $\sim 4.5 \times 10^{-11}$ s, and then a QCC $\approx$ 3.0 MHz for 0.064 M $CuClO_4$ in AN. It should be noted that the correlation time is 10 times shorter than that reported by Gill et al. in 1990.[8] The latter is based on the assumption that the discrepancy between the ratio of T_2's for ^{63}Cu and ^{65}Cu of 1.186 and the value of 1.1686 predicted[7] from the Q values is due to a failure of the extreme narrowing condition. It would appear that the authors have concluded later that this small difference is not meaningful. Most recently, Gill and

coworkers[12] have calculated a correlation time of 1.39×10^{-11} s in acetonitrile and used this to estimate that QCC = 5.46 MHz.

It was noted earlier that Marker and Gunter[3] observed temperature dependence of the ^{63}Cu linewidths (100 - 700 Hz) of the of Cu(I) trimethyl and triethyl phosphite in CD_2Cl_2 and $CDCl_3$, that is analogous to that observed in the AN system, with a minimum in the 0 to 20 °C range.

No attempt has previously been made to compare or correlate the results of these various studies. In a general sense, the observations suggest that some species of lower symmetry is forming in increasing amounts above ~-5 °C in AN and ~0 °C in the phosphite systems. The lower symmetry species might be ion-pairs, or complexes with different numbers and/or types of ligands. From the point of view of applications of ^{63}Cu(I) NMR, it would be advantageous to know the source of the wide lines often observed, with a view to designing methods or conditions for overcoming the problem and increasing the sensitivity.

Of the results in Figure 5.2, the observations of Ochsenbein and Schläpfer[1] on the PF_6^- salt are clearly unique. The concentration dependence is much more dramatic with an overall change in linewidth of ~400 Hz compared to ~50 Hz for the other anions. The temperature dependence (not shown) also is anomalous with a minimum at ~10 °C vs. -5 °C for the others, and with a much larger linewidth in the low temperature limit. Caulton et al.[13] have reported a linewidth of 400 Hz for a "nearly saturated" solution of $Cu(NCCH_3)_4PF_6$ at 25 °C, compared to ~850 Hz at 0.22 M reported by Ochsenbein and Schläpfer.[1] In this study, 0.0613 M $CuClO_4$ containing 0.050 M $(Et_4N)PF_6$ was found to have a linewidth of 447 Hz, entirely consistent with other samples at the same total salt

concentration. These anomalies suggest that the sample of Ochsenbein and Schläpfer[1] was contaminated in some way, and these results will not be included in the further analysis.

If a two species model consisting of $Cu(AN)_4^+$ and either an ion-pair or another species of different coordination or symmetry is assumed for the Cu(I)-acetonitrile system, then there are some simple expectations one should have for these results. In the low concentration limit, all of the salts should give the same linewidth, at a particular temperature. However, extrapolated values at 25 °C from the earlier studies (Figure 5.2) on the BF_4^- and ClO_4^- salts are ~ 470 and ~490 Hz, respectively, while this study gives much smaller values of ~415 and 420 Hz for the triflate and ClO_4^-, respectively. Similarly, below -5 °C where the temperature dependence is that expected for quadrupolar relaxation, all the salts should converge to the linewidth expected for the $Cu(AN)_4^+$ ion. This expectation does seem to be realized from the data in Figure 5.1 for the ~0.1 M triflate, perchlorate (present study) and tetrafluoroborate salts, and other deviations might be due to concentration differences.

Viscosity effects. It was noted earlier that $W_{1/2} \propto \tau_Q$ and the Stokes-Einstein relationship suggests that $\tau_Q \propto \eta/T$ where τ_Q is the correlation time and η is the viscosity of the solvent. Since many studies have shown that viscosity increases with salt concentration[14], then the simplest explanation for the concentration effects would be that they are due to the increase in viscosity with salt concentration which causes τ_Q and hence $W_{1/2}$ to increase.

Gill and coworkers[15] have studied the viscosity of $CuClO_4$ in acetonitrile. The concentration dependence of the viscosity is similar to that of tetra(n-propyl)ammonium

bromide studied by Saha and Das,[16] who also studied the temperature dependence of the viscosity for n-Pr_4NBr in AN. Nikam and Sawant[17] also studied the concentration dependence of the latter system. Gill and coworkers[15] found that the variation of viscosity with concentration of $CuClO_4$ is given by $\eta = \eta_o(1 + A\,[Salt]^{1/2} + B\,[Salt])$ with $A = 1.76 \times 10^{-2}$ and $B = 0.77$ at 25 °C. The data for n-Pr_4NBr[16] suggest that $B = 0.77 \times (1 + 4.0 \times 10^{-3}(298-T))$ for temperature dependence of B (15 to 45 °C) but A has no discernable temperature dependence, probably because this factor makes a small contribution to the overall effect. The temperature dependence of the viscosity of pure acetonitrile was determined between -40 and 20 °C by Kanes[18] and is given by $\eta_o = 0.152\exp(924.7/T)$. The concentration dependence for $CuClO_4$ viscosity from Gill and coworkers,[15] and the temperature dependencies from Saha and Das,[16] and Kanes[18] can be combined to estimate the viscosity of $CuClO_4$ in AN, with the assumption that $CuClO_4$ and n-Pr_4NBr have the same temperature dependence.

It is noteworthy that both the linewidths (Figure 5.2) and the viscosity have an essentially linear dependence on concentration. Since all of the concentration studies have been done at 25 °C, it is convenient for purposes of comparison to analyze the data in terms of the reduced viscosity, η/η_o, where η_o is the viscosity of the pure solvent (3.41 millipoise) and η is the viscosity of the salt solution. If $W_{1/2} \propto \tau_Q$ and $\tau_Q \propto \eta/T$ then

$$\left(\frac{\eta_o}{\eta}\right)W_{1/2} = \frac{C_v\eta_o}{T} = \left(W_{1/2}\right)_{0,T} \qquad (5.3)$$

where C_v is a proportionality constant and $(W_{1/2})_{0,T}$ is the linewidth in the pure solvent at temperature T. If viscosity is the only factor affecting the linewidth, then a plot of the

factor $(\eta_o/\eta)W_{1/2}$ vs. salt concentration should be a constant, independent of the salt concentration.

The appropriate plots are shown in Figure 5.3. The results suggest that linewidth times reduced viscosity is essentially constant for the perchlorate and tetrafluoroborate salts, and that the concentration effect with these salts is primarily due to the viscosity change. The anomaly of different $(W_{1/2})_{0,T}$ values from different salts and sources remains. However, there appears to be a significant remaining effect of salt concentration on linewidths for the triflate salt.

The apparently different behavior of Cu(I) triflate might be ascribed to quite different viscosity effects of the perchlorate and triflate anions, resulting in a much larger B value for the latter. But a rather large value of B ≈ 1.4 is required to linearize the $Cu(F_3CSO_3)$ data. This seems unlikely from a comparison of the viscosities of sodium perchlorate and triflate in DMSO.[19] The two salts show essentially the same concentration dependence in DMSO, and B values in AN and DMSO are generally of similar magnitude.[14] Results described later will show that there actually is a triflate ion effect on the linewidth which can be explained by ion-pairing.

The viscosity/temperature dependence has been tested by comparing the temperature dependence of the ^{14}N NMR linewidths in pure acetonitrile[20,21] to those of a 0.045 M $Cu(F_3CSO_3)$ solution. The results, shown in Figure 5.4, show that the viscosity-corrected linewidths of the $Cu(F_3CSO_3)$ solution agree with those of the of the pure solvent, and both have the temperature dependence expected from the viscosity.

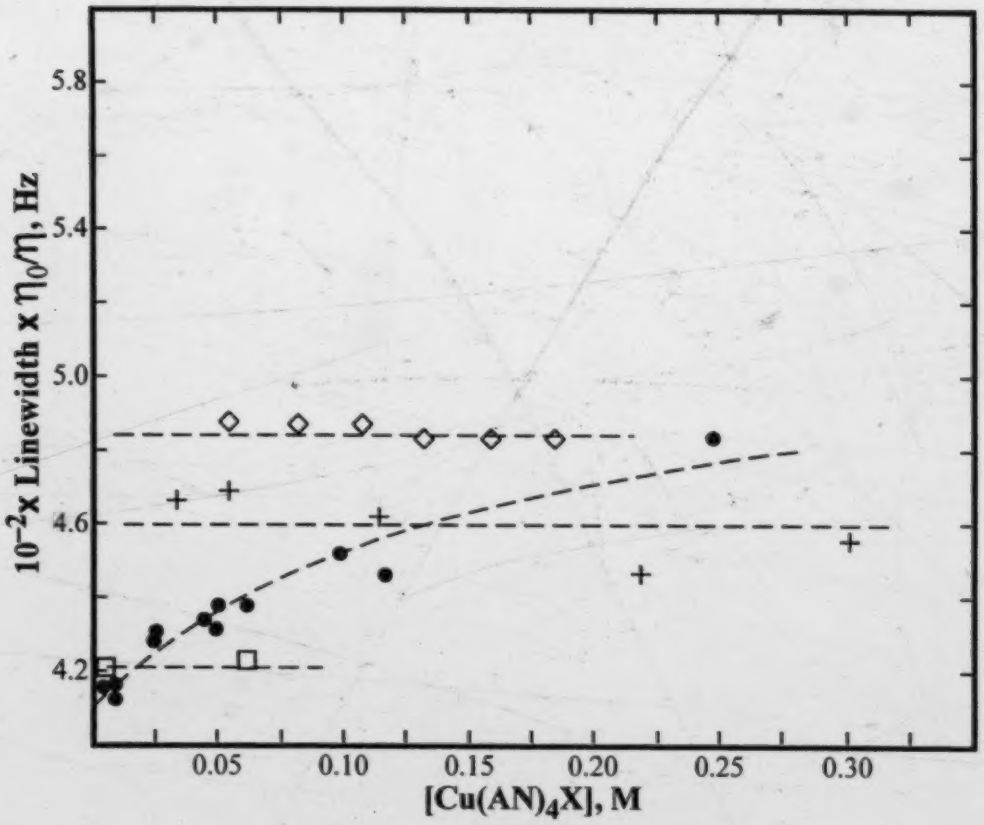

Figure 5.3. Concentration dependence of the ^{63}Cu(I) linewidth for $Cu(AN)_4X$ salts in acetonitrile. (●) X = $F_3CSO_3^-$; present study. (◇) X = ClO_4^-; reference 2. (□) X = ClO_4^-; present study. (+) X = BF_4^-; reference 1: Dashed lines are eye guides only.

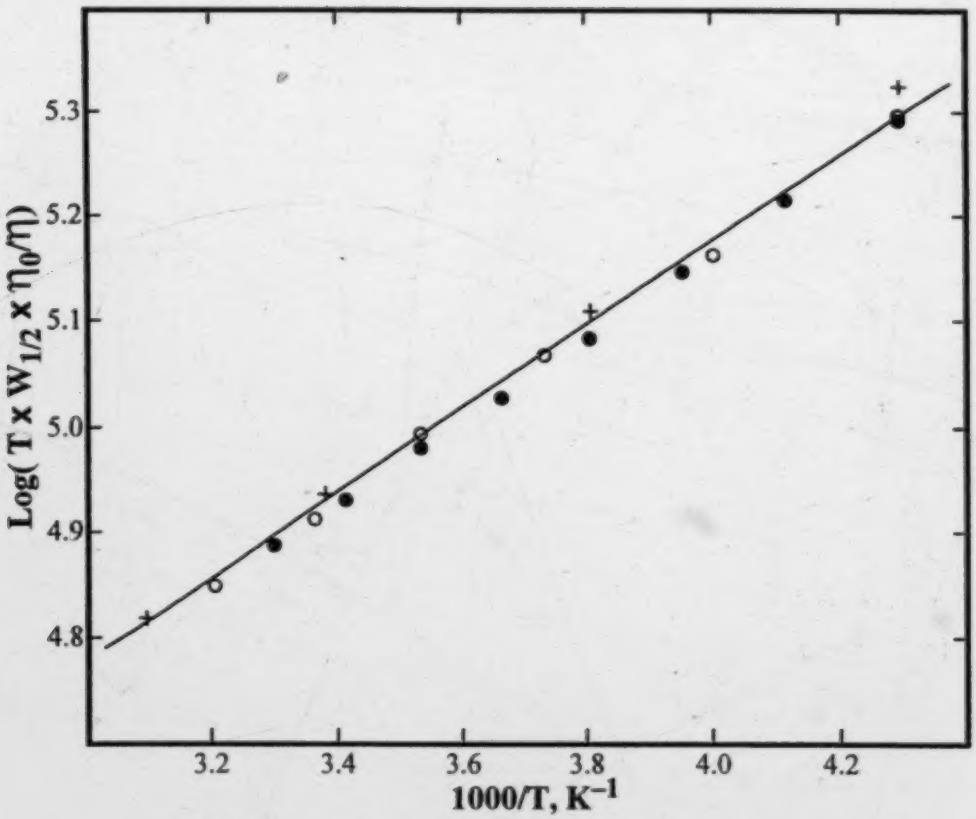

Figure 5.4. Temperature dependence of ^{14}N linewidths $W_{1/2}$ (Hz) after viscosity normalization: in pure CD_3CN (●) Reference 20, (○) Reference 21 and 0.045 M $Cu(F_3CSO_3)$ in CH_3CN (+).

Water and Cu(II) Effects. A possible explanation for the concentration dependence, and the different linewidths with zero salt also is the presence of Cu(II) and/or adventitious water. The latter might be present in the solvent, or be introduced along with the salt. Water could act as a ligand in a lower symmetry complex and also would increase the viscosity.[17] This might also account for some of the variability between reported linewidths noted in Table 5.1.

The effect of water has been examined in this study by preparing samples under vacuum and adding known amounts of water by dehydrating weighed amounts of $[Co(NH_3)_5OH_2]Br_3$ at ~100 °C[5] and condensing the water in the Cu(I)-AN solution in a dry ice slush. In addition, through a series of determinations of the density of various volume % of AN/H_2O (see Appendix 5.1), it has been possible to convert the earlier observations of Kroneck et al.[2] to water molarities for comparison to this study. As part of the same study, Kroneck et al.[2] also added submillimolar concentrations of Cu(II) to the solutions. These results are summarized in Table 5.2. It appears that the viscosity effect is not sufficient to account for the linewidth increases beyond $[H_2O] > 0.5$ M.

The results in Table 5.2 for the BF_4^- and $F_3CSO_3^-$ are in agreement with regard to the trend with increasing $[H_2O]$ and indicate a marked increase in linewidth for $[H_2O] \geq 0.5$ M, with an essentially linear increase with $[H_2O]$. The somewhat larger linewidths observed by Kroneck et al.[2] at lower $[H_2O]$ might be due to water already present from the solvent, and suggest that the $[H_2O] \approx 0.5$ M, i.e. 99% by volume AN, in Kroneck's samples. The effect of Cu(II) with BF_4^- seems to be minor, but the ClO_4^- samples of Kroneck et al.[2] are anomalous in showing an apparently large Cu(II) effect, and more than twice the linewidth expected in 5.04 M water, compared to BF_4^-. This anomaly is

Table 5.2. Water Dependence of $^{63}Cu(I)$ NMR Linewidth for $Cu(AN)_4X$ in Acetonitrile

X^-	[Cu(I)]	AN	$[H_2O]$	η [b]	[Cu(II)][c]	$W_{1/2}$	$W_{1/2}(\eta_o/\eta)$
	M	Vol %	M	cp	mM	Hz	Hz
BF_4 [a]	0.087	100	0	0.363	0	540	508
BF_4 [a]	0.10	99	0.51	0.365	0.099	560	522
BF_4 [a]	0.10	98	1.08	0.370	0.196	620	573
BF_4 [a]	0.10	95.25	2.64	0.393	0	805	699
BF_4 [a]	0.10	95.25	2.64	0.393	0.476	850	716
BF_4 [a]	0.10	95	2.78	0.395	0	900	777
BF_4 [a]	0.10	90	5.61	0.440	0	1215	941
ClO_4 [g]	0.062	100	0	0.356	0	443	422
ClO_4 [a]	0.061	100	0	0.356	0	550	525
ClO_4 [a]	0.089	91	5.04	0.428	0	2700	2152
ClO_4 [a]	0.062	91	5.04	0.420	0.18	4800	3887
ClO_4 [d]	0.064	100	0	0.403[e] (0.36)[f]	0	520	(491)
ClO_4 [d]	0.064		2.69	0.423[e]	0	997	805
ClO_4 [d]	0.064		5.36	0.440[e]	0	1221	948
ClO_4 [g]	0.061	90	5.61	0.429	0	1235	982
ClO_4 [d]	0.064		14.5	0.627[e]	0	2850	1552
ClO_4 [d]	0.064		23.2	0.849[e]	0	4300	1725
ClO_4 [d]	0.064		28.3	0.977[e]	0	5160	1800
ClO_4 [d]	0.064		32.9	1.124[e]	0	6400	1940

Table 5.2. (Continued)

X^-	[Cu(I)] M	AN Vol %	$[H_2O]$ M	η [b] cp	[Cu(II)][c] mM	$W_{1/2}$ Hz	$W_{1/2}(\eta_o/\eta)$ Hz
F_3CSO_3 [g]	0.045	100	0	0.350	0	450	433
F_3CSO_3 [g]	0.045		0.20	0.350	0	460	447
F_3CSO_3 [g]	0.045		0.53	0.351	0	500	484
F_3CSO_3 [g]	0.045		1.00	0.355	0	640	615

[a] Reference 2. [b] Calculated from densities and viscosities compiled in reference 17 for AN/H_2O solutions unless otherwise indicated. [c] The source of Cu(II) is not specified. [d] Reference 12 in AN/D_2O solutions. [e] Viscosities measured for the Cu(I)/AN/ D_2O solutions. [f] Calculated value consistent with earlier $CuClO_4$/AN viscosity vs. concentration results in reference 15. [g] Determined in this study in AN or AN/H_2O solutions.

further shown by the fact that Gill's results for ClO_4^- are in good agreement with those of Kroneck for BF_4^-, but not with the latter's ClO_4^- data.

There is a further anomaly with the ClO_4^- salt in the 91% AN sample of Kroneck et al.[2] in that the temperature dependence of the linewidth shows it increasing up to ~30 °C and then decreasing as the temperature is raised further to ~60 °C. This is almost the exact opposite of the temperature dependence observed for the same salt in pure AN which shows a minimum at about -5 °C. The authors admit to having no explanation for this behavior, especially in light of the fact that their ^{63}Cu chemical shifts in the two solutions show the same temperature dependence. Unfortunately, Gill et al.[12] did not do any temperature dependence studies on the ClO_4^- in AN/D_2O solutions. In this study, the temperature dependence of 0.0613 M $CuClO_4$ in 90% AN/H_2O was found to have a linewidth at 25 °C Hz in agreement with Gill et al.[12] (see Table 5.2), and the temperature dependence shown in Figure 5.5 was analogous to that in pure AN. It appears that the sample of Kroneck et al.[2] was contaminated in some way.

It was noted previously that the PF_6^- sample of Ochsenbein and Schläpfer[1] had anomalously large linewidths. If this was due to water in the sample, the sample would need to have been ~5 M in H_2O, or ~95% AN. This would seem to be unlikely. It has been my observation that samples prepared in air from freshly opened acetonitrile as supplied by the manufacturer, and simply sealed with a plastic cap and parafilm, show no effects of water in their NMR linewidths.

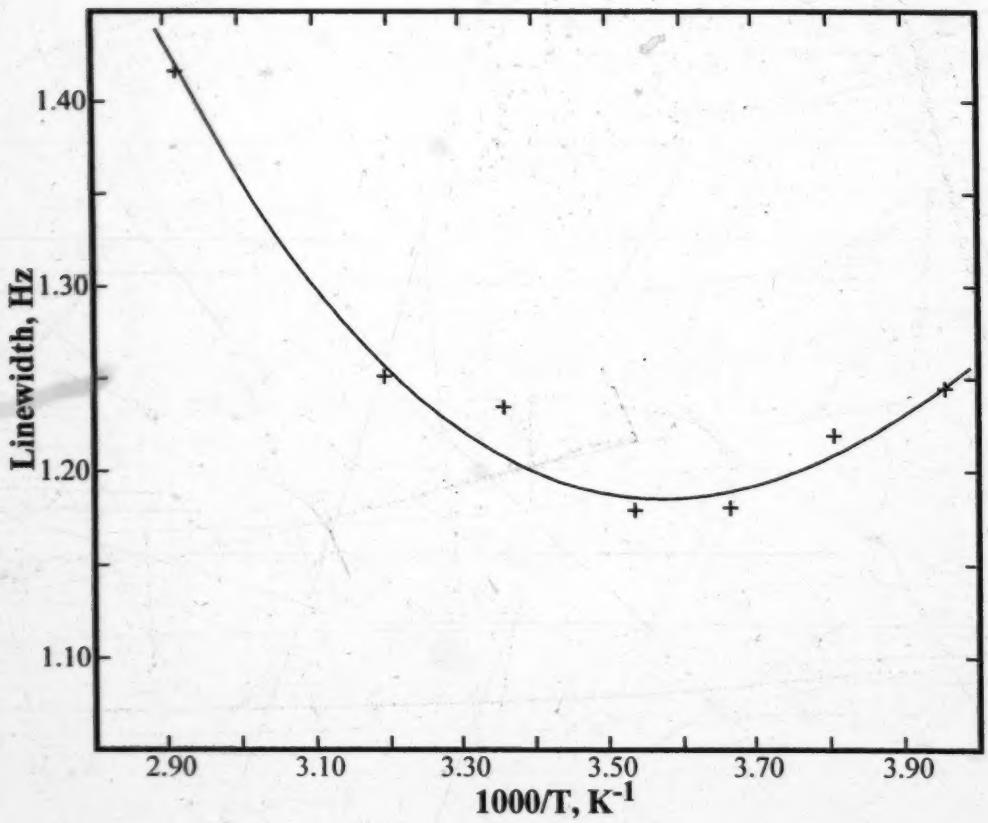

Figure 5.5. Temperature dependence of ^{63}Cu(I) NMR linewidth for 0.0613 M Cu(I) perchlorate in 10% water, 90% acetonitrile. The solvent composition is 10% H_2O, 10% CD_3CN and 80% CH_3CN.

Chloride ion effect. The variation in linewidths observed by various workers might be caused by the presence of traces of potential ligands for Cu(I). Chloride ion is one of the more ubiquitous of such species and its effect on the linewidths has been investigated by adding Et_4NCl to 0.0613 M $CuClO_4$ in AN. For chloride ion concentrations of 0.0015, 0.0031, 0.015 and 0.031 M, it was found that the ^{63}Cu linewidths are 1089, 1874, 4370 and 7557 Hz, respectively, at 25 °C. Clearly even millimolar amounts of chloride ion have a large effect on the linewidth. These observations emphasize that traces of complexing anions can have very significant effects on the observed linewidths.

Temperature and concentration dependence models. The assumption is made that the system can be described by two species, **A** and **B**, in a rapid equilibrium:

$$\mathbf{A} \underset{\longleftarrow}{\overset{X}{\longrightarrow}} \mathbf{B} \qquad (5.4)$$

where **A**, dominant at low temperatures is expected to be $Cu(AN)_4^+$ and **B** is a lower symmetry species with a larger linewidth and is favored at higher temperatures and concentrations. The reaction could be a simple structural change or involve the anion (X) to form an ion-pair. The model also should give a rationalization for the observation that only triflate seems to show an appreciable concentration effect. In any case, if quadrupolar relaxation is dominant for both species, then the linewidth ($W_{1/2}$) and relaxation rate (T_2^{-1}) will be related to the species concentrations by eq. 5.5

$$\pi W_{1/2} = T_2^{-1} = C_A^0\left(\frac{[A]}{[A+B]}\right)\tau_{QA} + C_B^0\left(\frac{[B]}{[A+B]}\right)\tau_{QB} \qquad (5.5)$$

where C_A^0 and C_B^0 are temperature independent constants, and τ_Q is the correlation time governing the quadrupolar relaxation. If the Stokes-Einstein relationship is assumed, then $\tau_Q \propto \eta/T$, where η is the viscosity of the solvent, and substitution into eq. 5.5 and rearrangement gives

$$\frac{\pi W_{1/2}}{\eta} = \frac{T_2^{-1}}{\eta} = \frac{C_A}{T}\left(\frac{[A]}{[A+B]}\right) + \frac{C_B}{T}\left(\frac{[B]}{[A+B]}\right) \qquad (5.6)$$

The temperature dependence of the right-hand-side of eq. 5.6 depends only on the thermodynamic parameters, $\Delta H°$ and $\Delta S°$ which characterize the **A** to **B** equilibrium. These parameters and the total concentration of Cu(I) and X can be used to calculate **[A]** and **[B]** and thence to fit the relaxation rate data as a function of temperature and concentration.

Concentration dependence: ion-pair model. The ion-pair model has been tested first because it seems the most natural way to account for the concentration dependence, and might have some dependence on the nature of the anion. Thus the lack of real concentration dependence with ClO_4^- and BF_4^-, beyond the viscosity effect noted above, could be ascribed to the low charge density and polarity of these ions compared to $F_3CSO_3^-$. Gejji et al.[22] have considered the theoretical aspects of ion-pairing of Li^+, Na^+ and NH_4^+ with $F_3CSO_3^-$ in the gas phase. The Eigen-Fuoss model[23] predicts that K_i might be in the range of 1 to 5 M^{-1} for outer-sphere ion association between unit charged

species in acetonitrile at 25 °C.

For the Cu(I)-triflate solutions, a preliminary examination revealed that the linewidth increased nearly linearly with the concentration up to ~0.05 M. This suggests that the concentration of the ion-pair is small relative to the total Cu(I), so that $K_i \leq 3\ M^{-1}$ for such solutions. A visual analysis, with $K_i = 2$, produced a good fit of the data at 298 K for all the $Cu(F_3CSO_3)$ solutions. It also was found that four solutions with $Bu_4N(F_3CSO_3)/Cu(X)$ concentrations of 0.05/0.0613, 0.10/0.0613 ($X = ClO_4^-$) and 0.20/0.0624, 0.401/0.135 ($X = F_3CSO_3^-$) have linewidths consistent with this model. However, solutions with $Li(F_3CSO_3)$ added to $Cu(ClO_4)$ or $Cu(F_3CSO_3)$ are not fitted as well, with linewidths consistently smaller than predicted, and the $Cu(F_3CSO_3)$ solutions have consistently larger linewidths than corresponding solutions of $Cu(ClO_4)$. This suggests that the total triflate concentration does affect the linewidth, but the effective triflate ion concentration in Li^+ solutions is smaller than the expected value. One possible explanation for this is through ion-pairing of Li^+ and $F_3CSO_3^-$. There do not seem to be any studies relating to ion-pairing of lithium triflate in AN, but Salomon and coworkers[24] have interpreted conductivity measurements to indicate a $K_i = 18.4$ for $Li(ClO_4)$ in AN. Lithium triflate has been studied in butyrolactone,[25] which has a dielectric constant similar to AN, and found to have $K_i \approx 20$.

In the final analysis, the model included the coupled equilibria for triflate ion-pairing with Cu^+ and Li^+, and the contributions of Cu^+ and the ion-pair $Cu^+(F_3CSO_3)$ to the linewidth, while taking viscosity effects into account, using the parameters of Gill et al.[15] It was assumed that the viscosity B coefficient was the same for Cu^+, Li^+ and Bu_4N^+, since the values are known to be quite similar.[14] The contributions of the ion-pairs

$Cu^{\bullet}(F_3CSO_3)$ and $Li^{\bullet}(F_3CSO_3)$ to the viscosity are problematic, and it was assumed that these neutral species did not make a significant contribution. Then the linewidths were fitted by least-squares to eq. 5.7.

$$W_{1/2} = \eta\left\{\frac{C_A}{T}\left(\frac{[Cu^+]}{[Cu(I)]_{tot}}\right) + \frac{C_B}{T}\left(\frac{[Cu \bullet F_3CSO_3]}{[Cu(I)]_{tot}}\right)\right\} \qquad (5.7)$$

where η is the viscosity in mp. The best-fit gave K_i values for Cu^+ and Li^+ of 1.51 ± 0.48 and $9.0 \pm 1.3\ M^{-1}$, respectively, with $(C_A/T) = 1.213 \pm 0.007 \times 10^3$ and $(C_B/T) = 2.16 \pm 0.15 \times 10^3$.

The solution compositions and results for the ion-pair model are summarized in Table 5.3. The excellent agreement between the observed and calculated linewidths, and the quite reasonable magnitudes of the K_i's seem to vindicate the model as an explanation for the concentration effects. It should be noted that the latter depend on the details of the viscosity correction, but similar values are obtained with any model assuming a normal dependence of viscosity on salt concentration.

Temperature Dependence

Ion-pair model. The ability to explain the temperature dependence also is a critical requirement of any successful model. The Cu^+-$F_3CSO_3^-$ ion-pair model assumes that there is more ion-pairing at higher temperature in order to explain the increasing linewidths above -5 °C. This implies in turn that there should be a more pronounced concentration dependence of the linewidths at higher temperature. The $\Delta H°$ for K_i will be determined essentially by the observed temperature dependence of the linewidths.

Table 5.3. Triflate Ion Dependence of ^{63}Cu(I) NMR Linewidths in Acetonitrile

Cu(I) Source	$[Cu(I)]_t$ mM	Added Salt mM	$[Triflate]_t$ mM	$W_{1/2}$, Hz [a] obsd	calcd
$Cu(F_3CSO_3)$	4.94	0	4.94	417	418
$Cu(F_3CSO_3)$	9.63	0	9.63	416	422
$Cu(F_3CSO_3)$	9.88	0	9.88	420 [b]	422
$Cu(F_3CSO_3)$	24.7	0	24.7	437	434
$Cu(F_3CSO_3)$	26.0	0	26.0	440 [b]	435
$Cu(F_3CSO_3)$	49.4	0	49.4	449	452
$Cu(F_3CSO_3)$	50.6	0	50.6	456	453
$Cu(F_3CSO_3)$	50.6	0	50.6	449 [b,f]	453
$Cu(F_3CSO_3)$	62.0	0	62.0	460 [b]	461
$Cu(F_3CSO_3)$	98.8	0	98.8	488	484
$Cu(F_3CSO_3)$	117.0	0	117	488	495
$Cu(F_3CSO_3)$	117.0	0	117	482 [b]	495
$Cu(F_3CSO_3)$	247.0	0	247	579	562
$Cu(ClO_4)$	61.3	500 [c]	50	477	473
$Cu(ClO_4)$	61.3	50 [c]	50	475	473
$Cu(ClO_4)$	61.3	100 [c]	100	513	510
$Cu(F_3CSO_3)$	62.4	200.0 [c]	262	603	600
$Cu(F_3CSO_3)$	135.0	401 [c]	536	748	758
$Cu(F_3CSO_3)$	62.4	50 [d]	112	482	481

Table 5.3. (Continued)

Cu(I) Source	$[Cu(I)]_t$ mM	Added Salt mM	$[Trif]_t$ mM	$W_{1/2}$, Hz [a] obsd	calcd
$Cu(F_3CSO_3)$	62.4	100 [d]	162.4	497	498
$Cu(ClO_4)$	61.3	100 [d]	100	484	484
$Cu(F_3CSO_3)$	62.4	201 [d]	263.4	527	524
$Cu(ClO_4)$	61.3	200 [d]	200	513	515
$Cu(ClO_4)$	61.3	200 [d,e]	200	513	515
$Cu(ClO_4)$	61.3	500[d]	500	576	576

[a] Measured on Varian S400 MHz spectrometer in 5 mm tubes unless otherwise indicated. [b] Measured on Bruker AM-200 MHz spectrometer. [c] Added as $Bu_4N(F_3CSO_3)$. [d] Added as $Li(F_3CSO_3)$. [e] Salt oven-dried immediately before sample preparation. [f] In 10 mm tube on Bruker AM-200 system.

The ion-pair model was tested on the temperature dependence results of 0.00494, 0.045 and 0.117 M $Cu(F_3CSO_3)$ solutions in acetonitrile. A qualitative examination of the linewidths revealed that there is not a marked sensitivity to concentration at the higher temperature, and it would appear that this model may not work, unless the $\Delta H°$ is sufficiently small so that K_i does not change too much between 25 and 70 °C. Small K_i variation and $\Delta H°$ values also are suggested by the fact that the temperature of the minimum linewidth does not seem to shift much with concentration. Otherwise, one would expect the higher temperature section to become more important at higher concentrations, and the minimum would shift to lower temperature. The value of $K_i = 1.5$ at 25 °C was taken from the previous analysis and various $\Delta H°$ values (1 - 10 kcal mol^{-1}) were assumed and the $\Delta S°$ calculated. It was found that a $\Delta H°$ in the range of 5 - 6 kcal mol^{-1} is required to reproduce the observed temperature dependence of the linewidths. Such $\Delta H°$ values are clearly in conflict with the implication of the data that K_i does not change much from 25 to 70 °C. This was confirmed by model calculations based on fitting the lowest concentration data with $K_i = 1.5$ (25 °C), $\Delta H° = 6.0$ kcal mol^{-1} and $\Delta S° = 20.93$ cal mol^{-1} K^{-1} (solid curve in Figure 5.6).

If the same parameters are used to calculate the curve for twice the total $Cu(F_3CSO_3)$ concentration (0.00988 M) (dashed curve in Figure 5.6), the predicted linewidths are much larger than those observed even in the 0.117 M solution. The calculated curve follows the expectations of increasing linewidth change at higher temperature and shift of the minimum to lower temperature, but it simply cannot reproduce the experimental observations.

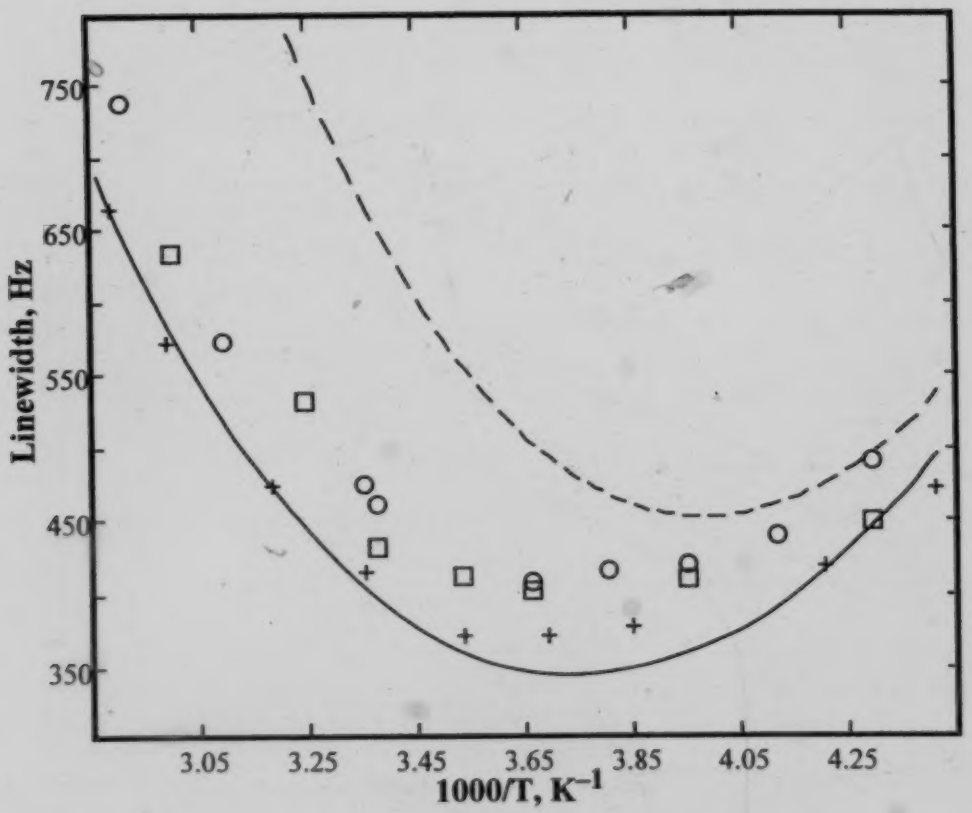

Figure 5.6. Temperature and concentration dependence of the $^{63}Cu(I)$ linewidth for $Cu(AN)_4(F_3CSO_3)$ in acetonitrile. (+) 0.00494 M. (□) 0.045 M. (○) 0.117 M. (–) curve calculated from the ion-pair model for 0.00494 M, $K_i = 1.5$ (25 °C), $\Delta H° = 6.0$ kcal mol^{-1} and $\Delta S° = 20.93$ cal mol K^{-1}. (---) curve calculated for 0.00988 M and the same $\Delta H°$ and $\Delta S°$.

The conclusion from the above analysis is that the ion-pair model alone cannot account for the increase in linewidth with temperature. It can account for the small concentration effects, but the ion-pair formation constant must have a much smaller temperature dependence than the linewidths.

Coordination-change model. An alternative model assumes that **A** and **B** are just related by a difference in the coordinated ligands such that **B** is less symmetrical than **A** and therefore provides more effective quadrupolar relaxation. It should be noted that the minimal temperature dependence of the triflate concentration effect, noted above, shows that the coordination change does not involve formation of $Cu(AN)_3(F_3CSO_3)$. The concentration dependence is due in part to viscosity changes and to ion-pairing, but is relatively temperature-independent compared to the coordination change equilibrium.

The perchlorate samples studied here present a good initial test for this model. The concentration dependence is consistent with viscosity effects, so that there are no complications with the magnitude or temperature dependence of ion-pair formation. Minor modification of eq. 5.7 shows that

$$\frac{W_{1/2}}{\eta} = \frac{1}{T}\left\{C_A\left(\frac{[A]}{[A+B]}\right) + C_B\left(\frac{[B]}{[A+B]}\right)\right\} \qquad (5.8)$$

where **A** and **B** are the symmetrical and less symmetrical species, respectively, and C_A and C_B are temperature independent constants dependent on the QCC for the respective species. The concentration and temperature dependence of the viscosity, η, can be calculated as previously described. In the low temperature limit where [A] >> [B], a plot of $W_{1/2}/\eta$ vs. 1/T should be linear with a slope of C_A. In the opposite limit, the slope

would be C_B, but the data do not indicate that this limit is ever really reached for the accessible temperature range.

The appropriate plots for two samples of 0.00621 and 0.0621 M $Cu(ClO_4)$ are shown in Figure 5.7. The low temperature limit is clearly observed, and the viscosity change adequately corrects for the concentration dependence.

A nonlinear least-squares analysis gave an excellent fit of the data with $\Delta H° = 5.4$ kcal mol^{-1}, $\Delta S° = 9.78$ cal mol^{-1} K^{-1}, $C_A = 1.125 \times 10^4$ and $C_B = 17.86 \times 10^5$. However, because the latter value is not defined by the data, it was necessary to hold $\Delta H°$ constant during the fitting, and the values given produce the minimum standard error of the fit for $\Delta H°$ in the range of 4.5 to 8.0 kcal mol^{-1}. The curve in Figure 5.7 is calculated on the basis of the parameters given, and shows that the model does fit the data. Further justification for the model is difficult to provide because of the unknown nature of the lower symmetry species **B**. The $\Delta H°$ is similar to that found by Marker and Gunter[3] for the Cu(I)-phosphite systems.

The relative values of C_A and C_B should depend on the values of $(QCC)^2$ for the two species, assuming that they have very similar correlation times. The ratio $C_B/C_A = 158$ then suggests that **B** has a 12.6 times larger QCC than **A**. The value of C_A can be used to estimate that $W_{1/2} \approx 128$ Hz for species **A** at 25 °C, and then the most recent value of $\tau_Q \approx 1.4 \times 10^{-11}$ s, from Gill and coworkers,[12] yields QCC ≈ 2.7 MHz for $Cu(AN)_4^+$. The only other homoleptic tetrahedral Cu(I) species with a known QCC seems to be $Cu(CN)_4^{3-}$, for which QCC = 1.125 MHz has been determined by Kroeker and Wasylishen.[26]

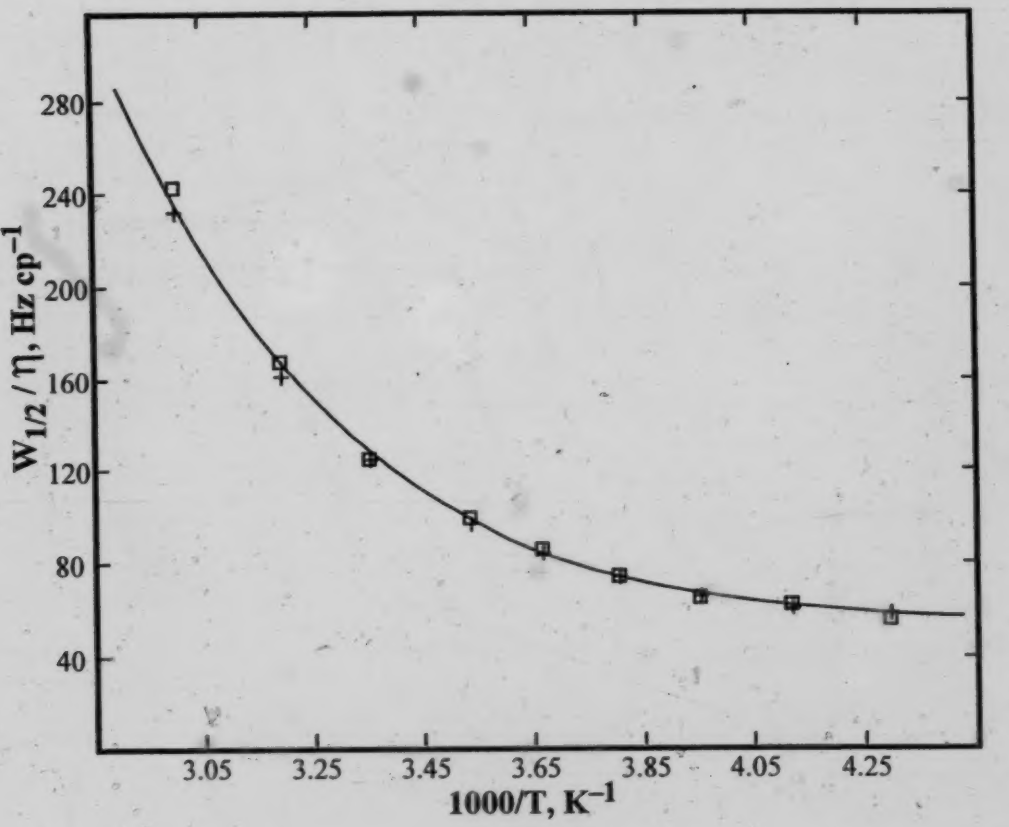

Figure 5.7. Temperature and concentration dependence of the ^{63}Cu(I) linewidth ($W_{1/2}$, Hz) divided by viscosity for the $Cu(AN)_4(ClO_4)$ in acetonitrile. (□) 0.00621M. (+) 0.0621M.

The value of QCC for species **A** and the ratio of C_B/C_A gives a QCC of ~34 MHz for species **B**. Lucken and coworkers[27] have reported NQR measurements for several Cu complexes with more complex ligand systems than AN. For 3-coordinate (2,6-lutidine)$_2$Cu(halide) and (2,6-lutidine)$_3$Cu$^+$ complexes the QCC (= $2\nu_{NQR}$) are in the range of 66 to 92 MHz. Asaro et al.[28] have used solid-state NMR to determined QCC values in the range of 17 to 27 MHz for several 4-coordinate species of the general type P_2CuS_2 and $PCuS_3$, and a 3-coordinate P_2CuO species with QCC of ~90 MHz. Two linear bis(tribenzylphosphine)Cu(I) salts have QCC in the range of 80 MHz.[29] Overall, a QCC value of ~34 MHz for species **B** falls within the wide range of values for asymmetric Cu(I) species.

The BF_4^- system previously studied by Ochsenbein and Schläpfer[1] and Kroneck et al.[2] is analogous to the perchlorate in that there is no indication of ion-pairing, so that the same parameters for K_C should describe the BF_4^- system. Plots of $W_{1/2}/\eta$ versus 1/T for this data are shown in Figure 5.8.

The results of the two studies generally are in agreement between about -15 and 20 °C, but Kroneck et al.[2] reported larger linewidths at higher temperatures and somewhat smaller values at lower temperatures. The curve through the data of Ochsenbein and Schläpfer[1] is drawn with essentially the same parameters as those for the perchlorate system, $C_A = 1.15 \times 10^4$ and $C_B = 17.9 \times 10^5$. However the data of Kroneck et al.[2] requires $C_A = 0.90 \times 10^4$ and $C_B = 21.6 \times 10^5$, which are ~20% lower and higher, respectively, than the others. These observations, combined with those for the triflate system described below, suggest that there is some systematic error in the observations of Kroneck et al.[2]

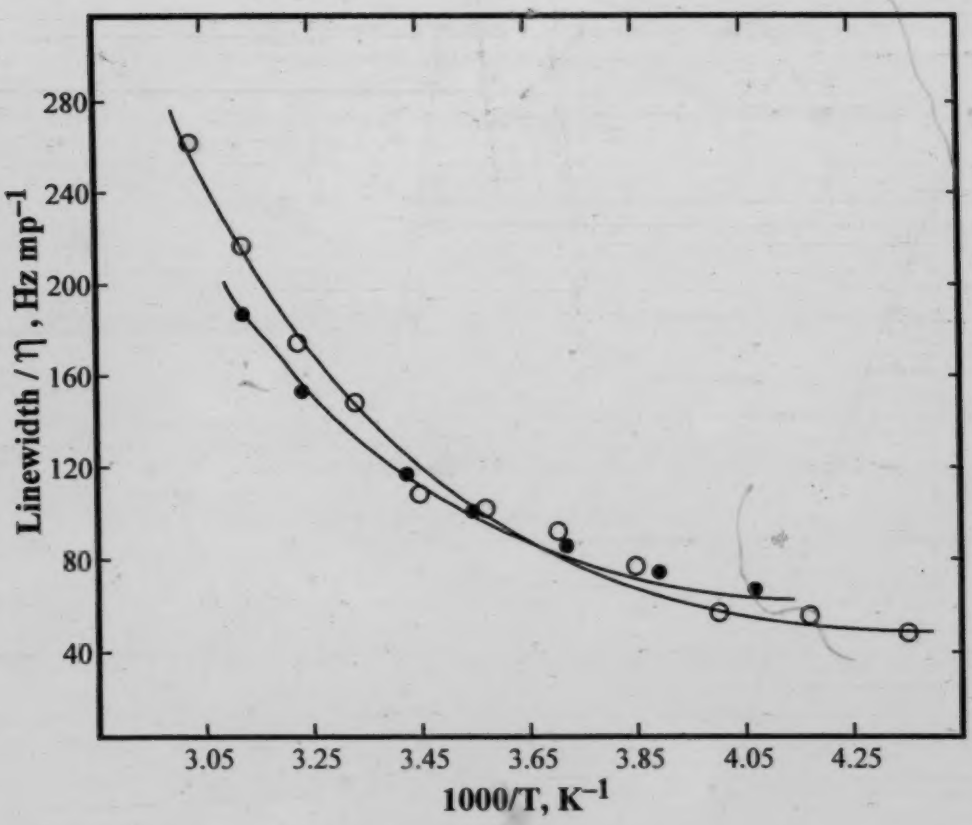

Figure 5.8. Temperature and concentration dependence of the ^{63}Cu(I) linewidth divided by viscosity for $Cu(AN)_4(BF_4)$ in acetonitrile. (●) 0.10 M; reference 1. (○) 0.09 M reference 2.

The temperature dependence for $Cu(F_3CSO_3)$ is more complex to analyze because the ion-pairing equilibrium is coupled to that for the coordination change. The plot of $W_{1/2}/\eta$ vs. 1/T is quite similar to that for the perchlorate system, aside from the slight changes with concentration. The results have been analyzed by solving the coupled equilibria in Scheme 5.1 for the four species, $Cu(AN)_4^+$, $Cu(AN)_4{\bullet}(F_3CSO_3)$, $Cu(AN)_n^+$, and $Cu(AN)_n{\bullet}(F_3CSO_3)$, where the latter two result from the coordination change.

Scheme 5.1

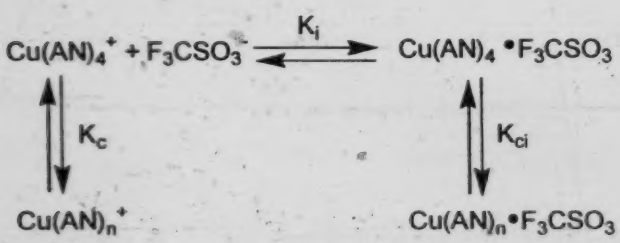

The analysis of the perchlorate system has given K_C and its temperature dependence, and some indication of the ratio of the QCC values for $Cu(AN)_4^+$ and $Cu(AN)_n^+$. The triflate system has shown that K_i = 1.5 at 25 °C with a small temperature dependence, and indicates that the ion-pair causes ~1.8 times more broadening than its parent. However, nothing is known about K_{Ci} or the magnitude of QCC for $Cu(AN)_n{\bullet}(F_3CSO_3)$. Therefore the simplest assumptions have been made in analyzing this system, namely that $K_{Ci} = K_C$ and that the broadening due to $Cu(AN)_n{\bullet}(F_3CSO_3)$ is 1.8 times that for $Cu(AN)_n^+$. Then the contributions from the $(AN)_4$ species and from the $(AN)_n$ species are given by F_4 and F_n, respectively.

$$F_4 = C_A[Cu(AN)_4^+] + 1.8\,[Cu(AN)_4 \bullet F_3CSO_3] \qquad (5.9)$$

$$F_n = C_B[Cu(AN)_n^+] + 1.8\,[Cu(AN)_n \bullet F_3CSO_3] \qquad (5.10)$$

Then the predicted linewidth divided by viscosity is given by

$$\frac{W_{1/2}}{\eta} = \frac{1}{T}\left(\frac{F_4 + F_n}{[Cu]_t}\right) \qquad (5.11)$$

where $[Cu]_t$ is the total Cu(I) concentration.

The analysis of the results initially indicated that the $\Delta H°$ for K_i is < 1 kcal mol^{-1}, and a value of 0.50 kcal mol^{-1} has been used, along with $\Delta S° = 2.48$ cal mol^{-1} K^{-1} to give $K_i = 1.5$ at 25 °C. For K_C, the thermodynamic parameters from the perchlorate system were used. The calculated curves are shown in Figure 5.9.

The curves in Figure 5.9, which reproduce the data very well, were calculated with $C_A = 1.06 \times 10^4$ and $C_B = 17.9 \times 10^5$. The latter value is identical to that found to fit the perchlorate system, and the former is 6% smaller than for the perchlorate salt.

In theory, if the viscosity/concentration effect in both systems and the ion-pair effect with triflate have been correctly evaluated, then the two systems should give the same values for C_A and C_B. The agreement found gives substantial support for the generic, coordination-change model to explain the large ^{63}Cu linewidths and their anomalous temperature dependence.

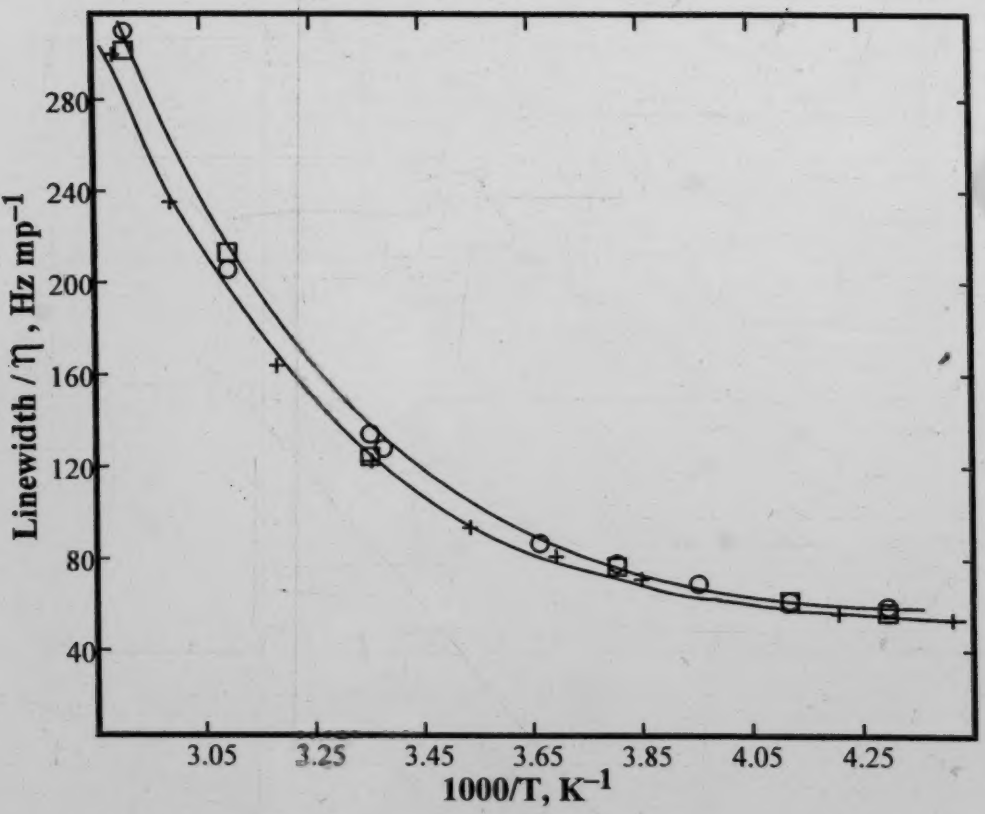

Figure 5.9. Temperature and concentration dependence of the $^{63}Cu(I)$ linewidth divided by viscosity for $Cu(AN)_4(F_3CSO_3)$ in acetonitrile. (+) 0.00494 M (□) 0.00988 M (○) 0.117 M. The calculated curves for first two solutions are indistinguishable.

Conclusion

Of the tetrakis(acetonitrile)copper(I) solutions studied, only the triflate shows an ion-pairing effect on the ^{63}Cu(I) NMR linewidths in acetonitrile. The concentration effects on the linewidths of acetonitrile solutions of the ClO_4^-, BF_4^- and PF_6^- salts at a given temperature are due to the accompanying viscosity changes. The quantitative model developed here shows that the anomalous temperature dependence above ~-5 °C, which leads to observation of unusually large ^{63}Cu(I) linewidths at ambient temperatures, is consistent with the presence of a species $Cu(AN)_n^+$, having different coordination number than the crystallographically observed value of 4 (see Chapter 2). The identity of $Cu(AN)_n^+$ has not been established. It has however been established that it is neither an ion-pair, $Cu(AN)_n \cdot X$ nor the stoichiometrically equivalent inner-sphere complex, $Cu(AN)_3X$. Based on the general coordination chemistry of Cu(I), a coordination number greater than 4 is very improbable. So $Cu(AN)_3^+$ is the most likely possibility.

References

(1) Ochsenbein, U.; Schläpfer C. W. *Helv. Chim. Acta* **1980**, *63*, 1926.

(2) Kroneck, P.; Kodweiss, J.; Lutz, O.; Nolle, A.; Zepf, D. *Z. Naturforsch.* **1982**, *37a*, 186.

(3) Marker, A.; Gunter, M. J. *J. Magnet. Reson.* **1982**, *47*, 118.

(4) Hemmerich, P.; Sigwart, C. *Experientia* **1963**, *19*, 488.

(5) Jordan, R. B.; Taube, H. *J. Am. Chem. Soc.* **1966**, *88*, 4406.

(6) Lutz, O.; Oehler, H.; Kroneck, P. *Zeit. Physik A* **1978**, *288*, 17.

(7) Raghavan, P. *Atom Data Nucl. Data. Tab.* **1989**, *42*, 189.

(8) Gill, D. S.; Rodehüser, L.; Delpuech, J.-J. *J. Chem. Soc., Faraday Trans.* **1990**, *86*, 2847.

(9) Gill, D. S.; Rodehüser, L.; Rubini, P.; Delpuech, J.-J. *J. Chem. Soc., Faraday Trans.* **1995**, *91*, 2307.

(10) Gill, D. S.; Singh, R.; Ali, V.; Singh, J.; Rehan, S. K. *J. Chem. Soc., Faraday Trans.* **1994**, *90*, 583.

(11) Gill, D. S.; Byrne, L.; Quickenden, T. L. *Z. Naturforsch.* **1998**, *53a*, 1004.

(12) Gill, D. S.; Kamp, U.; Doelle, A.; Zeidler, M. D. *Ind. J. Chem.* **2001**, *40A*, 693.

(13) Geerts, R. L.; Huffman, J. C.; Folting, K.; Lemmen, T. H.; Caulton, K. G. *J. Am. Chem. Soc.* **1983**, *105*, 3503.

(14) Jenkins, H. D. B.; Marcus, Y. *Chem. Rev.* **1995**, *95*, 2695.

(15) Gill, D. S.; Cheema, J. S. *Z. Phys. Chemie (N. F.)* **1983**, *134*, 205. Gill, D. S.;

Chauhan, J. S. *Z. Phys. Chemie (N. F.)* **1984**, *140*, 149.

(16) Saha, N.; Das, B. *J. Chem. Eng. Data* **2000**, *45*, 1125.

(17) Nikam, P. S.; Sawant, A. B. *J. Chem. Eng. Data* **1997**, *42*, 1151.

(18) Kanes, J. P. *Diss. Abs.* **1967**, *26*, 1367.

(19) Yao, N.-P.; Benion, D. N. *J. Phys. Chem.* **1971**, *95*, 1727.

(20) Wakai, C.; Hirokazu, S.; Matubayasi, N.; Nakahara, M. *J. Chem. Phys.* **2000**, *112*, 1462.

(21) Yuan, P.; Schwartz, M. *J. Chem. Soc., Faraday Trans.* **1990**, *86*, 593.

(22) Gejji, S. P.; Suresh, C. H.; Bartolotti, L. J.; Gadre, S. R. *J. Phys. Chem. A* **1997**, *101*, 5678.

(23) Eigen, M. *Z. Electrochem.* **1960**, *64*, 115. Fuoss, R. M. *J. Am. Chem. Soc.* **1958**, *80*, 5059.

(24) D'Aprano, A.; Sesta, B.; Mauro, V.; Salomon M. *J. Inclusion Phenomena and Macrocyclic Chem.* **1999**, *35*, 451; *J. Soln. Chem.* **2000**, *29*, 1075.

(25) Caillon-Caravanier, M.; Bosser, G.; Claude-Montigny, B.; Lemordant, D. *J. Electrochem. Soc.* **2002**, *149*, E340.

(26) Kroeker, S.; Wasylishen, R. E. *Can. J. Chem.* **1999**, *77*, 1962.

(27) Lucken, E. A. C. *Z. Naturforsch.* **1994**, *49a*, 155. Ramaprabhu, S.; Lucken, E. A. C.; Bernardinelli, G. *J. Chem. Soc., Dalton Trans.* **1995**, 115, and references therein.

(28) Asaro, F.; Camus, A.; Gobetto, R.; Olivieri, A. C.; Pellizer, G. *Solid State Nuclear*

Magnetic Resonance **1997**, *8*, 81.

(29) Kroeker, S.; Hanna, J. V.; Wasylishen, R. E.; Ainscough, E. W.; Brodie, A. M. *J. Mag. Reson.* **1998**, *135*, 208.

Chapter 6. Conclusions

Preliminary literature review of the electron self-exchange between Cu(II) and Cu(I) acetonitrile (AN) solvates revealed that pertinent structural information was lacking. Therefore, crystal structures for the AN solvates of Cu(II,I) triflate salts have been determined. This study was given in Chapter 2. Then the self-exchange rate has been estimated for the Cu(II/I) couple in AN/water mixtures using rate constants for the reductions of Cu(II) with ferrocene (Fc) and 1,1′-dimethylferrocene (Dmfc). The effect of anions, namely nitrate and chloride, on the rate of these reactions also was studied. These studies are presented in Chapters 3 and 4. The results of these studies did indicate that the self-exchange rate for the Cu(II/I) couple could be too slow to measure directly, so that a planned $^{63/65}$Cu(I)-NMR study seemed unnecessary. Even so, it also had been noted from the previous studies that $^{63/65}$Cu(I) NMR linewidths showed anomalous temperature dependence which had not been explained. Thus, the Cu(I)-NMR linewidth for the Cu(I)-AN system has been studied and correlated with the previous work. This study is reported in Chapter 5.

In Chapter 2, X-ray crystallography structures are reported for the colorless $Cu(AN)_4(Trif)$, blue $Cu(AN)_2(H_2O)_2(Trif)_2$ and $Cu(AN)_4(Trif)_2$ crystals. The Cu(I) structure is tetrahedral and the features are essentially similar to those of the structures of the tetrafluoroborate,[1] perchlorate[2] and hexafluorophosphate[3] salts. The two Cu(II) salts are tetragonally distorted, and the triflate anions appear at bond distances of 2.36-2.42 Å. The Cu(II)-N and Cu(I)-N bond lengths are almost identical (within 1.99 ± 0.02 Å). This observation is generally consistent with X-ray scattering results for these ions in acetonitrile solution.[4,5]

The study of Henriques et al.[6] and the present work obtained only the tetrasolvate, $M(NCCH_3)_4X_2$ (M= Cr, Cu; X = BF_4^-, $F_3CSO_3^-$) structures, for the acetonitrile system, but the benzonitrile study of the $SbCl_6^-$ salt by Brownstein et al.[7] gave the tetragonally distorted Cu(II) hexasolvate. It seems that the BF_4^- and $F_3CSO_3^-$ anions compete with acetonitrile, whereas the $SbCl_6^-$ might not compete as effectively, due to its larger size. Therefore, if one is interested in the acetonitrile hexasolvate, counterions of lower charge density might be the better choice. Nonetheless, tetra and hexasolvates of Cr(II) or Cu(II) have been obtained, even with a common anion, as in the case of $M(OH_2)_n(SiF_6)$ (M= Cr, Cu),[8,9] where n = 4 or 6, depending on the preparation procedure.

The similar Cu-$NCCH_3$ distances of the two oxidation states of copper suggest that the same is quite probable for the aqua-species. Therefore it has been concluded that the bond length difference of ~0.14 Å suggested by Persson et al.[4] for the aqueous couple may be a substantial overestimate. It has also been noted that the similarity of the bond lengths for the two oxidation states is consistent with the commonly tabulated ionic radii[10] for 4-coordinate Cu(I) and Cu(II) of 0.74 and 0.71 Å, respectively.

As far as the structural study goes, the question that needed to be addressed was how important these might be in influencing the electron self-exchange rate for Cu(II/I) in AN. The reason for this is that many authors who have studied Cu(II/I) self-exchange with a variety of ligands, often quote the Vallee and Williams[11] proposal in 1968 that the reactions will tend to be rather slow because of the inner-sphere structural reorganization energy barrier. The findings in Chapter 2, for the Cu(II)- and Cu(I)-AN solvates, suggest that simple bond expansion and compression should not be a major contributor to the inner-sphere reorganization energy for the Cu(II/I) couple. Since the bond lengths are

very similar, it was concluded that coordination change is likely the main source of the structural reorganization energy in a reaction that involves interconversion between the two states.

The Cu(II,I)-AN bond lengths have been used in the kinetic study to estimate the coulombic work in the Cu(II)-ferrocenes reactions (eq. 6.1), in order to estimate the rate constant (k_{11}) for the Cu(II/I) self-exchange (eq. 6.2) using the Marcus cross-relationship.

$$\begin{aligned} &Fc + Cu(II) \rightarrow Fc^{+} + Cu(I) \\ &Dmfc + Cu(II) \rightarrow Dmfc^{+} + Cu(I) \end{aligned} \qquad (6.1)$$

$$Cu(II) + {}^{*}Cu(I) \underset{k_{11}}{\overset{k_{11}}{\rightleftharpoons}} Cu(I) + {}^{*}Cu(II) \qquad (6.2)$$

In these equations, Cu(II) and Cu(I) species are the solvated ions while Fc^{+} and $Dmfc^{+}$ are the oxidized states for ferrocene and dimethylferrocene, respectively. The calculation of k_{11} was done in Chapter 3, and the relevant details of the Marcus cross-relationship are given therein.

Essential to the calculation of k_{11} are the equilibrium and rate constants for the Cu(II)-ferrocene reactions (eq. 6.1) and the self-exchange rate constant for the ferrocenes. The equilibrium constants were calculated using reduction potentials reported by Cox et al.[12] and Nelsen et al.[13] The rate constants for eq. 6.1 were obtained in 50, 80, 90, 95 and 97.5% AN, and they are collected in Table 3.6. The self-exchange rate constant of 9.3 x 10^{6} M^{-1} s^{-1} for ferrocene in acetonitrile was taken from Hunt and coworkers.[14] It was assumed that the self-exchange rate constant for dimethylferrocene is the same as that for ferrocene and that both rate constants are solvent-independent.

Application of the cross-relationship gave k_{11} value of 0.5-16 x 10^{-9} M^{-1} s^{-1} for the Cu(II/I) self-exchange in the AN/water mixtures (see Table 3.6). However, there was no apparent trend with increasing % AN, and the differences are attributed to experimental errors in the parameters used for the calculation. Therefore, the average value of ~5 x 10^{-9} M^{-1} s^{-1} has been estimated for the Cu(II/I) self-exchange rate constant in acetonitrile. This result is in sharp contrast to the 1967 estimate of ≥ 0.3 M^{-1} s^{-1} by Manahan[15] and implies that Manahan's value or method may be in error.

If the Cu(II)-ferrocenes reactions in eq. 6.1 are studied in the reverse direction, information might be obtained that would be useful in providing further insight into structural reorganization requirements for the Cu(II/I) couple. In principle, the reverse reaction rate can be measured if the solvent is changed to water or dilute aqueous acetonitrile (< 2% AN). The cross-reactions would then be exoergic, and the equilibrium constants would be in the order of ≤ 10^4 and ≤ 10^2 for the Cu(I)-Fc^+ and Cu(I)-$Dmfc^+$ systems, respectively. If the Marcus cross-relationship is obeyed, and the self-exchange rate constants for the cross-reaction partners are not much different from those given in Chapter 3 for 100% AN, then reduction potentials from Cox et al.[12] and Nelsen et al.[13] suggest cross-reaction rate constant of < 25 and < 3 M^{-1} s^{-1} for the Cu(I)-Fc^+ and Cu(I)-$Dmfc^+$ systems, respectively. These values give half lives of a few minutes for millimolar reagent concentrations and imply that the kinetics can be measured under these conditions. In practice, the study might be limited by the instability of aqueous Cu(I) and by the poor solubility of ferrocene (2.6 x 10^{-4} and 3.3 x 10^{-5} M in 10% AN and water, respectively, compared to 0.186 M at 25 °C in acetonitrile).[16]

When the results above were considered together with the current estimate of ~5 x

10^{-7} M^{-1} s^{-1} for the aqueous Cu(II/I)[17] it was concluded that the self-exchange is so slow in these solvents that it is unlikely to be determined by direct methods. It has been pointed out previously that the slowness may be due to the large coordination number and geometry difference between the two oxidation states. The reactants must have the appropriate configurations before becoming products. Therefore, the electron-transfer step is preceded by inner- and outer-sphere structural reorganization, so that the activation energy is larger the greater the structural difference.

Previous kinetic data on Cu(II/I) complexes, both in water and in AN, have shown that the Marcus cross-relationship may yield k_{11} values that differ by 10^4 or more from oxidation and reduction cross-reactions.[18] To test if such a situation applies in the systems studied here, oxidation of Cu(I) with suitable oxidants, such as $M(bpy \text{ or } phen)_3^{3+}$ (M = Fe or Ru),[19] could be done in AN. Then if k_{11} values from the reduction cross-reactions differ from those from oxidation cross-reactions, it might be that there are two competing pathways in which a conformational or geometric change and the electron-transfer step occur sequentially. However, it should be noted that the solvated ions are quite labile and similar values of k_{11} for the aqueous Cu(II/I) system (see Table 1.1) are calculated from both reduction and oxidation cross-reactions.

In Chapter 4, formation constants and molar extinction coefficients for $Cu(II)X_n$ ($X = NO_3^-$, Cl^-; n = 0, 1, 2, or 3) complexes in 80 and 95% AN/water are reported. The complexation results showed appreciably strong coordination of both nitrate and chloride ions with Cu(II) in 80 and 95% AN, with overall formation constants (β's) $\geq 10^3$. These values are much larger than the calculated Eigen-Fuoss ion-pair formation constant, K_{ip}, of < 100 M^{-1}. It was therefore concluded that the β's have the predominant contribution

from inner-sphere coordination. This coordination was stronger in 95% AN than in 80% AN, and the β's were 10^2 times larger for the chloride ion than for the nitrate in 95% AN but β_1's were similar for both ions in 80% AN.

The kinetics involves reduction of a Cu(II) complex to a Cu(I) complex, so that formation constants for both oxidation states are important in the Marcus theory interpretation of observed effects. Therefore, it is worthwhile to note that the β values in 100% AN show stronger preferential coordination of chloride to Cu(II)[20] than to Cu(I)[20b,21,22], in contrast to the situation in water where the β values for Cu(I)[23] are larger than those for Cu(II).[24] Between water and 100% AN, the β_1 for Cu(II) increases by 2 x 10^9 times compared to the corresponding increase of only about 50 times for Cu(I).

The kinetics were measured under controlled concentrations of X, which limited the Cu(II)X_n complexes to mono, bis and tris (chloride, 80% AN). The nitrate appears to inhibit the electron-transfer rate for Cu(II)-ferrocenes in ≥95% AN but had no detectable effect in ≤80% AN. The chloride ion showed catalytic effects in both 80 and 95% AN.

The β values for the complexation of Cu(II) and Cu(I) by the chloride ion in 100% AN show that the E° value for the $CuCl^+$/CuCl couple should be 0.893 V, which is about 0.3 V smaller than the 1.181 V value for the free couple. Therefore, one may expect chloride ion to have an adverse effect on the rate of Cu(II)-ferrocenes reaction in 100% AN. Because the study in Chapter 4 showed that a catalytic chloride effect was greater in 95% than in 80% AN, the effect might be expected to be even larger in 100% AN. As discussed below, in terms of the Marcus theory, this situation is possible if the self-exchange rate constant for the complex species is greater than that for the free ions and increases with % AN. If the self-exchange rate constant for the complex is large

enough to offset the effect of decreasing driving force, then catalysis can be observed; otherwise the rate will be inhibited.

According to the Marcus cross-relationship, if the self-exchange rate constants for the ferrocenes are independent of the added anion, then the ratio of the self-exchange of the complex species to that of the free species can be estimated using eq. 6.3.

$$\left(\frac{k_{11}^{n}}{k_{11}^{0}}\right) \approx \left(\frac{k_n}{k_0}\right)^2 \left(\frac{\beta_n^{I}}{\beta_n^{II}}\right)^{-1} \tag{6.3}$$

The β_n^{I} values for the Cu(II)-Cl^- system were assumed not to change much between 80 and 95% AN, because they do not change much between water and 100% AN (see Table 4.14). For the Cu(II)-NO_3^- system, the β_n^{I} values are assumed to be < 5, which is the upper limit determined by Senne and Kratochvil[21] for the system in 100% AN. When the k_n values from Chapter 4 were used, it was shown that k_{11} does increase with increasing n (see Table 4.16). It was concluded that the catalysis of the Cu(II)-Fc and Cu(II)-Dmfc reactions by the chloride ion is primarily due to the increase in the self-exchange rate constant for the Cu(II/I)Cl_n species, thereby compensating for the smaller driving force. There also is an increase in the self-exchange rate constant for the Cu(II/I)$(NO_3)_n$ species, so the inhibition of the cross-reaction rate above 95% AN must be due to the much stronger complexation of Cu(II) which is only partially compensated by increases in the self-exchange rate constants.

A determination of the formation constants for Cu(I) in 80 and 95% AN would be desirable for a better understanding of the extent to which thermodynamic changes affect

the Cu(II)-ferrocenes electron-transfer in the presence of the anions, and thus the Cu(II/I) electron self-exchange. Polarography or ion-selective electrodes can be used, as has been done in 100% AN in the previous studies.[20-22] Polarographic methods use the difference in the half-wave potentials for the complex and the free ion, and they are not very useful if this difference is too small.

The study on the ^{63}Cu(I) NMR linewidth for the Cu(I)-AN system was given in Chapter 5. The linewidths from my studies with the triflate and perchlorate salts are ~100 - 150 Hz (see Table 5.1) smaller than those in the literature. The ~15% difference in the linewidths may appear small for measurements done over a 20-year range. However, it has been found in the present studies that addition of possible contaminants such as water and chloride ion do have a significant effect on the measured linewidth. Addition of ≤ 0.5 M water (~ 99% AN) showed linewidth increases ascribable to increases in solution viscosity. Beyond 0.5 M water, the linewidths are larger than can be accounted for by viscosity changes alone, and lower symmetry Cu(I) species should be contributing. Chloride effects are much more prominent. As little as 1.5 mM chloride added to 0.061 M Cu(I) almost tripled the linewidth at 25 °C, and low symmetry $Cu(I)Cl_n$ species must be contributing. Although Cu(II) also is a likely contaminant, millimolar concentrations of Cu(II) triflate added to 0.06 M Cu(I) had minor effects, which are likely due to triflate ion pairing (see below). Therefore, the differences in the linewidths reported by the various authors could be due to the presence of water or other contaminants, which might be present in the solvent, or be introduced along with the salt.

The dependence of the Cu(I)-NMR linewidth on concentration and temperature was found to be qualitatively similar to that found by Ochsenbein and Schläpfer[25] and

Kroneck et al.[26] These authors did not correct their linewidths for viscosity changes with concentration and/or temperature, and they offered unsubstantiated rationalizations for the temperature dependence - coordination change[25] or ion-pairing.[26] My results in Chapter 5 and those from Ochsenbein and Schläpfer[25] and Kroneck et al.[26] have been subjected to quantitative analysis which included viscosity corrections. The results showed that triflate has a small ion-pairing effect (K_i = 1.5 M^{-1}) which contributes to the concentration dependence of the linewidth. For the other salts, namely, ClO_4^-, BF_4^-, PF_6^-, the concentration effects are entirely a viscosity effect. Further analysis of the ClO_4^-, BF_4^- and triflate using a coordination change model, revealed that the Cu(I) solutions contain temperature-dependent amounts of some species, suggested to be most likely $Cu(CH_3CN)_3^+$. Therefore, the high symmetry $Cu(CH_3CN)_4^+$ ion and the lower symmetry 3-coordinate species, relaxing by a predominantly quadrupolar mechanism, determine the ^{63,65}Cu(I)-NMR linewidths. The observed linewidth depends on the relative proportions of these species. Ion pairing, if present, makes a smaller but significant contribution. The commonly observed 4-coordinate tetrahedral structure in the crystals (see Chapter 2) was shown to have a linewidth of ~128 Hz at 25 °C and a quadrupole coupling constant (QCC) of ~2.7 MHz. The QCC for the 3-coordinate Cu(I) was estimated to be ~34 MHz.

It was indicated in Chapter 1 that it may be possible to measure the self-exchange for the Cu(II/I) couple in acetonitrile by monitoring the decrease in intensity of enriched ^{63}Cu(I) NMR signal, as normal abundance Cu(II) is added. Then it was suggested from the results in Chapter 3 that the rate may be too slow, as indicated by my Marcus theory estimates. This slowness was attributed to the large differences in the coordination geometries noted in Chapter 2. The conclusions from Chapter 5 further point to the

importance of the structural rearrangement for the Cu(II/I) self-exchange and suggest that there may be larger disparity in solution structures than is the case in the solid state. Thus, a 5- or 6-coordinate Cu(II) could possibly have to rearrange to 3- or 4-coordinate Cu(I) in AN solution, prior to the electron-transfer step. These factors then lead to a somewhat unique situation for the Cu(II/I) couple and strongly suggest that the self-exchange rate may be too slow indeed - perhaps in the range indicated by the Marcus cross-relationship. It may be considered that increasing temperature could increase the rate. However, the analysis in Chapter 5 gave $\Delta H° = 5.4$ kcal mol^{-1} and $\Delta S° = 9.78$ cal mol^{-1} K^{-1} for the coordination change equilibria, so that the 3-coordinate species is always favored at the higher temperature. Therefore, temperature increase is not beneficial if the presence of the lower coordination geometry has an adverse effect on the rate. The conclusion is that the self-exchange rate in acetonitrile is so slow that it is unlikely to be determined directly.

The QCC value of ~ 2.7 MHz for the $Cu(AN)_4^+$ ion is consistent with the QCC for $Cu(CN)_4^{3-}$ of 1.125 MHz,[27] whereas the value of ~34 MHz for $Cu(AN)_3^+$ seems to fit in the wide range of 17-90 MHz for low symmetry Cu(I) complexes.[28,29] It would be great, if the results of the present analysis could be compared with measured values for this and similar salts. Current studies to determine the QCC for the $Cu(AN)_4^+$ ion and other CuN_4^+ compounds, such as $Cu(benzonitrile)_4^+$ and $Cu(phenanthroline)_2^+$, are being undertaken with the assistance of Professor R. E. Wasylishen's group. These studies also might shed more light on the significance of the angular distortions observed in the X-ray structures.

References

(1) Jones, P. G.; Crespo, O. *Acta Cryst.* **1998**, *C54*, 18.

(2) Csoregh, I.; Kierkegaard, P.; Norrestam, R. *Acta Cryst.* **1975**, *B31*, 314.

(3) Black, J. R.; Levason, W.; Webster, M. *Acta Cryst.* **1995**, *C51*, 623.

(4) Persson, I.; Penner-Hahn, J. E.; Hodgson, K. O. *Inorg. Chem.* **1993**, *32*, 2497.

(5) Inamo, M.; Kamiya, N.; Inada, Y.; Nomura, M.; Funahashi, S. *Inorg. Chem.* **2001**, *40*, 5636.

(6) Henriques, R. T.; Herdtweck, E.; Kühn, F. E; Lopes, A. D.; Mink, J.; Romão, C. C. *J. Chem. Soc., Dalton Trans.* **1998**, 1293.

(7) Brownstein, S.; Han, N. F.; Gabe, E.; Le Page, Y. *Can. J. Chem.* **1989**, *67*, 2222.

(8) Cotton, F. A.; Daniels, L. M.; Murillo, C. A. *Inorg. Chem.* **1993**, *32,* 4868.

(9) Cotton, F. A.; Daniels, L. M.; Murillo, C. A.; Quesada, J. F. *Inorg. Chem.* **1993**, *32,* 4861.

(10) Huheey, J. E.; Keiter, E. A.; Keiter, R. L. *Inorganic Chemistry: Principles of Structure and Reactivity*, HarperCollins, New York, **1994**.

(11) Vallee, B. L.; Williams, R. J. P. *Proc. Natl. Acad. Sci., USA* **1968**, *59*, 498.

(12) Cox, B. G.; Jedral, W.; Palou, J. *J. Chem. Soc., Dalton Trans.* **1988**, 733.

(13) Nelsen, S. F; Chen, L-J; Ramm, M. T.; Voy, G. T.; Powell, D. R.; Accola, M. A., Seehafer, T. R.; Sabelko, J. J.;. Pladziewicz, J. R. *J. Org. Chem.* **1996,** *61,* 1405.

(14) Kirchner, K.; Dang, S.-Q.; Stebler, M.; Dodgen, H. W.; Wherland, S.; Hunt, J. P. *Inorg. Chem.* **1989**, *28*, 3604.

(15) Manahan, S. E. *Can. J. Chem.* **1967**, *45*, 2451.

(16) Brisset, J.-L. *J. Chem. Eng. Data* **1982**, *27*, 153.

(17) Sisley, M. J.; Jordan, R. B. *Inorg. Chem.* **1992**, *31*, 2880.

(18) Rorabacher, D. B. *Chem. Rev.* **2004**, *104*, 651, and references therein.

(19) Fukuzumi, S.; Nakanishi, I.; Tanaka, K.; Suenobu, T.; Tabard, A.; Guilard, R.; Van Caemelbecke, E.; Kadish K. M. *J. Am. Chem. Soc.* **1999**, *121*, 785.

(20) (a) Ishiguro, S.-I.; Jeliazkova, B. G.; Ohtaki, H. *Bull. Chem. Soc. Jpn.* **1985**, *58*, 1749. (b) Manahan, S. E.; Iwamoto, R. T. *Inorg. Chem.* **1965**, *4*, 1409.

(21) Senne, J. K.; Kratochvil, B. *Anal. Chem.* **1971**, *43*, 79.

(22) Heerman, L. F.; Rechnitz, G. A. *Anal. Chem.* **1972**, *44*, 1655.

(23) Smith, R. M.; Martell A. E.; Motekaitis, R. *NIST Critically Selected Stability Constants of Metal Complexes Database*, Version 2; NIST: Washington DC, **1995**.

(24) Ramette, R. W. *Inorg. Chem.* **1986**, *25*, 2481.

(25) Ochsenbein, U.; Schläpfer C. W. *Helv. Chim. Acta* **1980**, *63*, 1926.

(26) Kroneck, P.; Kodweiss, J.; Lutz, O.; Nolle, A.; Zepf, D. *Z. Naturforsch.* **1982**, *37a*, 186.

(27) Kroeker, S.; Wasylishen, R. E. *Can. J. Chem.* **1999**, *77*, 1962.

(28) Lucken, E. A. C. *Z. Naturforsch.* **1994**, *49a*, 155. Ramaprabhu, S.; Lucken, E. A. C.; Bernardinelli, G. *J. Chem. Soc., Dalton Trans.* **1995**, 115, and references therein.

(29) Asaro, F.; Camus, A.; Gobetto, R.; Olivieri, A. C.; Pellizer, G. *Solid State Nuclear Magnetic Resonance* **1997**, *8*, 81.

Appendix. Figures and Tables of Experimental Data

Appendix 2.1. Structure[a] and Data[b] Refinement for $Cu(NCCH_3)_2(OH_2)_2(F_3CSO_3)_2$ (**1a**), $Cu(NCCH_3)_4(F_3CSO_3)_2$ (**1b**) and $Cu(NCCH_3)_4(F_3CSO_3)$ (**2**)

	1a	**1b**	**2**
Formula	$CuC_6F_6H_{10}N_2O_8S_2$	$CuC_{10}F_6H_{12}N_4O_6S_2$	$C_9H_{12}CuF_3N_4O_3S$
MW (g mol^{-1})	479.82	525.90	376.83
Dimensions, mm	0.40 x 0.25 x 0.07	0.46 x 0.41 x 0.27	0.81 × 0.69 × 0.58
Crystal system	Triclinic	Orthorhombic	Monoclinic
Space group	PI (No. 2)	Pbca (No. 61)	$P2_1/c$ (No. 14)
a (Å) [c]	5.7426 (9)	13.5406 (17)	15.2062 (14)
b (Å) [c]	7.2723 (11)	10.8441 (14)	14.1400 (13)
c (Å) [c]	10.5221 (16)	27.725 (4)	22.399 (2)
α (degree) [c]	79.855 (3)		
β (degree) [c]	84.183 (3)		94.527 (2)
γ (degree) [c]	78.537 (3)		
V ($Å^3$) [c]	422.92 (11)	4071.1 (9)	4801.2 (8)
Z	1	8	12
ρ_{calcd} (g cm^{-3})	1.884	1.716	1.564
μ (mm^{-1})	1.638	1.366	1.538
2θ limit	52.84°	52.82°	52.76°
Total data	2363	17961	31788
Total Reflections	1710	4170 (R_{int} = 0.0485)	9759 (R_{int} = 0.0249)

Appendix 2.1. (Continued)

	1a	**1b**	**2**
NO [d]	1523	3565	6972
Data	1710	4170	9759
Restraints/parameters	0/117	0/266	38 [e]/572
S [f]	1.061	1.040	1.071
Final R_1 [g]	0.0420	0.0391	0.0827
Final wR_2 [h]	0.1236	0.1083	0.2706
Max/min in diff map	1.018/-0.683 e Å^{-3}	0.806/-0.752 e Å^{-3}	1.623/-1.158 e Å^{-3}

[a] Reference 12, Chapter 2. [b] Reference 13, Chapter 2. [c] Obtained from least squares refinement of 2106 centered reflections (**1a**), 4662 reflections with $5.03° < 2\theta < 52.74°$ (**1b**), and 5716 reflections with $4.43° < 2\theta < 52.62°$ (**2**). [d] The number of observed reflections (*NO*). Refinement on F_o^2 for all reflections (all of these having $F_o^2 \geq -3\sigma(F_o^2)$). Weighted R-factors wR_2 and all goodness of fit S are based on F_o^2; conventional R-factors R_1 are based on F_o, with F_o set to zero for negative F_o^2. The observed criterion of $F_o^2 \geq 2\sigma(F_o^2)$ is used only for calculating R_1, and is not relevant to the choice of reflections for refinement. R-factors based on F_o^2 are statistically about the twice as large as those on F_o, and R-factors based on all data will be even larger. [e] The interatomic distances within the disordered triflate ion were restrained to be: S-C, 1.80 (1) Å; S-O, 1.45 (1) Å; C-F, 1.35 (1) Å; O···O, 2.37 (1) Å; F···F, 2.20 (1) Å; and O···F, 3.04 (1) Å. [f] Goodness of fit with $[F_o^2 \geq -3\sigma(F_o^2)]$; $S = [\sigma w(F_o^2 - F_c^2)^2/(n-p)]^{1/2}$ (n = number of data; p = number of parameters varied; $w = [\sigma^2(F_o^2) + (0.1479P)^2 + 10.0873P]^{-1}$ (**2**) or $w = [\sigma^2(F_o^2) + (0.0976P)^2]^{-1}$ (**1a**) or $w = [\sigma^2(F_o^2) + (0.0708P)^2 + 1.0748P]^{-1}$ (**1b**), where $P = [\text{Max}(F_o^2, 0) + 2F_c^2]/3$). [g] $R_1 = \Sigma||F_o| - |F_c||/\Sigma|F_o|$. [h] $wR_2 = [\Sigma w(F_o^2 - F_c^2)^2/\Sigma w(F_o^4)]^{1/2}$.

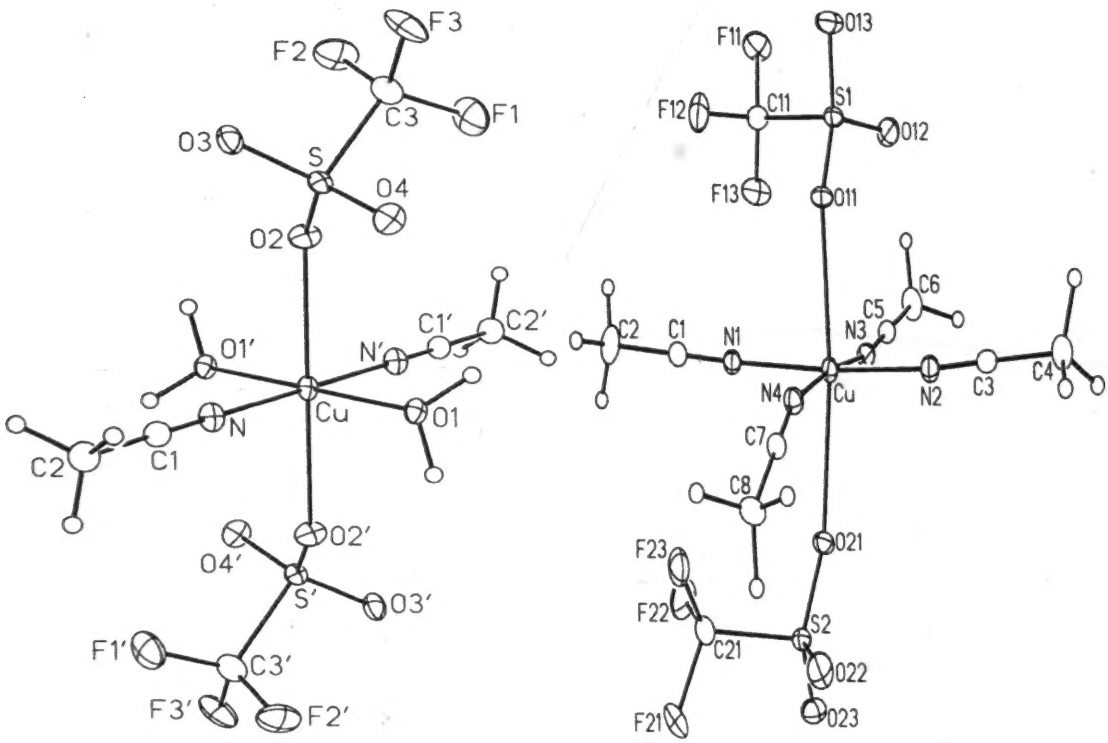

1a **1b**

Appendix 2.2. Perspective views of the $[Cu(NCCH_3)_2(OH_2)_2(F_3CSO_3)_2]$ (**1a**) and of the *trans*-$[Cu(NCCH_3)_4(F_3CSO_3)_2]$ (**1b**) molecules showing the atom labeling scheme. Non-hydrogen atoms are represented by Gaussian ellipsoids at the 20% probability level. Hydrogen atoms are shown with arbitrarily small thermal parameters. Primed atoms are related to unprimed ones via the crystallographic inversion center (0, 0, 0) upon which the copper center in **1a** is located.

Appendix 2.3. Atomic Coordinates and Equivalent Isotropic Displacement Parameters for **1a**

Atom	x	y	z	U_{eq} A^2
Cu	0.0000	0.0000	0.0000	0.0235(2)*
S	0.20856(12)	0.27324(9)	0.20010(6)	0.0253(2)*
F1	-0.0913(5)	0.2438(4)	0.4035(2)	0.0694(7)*
F2	0.2648(5)	0.1036(4)	0.4385(2)	0.0692(7)*
F3	0.1741(5)	0.4065(4)	0.4169(2)	0.0653(7)*
O1	-0.2301(3)	0.2409(3)	-0.02081(18)	0.0263(4)*
O2	0.1662(4)	0.0966(3)	0.1718(2)	0.0372(5)*
O3	0.4542(4)	0.2938(3)	0.1885(2)	0.0391(5)*
O4	0.0472(4)	0.4398(3)	0.1470(2)	0.0396(5)*
N	0.2215(4)	0.1201(3)	-0.1291(2)	0.0306(5)*
C1	0.3399(5)	0.1991(4)	-0.2017(3)	0.0278(6)*
C2	0.4900(6)	0.3030(4)	-0.2949(3)	0.0363(7)*
C3	0.1341(6)	0.2545(5)	0.3742(3)	0.0411(7)*

Anisotropically-refined atoms are marked with an asterisk (*). The form of the anisotropic displacement parameter is: $\exp[-2\pi^2(h^2a^{*2}U_{11} + k^2b^{*2}U_{22} + l^2c^{*2}U_{33} + 2klb^*c^*U_{23} + 2hla^*c^*U_{13} + 2hka^*b^*U_{12})]$

Appendix 2.4. Atomic Coordinates and Equivalent Isotropic Displacement Parameters for **1b**

Atom	x	y	z	U_{eq} A^2
Cu	0.03116(2)	0.02062(3)	0.135667(10)	0.02328(12)*
S1	0.10859(5)	-0.25939(6)	0.07795(2)	0.02969(16)*
S2	-0.09679(5)	0.29058(6)	0.18920(2)	0.02897(16)*
F11	-0.01391(15)	-0.40479(19)	0.03171(9)	0.0671(7)*
F12	-0.01245(17)	-0.2181(2)	0.00583(8)	0.0679(6)*
F13	-0.08517(12)	-0.26200(18)	0.07215(8)	0.0562(5)*
F21	-0.2021(2)	0.4432(2)	0.13768(8)	0.0766(7)*
F22	-0.23920(14)	0.2536(2)	0.12712(8)	0.0692(7)*
F23	-0.10795(15)	0.3253(2)	0.09498(7)	0.0589(6)*
O11	0.10738(13)	-0.12610(16)	0.08485(6)	0.0305(4)*
O12	0.09799(18)	-0.3305(2)	0.12140(8)	0.0478(5)*
O13	0.18259(16)	-0.3005(2)	0.04460(8)	0.0485(6)*
O21	-0.06770(15)	0.16367(17)	0.18200(7)	0.0347(4)*
O22	-0.01632(16)	0.3766(2)	0.18891(9)	0.0532(6)*
O23	-0.16994(17)	0.3074(2)	0.22621(8)	0.0509(6)*
N1	-0.07829(16)	0.02247(19)	0.08760(8)	0.0272(4)*
N2	0.14815(16)	0.0162(2)	0.17908(8)	0.0290(5)*
N3	-0.03163(15)	-0.1149(2)	0.17268(8)	0.0276(5)*
N4	0.09138(15)	0.1668(2)	0.10397(8)	0.0283(5)*

Appendix 2.4. (Continued)

Atom	x	y	z	U_{eq} A^2
C1	-0.13743(19)	0.0224(2)	0.05892(9)	0.0284(5)*
C2	-0.2135(2)	0.0230(3)	0.02188(11)	0.0489(8)*
C3	0.22051(19)	0.0146(2)	0.19959(9)	0.0280(5)*
C4	0.3132(2)	0.0144(3)	0.22590(11)	0.0429(7)*
C5	-0.05585(18)	-0.2044(2)	0.18981(9)	0.0270(5)*
C6	-0.0874(2)	-0.3197(3)	0.21167(12)	0.0433(7)*
C7	0.11401(17)	0.2649(2)	0.09584(9)	0.0260(5)*
C8	0.1397(2)	0.3930(2)	0.08621(11)	0.0366(6)*
C11	-0.0067(2)	-0.2869(3)	0.04547(11)	0.0391(7)*
C21	-0.1650(2)	0.3299(3)	0.13441(10)	0.0414(7)*

Anisotropically-refined atoms are marked with an asterisk (*). The form of the anisotropic displacement parameter is: $\exp[-2\pi^2(h^2a^{*2}U_{11} + k^2b^{*2}U_{22} + l^2c^{*2}U_{33} + 2klb^*c^*U_{23} + 2hla^*c^*U_{13} + 2hka^*b^*U_{12})]$

Appendix 2.5. Derived Atomic Coordinates and Displacement Parameters for Hydrogen Atoms in **1a** (top) and **1b** (bottom)

Atom	*x*	*y*	*z*	U_{eq}, Å^2
H1OA	-0.3307	0.2509	0.0596	0.040
H1OB	-0.3300	0.2446	-0.0917	0.040
H2A	0.4539	0.2960	-0.3827	0.044
H2B	0.6577	0.2471	-0.2825	0.044
H2C	0.4601	0.4363	-0.2823	0.044
H2A	-0.2224	-0.0608	0.0094	0.059
H2B	-0.1936	0.0779	-0.0045	0.059
H2C	-0.2758	0.0523	0.0358	0.059
H4A	0.3444	0.0956	0.2232	0.051
H4B	0.3572	-0.0484	0.2123	0.051
H4C	0.3006	-0.0042	0.2599	0.051
H6A	-0.1594	-0.3194	0.2154	0.052
H6B	-0.0563	-0.3287	0.2434	0.052
H6C	-0.0679	-0.3887	0.1910	0.052
H8A	0.1033	0.4469	0.1083	0.044
H8B	0.1224	0.4136	0.0529	0.044
H8C	0.2108	0.4047	0.0910	0.044

Appendix 2.6. Selected Interatomic Distances (Å) in **1a** (top) and **1b** (bottom)

Atom1	Atom2	Distance	Atom1	Atom2	Distance
Cu	O1	1.9666(18)	S	C3	1.826(3)
Cu	O2	2.3949(19)	F1	C3	1.315(4)
Cu	N	1.975(2)	F2	C3	1.319(4)
S	O2	1.439(2)	F3	C3	1.331(4)
S	O3	1.438(2)	N	C1	1.127(4)
S	O4	1.434(2)	C1	C2	1.450(4)
Cu	O11	2.3625(17)	F11	C11	1.337(3)
Cu	O21	2.4184(18)	F12	C11	1.331(4)
Cu	N1	1.993(2)	F13	C11	1.322(4)
Cu	N2	1.990(2)	F21	C21	1.330(4)
Cu	N3	1.984(2)	F22	C21	1.318(4)
Cu	N4	1.987(2)	F23	C21	1.339(3)
S1	O11	1.4581(19)	N1	C1	1.129(3)
S1	O12	1.437(2)	N2	C3	1.133(3)
S1	O13	1.435(2)	N3	C5	1.129(3)
S1	C11	1.827(3)	N4	C7	1.130(3)
S2	O21	1.4454(19)	C1	C2	1.455(4)
S2	O22	1.434(2)	C3	C4	1.452(4)
S2	O23	1.438(2)	C5	C6	1.454(4)
S2	C21	1.828(3)	C7	C8	1.457(4)

Appendix 2.7. Selected Interatomic Angles (deg) in **1a** [a]

Atom1	Atom2	Atom3	Angle	Atom1	Atom2	Atom3	Angle
O1	Cu	O1′	180.0	O2	S	O3	115.33(13)
O1	Cu	O2	90.14(7)	O2	S	O4	115.27(13)
O1	Cu	O2′	89.86(7)	O2	S	C3	102.99(14)
O1	Cu	N	89.09(9)	O3	S	O4	114.46(13)
O1	Cu	N′	90.91(9)	O3	S	C3	102.74(15)
O1′	Cu	O2	89.86(7)	O4	S	C3	103.56(15)
O1′	Cu	O2′	90.14(7)	Cu	O2	S	135.75(12)
O1′	Cu	N	90.91(9)	Cu	N	C1	175.8(2)
O1′	Cu	N′	89.09(9)	N	C1	C2	179.2(3)
O2	Cu	O2′	180.0	S	C3	F1	111.6(2)
O2	Cu	N	90.89(9)	S	C3	F2	111.4(3)
O2	Cu	N′	89.11(9)	S	C3	F3	110.3(2)
O2′	Cu	N	89.11(9)	F1	C3	F2	108.2(3)
O2′	Cu	N′	90.89(9)	F1	C3	F3	107.7(3)
N	Cu	N′	180.0	F2	C3	F3	107.5(3)

[a] Primed atoms are related to unprimed ones via the crystallographic inversion center (0, 0, 0)

Appendix 2.8. Selected Interatomic Angles (deg) in **1b**

Atom1	Atom2	Atom3	Angle	Atom1	Atom2	Atom3	Angle
O11	Cu	O21	172.13(6)	O22	S2	C21	103.12(15)
O11	Cu	N1	86.15(8)	O23	S2	C21	102.46(14)
O11	Cu	N2	89.81(8)	Cu	O11	S1	138.65(11)
O11	Cu	N3	89.82(8)	Cu	O21	S2	146.61(12)
O11	Cu	N4	95.40(8)	Cu	N1	C1	177.1(2)
O21	Cu	N1	86.40(8)	Cu	N2	C3	172.9(2)
O21	Cu	N2	97.74(8)	Cu	N3	C5	168.2(2)
O21	Cu	N3	87.89(8)	Cu	N4	C7	161.9(2)
O21	Cu	N4	87.16(8)	N1	C1	C2	179.7(3)
N1	Cu	N2	175.20(9)	N2	C3	C4	179.2(3)
N1	Cu	N3	91.99(8)	N3	C5	C6	179.7(3)
N1	Cu	N4	90.08(9)	N4	C7	C8	177.8(3)
N2	Cu	N3	90.61(9)	S1	C11	F11	111.0(2)
N2	Cu	N4	87.70(9)	S1	C11	F12	111.4(2)
N3	Cu	N4	174.51(9)	S1	C11	F13	112.2(2)
O11	S1	O12	114.87(12)	F11	C11	F12	107.2(3)
O11	S1	O13	113.62(13)	F11	C11	F13	107.3(3)
O11	S1	C11	102.54(12)	F12	C11	F13	107.5(3)
O12	S1	O13	116.31(14)	S2	C21	F21	110.5(2)

Appendix 2.8. (Continued)

Atom1	Atom2	Atom3	Angle	Atom1	Atom2	Atom3	Angle
O12	S1	C11	103.88(15)	S2	C21	F22	111.5(2)
O13	S1	C11	103.19(14)	S2	C21	F23	112.25(19)
O21	S2	O22	114.29(13)	F21	C21	F22	107.6(3)
O21	S2	O23	114.01(13)	F21	C21	F23	108.0(3)
O21	S2	C21	104.19(13)	F22	C21	F23	106.9(3)
O22	S2	O23	116.42(15)				

Appendix 2.9. Torsional Angles (deg) in **1a** [a]

Atom1	Atom2	Atom3	Atom4	Angle
O1	Cu	O2	S	-35.2(2)
O1′	Cu	O2	S	144.8(2)
O2′	Cu	O2	S	73(100)
N	Cu	O2	S	53.9(2)
N′	Cu	O2	S	-126.1(2)
O1	Cu	N	C1	17(3)
O1′	Cu	N	C1	-163(3)
O2	Cu	N	C1	-74(3)
O2′	Cu	N	C1	106(3)
N′	Cu	N	C1	79(100)
O3	S	O2	Cu	-108.2(2)
O4	S	O2	Cu	28.7(3)
C3	S	O2	Cu	140.7(2)
O2	S	C3	F1	-62.9(3)
O2	S	C3	F2	58.1(3)
O2	S	C3	F3	177.4(2)
O3	S	C3	F1	176.9(2)
O3	S	C3	F2	-62.0(3)
O3	S	C3	F3	57.3(3)

Appendix 2.9. (Continued)

Atom1	Atom2	Atom3	Atom4	Angle
O4	S	C3	F1	57.5(3)
O4	S	C3	F2	178.5(2)
O4	S	C3	F3	-62.1(3)
Cu	N	C1	C2	-3(26)

[a] Primed atoms are related to unprimed ones via the crystallographic inversion center (0, 0, 0)

Appendix 2.10. Torsional Angles (deg) in **1b**

Atom1	Atom2	Atom3	Atom4	Angle
O21	Cu	O11	S1	-69.4(5)
N1	Cu	O11	S1	-88.35(17)
N2	Cu	O11	S1	94.27(17)
N3	Cu	O11	S1	3.66(17)
N4	Cu	O11	S1	-178.06(17)
O11	Cu	O21	S2	-101.9(5)
N1	Cu	O21	S2	-82.9(2)
N2	Cu	O21	S2	94.6(2)
N3	Cu	O21	S2	-175.1(2)
N4	Cu	O21	S2	7.3(2)
O11	Cu	N1	C1	-30(4)
O21	Cu	N1	C1	152(4)
N2	Cu	N1	C1	3(5)
N3	Cu	N1	C1	-120(4)
N4	Cu	N1	C1	65(4)
O11	Cu	N2	C3	45.9(17)
O21	Cu	N2	C3	-136.3(17)
N1	Cu	N2	C3	13(2)
N3	Cu	N2	C3	135.7(17)

Appendix 2.10. (Continued)

Atom1	Atom2	Atom3	Atom4	Angle
N4	Cu	N2	C3	-49.5(17)
O11	Cu	N3	C5	15.1(10)
O21	Cu	N3	C5	-172.4(10)
N1	Cu	N3	C5	101.3(10)
N2	Cu	N3	C5	-74.7(10)
N4	Cu	N3	C5	-146.7(10)
O11	Cu	N4	C7	-173.2(7)
O21	Cu	N4	C7	14.3(7)
N1	Cu	N4	C7	100.6(7)
N2	Cu	N4	C7	-83.6(7)
N3	Cu	N4	C7	-11.5(13)
O12	S1	O11	Cu	-33.8(2)
O13	S1	O11	Cu	-171.20(15)
C11	S1	O11	Cu	78.16(19)
O11	S1	C11	F11	174.0(2)
O11	S1	C11	F12	54.5(2)
O11	S1	C11	F13	-66.0(2)
O12	S1	C11	F11	-66.1(3)
O12	S1	C11	F12	174.4(2)

Appendix 2.10. (Continued)

Atom1	Atom2	Atom3	Atom4	Angle
O12	S1	C11	F13	53.9(2)
O13	S1	C11	F11	55.7(3)
O13	S1	C11	F12	-63.8(2)
O13	S1	C11	F13	175.7(2)
O22	S2	O21	Cu	-45.8(3)
O23	S2	O21	Cu	176.9(2)
C21	S2	O21	Cu	66.0(2)
O21	S2	C21	F21	175.8(2)
O21	S2	C21	F22	56.3(2)
O21	S2	C21	F23	-63.6(3)
O22	S2	C21	F21	-64.6(3)
O22	S2	C21	F22	175.9(2)
O22	S2	C21	F23	56.0(3)
O23	S2	C21	F21	56.7(3)
O23	S2	C21	F22	-62.8(2)
O23	S2	C21	F23	177.3(2)
Cu	N1	C1	C2	-78(81)
Cu	N2	C3	C4	88(18)
Cu	N3	C5	C6	-96(100)
Cu	N4	C7	C8	-30(8)

Appendix 2.11. Anisotropic Displacement Parameters (U_{ij}, Å^2) for **1a**

Atom	U_{11}	U_{22}	U_{33}	U_{23}	U_{13}	U_{12}
Cu	0.0228(3)	0.0135(3)	0.0338(3)	-0.00564(18)	0.00183(19)	-0.00256(18)
S	0.0305(4)	0.0165(4)	0.0299(4)	-0.0077(2)	-0.0003(3)	-0.0041(3)
F1	0.0626(15)	0.0840(19)	0.0629(14)	-0.0089(12)	0.0257(11)	-0.0344(13)
F2	0.098(2)	0.0578(16)	0.0458(12)	0.0087(10)	-0.0221(12)	-0.0075(13)
F3	0.0990(19)	0.0588(15)	0.0495(12)	-0.0344(10)	0.0192(12)	-0.0314(13)
O1	0.0252(9)	0.0171(9)	0.0361(10)	-0.0069(7)	-0.0011(7)	-0.0007(7)
O2	0.0499(14)	0.0174(10)	0.0481(12)	-0.0107(8)	-0.0153(10)	-0.0044(9)
O3	0.0338(11)	0.0393(13)	0.0486(12)	-0.0222(10)	0.0079(9)	-0.0092(9)
O4	0.0442(13)	0.0198(11)	0.0517(13)	0.0000(9)	-0.0068(10)	-0.0014(9)
N	0.0325(13)	0.0176(11)	0.0406(12)	-0.0050(9)	0.0027(10)	-0.0043(9)
C1	0.0300(13)	0.0180(12)	0.0363(13)	-0.0078(10)	-0.0034(11)	-0.0025(10)
C2	0.0401(16)	0.0295(16)	0.0388(15)	-0.0001(12)	0.0010(12)	-0.0117(12)
C3	0.052(2)	0.0380(18)	0.0358(14)	-0.0078(12)	0.0050(13)	-0.0155(15)

The form of the anisotropic displacement parameter is: $\exp[-2\pi^2(h^2a^{*2}U_{11} + k^2b^{*2}U_{22} + l^2c^{*2}U_{33} + 2klb^*c^*U_{23} + 2hla^*c^*U_{13} + 2hka^*b^*U_{12})]$

Appendix 2.12. Anisotropic Displacement Parameters (U_{ij}, Å^2) for **1b**

Atom	U_{11}	U_{22}	U_{33}	U_{23}	U_{13}	U_{12}
Cu	0.02702(18)	0.01832(19)	0.02451(18)	0.00295(11)	-0.00321(11)	-0.00287(11)
S1	0.0348(3)	0.0212(3)	0.0331(3)	-0.0069(2)	-0.0027(3)	0.0049(2)
S2	0.0320(3)	0.0226(3)	0.0324(3)	-0.0043(2)	-0.0031(2)	0.0023(2)
F11	0.0667(12)	0.0395(12)	0.0951(17)	-0.0389(11)	-0.0246(11)	0.0038(9)
F12	0.0799(14)	0.0763(16)	0.0476(12)	0.0031(11)	-0.0241(11)	0.0079(12)
F13	0.0357(9)	0.0479(12)	0.0851(14)	-0.0226(10)	0.0051(9)	-0.0041(8)
F21	0.0887(17)	0.0621(15)	0.0790(15)	-0.0011(11)	-0.0229(12)	0.0465(14)
F22	0.0422(11)	0.0970(19)	0.0683(13)	-0.0150(12)	-0.0197(9)	-0.0074(11)
F23	0.0617(12)	0.0764(15)	0.0386(10)	0.0160(9)	0.0008(8)	0.0196(10)
O11	0.0357(9)	0.0197(9)	0.0361(10)	-0.0056(7)	0.0041(7)	0.0005(7)
O12	0.0782(16)	0.0267(11)	0.0386(11)	0.0030(9)	-0.0063(11)	0.0069(10)
O13	0.0433(11)	0.0419(13)	0.0605(14)	-0.0204(10)	0.0071(10)	0.0100(9)
O21	0.0455(10)	0.0237(10)	0.0347(10)	-0.0005(8)	0.0047(8)	0.0061(8)
O22	0.0513(12)	0.0344(13)	0.0739(17)	-0.0017(11)	-0.0185(11)	-0.0124(10)
O23	0.0607(14)	0.0505(14)	0.0415(12)	-0.0101(10)	0.0103(10)	0.0136(11)
N1	0.0322(11)	0.0211(11)	0.0282(10)	-0.0002(8)	-0.0044(9)	-0.0014(8)
N2	0.0313(11)	0.0243(11)	0.0313(11)	0.0009(8)	-0.0052(9)	-0.0013(9)
N3	0.0334(11)	0.0228(12)	0.0266(11)	0.0008(9)	0.0008(8)	-0.0017(9)
N4	0.0307(10)	0.0240(12)	0.0303(11)	0.0022(9)	-0.0005(8)	-0.0005(9)

Appendix 2.12. (Continued)

Atom	U_{11}	U_{22}	U_{33}	U_{23}	U_{13}	U_{12}
C1	0.0332(13)	0.0220(13)	0.0302(13)	0.0021(10)	0.0022(11)	-0.0003(10)
C2	0.0460(16)	0.061(2)	0.0394(16)	0.0078(15)	-0.0128(13)	-0.0143(15)
C3	0.0344(13)	0.0216(13)	0.0279(12)	-0.0028(9)	0.0021(10)	0.0003(10)
C4	0.0337(14)	0.051(2)	0.0436(16)	-0.0007(14)	-0.0085(12)	0.0021(13)
C5	0.0304(12)	0.0244(13)	0.0263(12)	0.0006(10)	-0.0004(10)	0.0003(10)
C6	0.0467(16)	0.0320(17)	0.0512(18)	0.0154(13)	-0.0046(13)	-0.0110(12)
C7	0.0278(11)	0.0242(14)	0.0260(12)	0.0016(9)	0.0006(9)	0.0005(10)
C8	0.0427(14)	0.0190(13)	0.0480(16)	0.0031(11)	0.0051(12)	-0.0013(11)
C11	0.0421(15)	0.0306(16)	0.0447(16)	-0.0134(13)	-0.0080(12)	0.0024(12)
C21	0.0363(14)	0.0466(19)	0.0413(16)	-0.0025(13)	-0.0063(12)	0.0143(13)

The form of the anisotropic displacement parameter is: $\exp[-2\pi^2(h^2a^{*2}U_{11} + k^2b^{*2}U_{22} + l^2c^{*2}U_{33} + 2klb^*c^*U_{23} + 2hla^*c^*U_{13} + 2hka^*b^*U_{12})]$

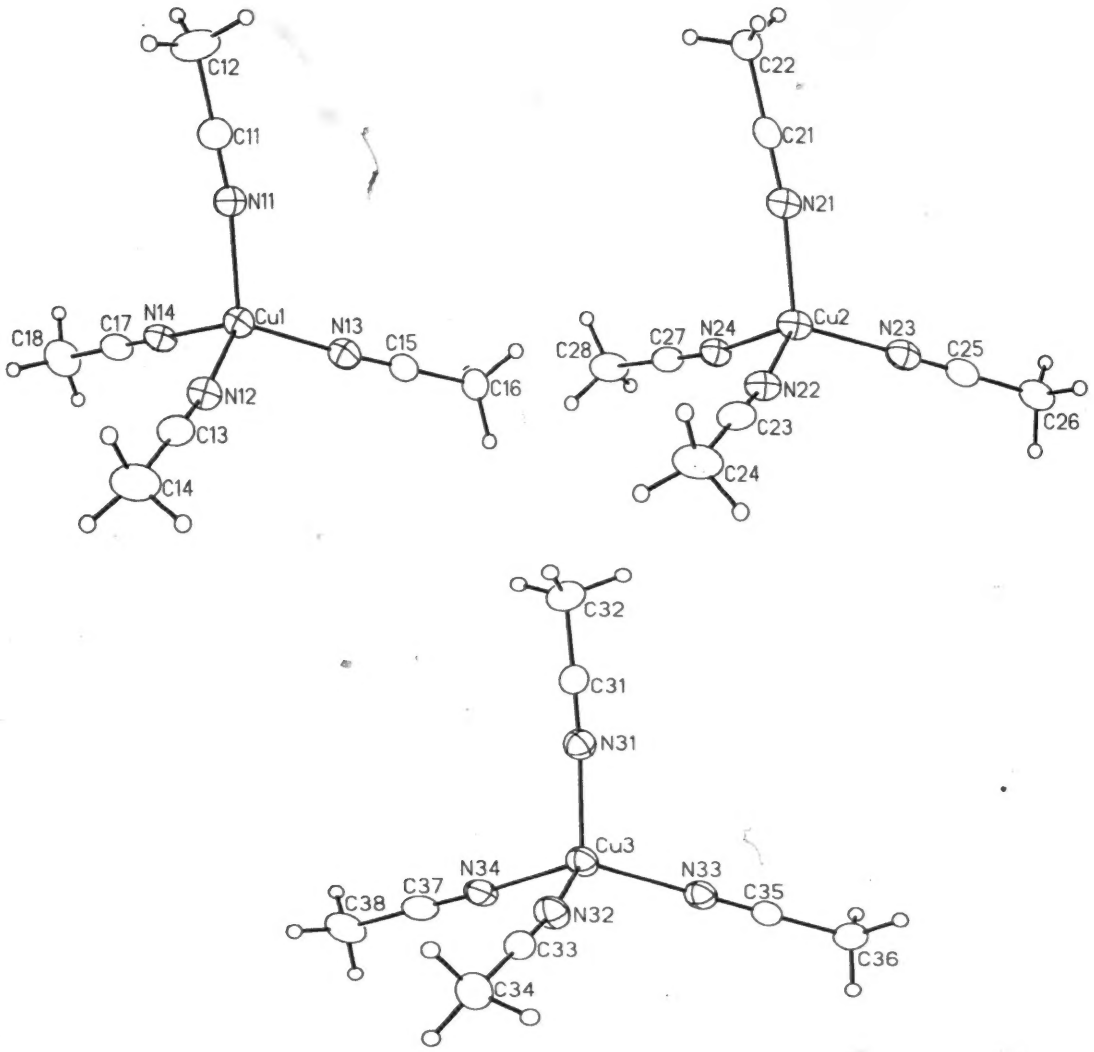

Appendix 2.13. Perspective views of the three crystallographically unique tetrakis(acetonitrile)copper(I) cations of **2**, showing the atom labeling scheme. Non-hydrogen atoms are represented by Gaussian ellipsoids at the 20% probability level. Hydrogen atoms are shown with arbitrarily small thermal parameters.

Appendix 2.14. Atomic Coordinates and Equivalent Isotropic Displacement Parameters for **2**

(a) atoms of the tetrakis(acetonitrile)copper(I) cations

Atom	x	y	z	Ueq, Å^2
Cu1	0.21050(5)	0.11427(5)	0.20652(4)	0.0602(2)*
N11	0.1827(3)	0.0031(4)	0.1521(2)	0.0591(12)*
N12	0.3411(3)	0.1094(3)	0.2267(3)	0.0610(12)*
N13	0.1466(4)	0.1126(4)	0.2802(3)	0.0633(13)*
N14	0.1851(3)	0.2307(4)	0.1580(3)	0.0607(12)*
C11	0.1783(4)	-0.0558(5)	0.1183(3)	0.0636(15)*
C12	0.1717(7)	-0.1316(6)	0.0751(4)	0.105(3)*
C13	0.4157(4)	0.1037(4)	0.2314(3)	0.0601(15)*
C14	0.5116(5)	0.0967(6)	0.2371(4)	0.090(3)*
C15	0.1055(4)	0.1106(4)	0.3207(3)	0.0513(13)*
C16	0.0535(4)	0.1078(5)	0.3715(3)	0.0618(15)*
C17	0.1746(4)	0.2956(5)	0.1300(3)	0.0612(15)*
C18	0.1614(6)	0.3797(5)	0.0934(4)	0.091(3)*
Cu2	0.14514(5)	0.12960(6)	-0.06397(4)	0.0640(3)*
N21	0.2239(3)	0.0169(4)	-0.0685(2)	0.0601(12)*
N22	0.2244(3)	0.2444(3)	-0.0630(2)	0.0598(12)*
N23	0.0744(4)	0.1241(4)	0.0074(3)	0.0676(15)*
N24	0.0680(3)	0.1349(4)	-0.1413(3)	0.0588(12)*

Appendix 2.14. (Continued)

(a) atoms of the tetrakis(acetonitrile)copper(I) cations

Atom	x	y	z	Ueq, Å^2
C21	0.2713(4)	-0.0437(4)	-0.0783(2)	0.0502(12)*
C22	0.3305(4)	-0.1191(4)	-0.0900(3)	0.0582(14)*
C23	0.2734(4)	0.3028(4)	-0.0673(3)	0.0593(15)*
C24	0.3345(5)	0.3803(5)	-0.0740(4)	0.085(3)*
C25	0.0343(4)	0.1222(4)	0.0478(3)	0.0586(15)*
C26	-0.0172(4)	0.1213(4)	0.0995(4)	0.0690(18)*
C27	0.0342(4)	0.1327(4)	-0.1882(3)	0.0579(14)*
C28	-0.0098(6)	0.1281(5)	-0.2482(4)	0.093(3)*
Cu3	0.55325(5)	-0.10589(5)	0.37028(3)	0.0608(3)*
N31	0.4257(4)	-0.1084(4)	0.3395(2)	0.0627(13)*
N32	0.5838(3)	-0.2276(4)	0.4138(2)	0.0627(13)*
N33	0.5754(3)	0.0040(4)	0.4248(2)	0.0608(12)*
N34	0.6267(3)	-0.1134(4)	0.3009(2)	0.0612(13)*
C31	0.3550(4)	-0.1116(4)	0.3196(3)	0.0539(13)*
C32	0.2644(5)	-0.1149(5)	0.2930(4)	0.0724(18)*
C33	0.6056(4)	-0.2997(4)	0.4307(2)	0.0513(12)*
C34	0.6353(5)	-0.3915(4)	0.4516(3)	0.0683(17)*
C35	0.5868(3)	0.0657(4)	0.4572(2)	0.0489(12)*
C36	0.6012(4)	0.1431(5)	0.4985(3)	0.0627(15)*
C37	0.6662(4)	-0.1274(5)	0.2604(3)	0.0596(15)*

Appendix 2.14. (Continued)

(a) atoms of the tetrakis(acetonitrile)copper(I) cations

atom	x	y	z	Ueq, Å^2
C38	0.7173(5)	-0.1463(7)	0.2103(3)	0.086(2)*

(b) atoms of the triflate ions

atom	x	y	z	Ueq, Å^2
S1	0.50712(10)	0.13064(10)	-0.09238(7)	0.0569(4)*
F11	0.6092(4)	0.2574(4)	-0.1330(2)	0.123(2)*
F12	0.5165(5)	0.1949(6)	-0.1991(2)	0.163(3)*
F13	0.6263(4)	0.1183(5)	-0.1673(3)	0.153(3)*
O11	0.4674(3)	0.0474(3)	-0.1168(2)	0.0818(14)*
O12	0.5790(6)	0.1160(4)	-0.0465(3)	0.115(3)*
O13	0.4499(4)	0.2031(5)	-0.0782(4)	0.125(3)*
C1	0.5676(5)	0.1772(6)	-0.1497(4)	0.081(2)
S2	0.85334(9)	0.13767(12)	0.56510(6)	0.0540(4)*
F21	0.8142(4)	0.1208(4)	0.4512(2)	0.120(2)*
F22	0.9226(4)	0.0343(5)	0.4864(3)	0.151(3)*
F23	0.9430(4)	0.1827(5)	0.4770(3)	0.139(2)*
O21	0.9347(3)	0.1338(4)	0.6017(2)	0.0761(13)*
O22	0.8128(3)	0.2284(4)	0.5587(3)	0.101(2)*
O23	0.7955(4)	0.0607(6)	0.5740(3)	0.123(3)*
C2	0.8844(5)	0.1177(5)	0.4906(4)	0.0731(18)

Appendix 2.14. (Continued)

(b) atoms of the triflate ions

atom	x	y	z	Ueq, Å^2
S3[a]	-0.1911(2)	0.1279(2)	0.28486(13)	0.0645(8)*[a]
F31[a]	-0.0413(2)	0.1304(5)	0.2370(3)	0.104(3)[a]
F32[a]	-0.1470(4)	0.0511(4)	0.1865(2)	0.120(3)[a]
F33[a]	-0.1492(4)	0.2066(4)	0.18656(19)	0.093(3)[a]
O31[a]	-0.2844(2)	0.1264(5)	0.2658(2)	0.201(11)[a]
O32[a]	-0.1705(4)	0.2118(3)	0.32033(19)	0.082(3)[a]
O33[a]	-0.1681(4)	0.0442(3)	0.3202(2)	0.114(4)[a]
C3[a]	-0.1285(3)	0.1291(3)	0.21995(16)	0.059(3)[a]
S3B	-0.1488(2)	0.1203(3)	0.25841(17)	0.0948(17)*[a]
F31B	-0.3011(3)	0.2028(4)	0.2582(3)	0.094(3)[a]
F32B	-0.3052(3)	0.0536(5)	0.2303(3)	0.146(4)[a]
F33B	-0.2775(3)	0.0903(4)	0.3254(2)	0.0708(19)[a]
O31B	-0.1109(3)	0.0275(4)	0.2700(3)	0.118(4)[a]
O32B	-0.1065(3)	0.1882(4)	0.2999(3)	0.204(9)[a]
O33B	-0.1363(4)	0.1487(5)	0.1975(2)	0.211(10)[a]
C3B	-0.2650(2)	0.1166(3)	0.26873(19)	0.065(4)[a]

Anisotropically-refined atoms are marked with an asterisk (*). The form of the anisotropic displacement parameter is: $\exp[-2\pi^2(h^2a^{*2}U_{11} + k^2b^{*2}U_{22} + l^2c^{*2}U_{33} + 2klb^*c^*U_{23} + 2hla^*c^*U_{13} + 2hka^*b^*U_{12})]$. [a] Refined with an occupancy factor of 0.5.

Appendix 2.15. Selected Interatomic Distances (Å) for **2**

(a) within the tetrakis(acetonitrile)copper(I) cations

Atom1	Atom2	Distance	Atom1	Atom2	Distance	Atom1	Atom2	Distance
Cu1	N11	2.015(5)	Cu2	N21	2.001(5)	Cu3	N31	2.007(6)
Cu1	N12	2.003(5)	Cu2	N22	2.022(5)	Cu3	N32	2.014(5)
Cu1	N13	1.980(6)	Cu2	N23	1.997(7)	Cu3	N33	1.988(6)
Cu1	N14	1.994(5)	Cu2	N24	2.016(5)	Cu3	N34	1.987(5)
N11	C11	1.123(8)	N21	C21	1.152(7)	N31	C31	1.132(8)
N12	C13	1.134(8)	N22	C23	1.121(7)	N32	C33	1.127(7)
N13	C15	1.143(8)	N23	C25	1.131(8)	N33	C35	1.140(7)
N14	C17	1.115(8)	N24	C27	1.131(8)	N34	C37	1.144(8)
C11	C12	1.441(10)	C21	C22	1.433(8)	C31	C32	1.458(9)
C13	C14	1.456(10)	C23	C24	1.452(9)	C33	C34	1.442(8)
C15	C16	1.436(9)	C25	C26	1.448(11)	C35	C36	1.440(9)
C17	C18	1.449(10)	C27	C28	1.456(9)	C37	C38	1.440(10)

(b) within the triflate ions

Atom1	Atom2	Distance	Atom1	Atom2	Distance	Atom1	Atom2	Distance
S1	O11	1.413(5)	S2	C2	1.792(8)	F33A	C3A	1.35(1)†
S1	O12	1.455(6)	F21	C2	1.331(9)	S3B	O31B	1.45(1)†
S1	O13	1.397(6)	F22	C2	1.321(9)	S3B	O32B	1.45(1)†
S1	C1	1.764(8)	F23	C2	1.332(9)	S3B	O33B	1.45(1)†

Appendix 2.15. (Continued)

(b) within the triflate ions

Atom1	Atom2	Distance	Atom1	Atom2	Distance	Atom1	Atom2	Distance
F11	C1	1.338(9)	S3A	O31A	1.45(1)†	S3B	C3B	1.80(1)†
F12	C1	1.324(9)	S3A	O32A	1.45(1)†	F31B	C3B	1.35(1)†
F13	C1	1.304(10)	S3A	O33A	1.45(1)†	F32B	C3B	1.35(1)†
S2	O21	1.430(5)	S3A	C3A	1.80(1)†	F33B	C3B	1.35(1)†
S2	O22	1.425(5)	F31A	C3A	1.35(1)†			
S2	O23	1.423(6)	F32A	C3A	1.35(1)†			

†Distance restrained during refinement.

Appendix 2.16. Selected Interatomic Angles (deg) for **2**

(a) within the tetrakis(acetonitrile)copper(I) cations

Atom1	Atom2	Atom3	Angle	Atom1	Atom2	Atom3	Angle
N11	Cu1	N12	105.5(2)	Cu2	N22	C23	172.1(5)
N11	Cu1	N13	113.7(2)	Cu2	N23	C25	179.1(5)
N11	Cu1	N14	107.0(2)	Cu2	N24	C27	170.6(5)
N12	Cu1	N13	110.8(2)	N21	C21	C22	179.5(7)
N12	Cu1	N14	107.3(2)	N22	C23	C24	178.0(7)
N13	Cu1	N14	112.2(2)	N23	C25	C26	179.2(7)
Cu1	N11	C11	170.1(6)	N24	C27	C28	179.0(8)
Cu1	N12	C13	172.0(6)	N31	Cu3	N32	109.3(2)
Cu1	N13	C15	176.1(5)	N31	Cu3	N33	109.7(2)
Cu1	N14	C17	176.8(5)	N31	Cu3	N34	108.6(2)
N11	C11	C12	179.4(9)	N32	Cu3	N33	110.5(2)
N12	C13	C14	179.6(9)	N32	Cu3	N34	102.1(2)
N13	C15	C16	179.8(8)	N33	Cu3	N34	116.3(2)
N14	C17	C18	179.7(9)	Cu3	N31	C31	176.6(5)
N21	Cu2	N22	106.4(2)	Cu3	N32	C33	170.1(5)
N21	Cu2	N23	111.8(2)	Cu3	N33	C35	178.0(5)
N21	Cu2	N24	107.2(2)	Cu3	N34	C37	172.8(5)
N22	Cu2	N23	112.4(2)	N31	C31	C32	179.0(7)
N22	Cu2	N24	106.6(2)	N32	C33	C34	178.7(7)
N23	Cu2	N24	112.0(2)	N33	C35	C36	179.6(6)

Appendix 2.16. (Continued)

(a) within the tetrakis(acetonitrile)copper(I) cations

Atom1	Atom2	Atom3	Angle	Atom1	Atom2	Atom3	Angle
Cu2	N21	C21	171.2(5)	N34	C37	C38	178.7(7)

(b) within the triflate ions

Atom1	Atom2	Atom3	Angle	Atom1	Atom2	Atom3	Angle
O11	S1	O12	115.5(3)	O31A	S3A	O32A	109.7(1)†
O11	S1	O13	116.3(4)	O31A	S3A	O33A	109.7(1)†
O11	S1	C1	105.1(4)	O31A	S3A	C3A	109.3(1)†
O12	S1	O13	112.9(5)	O32A	S3A	O33A	109.7(1)†
O12	S1	C1	99.3(4)	O32A	S3A	C3A	109.2(1)†
O13	S1	C1	105.2(4)	O33A	S3A	C3A	109.2(1)†
S1	C1	F11	112.0(6)	S3A	C3A	F31A	109.9(1)†
S1	C1	F12	111.9(6)	S3A	C3A	F32A	109.9(1)†
S1	C1	F13	113.0(6)	S3A	C3A	F33A	109.9(1)†
F11	C1	F12	107.8(7)	F31A	C3A	F32A	109.0(1)†
F11	C1	F13	107.8(7)	F31A	C3A	F33A	109.1(1)†
F12	C1	F13	103.8(8)	F32A	C3A	F33A	109.0(1)†
O21	S2	O22	116.1(3)	O31B	S3B	O32B	109.5(1)†
O21	S2	O23	113.9(3)	O31B	S3B	O33B	109.9(1)†

Appendix 2.16. (Continued)

(b) within the triflate ions

Atom1	Atom2	Atom3	Angle	Atom1	Atom2	Atom3	Angle
O21	S2	C2	104.4(3)	O31B	S3B	C3B	109.3(1)†
O22	S2	O23	115.8(4)	O32B	S3B	O33B	109.6(1)†
O22	S2	C2	101.1(4)	O32B	S3B	C3B	109.1(1)†
O23	S2	C2	102.8(4)	O33B	S3B	C3B	109.4(1)†
S2	C2	F21	110.9(6)	S3B	C3B	F31B	109.9(1)†
S2	C2	F22	110.9(6)	S3B	C3B	F32B	109.7(1)†
S2	C2	F23	109.5(6)	S3B	C3B	F33B	109.9(1)†
F21	C2	F22	108.4(7)	F31B	C3B	F32B	109.1(1)†
F21	C2	F23	110.0(7)	F31B	C3B	F33B	109.1(1)†
F22	C2	F23	107.1(7)	F32B	C3B	F33B	109.1(1)†

†Angle restrained during refinement.

Appendix 2.17. Torsional Angles (deg) for **2**

Atom1	Atom2	Atom3	Atom4	Angle
N12	Cu1	N11	C11	-39(3)
N13	Cu1	N11	C11	-160(3)
N14	Cu1	N11	C11	75(3)
N11	Cu1	N12	C13	39(4)
N13	Cu1	N12	C13	163(4)
N14	Cu1	N12	C13	-75(4)
N11	Cu1	N13	C15	-48(7)
N12	Cu1	N13	C15	-166(7)
N14	Cu1	N13	C15	74(7)
N11	Cu1	N14	C17	-86(10)
N12	Cu1	N14	C17	26(10)
N13	Cu1	N14	C17	148(10)
Cu1	N11	C11	C12	-180(100)
Cu1	N12	C13	C14	48(100)
Cu1	N13	C15	C16	33(100)
Cu1	N14	C17	C18	23(100)
N22	Cu2	N21	C21	-66(3)
N23	Cu2	N21	C21	171(3)
N24	Cu2	N21	C21	48(3)

Appendix 2.17. (Continued)

Atom1	Atom2	Atom3	Atom4	Angle
N21	Cu2	N22	C23	40(4)
N23	Cu2	N22	C23	163(4)
N24	Cu2	N22	C23	-74(4)
N21	Cu2	N23	C25	149(35)
N22	Cu2	N23	C25	30(35)
N24	Cu2	N23	C25	-90(35)
N21	Cu2	N24	C27	-32(3)
N22	Cu2	N24	C27	82(3)
N23	Cu2	N24	C27	-155(3)
Cu2	N21	C21	C22	143(100)
Cu2	N22	C23	C24	103(22)
Cu2	N23	C25	C26	7(79)
Cu2	N24	C27	C28	91(44)
N32	Cu3	N31	C31	-92(9)
N33	Cu3	N31	C31	147(9)
N34	Cu3	N31	C31	19(9)
N31	Cu3	N32	C33	99(3)
N33	Cu3	N32	C33	-141(3)
N34	Cu3	N32	C33	-16(3)

Appendix 2.17. (Continued)

Atom1	Atom2	Atom3	Atom4	Angle
N31	Cu3	N33	C35	70(15)
N32	Cu3	N33	C35	-50(15)
N34	Cu3	N33	C35	-166(15)
N31	Cu3	N34	C37	-71(4)
N32	Cu3	N34	C37	44(4)
N33	Cu3	N34	C37	164(4)
Cu3	N31	C31	C32	-50(48)
Cu3	N32	C33	C34	43(34)
Cu3	N33	C35	C36	38(89)
Cu3	N34	C37	C38	-73(38)
O11	S1	C1	F11	179.8(6)
O11	S1	C1	F12	58.5(7)
O11	S1	C1	F13	-58.3(7)
O12	S1	C1	F11	-60.5(7)
O12	S1	C1	F12	178.3(7)
O12	S1	C1	F13	61.4(7)
O13	S1	C1	F11	56.5(7)
O13	S1	C1	F12	-64.8(8)
O13	S1	C1	F13	178.4(7)
O21	S2	C2	F21	-179.1(5)

Appendix 2.17. (Continued)

Atom1	Atom2	Atom3	Atom4	Angle
O21	S2	C2	F22	60.4(6)
O21	S2	C2	F23	-57.6(6)
O22	S2	C2	F21	-58.3(6)
O22	S2	C2	F22	-178.8(6)
O22	S2	C2	F23	63.3(6)
O23	S2	C2	F21	61.7(6)
O23	S2	C2	F22	-58.8(7)
O23	S2	C2	F23	-176.8(6)
O31A	S3A	C3A	F31A	-180.0(1)†
O31A	S3A	C3A	F32A	-60.0(1)†
O31A	S3A	C3A	F33A	60.0(1)†
O32A	S3A	C3A	F31A	59.9(1)†
O32A	S3A	C3A	F32A	180.0(1)†
O32A	S3A	C3A	F33A	-60.1(1)†
O33A	S3A	C3A	F31A	-60.0(1)†
O33A	S3A	C3A	F32A	60.1(1)†
O33A	S3A	C3A	F33A	180.0(1)†
O31B	S3B	C3B	F31B	179.8(1)†
O31B	S3B	C3B	F32B	-60.2(1)†

Appendix 2.17. (Continued)

Atom1	Atom2	Atom3	Atom4	Angle
O31B	S3B	C3B	F33B	59.7(1)†
O32B	S3B	C3B	F31B	60.1(1)†
O32B	S3B	C3B	F32B	-180.0(1)†
O32B	S3B	C3B	F33B	-60.0(1)†
O33B	S3B	C3B	F31B	-59.8(1)†
O33B	S3B	C3B	F32B	60.1(1)†
O33B	S3B	C3B	F33B	-179.9(1)†

†Angle restrained during refinement.

Appendix 2.18. Anisotropic Displacement Parameters (U_{ij}, Å^2) for **2**

Atom	U_{11}	U_{22}	U_{33}	U_{23}	U_{13}	U_{12}
Cu1	0.0569(4)	0.0560(4)	0.0678(5)	-0.0025(3)	0.0061(3)	0.0036(3)
N11	0.062(3)	0.052(3)	0.061(3)	0.000(2)	-0.005(2)	0.003(2)
N12	0.057(3)	0.056(3)	0.070(3)	-0.003(2)	0.002(2)	0.004(2)
N13	0.057(3)	0.055(3)	0.078(4)	-0.007(2)	0.008(3)	0.002(2)
N14	0.053(3)	0.051(3)	0.077(3)	-0.004(3)	-0.007(2)	0.000(2)
C11	0.073(4)	0.055(3)	0.061(4)	0.002(3)	-0.011(3)	0.004(3)
C12	0.146(9)	0.075(5)	0.087(6)	-0.028(4)	-0.029(6)	0.015(5)
C13	0.061(4)	0.054(3)	0.064(4)	-0.009(3)	-0.007(3)	0.003(3)
C14	0.054(4)	0.099(6)	0.114(7)	-0.031(5)	-0.014(4)	0.005(4)
C15	0.044(3)	0.046(3)	0.064(3)	-0.002(2)	0.003(3)	0.001(2)
C16	0.053(3)	0.071(4)	0.062(4)	0.008(3)	0.007(3)	-0.006(3)
C17	0.054(3)	0.053(3)	0.075(4)	-0.007(3)	-0.009(3)	0.001(3)
C18	0.091(6)	0.065(5)	0.115(7)	0.023(4)	-0.008(5)	0.006(4)
Cu2	0.0558(5)	0.0566(5)	0.0767(6)	-0.0042(4)	-0.0133(4)	-0.0002(3)
N21	0.054(3)	0.053(3)	0.071(3)	-0.004(2)	-0.010(2)	-0.002(2)
N22	0.051(3)	0.052(3)	0.074(3)	-0.006(2)	-0.011(2)	0.002(2)
N23	0.061(3)	0.060(3)	0.078(4)	0.001(3)	-0.017(3)	0.001(2)
N24	0.053(3)	0.055(3)	0.066(3)	0.000(2)	-0.010(2)	0.001(2)
C21	0.049(3)	0.047(3)	0.053(3)	0.006(2)	-0.006(2)	-0.012(2)

Appendix 2.18. (Continued)

Atom	U_{11}	U_{22}	U_{33}	U_{23}	U_{13}	U_{12}
C22	0.052(3)	0.054(3)	0.069(4)	0.005(3)	0.007(3)	-0.004(2)
C23	0.046(3)	0.049(3)	0.081(4)	-0.011(3)	-0.009(3)	0.008(3)
C24	0.058(4)	0.052(4)	0.144(8)	0.002(4)	0.006(5)	0.000(3)
C25	0.044(3)	0.052(3)	0.076(4)	0.010(3)	-0.011(3)	-0.001(2)
C26	0.050(3)	0.060(4)	0.096(5)	0.019(3)	0.003(3)	-0.003(3)
C27	0.053(3)	0.049(3)	0.070(4)	-0.006(3)	-0.007(3)	0.008(2)
C28	0.111(7)	0.082(5)	0.079(5)	-0.017(4)	-0.043(5)	0.032(5)
Cu3	0.0655(5)	0.0618(5)	0.0551(4)	0.0036(3)	0.0046(3)	0.0156(3)
N31	0.069(3)	0.069(3)	0.050(3)	0.001(2)	0.003(2)	0.012(2)
N32	0.071(3)	0.060(3)	0.059(3)	0.008(2)	0.008(2)	0.013(2)
N33	0.062(3)	0.058(3)	0.063(3)	0.004(3)	0.005(2)	0.011(2)
N34	0.053(3)	0.072(3)	0.058(3)	0.007(2)	0.006(2)	0.012(2)
C31	0.067(4)	0.050(3)	0.045(3)	-0.001(2)	0.000(3)	0.007(2)
C32	0.073(4)	0.064(4)	0.077(5)	0.002(3)	-0.015(3)	0.002(3)
C33	0.054(3)	0.053(3)	0.047(3)	-0.006(2)	0.001(2)	0.005(2)
C34	0.084(5)	0.052(3)	0.069(4)	-0.003(3)	0.004(3)	0.013(3)
C35	0.047(3)	0.050(3)	0.049(3)	0.009(2)	0.003(2)	0.010(2)
C36	0.062(4)	0.061(4)	0.063(4)	0.002(3)	-0.003(3)	0.007(3)
C37	0.048(3)	0.070(4)	0.060(4)	0.016(3)	0.000(3)	0.002(3)
C38	0.069(4)	0.119(6)	0.074(5)	0.019(4)	0.023(4)	0.023(4)
S1	0.0641(9)	0.0486(7)	0.0604(9)	-0.0044(6)	0.0192(7)	-0.0095(6)

Appendix 2.18. (Continued)

Atom	U_{11}	U_{22}	U_{33}	U_{23}	U_{13}	U_{12}
F11	0.168(5)	0.102(4)	0.106(4)	-0.019(3)	0.050(3)	-0.087(4)
F12	0.239(8)	0.178(6)	0.067(3)	0.044(4)	-0.032(4)	-0.098(6)
F13	0.118(5)	0.177(7)	0.176(7)	-0.068(5)	0.092(5)	-0.018(4)
O11	0.094(3)	0.066(3)	0.086(3)	-0.015(2)	0.013(3)	-0.033(3)
O12	0.184(7)	0.077(4)	0.075(4)	0.011(3)	-0.050(4)	-0.008(4)
O13	0.092(4)	0.100(4)	0.194(7)	-0.035(5)	0.071(4)	0.008(3)
S2	0.0460(7)	0.0702(9)	0.0462(7)	-0.0051(6)	0.0054(6)	0.0013(6)
F21	0.144(5)	0.156(5)	0.056(3)	-0.023(3)	-0.030(3)	0.018(4)
F22	0.161(5)	0.149(5)	0.138(5)	-0.092(4)	-0.018(4)	0.071(4)
F23	0.123(4)	0.194(7)	0.107(4)	0.040(4)	0.054(3)	-0.017(4)
O21	0.071(3)	0.087(3)	0.067(3)	-0.008(2)	-0.016(2)	0.007(2)
O22	0.077(3)	0.099(4)	0.122(5)	-0.056(4)	-0.025(3)	0.043(3)
O23	0.082(4)	0.164(6)	0.120(5)	0.065(5)	-0.009(3)	-0.049(4)
S3A	0.076(2)	0.0625(19)	0.0541(18)	0.0056(14)	-0.0020(17)	-0.0080(15)
S3B	0.0545(19)	0.156(4)	0.079(2)	0.055(3)	0.0384(19)	0.043(2)

The form of the anisotropic displacement parameter is: $\exp[-2\pi^2(h^2a^{*2}U_{11} + k^2b^{*2}U_{22} + l^2c^{*2}U_{33} + 2klb^*c^*U_{23} + 2hla^*c^*U_{13} + 2hka^*b^*U_{12})]$.

Appendix 2.19. Derived Atomic Coordinates and Displacement Parameters for Hydrogen Atoms in **2**

Atom	x	y	z	Ueq, $Å^2$
H12A	0.1581	-0.1908	0.0953	0.125
H12B	0.2278	-0.1382	0.0568	0.125
H12C	0.1245	-0.1175	0.0440	0.125
H14A	0.5316	0.0801	0.2784	0.108
H14B	0.5371	0.1576	0.2268	0.108
H14C	0.5304	0.0478	0.2099	0.108
H16A	0.0868	0.1367	0.4061	0.074
H16B	0.0398	0.0420	0.3808	0.074
H16C	-0.0014	0.1429	0.3624	0.074
H18A	0.1497	0.4338	0.1190	0.109
H18B	0.1110	0.3702	0.0640	0.109
H18C	0.2145	0.3921	0.0726	0.109
H22A	0.3074	-0.1788	-0.0755	0.070
H22B	0.3885	-0.1064	-0.0693	0.070
H22C	0.3361	-0.1235	-0.1332	0.070
H24A	0.3948	0.3556	-0.0729	0.102
H24B	0.3300	0.4256	-0.0413	0.102
H24C	0.3198	0.4120	-0.1124	0.102

Appendix 2.19. (Continued)

Atom	x	y	z	Ueq, Å^2
H26A	0.0224	0.1268	0.1361	0.083
H26B	-0.0502	0.0618	0.1004	0.083
H26C	-0.0585	0.1746	0.0971	0.083
H28A	-0.0736	0.1224	-0.2456	0.112
H28B	0.0116	0.0729	-0.2692	0.112
H28C	0.0029	0.1857	-0.2702	0.112
H32A	0.2310	-0.0618	0.3079	0.087
H32B	0.2369	-0.1745	0.3038	0.087
H32C	0.2642	-0.1106	0.2493	0.087
H34A	0.5940	-0.4399	0.4354	0.082
H34B	0.6382	-0.3929	0.4955	0.082
H34C	0.6941	-0.4040	0.4383	0.082
H36A	0.5885	0.2030	0.4775	0.075
H36B	0.6627	0.1428	0.5152	0.075
H36C	0.5621	0.1364	0.5310	0.075
H38A	0.7774	-0.1225	0.2190	0.104
H38B	0.6901	-0.1147	0.1745	0.104
H38C	0.7191	-0.2147	0.2032	0.104

Appendix 3.1. Absorbance-Time Data for the Reaction of 3.85 x 10^{-4} M Cu(II) Triflate With 2.08 x 10^{-4} M Dimethylferrocene in 80% AN at 25 °C

Time (s)	Absorbance[a]	Time (s)	Absorbance [a]
0	0.013	160	0.098
5	0.021	200	0.106
10	0.026	240	0.112
15	0.032	280	0.117
20	0.036	330	0.120
30	0.045	380	0.123
40	0.052	430	0.126
60	0.065	480	0.128
80	0.074	580	0.129
100	0.081	680	0.129
120	0.088	780	0.130

[a] In a 2 cm cell.

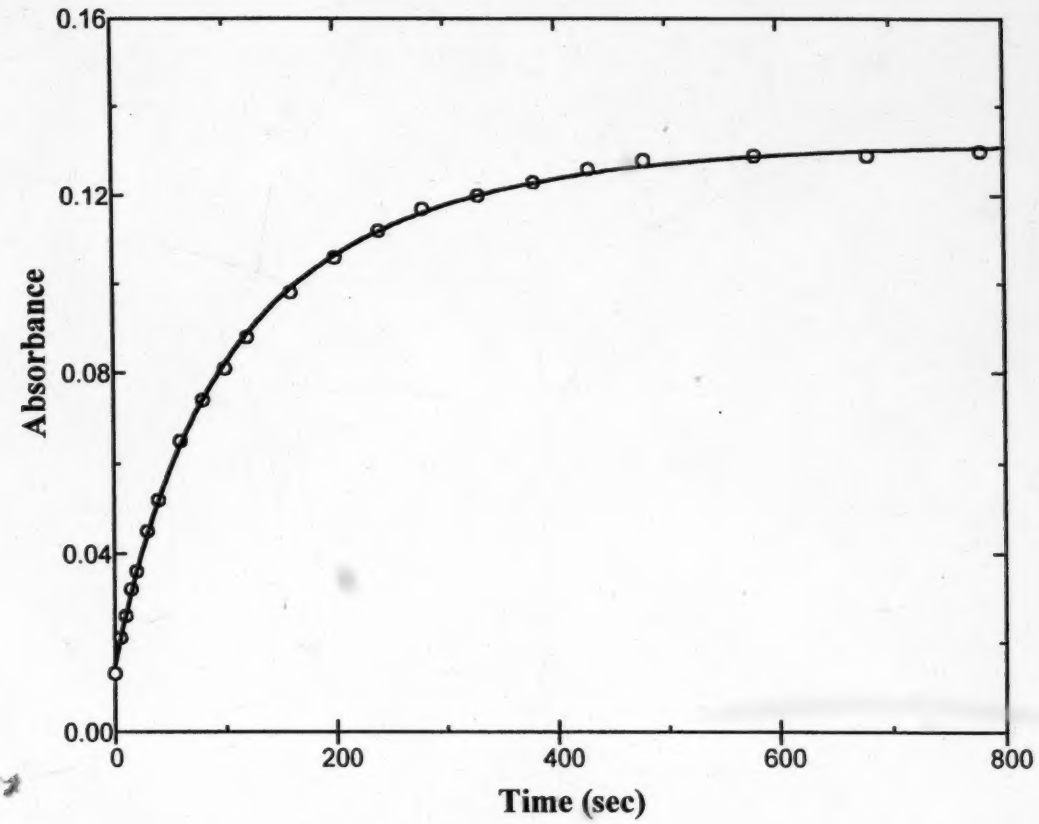

Appendix 3.2. Second-order kinetic fit for the reaction of 3.85 x 10^{-4} M $Cu(CF_3SO_3)_2$ with 2.08 x 10^{-4} M dimethylferrocene in 80% AN at 25 °C. The path length was 2 cm. The curve represents values calculated using the initial concentrations and parameters values 0.00126 (fixed), 0.131 (fixed), 28.5 ± 0.5, 9.05 ± 0.44, 0.0015 ± 0.0005 for initial absorbance, final absorbance, rate constant (M^{-1} s^{-1}), dead-time (s) and blank absorbance respectively.

Appendix 5.1. Determination of Densities, Volume %, Molarities and Mole Fractions of Acetonitrile/Water Mixtures at Ambient Temperature (~22 °C)

mL H_2O	mL AN	Density[c]	Vol %AN	M H_2O[d]	M, AN[d]	χ, H_2O[e]
13.12 [a]	12.50	0.914	48.79	29.06	9.50	0.754
12.50 [b]	12.98	0.904	50.94	27.69	9.87	0.737
5.30 [a]	20.00	0.836	79.05	11.74	15.20	0.436
5.00 [b]	20.35	0.835	80.28	11.08	15.47	0.417
2.88 [a]	22.50	0.817	88.65	6.38	17.10	0.272
2.50 [b]	22.66	0.807	90.06	5.54	17.22	0.243
1.36 [a]	23.75	0.795	94.58	3.01	18.05	0.143
1.25 [b]	23.80	0.792	95.01	2.77	18.09	0.133
0.67 [a]	24.38	0.788	97.29	1.51	18.53	0.0753
0.625 [b]	24.38	0.786	97.50	1.38	18.53	0.0693

[a] Water added to AN to give 25.00 mL. [b] AN added to Water to give 25.00 mL. [c] In g mL^{-1}, based on total volume of 25.00 mL and mass calculated using pure liquid densities of 0.998 and 0.780 g mL^{-1} for H_2O and AN, respectively. [d] Calculated molarity. [e] Mole fraction of H_2O.